Bioanalytical Techniques to Investigate the Consequences of Photosensitized Lipid Oxidation on Lipid Bilayer Formation and Structure

Bioanalytical Techniques to Investigate the Consequences of Photosensitized Lipid Oxidation on Lipid Bilayer Formation and Structure

by

Ashley M. Baxter

A Dissertation

Presented to the Graduate and Research Committee

of Lehigh University

in Candidacy for the Degree of

Doctor of Philosophy

in

Chemistry

Lehigh University

May 2022

Approved and recommended for acceptance as a dissertation in partial fulfillment of the requirements for the degree of Doctor of Philosophy

Ashley M. Baxter
Bioanalytical Techniques to Investigate the Consequences of Photosensitized Lipid Oxidation on Lipid Bilayer Formation and Structure

April 28, 2022

Defense Date

Dissertation Director
Nathan Wittenberg, PhD

Approved Date

Committee Members:

Damien Thévenin, PhD

Elizabeth Young, PhD

Aurelia Honerkamp-Smith, PhD

Acknowledgements

Curiosity begins in childhood. Thank you to all of my past teachers for instilling a thirst for knowledge and giving me the tools that have gotten me through twenty-three years of schooling. Thank you especially to the professors at DeSales University, particularly Dr. Sara Hayik, who took a chance on me as an undergraduate researcher on a p-chem project, but who gave me the skills I needed to become a graduate researcher. I also want to thank Drs. Julie Himmelberger, Rodger Berg, Steve Sweeney, and Fran Mayville, all of whom helped me on my journey through undergrad, and who have been supportive throughout my grad school career. And thank you to Toni LaBelle, who was the best randomly-assigned freshman-year roommate I ever could have asked for, and Ryan Fischer, who was with me all throughout high school and undergrad. You two were the best study buddies and my dearest friends, and you were absolute rocks for me while we were all at DeSales.

I want to thank my graduate advisor, Nate Wittenberg, for his kindness, patience, and guidance these last six years. Thank you for being a wonderful boss to work for, and for all of the help you have provided with my project. Along those line, I want to thank my lab mates for being great colleagues to work with. Especially thank you to Megan Blauch, who has been the best source of encouragement and support throughout this journey, Jennie Cawley, who always asked the questions to make me think harder and reach farther, and Luke Jordan, for taking the time to train and mentor me when I first joined the Wittenberg lab. More broadly, thank you to the Lehigh Chemistry Department for all the resources and support throughout my graduate career.

Next up, thank you to a whole host of friends, near and far, for your endless encouragement. There are so many to thank, and unfortunately, I know I will leave some out, but especially thank you to Lindsay, Ambre, Sahra, Vicky, and Lauren. You're all stars.

Penultimately, thank you to my family at large. A majority of them are not scientists and probably couldn't tell you what my research is about, but nevertheless, they would always ask me how my lipids were doing. My lipids are doing great.

Finally, none of this would have been possible without my parents. My dad has been gone for nearly seven years, and yet his voice will never fade in my memory, telling me how much he loves me, and how proud he is of me. My mom... there aren't enough words in the English language to thank my mom for all she has done for me. She provided me with more support and stability than I can ever hope to repay. She is the epitome of love, grace, and gentleness. I can only hope to one day be a fraction as patient and generous as she is.

TABLE OF CONTENTS

LIST OF FIGURES.....xii

LIST OF TABLES.....xvi

ABSTRACT.....1

CHAPTER 1. Lipids, Membranes, and Bioanalytical Techniques.....3

1.1 Introduction.....3

1.2 Lipids.....3

1.2.1 Phospholipids.....4

1.2.2 Glycolipids.....6

1.2.3 Sphingolipids.....6

1.2.4 Glycosphingolipids and Gangliosides.....8

1.2.5 Cholesterol.....9

1.3 Role of Phospholipids.....10

1.4 Lipid Shape.....11

1.5 Lipid Self-Assembly.....14

1.6 Plasma Cell Membrane.....16

1.7 Model Membrane Mimics.....17

1.7.1 Liposomes and Giant Vesicles.....18

1.7.2 Black Lipid Membranes.....19

1.7.3 Supported Lipid Bilayers.....19

1.7.3.1 Vesicle Fusion.....20

1.7.3.2 Solvent-Assisted Lipid Bilayer.....21

1.7.3.3 Bicelle SLB Formation.....22

1.7.3.4 Langmuir-Blodgett.....23

1.8 Reactive Oxygen Species....23

1.9 Lipid Oxidation....24

1.9.1 Oxidation-Induced Membrane Deformation....26

1.9.2 Antioxidants....28

1.10 Photosensitizers and Photodynamic Therapy....29

1.11 Bioanalytical Techniques....32

1.11.1 Quartz Crystal Microbalance with Dissipation Monitoring....32

1.11.2 Fluorescence Microscopy....35

1.11.2.1 Fluorescence Recovery After Photobleaching....36

1.11.2.2 Total Internal Reflection Fluorescence Microscopy....37

1.12 Thesis Overview....38

1.13 References....40

CHAPTER 2. Excitation of Fluorescent Lipid Probes Accelerates Supported Lipid Bilayer Formation via Photosensitized Lipid Oxidation....54

2.1 Abstract....54

2.2 Introduction....55

2.3 Results and Discussion....56

2.3.1 Phospholipid Structures and Excitation Spectra of Fluorophore-Lipid Conjugates....56

2.3.2 The Inclusion of a Lipid-Conjugated Fluorophore does not Impact SLB Formation....58

2.3.3 Accelerated SLB Formation....59

2.3.4 Concentration and Light Intensity Dependence....62

2.3.5 Excited Liposomes do not Spontaneously Rupture on Gold Surfaces....64

2.3.6 Larger Liposomes Also Show Accelerated SLB Formation....65

2.3.7 SLB Mass Decreases with Longer Illumination Times.....66
2.3.8 SLBs Formed from Excited Liposomes are Relatively Free of Defects.....67
2.3.9 Ambient Light has Negligible Effect on SLB Formation Process.....68
2.3.10 Fluorescence Micrographs of SLBs Formed from Illuminated Liposomes.....69
2.3.11 Accelerated SLB Formation Process Depends on Fluorophore Identity.....70
2.3.12 Mimicking the Effects of Photo-Oxidation.....72
2.3.13 Attenuation of Accelerated SLB Formation Process.....74
2.3.14 Evidence of Lipid Oxidation.....76
2.3.15 DLS and Zeta Potential of Liposomes.....78
2.3.16 Inclusion of Oxidation Products in Liposomes.....80
2.4 Conclusions.....82
2.5 Materials and Methods.....86
2.5.1 Preparation of Liposomes.....86
2.5.2 Collection of Spectra.....87
2.5.3 Liposome Illumination.....88
2.5.4 Quartz Crystal Microbalance with Dissipation Monitoring Measurements.....88
2.5.5 Lipid Monolayer Compression Isotherms.....89
2.5.6 FT-IR Spectroscopy.....89
2.5.7 Dynamic Light Scattering.....90
2.5.8 Zeta Potential Analysis.....90
2.5.9 Fluorescence Microscopy.....90
2.6 References.....92

CHAPTER 3. Tubulation of Supported Lipid Bilayer Membranes Induced by Photosensitized Lipid Oxidation.....97

3.1 Abstract.....97

3.2 Introduction.....98

3.3 Results and Discussion.....100

3.3.1 TF-PC Causes Membrane Tubulation.....100

3.3.2 Attenuation of Membrane Tubulation.....103

3.3.3 Correlation of Power Intensity and Lag Time of Membrane Tubules.....106

3.3.4 Tube-to-Liposome Transitions.....108

3.3.5 Tube and Liposome Growth Dynamics.....111

3.3.6 Tube Extension in Flow.....112

3.3.7 The Effects of Divalent Cations on Membrane Tubulation.....113

3.3.8 Mechanism of SLB Tubulation and Vesiculation.....116

3.4 Conclusions.....119

3.5 Materials and Methods.....120

3.5.1 Buffers.....120

3.5.2 Preparation of Liposomes.....120

3.5.3 Supported Bilayer Formation and Fluorescence Microscopy.....121

3.5.4 Fabrication of Microfluidic Channels.....121

3.6 References.....123

CHAPTER 4. Effects of Cholesterol on SLB Formation from Liposomes Containing Oxidized Lipids.....130

4.1 Abstract.....130

4.2 Introduction.....130

4.3 Results and Discussion.....132

4.3.1 Oxidized Phospholipids Alter Liposome Rupture Pathway.....132

4.3.2 Cholesterol Alters Rupture Pathway of Liposomes Containing Oxidized Lipids....134

4.4 Conclusions and Future Directions....139

4.5 Materials and Methods....139

4.5.1 Preparation of Liposomes....140

4.5.2 QCM-D Measurements....140

4.6 References....141

CHAPTER 5. Influence of Brain Gangliosides on the Formation and Properties of Supported Lipid Bilayers....144

5.1 Abstract....144

5.2 Introduction....145

5.3 Results and Discussion....147

5.3.1 Formation of SLBs Containing Brain Gangliosides....147

5.3.2 The Effect of Ca^{2+} on SLB Formation....157

5.3.3 The Influence of Gangliosides and Ca^{2+} on Lipid Diffusion....159

5.3.4 Measuring Antibody Binding Constants Using Ganglioside-Rich SLBs....168

5.3.5 Curve Fitting for Antibody Binding Assays....171

5.4 Summary and Conclusions....172

5.5 Materials and Methods....173

5.5.1 Reagents and Chemicals....173

5.5.2 Liposome Preparation....174

5.5.3 QCM-D Measurements....174

5.5.4 Zeta Potential Measurements....175

5.5.5 FRAP Measurements....175

5.5.6 Statistical Analysis....176
5.6 References....177

CHAPTER 6. Future Directions....184
6.1 Introduction....184
6.2 Binding Studies of CD36 to Oxidized Lipids....185
6.2.1 The Influence of Cholesterol on CD36 Binding....186
6.3 Spatiotemporal Response of Immune Cells to Oxidized Lipid Gradients....187
6.4 Cholesterol Modulation of Lipid-Lipid and Lipid-Protein Interactions....189
6.5 Conclusions....190
6.6 References....191

VITA....193

LIST OF FIGURES

Figure 1.1. The general structure of phospholipids and common head groups.....5

Figure 1.2. Structures of sphingosine, ceramide, and sphingomyelin.....7

Figure 1.3. The structure of the ganglioside GM1.....8

Figure 1.4. The structure of cholesterol.....9

Figure 1.5. Simulated systems demonstrating membrane curvature.....12

Figure 1.6. A schematic representation of lipid packing parameter.....14

Figure 1.7. A mechanism of lipid oxidation.....26

Figure 1.8. Oxidation changes lipid properties.....28

Figure 1.9. Mechanism of action of tocopherols.....29

Figure 1.10. Jablonski diagram of the excitation of a photosensitizer.....30

Figure 1.11. Mechanisms of contact-independent and contact-dependent photosensitizer-induced lipid oxidation.....31

Figure 1.12. Classical QCM-D response of SLB formation on a SiO_2 sensor.....35

Figure 1.13. The principle of TIRFM.....38

Figure 2.1. Structures of the phospholipids, fluorescently-conjugated lipids, and α-tocopherol.....57

Figure 2.2. Excitation spectra and spectrum of LED light source.....58

Figure 2.3. TF-PC does not significantly alter SLB formation.....58

Figure 2.4. Illumination does not affect DOPC liposomes.....60

Figure 2.5. Influence of illumination of TF-PC-containing liposomes on SLB formation..61

Figure 2.6. Influence of illumination of BODIPY-PE-containing liposomes on SLB formation.....62

Figure 2.7. Effect of illumination and TF-PC concentration on SLB formation.....63

Figure 2.8. Effect of illumination intensity on SLB formation.....63

Figure 2.9. Illuminated DOPC/TF-PC liposomes do not spontaneously rupture on a gold

surface.....65

Figure 2.10. SLB formation from liposomes extruded through 100 nm pore size filters.....66

Figure 2.11. Liposome illumination reduces final frequency and SLB mass.....67

Figure 2.12. Examination of SLB continuity by exposure to bovine serum albumin.....68

Figure 2.13. Effects of ambient light exposure.....69

Figure 2.14. Fluorescence micrographs of SLBs.....70

Figure 2.15. The influence of illumination on SLB formation from DOPC liposomes containing other fluorescently-conjugated lipid probes.....71

Figure 2.16. The influence of oxidized phospholipids on SLB formation.....72

Figure 2.17. Influence of DMSO on liposome adsorption, rupture, and SLB formation.....73

Figure 2.18. Influence of lipid saturation on SLB formation after liposome illumination...74

Figure 2.19. Influence of antioxidant on SLB formation after liposome illumination.....75

Figure 2.20. Surface pressure-area isotherms of monolayer of illuminated lipids.....77

Figure 2.21. FT-IR spectra of illuminated lipids.....78

Figure 2.22. Effect of hexanoic acid on SLB formation.....81

Figure 2.23. Schematic illustration of liposome rupture pathways.....85

Figure 3.1. Structures of the phospholipids, fluorescently-conjugated lipids, and α-tocopherol used in this study.....100

Figure 3.2. Fluorescence micrographs of DOPC/TF-PC SLBs.....101

Figure 3.3. Tubulation is reduced by lower concentration of fluorophore.....102

Figure 3.4. Tubulation is inhibited by saturated lipids.....104

Figure 3.5. Tubulation is inhibited by a non-sensitizer fluorophore.....105

Figure 3.6. Tubulation is inhibited by an antioxidant.....105

Figure 3.7. Light power dependence of SLB tubulation.....106

Figure 3.8. Membrane tube length and liposome size distributions.....108

Figure 3.9. Tube-to-liposome transitions.....110

Figure 3.10. Rate of tube length and liposome diameter growth.....111

Figure 3.11. Membrane tubules extend under flow.....113

Figure 3.12. Fluorescence micrographs of the influence of divalent cations on the progression of SLB tubulation.....115

Figure 4.1. Structures of phospholipids and cholesterol.....132

Figure 4.2. QCM-D response of SLB formation with increasing concentrations of oxidized lipids.....133

Figure 4.3. QCM-D response of SLB formation with 5 mol% PazePC and increasing concentrations of cholesterol.....134

Figure 4.4. QCM-D response of SLB formation with 7.5 mol% PazePC and increasing concentrations of cholesterol.....136

Figure 4.5. QCM-D response of SLB formation with 10 mol% PazePC and increasing concentrations of cholesterol.....137

Figure 5.1. Structures of GM1, GD1a, GD1b, and GT1b gangliosides.....147

Figure 5.2. Representative frequency and dissipation curves for QCM-D monitoring of the formation of DOPC SLBs.....149

Figure 5.3. Representative frequency and dissipation curves for QCM-D monitoring of the formation of ganglioside-rich SLBs.....150

Figure 5.4. Formation of SLBs containing 2–4% gangliosides.....151

Figure 5.5. Time course of adsorption and rupture of liposomes with 5% GD1a and 5% GT1b.....152

Figure 5.6. Influence of ganglioside type and concentration on liposomes adsorption and rupture.....153

Figure 5.7. Zeta potential of liposomes composed solely of DOPC and DOPC liposomes containing 5% GM1, GD1a, GD1b, and GT1b.....155

Figure 5.8. Effects of Ca^{2+} on the formation of ganglioside-rich SLBs.....157

Figure 5.9. Ratio of $t_{crit}(+Ca^{2+})/t_{crit}(Ca^{2+}\text{-free})$ of different gangliosides.....158

Figure 5.10. Influence of ganglioside concentration and Ca^{2+} on lipid diffusion coefficients in SLBs.....160

Figure 5.11. FRAP images of DOPC supported lipid bilayers before and after Ca^{2+} chelation with EDTA.....162

Figure 5.12. FRAP images of DOPC supported lipid bilayers containing 1, 3, or 5% GM1 before and after Ca^{2+} chelation with EDTA.....163

Figure 5.13. FRAP images of DOPC supported lipid bilayers containing 1, 3, or 5% GD1a before and after Ca^{2+} chelation with EDTA.....164

Figure 5.14. FRAP images of DOPC supported lipid bilayers containing 1, 3, or 5% GD1b before and after Ca^{2+} chelation with EDTA.....165

Figure 5.15. FRAP images of DOPC supported lipid bilayers containing 1, 3, or 5% GT1b before and after Ca^{2+} chelation with EDTA.....166

Figure 5.16. Formation of a SLB containing 1% GD1a in the presence of 2 mM Ca^{2+} monitored with QCM-D.....169

Figure 5.17. QCM-D frequency shift curves showing 1, 5, and 50 nM GD1a-1 antibody binding to SLBs with 1% GD1a.....170

Figure 5.18. Cholera toxin B subunit (CTB) binding to SLB with 5% GM1.....171

Figure 6.1. Approach to measure CD36-oxPC interaction kinetics and affinity.....186

Figure 6.2. Spatiotemporal macrophage response to linear oxPC gradients.....188

Figure 6.3. Spatiotemporal macrophage response to photochemically-generated oxPC gradients.....189

LIST OF TABLES

Table 2.1. Liposome radii, surface areas, and zeta potentials before and after illumination.....79

Table 5.1. Lipid diffusion coefficients determined from FRAP measurements.....161

ABSTRACT

Lipid membranes comprise the boundary of cells and organelles, providing structure, support, and protection. Model membrane systems can be formed through a variety of a techniques and are advantageous for studying lipid bilayer membranes in a controlled system. Reactive oxygen species (ROS) are found and produced endogenously within cells and organelles; however, unsaturated lipids are particularly susceptible to oxidation via ROS. Oxidation of these unsaturated fatty acid tails changes their chemical structure, rendering them more polar, which causes a number of physical changes to the lipid bilayer membrane. The consequences of lipid oxidation include an increase in the area per lipid molecule which causes lateral membrane expansion, a decrease in lipid order, membrane thinning, increased membrane permeability, and others. Studies have also shown the induction of highly curved membrane structures, such as buds or tubes, upon lipid oxidation. Furthermore, lipid oxidation has been linked with many degenerative diseases as well as aging.

The first half of my work investigates how the formation process of a supported lipid bilayer (SLB) is altered by lipid photo-oxidation through use of the lipid-conjugated fluorophore TopFluor-PC (TF-PC) as a photosensitizer. My studies using quartz crystal microbalance with dissipation monitoring (QCM-D) show that the traditional pathway of SLB formation is disrupted when vesicles have been photo-oxidized, suggesting a structural change to the lipids comprising the vesicles. This is further supported by the attenuation of the observed affects when an antioxidant such as α-tocopherol (vitamin E) or saturated phospholipids are incorporated into the lipid vesicles. The second half of my work uses fluorescence microscopy to observe the consequences of oxidation on a SLB,

namely the formation of membrane tubules followed by the formation vesicles from these tubes. Characterization of these defects shows a direct correlation between the length of the tube and the diameter of the resulting vesicle. Using geometric modeling, I can calculate the diameter of individual membrane nanotubes. Additionally, the presence of the antioxidant α-tocopherol attenuates the membrane defects brought about by photo-oxidation, and membranes made of fully-saturated lipids show no evidence of tubulation or vesiculation.

This work elucidates the physiological changes caused by membrane photo-oxidation, and investigates the importance and relevance of lipid oxidation as it pertains to biological and biochemical systems.

Chapter 1: Lipids, Membranes, and Bioanalytical Techniques

1.1 Introduction

Cells are the most basic yet fundamental unit of life, and countless scientists have dedicated their lives to furthering understanding of cells. This is no easy feat, since cells are composed of a complex mixture of biomolecules, such as lipids, proteins, nucleic acids, and carbohydrates.[1] Because of these complexities, researchers often use model membrane systems to mimic cell membranes. Model membranes allow researchers to hone in on just a few variables to further understand individual components of a cell.

This chapter will discuss at great length the fundamental building blocks of cell membranes: lipids. The focus will center around supported lipid bilayers (SLBs) and liposomes, both of which can act as model membrane mimics. It will also detail changes to membrane properties as a function of lipid identity and lipid shape, and ways that membrane properties can change upon the oxidation of the lipid molecules composing the membrane. There are a variety of bioanalytical techniques that can be used to investigate and monitor structural changes of lipids and biomembranes, which will also be discussed in this chapter.

1.2 Lipids

Lipids are among one of the four major classes of biologically-relevant macromolecules, sharing this title with proteins, nucleic acids, and carbohydrates.[1] There are several classes of lipid molecules, including fatty acids, phospholipids, steroids, and waxes;[2] however, phospholipids are, by far, the most prevalent and are the most common lipid type found within the plasma membrane of a cell.[3]

1.2.1 Phospholipids

Phospholipids are amphipathic molecules, meaning they have both hydrophilic (water loving) and hydrophobic (water hating) moieties. Generally, phospholipids are made up of three parts: a phosphate head group, carbon-chain tail group(s), and a glycerol backbone. The hydrophobic part is the fatty acid tail, which is made up of acyl chains, which are covalently bonded to two of the three hydroxyl groups of the glycerol backbone. These fatty acid tails can differ in length, though, on average, they tend to be 14–24 carbon atoms long;[3] however, some lipid molecules can be shorter or longer. There may be points of unsaturation within the fatty acid tail, meaning that there is a carbon-carbon double bond. The double bond can be in either the *cis* or *trans* conformation, depending on the orientation. Lipids tend to have two fatty acid tails, though some can have more or fewer.[3]

The length of these fatty acid tails as well as the specific nature of the hydrophilic headgroup differentiates one lipid from another. Some head groups may be charged or be differently-sized, which will innately change its physical properties and behavior.[4] The specific structure of the headgroup often denotes the name of the lipid. For example, if the headgroup contains a choline moiety, the name is phosphatidylcholine, or PC for short. Common head groups are amino acids (i.e. serine), saccharides, and primary or tertiary amines.

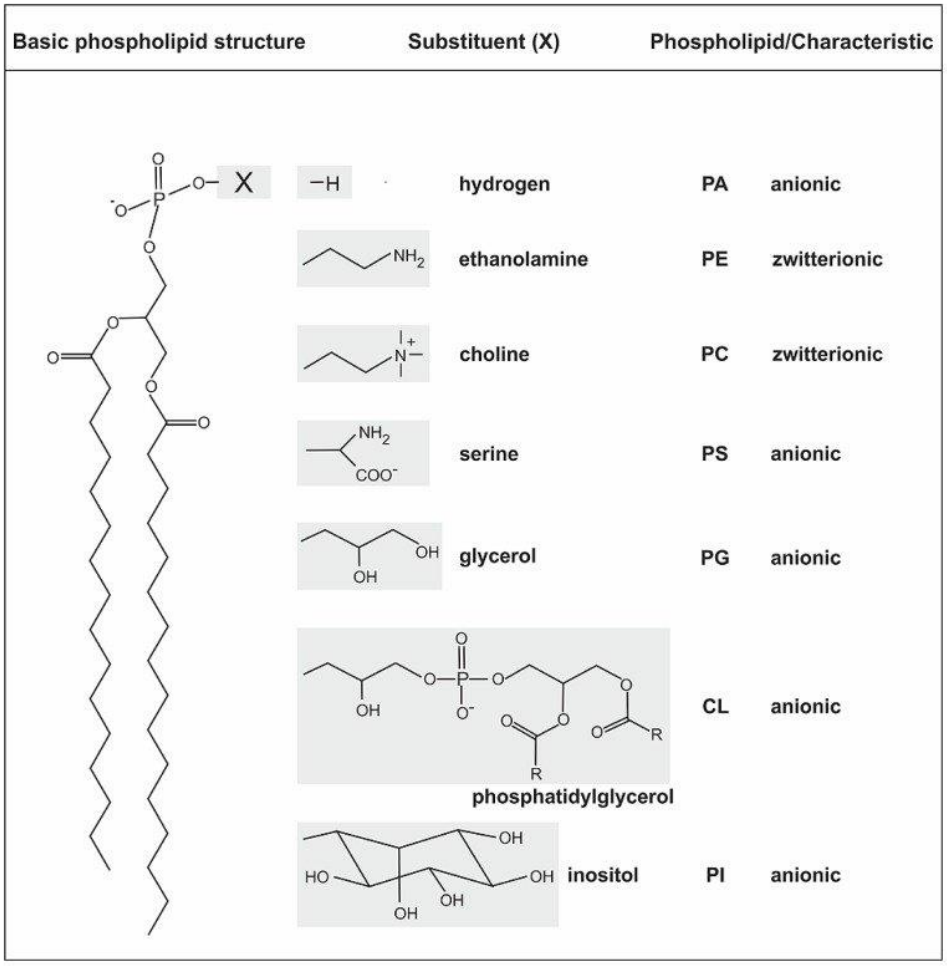

Figure 1.1. The general structure of phospholipids and common head groups. PA = phosphatidic acid; PE = phosphatidylethanolamine; PC = phosphatidylcholine; PS = phosphatidylserine; PG = phosphatidylglycerol; CL = cardiolipin; PI = phosphatidylinositol.[5]

The precise physical and mechanical properties of a cell membrane depend on the types of lipids that comprise it.[6] The packing of lipids within a membrane is dependent on many things. Environmental factors (pH, temperature, ionic composition, etc.) can drastically change the physical properties of a lipid and thus impact how lipids organize into complex structures.[7] As mentioned earlier, the length and degree of saturation of the fatty acid chains of a phospholipid differs between lipids. These factors impact membrane

stiffness or fluidity. Lipids with long fatty acid tails often lead to stiffer membranes with higher melting temperatures due to the increased number of van der Waals interactions between the hydrophobic tails clustered within the center of the membrane.[8] Similarly, phospholipids that are completely saturated (i.e. have no double bonds within the fatty acid tail) can cluster together more tightly than lipids that have "kinks" in their tails due to the presence of double bonds. This tighter packing leads to a stiffer membrane.

The addition of cholesterol can impact membrane fluidity by filling in gaps or pores within the membrane, thus stiffening it; conversely, if cholesterol is within straight-chain lipid membranes, which pack together tightly, the cholesterol molecule disrupts the van der Waals interactions, thus decreasing stiffness, decreasing the melting point, and increasing membrane fluidity.[9]

1.2.2 Glycolipids

Glycolipids are a subclass of lipid molecules that have sugar molecules (glycans) as a head group. While glycolipids are fairly simple molecules, particularly if just one sugar moiety is covalently bonded to the lipid head group, they can have a range of biological functions. Glycolipids are found on the surface of cell membranes, and are involved with facilitating cell-cell interactions as well as acting as target receptors for viruses or other pathogens seeking to enter a cell.[10] Glycolipids are often enriched in lipid microdomains or lipid rafts. Because of this, their presence can alter the function of nearby molecules (such as proteins) within these rafts.[11]

1.2.3 Sphingolipids

Sphingolipids are another class of lipids found within cell membranes. They have a sphingosine backbone, which is a serine moiety with an attached fatty acid. Sphingolipids are highly enriched in the nervous system, where they serve important signaling and regulatory roles.[12] Because of this, these molecules have become the focus of study of neurological disorders and neurodegenerative diseases.

A specific type of sphingolipid is sphingomyelin (SM). SM and PC lipids are the most prevalent lipids in the external leaflet of cell membranes, though SM is more highly enriched in specialized tissues such as brain tissue.[12,13] The structure of SM is similar to other sphingolipids; however, their sphingosine backbone has an additional fatty acid and a PC head group.

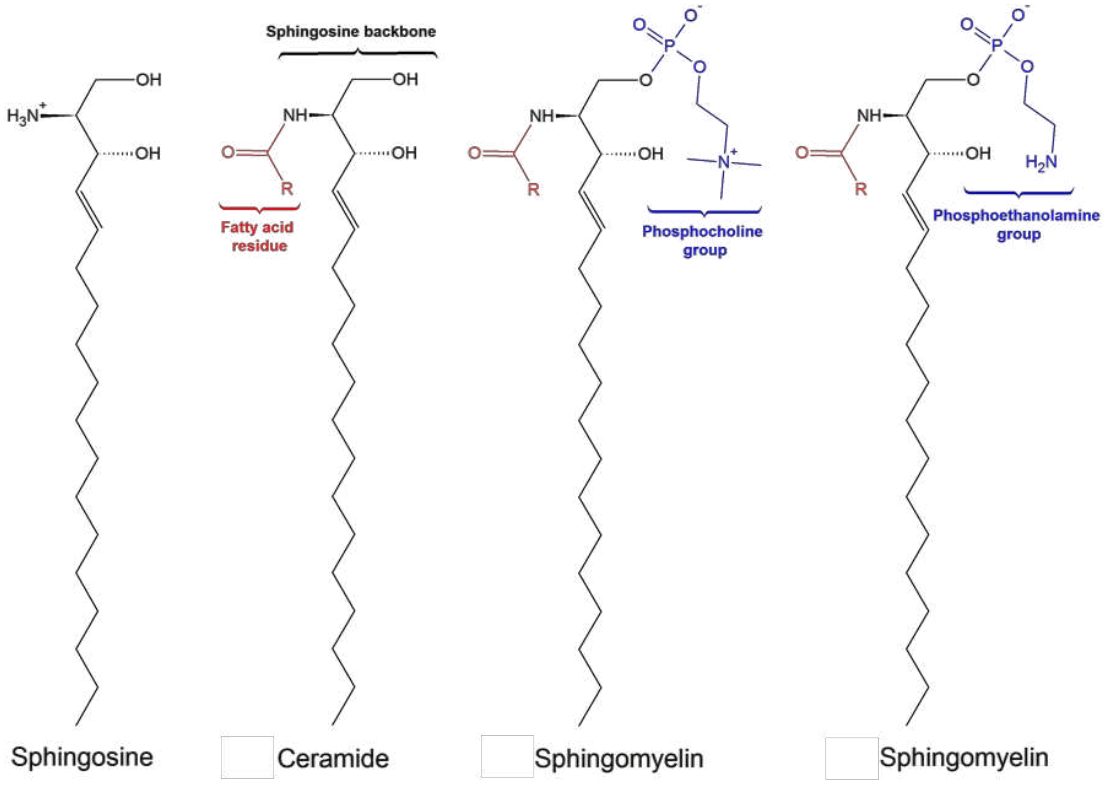

Figure 1.2. Structures of sphingosine, ceramide, and sphingomyelin with either a phosphocholine or phosphoethanolamine headgroup. Reproduced from reference 14.[14]

1.2.4 Glycosphingolipids and Gangliosides

Glycosphingolipids (GSLs) are a combination of glycolipids and sphingolipids. GSLs are involved in the initial steps of virus/pathogen-cell interactions, where they mediate host cell membrane recognition.[15] They are present on the surface of cell membranes and are very abundant in the brain in the form of gangliosides.[11] Gangliosides are molecules composed of a glycosphingolipid with one or more sialic acids linked to the sugar moiety. The most common sialic acid among human brain gangliosides is N-acetylneuraminic acid.[16]

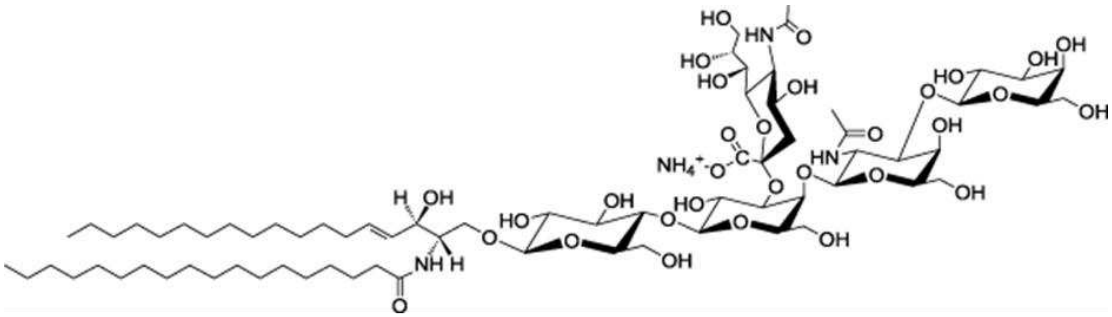

Figure 1.3. The structure of the ganglioside GM1. © Avanti Polar Lipids.

Gangliosides are differentiated from one another by the differing number of sialic acid groups; because of this, different gangliosides carry different head group charges. These negative charges create electrostatic repulsions between ganglioside molecules and substrates, making it difficult to create ganglioside-rich supported lipid bilayers (SLBs).

Gangliosides often phase separate, and are typically found in the liquid ordered phase.[17] This phase separation is responsible for the formation of microdomains or lipid rafts.

1.2.5 Cholesterol

Cholesterol falls under the class of lipids known as sterols. Sterol molecules are crucial to eukaryotic cell structure, and cholesterol is biosynthesized by all eukaryotic cells.[18] Cholesterol has a fused-ring structure (three six-membered rings and one five-membered ring), which is vastly different from the long-chain structures of lipids that have been discussed thus far.

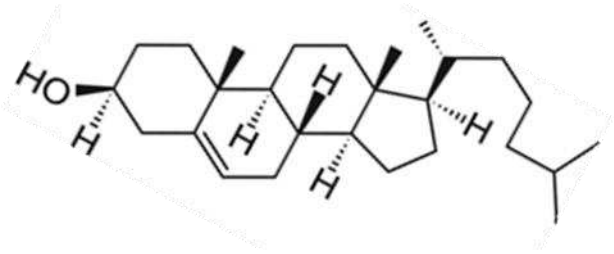

Figure 1.4. The structure of cholesterol. © Avanti Polar Lipids.

Cholesterol is found in high percentages in eukaryotic cells, ranging from approximately 30–40 mol%.[19] While the bulk of the cholesterol molecule is very hydrophobic, it also has a polar hydroxyl head group. This causes cholesterol to orient itself within a lipid membrane such that the hydroxyl moiety is pointing towards the aqueous interface, while the body of the molecule is embedded within the hydrophobic core of the membrane. This orientation effects the lipid packing of a bilayer. When cholesterol is

abundantly present amid phospholipids, there is much tighter packing within the bilayer, which in turn can affect the biophysical properties (mobility, melting point, etc.) of the membrane.

1.3 Role of Phospholipids

Phospholipids have the important task of creating the protective boundary around cells and organelles; this aids both in the cell's protection, organization, and compartmentalization. Lipids are one of the most abundant molecules, and they comprise approximately 50% of animal cell membranes, with the other 50% being proteins.[3]

The cell is a complex structure that has need of small molecules to assist in inter- and intracellular signaling. In addition to providing structural support of cell membranes, phospholipids act as sources of energy and signaling molecules.[20] Phosphatidic acid (PA), diacylglycerol (DAG), and phosphorylated forms of phosphatidylinositol (PI), called phosphoinositides, are just a few examples of cellular signaling molecules that are derived from lipids.[21]

Mammalian cells endogenously synthesize phospholipids in the cytosolic side of the endoplasmic reticulum (ER) membrane, which is full of proteins that catalyze and assist with phospholipid biosynthesis.[22,23] The precursor molecule for phospholipids is a glycerol molecule or fatty acid, which is phosphorylated by a glycerokinase and converted into glycerol-3-phosphate. Glycerol-3-phosphate acyltransferase or acyl-CoA synthase enzymes react with the glycerol-3-phosophate or fatty acid molecules, respectively, to create phosphatidic acid (PA). If PA is reacted upon by phosphatidic acid phosphatase, it is converted to diacylglycerol (DAG), which can further be converted to

phosphatidylcholine (PC), phosphatidylserine (PS), or phosphatidylethanolamine (PE) by other enzymatic pathways. Eventually, vesicles containing these newly-synthesized phospholipids will bud off from the ER membrane. From there, they will be transported to the plasma membrane for incorporation to either the inner or outer leaflet of the membrane.[23]

1.4 Lipid Shape

The ordering and packing of lipid molecules into higher-ordered structures is very much dependent upon the shape of the individual lipid molecule.[24] The overall shape and curvature of a membrane can also be dictated by the type of lipid composing the membrane. Positive curvature is defined as being concave in nature, when the membrane is viewed from above; negative curvature, on the other hand, is convex in nature (Figure 1.5)

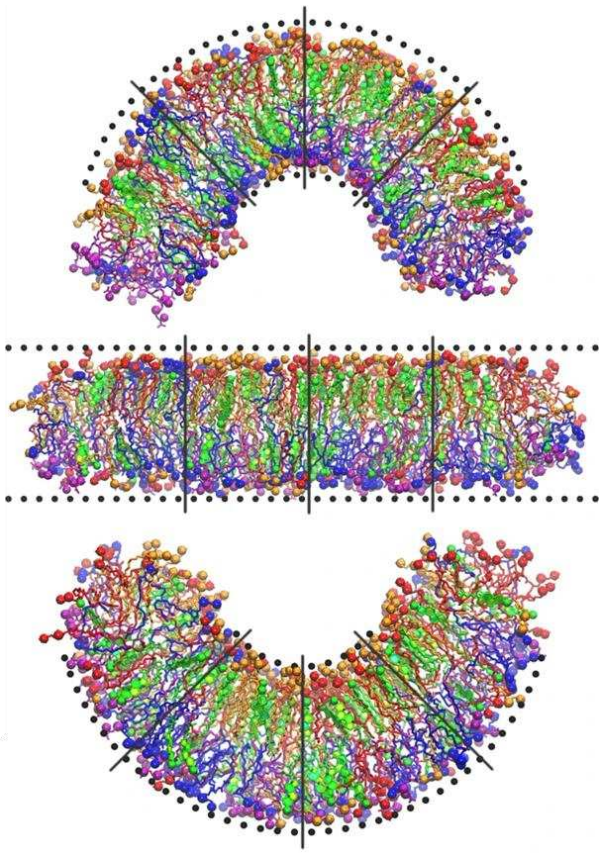

Figure 1.5. Simulated systems demonstrating membrane curvature.[25] The outer membrane leaflet is on top in each of these examples. Top: positive curvature with regards to the outer membrane leaflet. Middle: no curvature. Bottom: Negative membrane curvature with regards to the outer membrane leaflet.

There are three major classes of lipid shapes, which are dependent on the head group size relative to the lipid tail group size.[26] These three classes of lipid shape are inverted cone, cylinder, and cone. A mathematical formula has been derived to assign a numerical value of a lipid's packing parameter (*P*), which predicts whether the lipid is inverted cone, cylindrical, or cone-shaped:[7]

$$P = \frac{V}{a \cdot l} \qquad \text{eq 1.1}$$

In the above equation, V is the volume occupied by the tail group, a is the area of the lipid molecule, and l is the length of the acyl chain of the tail group.

When $P < 1$, the head group is larger than the tail group, and the lipid is inverse-cone shaped. Lipids with only one acyl chain group rather than two, such as detergents and lysophospholipids, are the molecules that primarily make up this shape category. This class of lipid favors sites of positive membrane curvature[27] and tends to form micellar structures.[26] These lipids also play an especially crucial and important role in membrane pore formation[28] and vesicle budding.[29]

When $P > 1$, the tail group is larger than the head group, and the lipid is cone-shaped. These structures tend to form inverted micelles and favor sites of negative membrane curvature.[27,30] Inverted cone-shaped lipids play an important role in cellular uptake processes due to the fact that the membrane has to bend inwards.[31]

Finally, when $P = 1$, the relative size of the head group and tail group are the same, and the lipid is cylindrical in shape. These lipids form planar lipid bilayers and liposomes,[26] arguably making them the most important lipid shape.

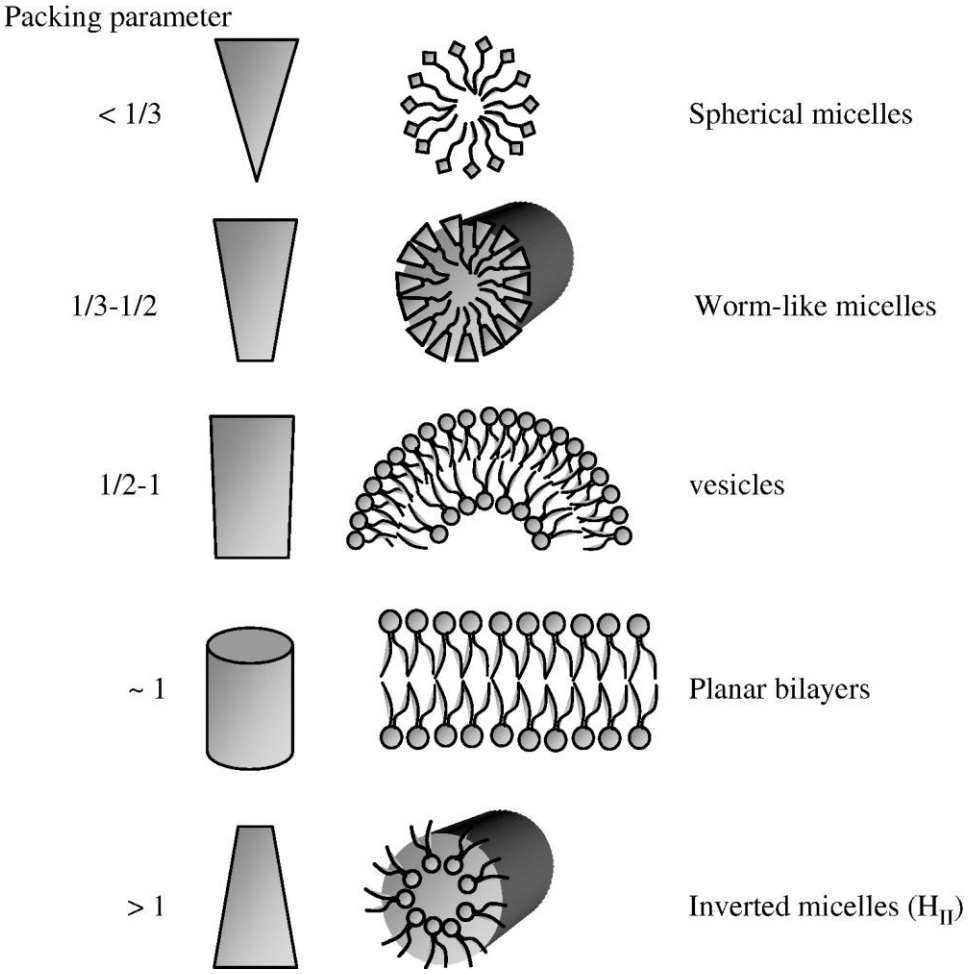

Figure 1.6. A schematic representation of lipid packing parameter and the resulting aggregate structure.[32]

1.5 Lipid Self-Assembly

The dual amphipathic nature of lipid molecules gives them the ability to spontaneously form ordered structures, such as micelles or vesicles/liposomes, when placed in an aqueous environment. Lipids form these ordered structures to shield their hydrophobic tails from water, while allowing their hydrophilic heads to interact favorably with the aqueous environment.[33,34]

This spontaneous, ordered aggregation is driven by the hydrophobic effect. In bulk aqueous solutions, water molecules are free to orient themselves at will, as long as hydrogen-bonding partners are made between hydrogen and oxygen atoms of different water molecules. The entropy of a system such as this is high, and thus favorable.

When hydrophobic molecules such as a lipid are introduced into an aqueous environment, the water molecules at the interface of the fatty acid tail must present themselves into a highly-ordered structure to maximize the number of hydrogen bonds, creating an unfavorable decrease in entropy and thus greatly increasing the free energy of the system. However, if the lipid molecules were to pack tightly together, the acyl chains of the lipid tails interact and form van der Waals interactions. Upon doing this, the water molecules that were caged around each individual lipid tail are now free to reorient themselves within the bulk solution, favorably increasing the entropy of the system once more. Thus, hydrophobic molecules will aggregate to minimize the free energy so that the fewest number of water molecules have to coat these hydrophobic regions.[3]

To keep the hydrophobic tails as protected from water as possible, lipids will self-organize into the most energetically favorable conformation.[35] For short-chain or lysolipids (lipids with just one single acyl chain rather than two), micelles tend to be the most common structures that form.[36] Micelles are one-layered spherical structures with the hydrophobic acyl chains facing inward to form a hydrophobic core, while the hydrophilic head groups face outward. If the environment is nonpolar, reverse micelles (or inverted micelles) form,[36] wherein the hydrophilic heads face inwards towards the core, and the hydrophobic tails face outward toward the environment. The hydrophobic core of a micelle can also enable the transport of hydrophobic cargo.[34]

Lipid vesicles (also referred to as liposomes, particularly when speaking of synthetically-made structures) are another type of ordered structure that lipids can adopt.[37] These structures are essentially an enclosed, spherical bilayer with a solvated interior compartment,[32] which allows for the transportation water-soluble cargo, and is an important method of transport that many cells utilize. A majority of the structures described in this section of the dissertation can be viewed schematically in Figure 1.6.

1.6 Plasma Cell Membrane

The most important higher-ordered lipid structure is the lipid bilayer, or plasma membrane. This structure makes up the exterior boundary of cells, providing structure and protection between a cell and its environment,[38] while also facilitating intra- and intercellular communication.[4] In eukaryotic cells, which are far more sophisticated and complex than their prokaryotic counterparts, plasma membranes allow intracellular organelles to be differentiated from each other within the same cell.[4,39]

The membrane of a cell is extremely complex and is responsible for overseeing the movement of molecules into or out of the cell. While passive diffusion (spontaneous movement of particles across a membrane) is possible for molecules that are sufficiently hydrophobic to pass through the core of a bilayer, membrane proteins are responsible for transporting more hydrophilic molecules across the membrane barrier. Other functions of membrane proteins include enzymatic reactions as well as intra- and intercellular signaling.[40] Studies have suggested that the identity of lipids present around these membrane proteins can influence the structure and activity of the membrane protein.[41–43] Approximately 50% of a cell membrane consists of phospholipids, while the remaining

50% consists of glycans, cholesterol, and proteins, thus making for an intricate and complex system to study.[3,4,39,44]

In 1972, S.J. Singer and Garth L. Nicolson introduced the fluid mosaic model of the cell membrane, wherein they presented the cell membrane as a two-dimensional viscous liquid whose components have the ability to freely diffuse throughout the area.[45] This model portrays membranes as patchwork "mosaics", consisting not only of phospholipids, but also proteins, carbohydrates, and cholesterol. All of these pieces are able to laterally diffuse throughout the membrane, hence the term "fluid".[46]

However, further research over the last several decades have created doubts over the validity of such a model. As more information about the true nature and structure of cell membranes has come to light, it has become more apparent that membranes are full of proteins and other biomolecules, which would significantly impact the truly "fluid" nature of a membrane. Therefore, other models have been suggested, with one of the most common being the lipid raft hypothesis. Research has shown that lipids partition into microdomains ("rafts"), and that these rafts can have highly specific and unique lipid compositions in contrast to the bulk composition of the cell membrane.[47]

1.7 Model Membrane Mimics

Biological membranes are extremely crowded. Because of their complex nature, true plasma membranes are extremely difficult to study; therefore, simplified models are often used instead.[44,48] Model membranes are often used to simplify complex cellular membrane structures for laboratory study. In a model membrane, the lipid bilayer is kept while additives such as proteins, cholesterol, or glycans are only included if desired and in

carefully-controlled ratios. This allows for unique components of a membrane to be studied while carefully controlling a variety of variables; simplified membranes make it possible to investigate cellular processes in more depth while still enabling control over the system to be studied.[49]

1.7.1 Liposomes and Giant Vesicles

Liposomes are one of the simplest model membrane mimics. With a SLB, there is an exposed edge of the acyl chain tail group, which is energetically unfavorable, as described earlier. Liposomes are closed spherical structures, thus eliminating this exposed membrane edge and creating a more stable structure. Liposomes can be created in a variety of ways, including but not limited to extrusion, sonication, centrifugation, freeze-thawing, dehydration/rehydration, and solvent dispersal.[50–52]

Giant unilamellar vesicles (GUVs) are yet another type of model membrane mimic. They are similar to liposomes, though are much larger, with diameters on the order of one to tens of microns, making them closer to biologically-relevant cell sizes.[53] GUVs have been crucial in furthering the understanding of lipid phase separation and domain/raft formation. The composition of lipids within GUVs can be very tightly controlled, allowing for the study of raft formation as a result of changes in lipid composition. There are two phases of a membrane: liquid ordered (L_O) domains, which are rich in saturated phospholipids, cholesterol, and sphingolipids, and liquid disordered (L_D) domains, which are rich in unsaturated phospholipids.[54,55] L_O domains are thought to best mimic raft formation as they occur in native cell membranes.

1.7.2 Black Lipid Membranes

Planar lipid bilayers and spherical liposomes were first artificially formed and characterized by the Bangham group in the 1960s.[56,57] Around the same time, the artificial formation of black lipid membranes was researched and discovered by Mueller, et al.[58] The name "black lipid membrane" comes from its optical properties—the light reflected off of the back face destructively interferes with the light reflected off of the front face due to the thickness of the formed membrane (only a few nanometers).[59]

There are several ways to create such black lipid membranes. With the first, a 1–2% phospholipid solution in organic solvent is "painted" across a tiny hole (typically 1 mm or smaller) made of a hydrophobic material (such as Teflon) that is submerged in aqueous media. The lipid film thins and spreads to form a uniform lipid bilayer.[58] The second method is a folded lipid bilayer. With this technique, two compartments are filled with aqueous solution, and separated by a wall with a small (~1 mm) hole. Phospholipids are deposited in one of the compartments, and the solution level in that compartment is slowly lowered, then raised again; this allows a lipid bilayer to form vertically, with aqueous phases on either side of the membrane.[49,60] These techniques gained traction for their use in measuring cross-membrane currents and voltages, because electrodes can be placed in the aqueous media on either side of the formed membrane.[61] Proteins can be incorporated into these membrane mimics as well, enabling the study of transmembrane proteins and protein channels.[62]

1.7.3 Supported Lipid Bilayers

However, a simpler and more popular membrane mimic is a supported lipid bilayer (SLB). A SLB consists of two leaflets (layers) of lipids, with their polar head groups pointing outwards and their acyl chain tail groups pointing inward away from the aqueous environment. As the name suggests, these lipids are formed on a solid substrate (support), with approximately 10-20 Å of trapped water molecules between the bottom layer and the solid support.[49] However, unlike the black lipid membrane described earlier, a SLB does not offer access to both sides of the membrane.

SLB substrates must be hydrophilic (so as not to repel the polar head groups) and smooth; thus, the most common SLB substrates are mica, glass, or SiO_2.[63] The components of a SLB are often synthetic phospholipids, and it has been well established that these substrates are conducive to the spontaneous formation of stable planar lipid bilayers.[63] Since their introduction, SLBs have become one of the most popular membrane mimics to provide insight and elucidation into the workings of cell-cell communication, protein-lipid interactions, cell signaling, and more.[64]

1.7.3.1 Vesicle Fusion

One of the most common and straightforward methods of forming a SLB is the vesicle fusion method, and it is the method used throughout a majority of this dissertation. With this technique, liposomes are deposited in the bulk solution atop a solid substrate. These liposomes adsorb to the surface then spontaneous rupture on the solid support.[65–69] There are competing forces (such as van der Waals or electrostatic forces) at play that determine the speed and readiness at which liposomes will rupture, and these are liposome–liposomes interactions, and liposome–substrate interactions.[70–73] Depending on the

strength of attractive or repulsive forces between the adsorbed liposomes and the solid support, then the liposomes may remain intact rather than rupturing. This is most often seen with supports such as gold or titanium dioxide,[74,75] or with anionic lipids on silica.[76] Conversely, lipids with strong attractive forces (i.e. cationic lipids on silica) will rupture immediately upon contact with the surface.[77]

While the vesicle fusion method remains one of the most popular and widely-used techniques, it has challenges that may make it difficult to form a SLB under certain conditions. Intrinsic liposome-specific factors such as lipid composition,[73] lipid concentration,[78] lipid phase,[79] liposome size,[80] and liposome lamellarity[81] can impact the success of SLB formation. External factors such as solution pH,[82] ionic strength[83] (including ion identity[84] and resulting osmotic pressure[85]), temperature,[86] and solid support properties such as nanomorphology/topography[87,88] and atomic composition.[89]

1.7.3.2 Solvent-Assisted Lipid Bilayer

Another technique of forming a SLB is the solvent-assisted lipid bilayer (SALB) method, which relies on controlling the adsorption and self-assembly of lipid molecules onto the solid support by tuning and varying the bulk solution in which the lipid molecules are dissolved.[90] With this technique, lipid molecules are dissolved in a water-miscible organic solvent (isopropyl alcohol) can be deposited on a SiO_2 surface, then the solvent can be gradually exchanged from isopropyl alcohol to an aqueous buffer.[91] As the bulk solution environment transitions from isopropyl alcohol to aqueous buffer, the lipids experience a series of shape transitions, morphing from free lipids and inverted micelles to micelles and spherical liposomes. Thus, once the solution environment becomes primarily

aqueous, a SLB can be formed on a SiO_2 surface in a similar manner as the vesicle-fusion method.

A key advantage to the SALB method is that allows for the formation of SLB on surfaces on which liposomes do not readily rupture (i.e. gold and titanium dioxide), and it allows for the formation of lipid monolayers on hydrophobic surfaces.[92,93] However, there are some drawbacks. Firstly, this method is typically unsuitable for protein incorporation into a bilayer, due to the fact that many proteins can be denatured in organic-aqueous mixtures.[94] Secondly, if the SLB is not thoroughly washed, trace amounts of isopropyl alcohol may be left behind (embedded in the bilayer), which can hinder further analysis or experimentation with the SLB.[95]

1.7.3.3 Bicelle SLB Formation

Bicelles are flat, two-dimensional disk structures composed of a mixture of long- and short-chain lipids. They assemble in such a way that the long-chain lipids assemble into a planar bilayer in the center of the disk, while the short-chain lipids arrange themselves around the edges of the disk in order to protect the lipid acyl chains from the surrounding aqueous environment. Bicelles have become popular in recent decades as a method of incorporating and studying membrane proteins.[96,97]

Bicelles have also become a method of forming SLBs. This technique mimics that of vesicle fusion,[98] though with a few key differences. Bicelle-induced SLB formation relies on the differences in solubility between long- and short-chain lipids. Short-chain lipids are slightly more soluble, and as such, once the bicelle makes contact with the solid

support on which the SLB will be formed, these short-chain lipids return to the bulk solution, leaving the long-chain lipids to assemble across the surface of the solid support.[95]

1.7.3.4 Langmuir-Blodgett

The Langmuir-Blodgett technique relies on the transfer of two lipid monolayers from an air-water interface to an air-solid interface. The lower leaflet of the bilayer is formed by pulling a solid substrate through a lipid monolayer; then the upper leaflet is then transferred by dipping the substrate horizontally into another lipid monolayer, forming the bilayer.[64,99,100] This technique is beneficial in that it works with a variety of lipid compositions, and it is a fairly simple and reliable method of forming asymmetric SLBs.[95] However, this technique requires the use of specialized equipment (a Langmuir trough), and thus expertise with this equipment and technique, making it a more inaccessible technique than the techniques previously discussed.

1.8 Reactive Oxygen Species

Living organisms use O_2 to perform many metabolic processes; however, in using O_2, reactive oxygen species (ROS) such as peroxides, superoxide, hydroxyl radicals, and singlet oxygen can be produced.[101] ROS are produced endogenously within cells and organelles such as the endoplasmic reticulum,[102] peroxisomes,[103] and mitochondria[104] during biochemical reactions. Specifically, mitochondrial membranes are enriched with unsaturated lipids, with easily-oxidized cardiolipin being one of the predominant lipids within the membrane.[105,106] Thus, the biological and physiological effects of lipid oxidation

are of great concern and interest as the consequences of lipid oxidation have been linked with a multitude of degenerative diseases and aging.[107,108]

At first believed to be dangerous and deleterious molecules, it was later discovered that some ROS are also important signaling molecules for many cells.[109] Therefore, to combat the potential dangers of ROS, living organisms have evolved to maintain a nonequilibrium steady-state of a highly reducing intracellular environment to keep ROS concentrations low, even amidst changes in cellular and metabolic activities.[110] Cells also have an antioxidant system comprised of enzymes and small molecules to help regulate ROS concentrations.[111,112] The fluctuating redox environment and concentrations of ROS are used by the cell in signaling pathways and gene expression to control a variety of cellular processes.[113] However, if the production of ROS exceeds normal cellular concentration, there are a variety of antioxidant processes designed to regulate the intracellular levels of ROS.[114] If the levels of ROS increase beyond the capacity of endogenous antioxidants to mitigate the damage, the cell comes under oxidative stress, wherein the ROS begins to damage cell structures,[115] including lipid membranes. An overabundance of ROS, and thus the buildup of oxidative cellular damage, has been linked with many degenerative diseases and aging,[107,108] making lipid oxidation a prominent emphasis of scientific research.

1.9 Lipid Oxidation

As alluded to in the above section, lipids—particularly unsaturated ones—are susceptible to oxidation via ROS. Lipid oxidation primarily occurs when ROS react with a site of unsaturation within the lipid tail, abstracting an allylic hydrogen atom at the site of

the double bond.[116,117] Allylic hydrogens are easier to abstract than non-allylic hydrogens due to their differences in bond dissociation energy.[118,119] The C–H bond adjacent to a C=C double bond is approximately 10 kcal mol^{-1} weaker than the C–H bond adjacent to a C–C single bond,[120] which is the reason saturated lipids are more resistant to oxidative damage than their unsaturated counterparts.

There are a variety of mechanisms by which lipid oxidation can occur, and the mechanism can vary depending upon the number of sites of unsaturation in the lipid tail as well as the exact ROS that is acting as the oxidizing agent. The process of lipid oxidation typically occurs in three phases: initiation, propagation, and finally termination.[121] Initiation is the first step, whereby ROS attacks the site of unsaturation within the lipid tail, abstracts a hydrogen atom, and generates a carbon radical. This radical species then reacts with oxygen to form lipid peroxide radicals. The next step is propagation, wherein these peroxide radicals react with nearby unoxidized lipids within the bilayer, which generates a lipid hydroperoxide and a newly generated carbon radical. This regeneration of carbon radicals continues until the termination step, which occurs if two lipid peroxide radicals react together to form a nonradical lipid species. Common oxidation products include lipid peroxides, aldehydes, and carboxylic acids.[122–124]

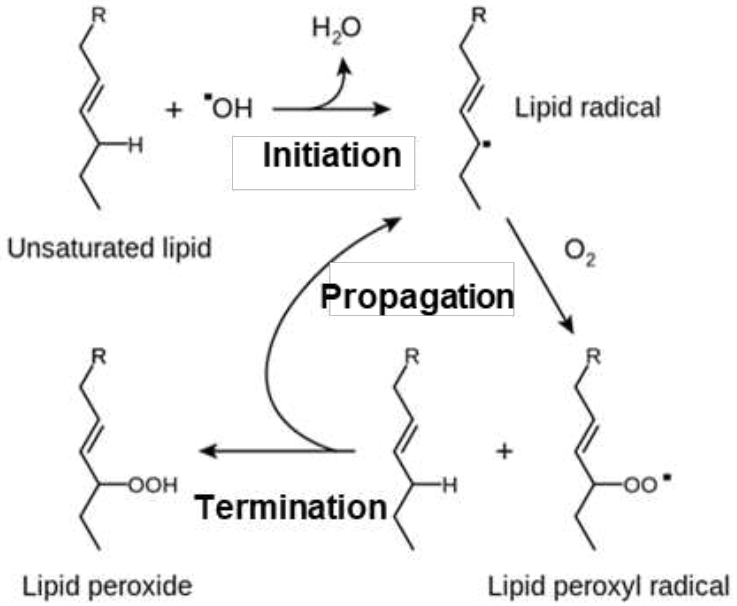

Figure 1.7. A mechanism of lipid oxidation, detailing the steps of initiation, propagation, and termination.[125]

1.9.1 Oxidation-Induced Membrane Deformation

Oxidized lipids cause a number of structural changes to the lipid bilayer membrane, and can even alter the function of membrane proteins.[126] Some of the consequences of lipid oxidation are an increase in the area per lipid molecule that causes lateral membrane expansion, decrease in lipid order, decreased membrane thickness, increased membrane permeability, increased lipid mobility, and increased lipid flip-flop.[127] Some studies have also shown the induction of highly curved membrane structures, such as buds or tubes, upon lipid oxidation.[128] Unlike GUVs, which are capable of inward or outward tubulation,[129] SLBs can only tubulate outward due to the presence of an underlying substrate.

Model membranes, such as GUVs,[130] liposomes,[131] micelles,[132] lipid monolayers,[133] and supported lipid bilayers[134] have enabled the discovery of many of the consequences of lipid oxidation initiated by direct chemical oxidizing agents and light-based photosensitizer methods. These model systems allow the user to tune the lipid composition as well as the size and morphology of the membrane structure. The morphology of a model membrane structure is determined by a number of factors such as the interactions with a substrate, surface area to volume ratio, the area ratio of the two membrane leaflets, and the molecular structure of the lipids in the membrane.[135] The molecular shape of the lipid components, for example cylindrical or conical, often dictates the shape and curvature a model membrane structure will adopt.[136]

Importantly, oxidation of lipid tail groups renders them much more polar, which alters the molecular shape and tail group orientation in the membrane, resulting in molecular reorganization,[137] area expansion of the membrane,[138] and sometimes membrane phase separation.[139] These reorganizations are at the root of the aforementioned consequences of lipid oxidation, including changes in membrane curvature. Khandeli and Mouritsen performed molecular dynamic (MD) simulations on oxidized POPC lipids to probe the change in structure and conformation that lipid oxidation has on a lipid bilayer.[140] The group showed that, since the oxidized tail is slightly more polar after oxidation, it is energetically more favorable for the oxidized tail group to be closer to the polar phosphate heads and the aqueous solution than buried in the membrane.

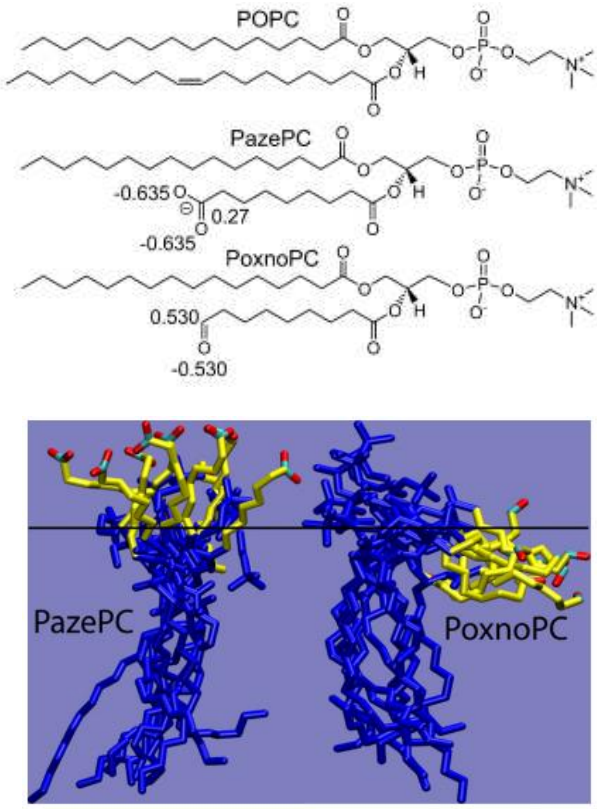

Figure 1.8. Oxidation changes lipid properties. Structures of POPC and oxidized POPC molecules (top) and the corresponding molecular dynamic simulation structures (bottom).[140] The small numbers in the top figure are the partial charges of the carbon and oxygen atoms of the carbonyl and carboxyl groups.

1.9.2 Antioxidants

The role of an antioxidant is to accept or donate electrons to free radical species. Antioxidants react directly with either the damaging ROS or the lipid radical intermediates, interrupting the propagation step of lipid oxidation.[141] Though the antioxidant then becomes a radical species, they are often less active and less dangerous than the lipid peroxide radicals that they formerly reacted with.[142] Antioxidants typically have an aromatic ring structure, which aids in the delocalization and thus stabilization of the unpaired electron radical. Tocopherols (Vitamin E), specifically, act as free-radical

scavengers and H-donors to the lipid radical, helping to minimize the oxidative damage to the membrane.[143–146]

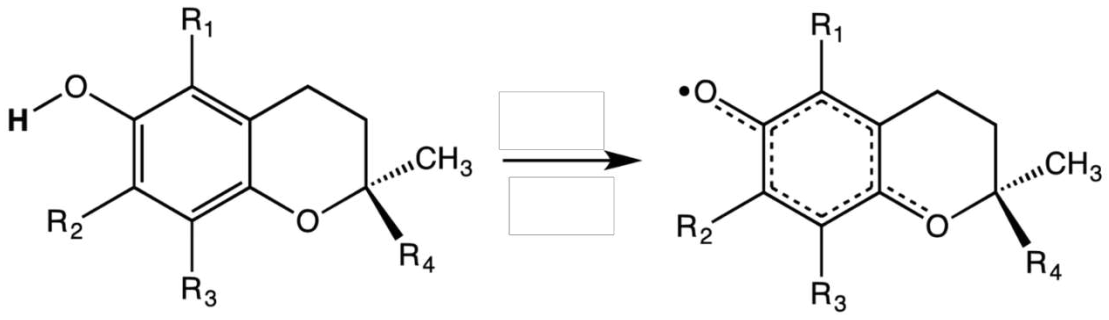

Figure 1.9. Mechanism of action of tocopherols.[147] Aromatic ring structures assist with the delocalization of an unpaired electron radical species.

Vitamin E can be regenerated back into its antioxidant form by interacting with ascorbic acid (Vitamin C) or coenzyme Q.[148] Vitamin C itself acts as another free radical scavenger within cells and the circulatory system. Coenzyme Q (ubiquinone) is an electron carrier and takes part in the electron transfer chain.[149] A reduced version of coenzyme Q (ubiquinol) can interact with Vitamin E to return it to its antioxidant state.

1.10 Photosensitizers and Photodynamic Therapy

Photosensitizers are molecules that absorb energy from light, get excited to a higher-energy state, and transfer that energy to a secondary molecule to cause physical or chemical changes to that secondary species. Photodynamic therapy (PDT) is a popular therapeutic technique that exploits this mechanism of action. Many cytotoxic effects can be caused by a photosensitizer acting in close proximity to cells; however, researchers have discovered the ability to selectively target specific areas in the body in which to create a

photosensitizer-induced response. Typically, the wavelength of light used to excite a photosensitizer is within the visible or infrared spectrum, especially if used therapeutically within the body. Infrared light can penetrate much deeper within the body and as such is the most advantageous wavelength range to use.

Effective photosensitizers are ones that have a high extinction coefficient, meaning they are able to effectively and efficiently absorb photons. They should also have a high quantum yield such that the triplet state should be long-lived, giving the photosensitizer enough time to react with their target secondary molecule. Most efficient photosensitizers have polycyclic structures (i.e. porphyrins) with plenty of π-electron double-bond conjugation.[150] Many energetically-excited photosensitizers are able to produce ROS, which then react with lipids to oxidize them in the manner described earlier in this dissertation.

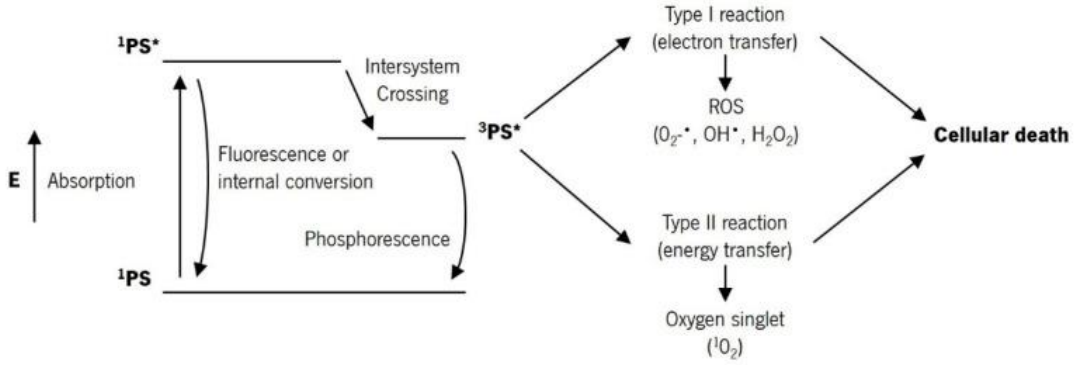

Figure 1.10. Jablonski diagram of the excitation of a photosensitizer and subsequent mechanisms of action of a photosensitizer to generate ROS, resulting in cell death.[151,152]

There are two primary reaction types through which a photosensitizer can act on lipids: Type 1, also known as a contact-dependent method, and Type 2, also known as a

contact-independent method. With the contact-dependent method, there is a direct reaction between the excited state of the photosensitizer and the lipid molecule. With this type of reaction, there are a multitude of reaction types that can occur, leading to a variety of oxidation products.[121] Conversely, with the contact-independent mechanism, the excited photosensitizer generates singlet oxygen, which reacts via an *ene* reaction with an allylic hydrogen of an unsaturated lipid. This mechanism of action primarily yields lipid peroxides as a final oxidation product.[121] Regardless of the specific type or mechanism of action of a photosensitizer, the end result is the same: lipid oxidation products leads to membrane destabilization. This destabilization is due to the altered chemical structure of an oxidized lipid, which leads to an increase in the area per lipid molecule, membrane thinning, increased membrane permeability, and more,[137-139] which will be discussed throughout this dissertation.

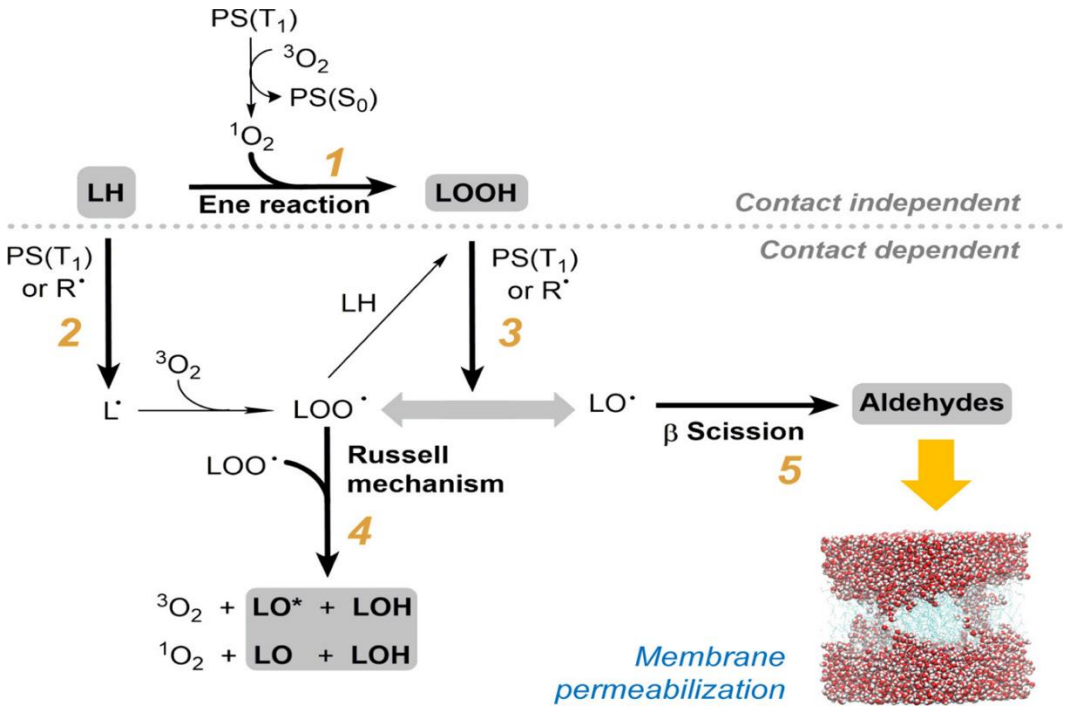

Figure 1.11. Mechanisms of contact-independent and contact-dependent photosensitizer-induced lipid oxidation.[153]

1.11 Bioanalytical Techniques

The use of analytical tools and techniques to study biochemical systems is the focus of the future chapters of this dissertation. Two primary instruments are used to aid in the investigation of lipid oxidation and the resulting effects oxidation has on SLBs. These two techniques will be discussed at length in the next several sections.

1.11.1 Quartz Crystal Microbalance with Dissipation Monitoring

A quartz crystal microbalance with dissipation monitoring (QCM-D) is an instrument that allows for the detection and measurement of mass variations per unit area. It is extremely sensitive, and is capable of measuring minute mass changes as low as the nanogram level.[154] This high level of sensitivity allows the QCM-D to be used for surface binding/interaction studies, where mass is gained or lost when ligands bind or release.[155]

QCM-D instruments collect two different signals: frequency and dissipation. To acquire a signal, an AC voltage is applied across a quartz crystal—quartz is used because of its piezoelectric property (the change in shape due to an applied voltage). This voltage causes the crystal to oscillate at a certain frequency, which is quantified and reported as a signal. This signal then changes depending on changes to the crystal, as frequency is directly correlated with a change in mass. When mass adsorbs to the crystal, the crystal oscillates more slowly; thus, when mass is adsorbed to the surface, the frequency will decrease (become more negative).

The exact mass that has been adsorbed to the crystal can be calculated using the Sauerbrey equation.[156] In the strictest sense, the Sauerbrey equation is only applicable to rigid films (films with zero dissipation). However, SLBs can be considered a thin rigid film and thus the Sauerbrey equation acts as a good model.

$$\Delta f = \frac{-2f_o^2}{A\sqrt{\rho_q \mu_q}}\Delta m \qquad \text{eq 1.2}$$

In the above question, f_o is the resonant frequency (Hz), A is the sensor surface area (cm^2), ρ_q is the density of quartz (2.648 g cm^{-3}), μ_q is the shear modulus of quartz crystal (2.947 x 10^{11} g cm^{-1} s^{-2}), Δm is the change in mass (g), and Δf is the change in frequency (Hz). However, the above equation can be simplified:

$$\Delta m = \frac{C}{n}\Delta f \qquad \text{eq 1.3}$$

where Δm is the change in mass, n is the overtone number, Δf is the change in frequency, and C is a constant that depends on the properties of the quartz crystal. However, C can be defined by the following equation:

$$C = \frac{t_q \rho_q}{f_o} \qquad \text{eq 1.4}$$

where t_q is the thickness of quartz, and ρ_q is the density of quartz, and f_o is the resonant frequency of the quartz crystal and is often 5 MHz.[154] Because all of these variables are constant when using the same style sensor, C can be simplified to -17.7 Hz ng cm^{-2}.

The second signal is dissipation, which is a measure of softness or rigidity (viscoelasticity) of the crystal's surface. Dissipation monitors the oscillation decay across the quartz crystal over time, since the rate of decay is proportional of the energy dissipation of the sensor.[154,157,158] The analysis of dissipation signals can provide insight into structural changes of the adsorbed layer, and it can provide information on film thickness, conformational changes, and hydration.[159] Both frequency and dissipation are collected simultaneously, making the QCM-D a useful tool in many bioanalytical investigations.

Quartz crystals can be coated with a variety of substrates. One of the most common for lipid bilayer studies is silica; the polar headgroup of lipid molecules will interact favorably with the polar surface of SiO_2. Gold-coated sensors can be used for monolayer studies, wherein the nonpolar tail groups will interact favorably with the nonpolar gold surface.

SLBs can easily be formed on SiO_2 surfaces via the vesicle-fusion method described earlier in this dissertation. The signal for SLB formation is distinct and can be directly monitored in real-time with a QCM-D instrument. Liposomes are injected into the flow cell of the QCM-D, where they then begin to adsorb, intact, onto the SiO_2 surface. The instrument registers this as a decrease in frequency, since there is mass accumulating on the surface of the crystal, and an increase in dissipation, since a layer of liposomes is much less rigid than a bare crystal. Liposomes continue to accumulate on the surface until a critical coverage is reached, at which point, liposomes begin to spontaneously rupture

across the surface. The frequency signal thus begins to increase (become less negative), since the mass of the sequestered solution inside of the liposomes is being lost. Conversely, the dissipation signal begins to decrease, since a SLB is more rigid than a layer of "soft" liposomes. Upon the completed formation of a SLB, the frequency and dissipation signals will plateau and subsequently remain unchanged. An intact SLB typically has a final frequency shift of approximately -26 Hz, and a final unitless dissipation shift of approximately 0.2 x 10^{-6}.[160]

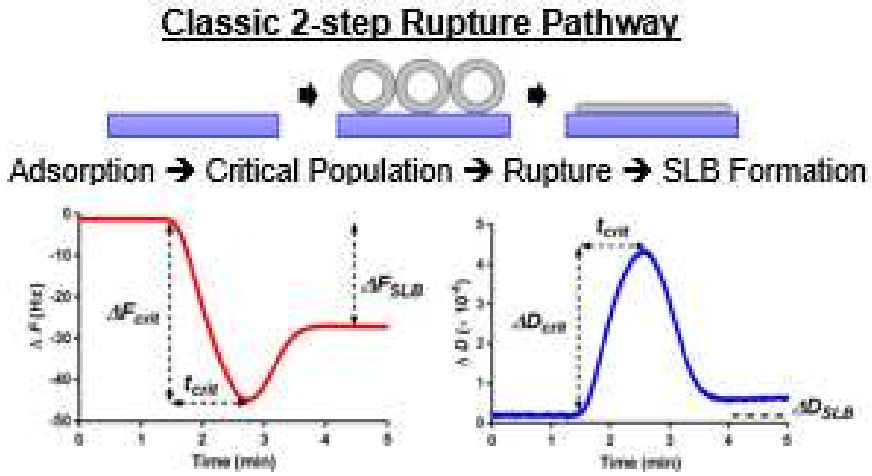

Figure 1.12. Classical QCM-D response of SLB formation on a SiO_2 sensor. ΔF_{crit} and ΔD_{crit} are, respectively, the minimum frequency and maximum dissipation signals prior to liposome rupture. t_{crit} is the corresponding time required to reach ΔF_{crit} and ΔD_{crit}. ΔF_{SLB} and ΔD_{SLB} are, respectively, the final frequency and final dissipation shifts due to SLB formation.

1.11.2 Fluorescence Microscopy

Fluorescence microscopy can be used to characterize supported lipid bilayers. With this technique, the sample or specimen of interest is fluorescently-labeled with a fluorophore, and illuminated with a high-energy light source. The fluorophore absorbs that

light energy, causing it to be excited to a higher energy level; the relaxation back down to ground state emits photons of a lower energy (i.e. longer wavelength) than what was used to excite the fluorophore. This emission is seen as fluorescence.[161] The difference in the wavelength at which a fluorophore is excited versus the wavelength at which it emits is called a Stokes shift.

Wide-field (the whole sample is illuminated) fluorescence microscopy allows for real-time imaging of fluorescent samples. Traditionally, for a wide-field fluorescence microscope, the light comes from a high-pressure xenon or mercury bulb. However, using light emitting diodes (LEDs) as a bright, single-wavelength light source is becoming increasingly more common. LEDs are advantageous because of their selective wavelength control and longevity; however, multiple LED sources are required for fluorophores that excite or emit in different wavelength ranges.[161]

1.11.2.1 Fluorescence Recovery After Photobleaching

Fluorescence microscopy can be used to confirm the formation of an intact SLB through use of fluorescence recovery after photobleaching (FRAP). During a FRAP experiment, the sample is irradiated with a high-power laser, which photobleaches the fluorophores in a particular region of interest (ROI), resulting in a uniform black spot on the sample. This is recorded as an abrupt decrease in fluorescence intensity. Because lipids in a bilayer are mobile, surrounding lipids will, over time, diffuse into the bleach spot, resulting in a gradual recovery of fluorescence. Fluorescence recovery will only be seen if a SLB has been formed, since there will be no wide-range diffusion if the surface is covered with intact liposomes or micelles.

FRAP measurements can provide useful information on lipid diffusion and lateral mobility through use of the following equation:[162]

$$D = \frac{0.224r^2}{t_{1/2}} \qquad \text{eq 1.5}$$

wherein D is the diffusion coefficient of the lipids in the sample, r is the radius of the uniform bleach laser, and $t_{1/2}$ is the time required for a bleach spot to recover half way between initial and final steady state fluorescence intensities. 0.224 is a predetermined constant from derivations performed by Soumpasis, which are described at length in reference 162.

1.11.2.2 Total Internal Reflection Fluorescence Microscopy

Another fluorescence microscope technique is total internal reflection fluorescence microscopy (TIRFM). The probing depth of this form of microscopy can be less than 100 nm from the substrate, which provides only a surface view of the sample. By contrast, the probing depth of confocal microscopy is approximately 500 nm, so TIRFM provides a much more surface-level image.[163,164]

The depth of the excitation field (or evanescent field) of TIRFM is dependent upon the angle of the laser as it relates to the substrate of the sample. The excitation light is totally internally reflected within the substrate (typically glass) at the solid-aqueous interface. This generates an evanescent wave (electromagnetic field) with the same frequency as the excitation light.[165,166] The intensity of this evanescent wave decreases

exponentially as the distance from the substrate increases; as such, only fluorescent molecules close to the substrate will be excited.

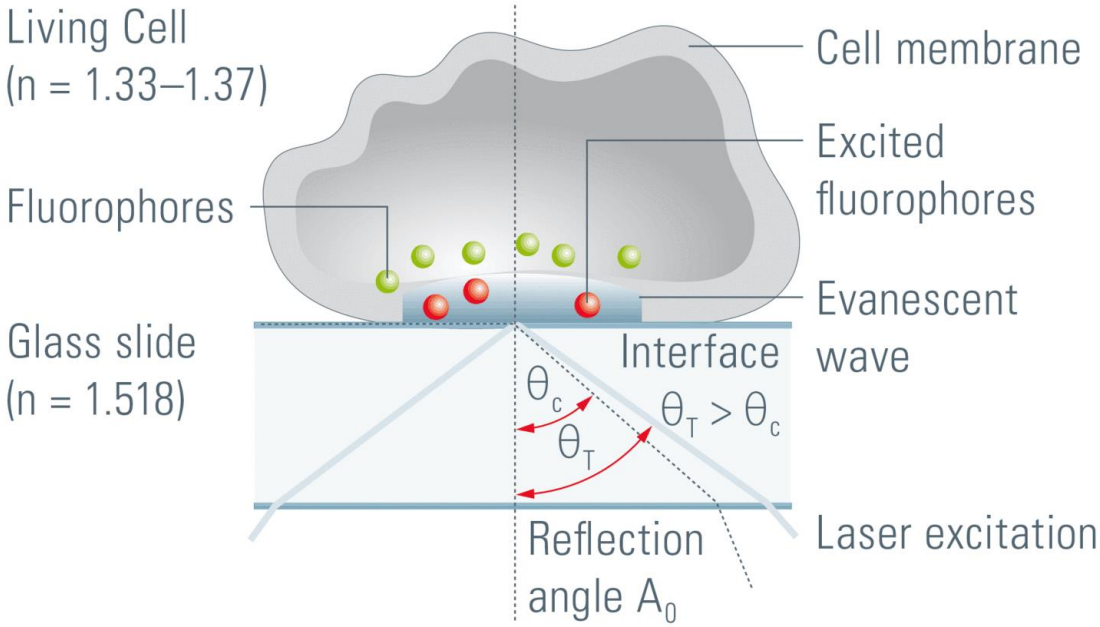

Figure 1.13. The principle of TIRFM.[167] TIRFM allows for surface-level imaging of a sample. θ_T = incident angle; θ_C = critical angle (the angle at which total internal reflection occurs); n = refractive index of the sample and the substrate upon which the sample sits.

TIRFM is advantageous due to its high signal-to-noise ratio, low interference from background fluorescence, and decreased exposure of the sample to the light, meaning this technique is less likely to photobleach the sample as the sample is being imaged. This technique is also beneficial for detecting single fluorescent molecules, allowing for the study of binding kinetics.[168] The dissociation rates of ligands can be calculated based off of residence times (the length of time that a ligand remained bound), which can provide insight into ligand–receptor binding, membrane–protein interactions, and more.

1.12 Thesis Overview

The research discussed herein is focused on the use of bioanalytical techniques to probe and investigate the consequences of photosensitized lipid oxidation on lipid bilayer formation and structure. This chapter should provide the necessary background about lipid oxidation and bioanalytical techniques that can and will be used to investigate the consequences of lipid oxidation. Chapter two will primarily discuss the changes that arise in how a SLB is formed when liposome precursors containing fluorescently-conjugated lipids are exposed to broadband visible light. The chapter also discusses the structural changes that arise to the lipids themselves which are responsible for the altered SLB rupture behavior that is observed. Chapter three is focused on characterizing membrane defects that arise across the surface of a SLB that contains a fluorescently-conjugated lipid when the SLB is illuminated with visible light. Chapter four discusses the preliminary results of changes observed in rupture behavior of liposomes that are made of oxidized lipids when varying concentrations of cholesterol are added to the liposomes. Chapter five is a slight derivation from lipid oxidation; however, the chapter involves work with gangliosides and the rupture behavior of liposomes that contain varying amounts of different gangliosides. The chapter also describes the behaviors in ganglioside-rich SLBs, and the effect that divalent cations (which are often used to assist in the rupture of non-rupture-prone liposomes) have on SLB properties. Finally, chapter six outlines the future of this project of oxidized lipids, and how the techniques and systems that I have used throughout this dissertation can be used to study the interactions between oxidized lipids and proteins that readily bind to oxidized lipids.

1.13 References

(1) Berg, J. M.; Tymoczko, J. L.; Stryer, L.; Berg, J. M.; Tymoczko, J. L.; Stryer, L. *Biochemistry*, 5th ed.; W H Freeman, 2002.

(2) Ahmed, S.; Shah, P.; Ahmed, O. Biochemistry, Lipids. In *StatPearls*; StatPearls Publishing: Treasure Island (FL), 2021.

(3) Alberts, B.; Johnson, A.; Lewis, J.; Raff, M.; Roberts, K.; Walter, P. The Lipid Bilayer. *Mol. Biol. Cell 4th Ed.* **2002**.

(4) Yeagle, P. L. The Structure of Biological Membranes; CRC Press: Boca Raton, 2012; pp 1–17.

(5) Aktas, M.; Danne, L.; Möller, P.; Narberhaus, F. Membrane Lipids in Agrobacterium Tumefaciens: Biosynthetic Pathways and Importance for Pathogenesis. *Front. Plant Sci.* **2014**, *5*, 109.

(6) Lewis, R. N. A. H.; McElhaney, R. N. Membrane Lipid Phase Transitions and Phase Organization Studied by Fourier Transform Infrared Spectroscopy. *Biochim. Biophys. Acta BBA - Biomembr.* **2013**, *1828* (10), 2347–2358.

(7) Israelachvili, J. N. *Intermolecular and Surface Forces*; Academic Press, 2011.

(8) Gennis, R. B. *Biomembranes: Molecular Structure and Function*; Gennis, R. B., Ed.; Springer Advanced Texts in Chemistry; Springer-Verlag: New York, 1989.

(9) Heimburg, T. *Thermal Biophysics of Membranes*; Wiley-VCH, 2007.

(10) Glycolipids - Latest research and news | Nature https://www.nature.com/subjects/glycolipids.

(11) Hirabayashi, Y. A World of Sphingolipids and Glycolipids in the Brain —Novel Functions of Simple Lipids Modified with Glucose—. *Proc. Jpn. Acad. Ser. B Phys. Biol. Sci.* **2012**, *88* (4), 129–143.

(12) Goins, L.; Spassieva, S. Sphingoid Bases and Their Involvement in Neurodegenerative Diseases. *Adv. Biol. Regul.* **2018**, *70*, 65–73.

(13) Koval, M.; Pagano, R. E. Intracellular Transport and Metabolism of Sphingomyelin. *Biochim. Biophys. Acta BBA - Lipids Lipid Metab.* **1991**, *1082* (2), 113–125.

(14) Chen, H.; Chan, A. Y.; Stone, D. U.; Mandal, N. A. Beyond the Cherry-Red Spot: Ocular Manifestations of Sphingolipid-Mediated Neurodegenerative and Inflammatory Disorders. *Surv. Ophthalmol.* **2014**, *59* (1), 64–76.

(15) Bally, M.; Gunnarsson, A.; Svensson, L.; Larson, G.; Zhdanov, V. P.; Höök, F. Interaction of Single Viruslike Particles with Vesicles Containing Glycosphingolipids. *Phys. Rev. Lett.* **2011**, *107* (18), 188103.

(16) Kolter, T. Ganglioside Biochemistry. *ISRN Biochem.* **2012**, *2012*, 506160.

(17) Sonnino, S.; Mauri, L.; Chigorno, V.; Prinetti, A. Gangliosides as Components of Lipid Membrane Domains. *Glycobiology* **2007**, *17* (1), 1R-13R.

(18) Cerqueira, N. M. F. S. A.; Oliveira, E. F.; Gesto, D. S.; Santos-Martins, D.; Moreira, C.; Moorthy, H. N.; Ramos, M. J.; Fernandes, P. A. Cholesterol Biosynthesis: A Mechanistic Overview. *Biochemistry* **2016**, *55* (39), 5483–5506.

(19) Purves, W. K.; Orians, G. H.; Heller, H. C. *Life, the Science of Biology*; Sinauer Associates, 1992.

(20) Ademowo, O. S.; Dias, H. K. I.; Burton, D. G. A.; Griffiths, H. R. Lipid (per) Oxidation in Mitochondria: An Emerging Target in the Ageing Process? *Biogerontology* **2017**, *18* (6), 859–879.

(21) Ivanova, P. T.; Milne, S. B.; Forrester, J. S.; Brown, H. A. LIPID Arrays: New Tools in the Understanding of Membrane Dynamics and Lipid Signaling. *Mol. Interv.* **2004**, *4* (2), 86–96.

(22) Vance, J. E.; Vance, D. E. Phospholipid Biosynthesis in Mammalian Cells. *Biochem. Cell Biol.* **2004**, *82* (1), 113–128.

(23) Kannan, M.; Lahiri, S.; Liu, L.-K.; Choudhary, V.; Prinz, W. A. Phosphatidylserine Synthesis at Membrane Contact Sites Promotes Its Transport out of the ER. *J. Lipid Res.* **2017**, *58* (3), 553–562.

(24) Cooke, I. R.; Deserno, M. Coupling between Lipid Shape and Membrane Curvature. *Biophys. J.* **2006**, *91* (2), 487–495.

(25) Yesylevskyy, S.; Rivel, T.; Ramseyer, C. Curvature Increases Permeability of the Plasma Membrane for Ions, Water and the Anti-Cancer Drugs Cisplatin and Gemcitabine. *Sci. Rep.* **2019**, *9* (1), 17214.

(26) Sych, T.; Mély, Y.; Römer, W. Lipid Self-Assembly and Lectin-Induced Reorganization of the Plasma Membrane. *Philos. Trans. R. Soc. B Biol. Sci.* **2018**, *373* (1747), 20170117.

(27) Thomas, A. Lipids: Defining the Shape of Things to Come. *Nat. Cell Biol.* **1999**, *1* (8), E192–E192.

(28) Reusch, R. Biogenesis of Ion Channels. *J. Biochem. Biophys.* **2014**, *1* (1).

(29) Sprong, H.; van der Sluijs, P.; van Meer, G. How Proteins Move Lipids and Lipids Move Proteins. *Nat. Rev. Mol. Cell Biol.* **2001**, *2* (7), 504–513.

(30) Rapp, M. The Ins and Outs of Membrane Proteins Topology Studies of Bacterial Membrane Proteins. **2021**.

(31) Jouhet, J. Importance of the Hexagonal Lipid Phase in Biological Membrane Organization. *Front. Plant Sci.* **2013**, *4*, 494.

(32) Stuart, M. C. A.; Boekema, E. J. Two Distinct Mechanisms of Vesicle-to-Micelle and Micelle-to-Vesicle Transition Are Mediated by the Packing Parameter of Phospholipid–Detergent Systems. *Biochim. Biophys. Acta BBA - Biomembr.* **2007**, *1768* (11), 2681–2689.

(33) Edidin, M. Lipids on the Frontier: A Century of Cell-Membrane Bilayers. *Nat. Rev. Mol. Cell Biol.* **2003**, *4* (5), 414–418.

(34) Escribá, P. V.; Ozaita, A.; Ribas, C.; Miralles, A.; Fodor, E.; Farkas, T.; García-Sevilla, J. A. Role of Lipid Polymorphism in G Protein-Membrane Interactions: Nonlamellar-Prone Phospholipids and Peripheral Protein Binding to Membranes. *Proc. Natl. Acad. Sci. U. S. A.* **1997**, *94* (21), 11375–11380.

(35) Tanford, C. Theory of Micelle Formation in Aqueous Solutions. *J. Phys. Chem.* **1974**, *78* (24), 2469–2479.

(36) Battig, M. R.; Wang, Y. Chapter 17 - Nucleic Acid Aptamers for Biomaterials Development. In *Natural and Synthetic Biomedical Polymers*; Kumbar, S. G., Laurencin, C. T., Deng, M., Eds.; Elsevier: Oxford, 2014; pp 287–299.

(37) Casem, M. L. Case Studies in Cell Biology - 1st Edition.

(38) van Meer, G.; Voelker, D. R.; Feigenson, G. W. Membrane Lipids: Where They Are and How They Behave. *Nat. Rev. Mol. Cell Biol.* **2008**, *9* (2), 112–124.

(39) Korn, E. D. Structure and Function of the Plasma Membrane. *J. Gen. Physiol.* **1968**, *52* (1), 257–278.

(40) Cournia, Z.; Allen, T. W.; Andricioaei, I.; Antonny, B.; Baum, D.; Brannigan, G.; Buchete, N.-V.; Deckman, J. T.; Delemotte, L.; del Val, C.; Friedman, R.; Gkeka, P.; Hege, H.-C.; Hénin, J.; Kasimova, M. A.; Kolocouris, A.; Klein, M. L.; Khalid, S.; Lemieux, M. J.; Lindow, N.; Roy, M.; Selent, J.; Tarek, M.; Tofoleanu, F.; Vanni, S.; Urban, S.; Wales, D. J.; Smith, J. C.; Bondar, A.-N. Membrane Protein Structure, Function, and Dynamics: A Perspective from Experiments and Theory. *J. Membr. Biol.* **2015**, *248* (4), 611–640.

(41) Bondar, A.-N.; del Val, C.; Freites, J. A.; Tobias, D. J.; White, S. H. Dynamics of SecY Translocons with Translocation-Defective Mutations. *Structure* **2010**, *18* (7), 847–857.

(42) Bondar, A.-N.; del Val, C.; White, S. H. Rhomboid Protease Dynamics and Lipid Interactions. *Structure* **2009**, *17* (3), 395–405.

(43) Kalvodova, L.; Kahya, N.; Schwille, P.; Ehehalt, R.; Verkade, P.; Drechsel, D.; Simons, K. Lipids as Modulators of Proteolytic Activity of BACE: INVOLVEMENT OF CHOLESTEROL, GLYCOSPHINGOLIPIDS, AND ANIONIC PHOSPHOLIPIDS IN VITRO*. *J. Biol. Chem.* **2005**, *280* (44), 36815–36823.

(44) Liu, H.-Y.; Chen, W.-L.; Ober, C. K.; Daniel, S. Biologically Complex Planar Cell Plasma Membranes Supported on Polyelectrolyte Cushions Enhance Transmembrane Protein Mobility and Retain Native Orientation. *Langmuir* **2018**, *34* (3), 1061–1072.

(45) Singer, S. J.; Nicolson, G. L. The Fluid Mosaic Model of the Structure of Cell Membranes. *Science* **1972**, *175* (4023), 720–731.

(46) Lombard, J. Once upon a Time the Cell Membranes: 175 Years of Cell Boundary Research. *Biol. Direct* **2014**, *9*, 32.

(47) Goñi, F. M. The Basic Structure and Dynamics of Cell Membranes: An Update of the Singer–Nicolson Model. *Biochim. Biophys. Acta BBA - Biomembr.* **2014**, *1838* (6), 1467–1476.

(48) Salehi-Reyhani, A.; Ces, O.; Elani, Y. Artificial Cell Mimics as Simplified Models for the Study of Cell Biology. *Exp. Biol. Med.* **2017**, *242* (13), 1309–1317.

(49) Castellana, E. T.; Cremer, P. S. Solid Supported Lipid Bilayers: From Biophysical Studies to Sensor Design. *Surf. Sci. Rep.* **2006**, *61* (10), 429–444.

(50) Batzri, S.; Korn, E. D. Single Bilayer Liposomes Prepared without Sonication. *Biochim Biophys Acta* **1973**, *298* (4), 1015–1019.

(51) Pick, U. Liposomes with a Large Trapping Capacity Prepared by Freezing and Thawing of Sonicated Phospholipid Mixtures. *Arch. Biochem. Biophys.* **1981**, *212* (1), 186–194.

(52) Riaz, M. Liposomes Preparation Methods. *Pak. J. Pharm. Sci.* **1996**, *9* (1), 65–77.

(53) Bhatia, T.; Husen, P.; Brewer, J.; Bagatolli, L. A.; Hansen, P. L.; Ipsen, J. H.; Mouritsen, O. G. Preparing Giant Unilamellar Vesicles (GUVs) of Complex Lipid Mixtures on Demand: Mixing Small Unilamellar Vesicles of Compositionally

Heterogeneous Mixtures. *Biochim. Biophys. Acta BBA - Biomembr.* **2015**, *1848* (12), 3175–3180.

(54) Fidorra, M.; Garcia, A.; Ipsen, J. H.; Härtel, S.; Bagatolli, L. A. Lipid Domains in Giant Unilamellar Vesicles and Their Correspondence with Equilibrium Thermodynamic Phases: A Quantitative Fluorescence Microscopy Imaging Approach. *Biochim. Biophys. Acta BBA - Biomembr.* **2009**, *1788* (10), 2142–2149.

(55) de Almeida, R. F. M.; Borst, J.; Fedorov, A.; Prieto, M.; Visser, A. J. W. G. Complexity of Lipid Domains and Rafts in Giant Unilamellar Vesicles Revealed by Combining Imaging and Microscopic and Macroscopic Time-Resolved Fluorescence. *Biophys. J.* **2007**, *93* (2), 539–553.

(56) Bangham, A. D. Physical Structure and Behavior of Lipids and Lipid Enzymes. *Adv. Lipid Res.* **1963**, *1*, 65–104.

(57) Bangham, A. D.; Horne, R. W. Negative Staining of Phospholipids and Their Structural Modification by Surface-Active Agents as Observed in the Electron Microscope. *J. Mol. Biol.* **1964**, *8* (5), 660–668.

(58) Mueller, P.; Rudin, D. O.; Tien, H. T.; Wescott, W. C. Methods for the Formation of Single Bimolecular Lipid Membranes in Aqueous Solution. *J. Phys. Chem.* **1963**, No. 67, 534.

(59) Tien, H. T.; Carbone, S.; Dawidowicz, E. A. Formation of "Black" Lipid Membranes by Oxidation Products of Cholesterol. *Nature* **1966**, *212* (5063), 718–719.

(60) Montal, M.; Mueller, P. Formation of Bimolecular Membranes from Lipid Monolayers and a Study of Their Electrical Properties. *Proc. Natl. Acad. Sci. U. S. A.* **1972**, *69* (12), 3561–3566.

(61) Mueller, P.; Rudin, D. O.; Ti Tien, H.; Wescott, W. C. Reconstitution of Cell Membrane Structure in Vitro and Its Transformation into an Excitable System. *Nature* **1962**, *194* (4832), 979–980.

(62) Rognlien, K. T.; Woodbury, D. J. Chapter 16 - Reconstituting SNARE Proteins into BLMs. In *Membrane Science and Technology*; Tien, H. T., Ottova-Leitmannova, A., Eds.; Planar Lipid Bilayers (BLMs) and Their Applications; Elsevier, 2003; Vol. 7, pp 479–488.

(63) Granéli, A.; Rydström, J.; Kasemo, B.; Höök, F. Formation of Supported Lipid Bilayer Membranes on SiO2 from Proteoliposomes Containing Transmembrane Proteins. *Langmuir* **2003**, *19* (3), 842–850.

(64) Tamm, L. K.; McConnell, H. M. Supported Phospholipid Bilayers. *Biophys. J.* **1985**, *47* (1), 105–113.

(65) Puu, G.; Gustafson, I. Planar Lipid Bilayers on Solid Supports from Liposomes – Factors of Importance for Kinetics and Stability. *Biochim Biophys Acta* **1997**, *1327* (2), 149–161.

(66) Cremer, P. S.; Boxer, S. G. Formation and Spreading of Lipid Bilayers on Planar Glass Supports. *J Phys Chem B* **1999**, 2554–2559.

(67) Keller, C. A.; Kasemo, B. Surface Specific Kinetics of Lipid Vesicle Adsorption Measured with a Quartz Crystal Microbalance. *Biophys. J.* **1998**, *75* (3), 1397–1402.

(68) Keller, C. A.; Glasmästar, K.; Zhdanov, V. P.; Kasemo, B. Formation of Supported Membranes from Vesicles. *Phys. Rev. Lett.* **2000**, *84* (23), 5443–5446.

(69) Reviakine, I.; Brisson, A. Formation of Supported Phospholipid Bilayers from Unilamellar Vesicles Investigated by Atomic Force Microscopy. *Langmuir* **2000**, *16* (4), 1806–1815.

(70) Zhdanov, V. P.; Kasemo, B. Comments on Rupture of Adsorbed Vesicles. *Langmuir* **2001**, *17* (12), 3518–3521.

(71) Cha, T.; Guo, A.; Zhu, X.-Y. Formation of Supported Phospholipid Bilayers on Molecular Surfaces: Role of Surface Charge Density and Electrostatic Interaction. *Biophys. J.* **2006**, *90* (4), 1270–1274.

(72) Cho, N.-J.; Wang, G.; Edvardsson, M.; Glenn, J. S.; Hook, F.; Frank, C. W. Alpha-Helical Peptide-Induced Vesicle Rupture Revealing New Insight into the Vesicle Fusion Process As Monitored in Situ by Quartz Crystal Microbalance-Dissipation and Reflectometry. *Anal. Chem.* **2009**, *81* (12), 4752–4761.

(73) Biswas, K. H.; Jackman, J. A.; Park, J. H.; Groves, J. T.; Cho, N.-J. Interfacial Forces Dictate the Pathway of Phospholipid Vesicle Adsorption onto Silicon Dioxide Surfaces. *Langmuir* **2018**, *34* (4), 1775–1782.

(74) Reimhult, E.; Höök, F.; Kasemo, B. Intact Vesicle Adsorption and Supported Biomembrane Formation from Vesicles in Solution: Influence of Surface Chemistry, Vesicle Size, Temperature, and Osmotic Pressure. *Langmuir* **2003**, *19* (5), 1681–1691.

(75) Reviakine, I.; Rossetti, F. F.; Morozov, A. N.; Textor, M. Investigating the Properties of Supported Vesicular Layers on Titanium Dioxide by Quartz Crystal Microbalance with Dissipation Measurements. *J. Chem. Phys.* **2005**, *122* (20), 204711.

(76) Reimhult, E.; Höök, F.; Kasemo, B. Vesicle Adsorption on SiO2 and TiO2: Dependence on Vesicle Size. *J. Chem. Phys.* **2002**, *117* (16), 7401–7404.

(77) Richter, R.; Mukhopadhyay, A.; Brisson, A. Pathways of Lipid Vesicle Deposition on Solid Surfaces: A Combined QCM-D and AFM Study. *Biophys. J.* **2003**, *85* (5), 3035–3047.

(78) Jackman, J. A.; Špačková, B.; Linardy, E.; Kim, M. C.; Yoon, B. K.; Homola, J.; Cho, N.-J. Nanoplasmonic Ruler to Measure Lipid Vesicle Deformation. *Chem. Commun.* **2015**, *52* (1), 76–79.

(79) Oh, E.; Jackman, J. A.; Yorulmaz, S.; Zhdanov, V. P.; Lee, H.; Cho, N.-J. Contribution of Temperature to Deformation of Adsorbed Vesicles Studied by Nanoplasmonic Biosensing. *Langmuir* **2015**, *31* (2), 771–781.

(80) Jackman, J. A.; Kim, M. C.; Zhdanov, V. P.; Cho, N.-J. Relationship between Vesicle Size and Steric Hindrance Influences Vesicle Rupture on Solid Supports. *Phys. Chem. Chem. Phys.* **2016**, *18* (4), 3065–3072.

(81) Jackman, J. A.; Zhao, Z.; Zhdanov, V. P.; Frank, C. W.; Cho, N.-J. Vesicle Adhesion and Rupture on Silicon Oxide: Influence of Freeze–Thaw Pretreatment. *Langmuir* **2014**, *30* (8), 2152–2160.

(82) Cho, N.-J.; Jackman, J. A.; Liu, M.; Frank, C. W. PH-Driven Assembly of Various Supported Lipid Platforms: A Comparative Study on Silicon Oxide and Titanium Oxide. *Langmuir* **2011**, *27* (7), 3739–3748.

(83) Boudard, S.; Seantier, B.; Breffa, C.; Decher, G.; Félix, O. Controlling the Pathway of Formation of Supported Lipid Bilayers of DMPC by Varying the Sodium Chloride Concentration. *Thin Solid Films* **2006**, *495* (1), 246–251.

(84) Dacic, M.; Jackman, J. A.; Yorulmaz, S.; Zhdanov, V. P.; Kasemo, B.; Cho, N.-J. Influence of Divalent Cations on Deformation and Rupture of Adsorbed Lipid Vesicles. *Langmuir* **2016**, *32* (25), 6486–6495.

(85) Jackman, J. A.; Choi, J.-H.; Zhdanov, V. P.; Cho, N.-J. Influence of Osmotic Pressure on Adhesion of Lipid Vesicles to Solid Supports. *Langmuir* **2013**, *29* (36), 11375–11384.

(86) Reimhult, E.; Höök, F.; Kasemo, B. Temperature Dependence of Formation of a Supported Phospholipid Bilayer from Vesicles on SiO2. *Phys. Rev. E* **2002**, *66* (5), 051905.

(87) Sundh, M.; Svedhem, S.; Sutherland, D. S. Formation of Supported Lipid Bilayers at Surfaces with Controlled Curvatures: Influence of Lipid Charge. *J. Phys. Chem. B* **2011**, *115* (24), 7838–7848.

(88) Pfeiffer, I.; Seantier, B.; Petronis, S.; Sutherland, D.; Kasemo, B.; Zäch, M. Influence of Nanotopography on Phospholipid Bilayer Formation on Silicon Dioxide. *J. Phys. Chem. B* **2008**, *112* (16), 5175–5181.

(89) Tero, R. Substrate Effects on the Formation Process, Structure and Physicochemical Properties of Supported Lipid Bilayers. *Materials* **2012**, *5* (12), 2658–2680.

(90) Szoka, F.; Papahadjopoulos, D. Procedure for Preparation of Liposomes with Large Internal Aqueous Space and High Capture by Reverse-Phase Evaporation. *Proc. Natl. Acad. Sci.* **1978**, *75* (9), 4194–4198.

(91) Hohner, A. O.; David, M. P. C.; Rädler, J. O. Controlled Solvent-Exchange Deposition of Phospholipid Membranes onto Solid Surfaces. *Biointerphases* **2010**, *5* (1), 1–8.

(92) Jackman, J. A.; Cho, N.-J. Supported Lipid Bilayer Formation: Beyond Vesicle Fusion. *Langmuir* **2020**, *36* (6), 1387–1400.

(93) Tabaei, S. R.; Choi, J.-H.; Haw Zan, G.; Zhdanov, V. P.; Cho, N.-J. Solvent-Assisted Lipid Bilayer Formation on Silicon Dioxide and Gold. *Langmuir* **2014**, *30* (34), 10363–10373.

(94) Griebenow, K.; Klibanov, A. M. On Protein Denaturation in Aqueous−Organic Mixtures but Not in Pure Organic Solvents. *J. Am. Chem. Soc.* **1996**, *118* (47), 11695–11700.

(95) Sut, T. N.; Yoon, B. K.; Jeon, W.-Y.; Jackman, J. A.; Cho, N.-J. Supported Lipid Bilayer Coatings: Fabrication, Bioconjugation, and Diagnostic Applications. *Appl. Mater. Today* **2021**, *25*, 101183.

(96) Sanders, C. R.; Oxenoid, K. Customizing Model Membranes and Samples for NMR Spectroscopic Studies of Complex Membrane Proteins. *Biochim. Biophys. Acta BBA - Biomembr.* **2000**, *1508* (1), 129–145.

(97) Dürr, U. H. N.; Soong, R.; Ramamoorthy, A. When Detergent Meets Bilayer: Birth and Coming of Age of Lipid Bicelles. *Prog. Nucl. Magn. Reson. Spectrosc.* **2013**, *69*, 1–22.

(98) Kolahdouzan, K.; Jackman, J. A.; Yoon, B. K.; Kim, M. C.; Johal, M. S.; Cho, N.-J. Optimizing the Formation of Supported Lipid Bilayers from Bicellar Mixtures. *Langmuir* **2017**, *33* (20), 5052–5064.

(99) Girard-Egrot, A. P.; Blum, L. J. Langmuir-Blodgett Technique for Synthesis of Biomimetic Lipid Membranes. In *Nanobiotechnology of Biomimetic Membranes*;

Martin, D. K., Ed.; Fundamental Biomedical Technologies; Springer US: Boston, MA, 2007; pp 23–74.

(100) Levine, Y. K.; Bailey, A. I.; Wilkins, M. H. F. Multilayers of Phospholipid Bimolecular Leaflets. *Nature* **1968**, *220* (5167), 577–578.

(101) Boveris, A. Mitochondrial Production of Superoxide Radical and Hydrogen Peroxide. In *Tissue Hypoxia and Ischemia*; Reivich, M., Coburn, R., Lahiri, S., Chance, B., Eds.; Advances in Experimental Medicine and Biology; Springer US: Boston, MA, 1977; pp 67–82.

(102) Cao, S. S.; Kaufman, R. J. Endoplasmic Reticulum Stress and Oxidative Stress in Cell Fate Decision and Human Disease. *Antioxid. Redox Signal.* **2014**, *21* (3), 396–413.

(103) De Duve, C.; Baudhuin, P. Peroxisomes (Microbodies and Related Particles). *Physiol. Rev.* **1966**, *46* (2), 323–357.

(104) Boveris, A.; Oshino, N.; Chance, B. The Cellular Production of Hydrogen Peroxide. *Biochem. J.* **1972**, *128* (3), 617–630.

(105) Paradies, G.; Paradies, V.; Ruggiero, F. M.; Petrosillo, G. Role of Cardiolipin in Mitochondrial Function and Dynamics in Health and Disease: Molecular and Pharmacological Aspects. *Cells* **2019**, *8* (7).

(106) Zorov, D. B.; Juhaszova, M.; Sollott, S. J. Mitochondrial Reactive Oxygen Species (ROS) and ROS-Induced ROS Release. *Physiol. Rev.* **2014**, *94* (3), 909–950.

(107) Dröge, W. Free Radicals in the Physiological Control of Cell Function. *Physiol. Rev.* **2002**, *82* (1), 47–95.

(108) Finkel, T. Radical Medicine: Treating Ageing to Cure Disease. *Nat. Rev. Mol. Cell Biol.* **2005**, *6* (12), 971–976.

(109) Corpas, F.; Gupta, D.; Palma, J. Production Sites of Reactive Oxygen Species (ROS) in Organelles from Plant Cells; 2015; pp 1–22.

(110) Schafer, F. Q.; Buettner, G. R. Redox Environment of the Cell as Viewed through the Redox State of the Glutathione Disulfide/Glutathione Couple. *Free Radic. Biol. Med.* **2001**, *30* (11), 1191–1212.

(111) Mittler, R. Oxidative Stress, Antioxidants and Stress Tolerance. *Trends Plant Sci.* **2002**, *7* (9), 405–410.

(112) Mittler, R.; Vanderauwera, S.; Gollery, M.; Van Breusegem, F. Reactive Oxygen Gene Network of Plants. *Trends Plant Sci.* **2004**, *9* (10), 490–498.

(113) Menon, S. G.; Goswami, P. C. A Redox Cycle within the Cell Cycle: Ring in the Old with the New. *Oncogene* **2007**, *26* (8), 1101–1109.

(114) Sies, H. Oxidative Stress: From Basic Research to Clinical Application. *Am. J. Med.* **1991**, *91* (3C), 31S-38S.

(115) Devasagayam, T. P. A.; Tilak, J. C.; Boloor, K. K.; Sane, K. S.; Ghaskadbi, S. S.; Lele, R. D. Free Radicals and Antioxidants in Human Health: Current Status and Future Prospects. *J. Assoc. Physicians India* **2004**, *52*, 794–804.

(116) Hayyan, M.; Hashim, M. A.; AlNashef, I. M. Superoxide Ion: Generation and Chemical Implications. *Chem. Rev.* **2016**, *116* (5), 3029–3085.

(117) Yin, H.; Xu, L.; Porter, N. A. Free Radical Lipid Peroxidation: Mechanisms and Analysis. *Chem. Rev.* **2011**, *111* (10), 5944–5972.

(118) Pratt, D. A.; Mills, J. H.; Porter, N. A. Theoretical Calculations of Carbon−Oxygen Bond Dissociation Enthalpies of Peroxyl Radicals Formed in the Autoxidation of Lipids. *J. Am. Chem. Soc.* **2003**, *125* (19), 5801–5810.

(119) Yin, H.; Xu, L.; Porter, N. A. Free Radical Lipid Peroxidation: Mechanisms and Analysis. *Chem. Rev.* **2011**, *111* (10), 5944–5972.

(120) Blanksby, S. J.; Ellison, G. B. Bond Dissociation Energies of Organic Molecules. *Acc. Chem. Res.* **2003**, *36* (4), 255–263.

(121) Bacellar, I. O. L.; Baptista, M. S. Mechanisms of Photosensitized Lipid Oxidation and Membrane Permeabilization. *ACS Omega* **2019**, *4* (26), 21636–21646.

(122) Reis, A.; Spickett, C. M. Chemistry of Phospholipid Oxidation. *Biochim. Biophys. Acta BBA - Biomembr.* **2012**, *1818* (10), 2374–2387.

(123) Spiteller, G. The Important Role of Lipid Peroxidation Processes in Aging and Age Dependent Diseases. *Mol. Biotechnol.* **2007**, *37* (1), 5–12.

(124) Vieira, S. A.; Zhang, G.; Decker, E. A. Biological Implications of Lipid Oxidation Products. *J. Am. Oil Chem. Soc.* **2017**, *94* (3), 339–351.

(125) Dhingra, S. Oxidants and Antioxidants in Complementary and Alternative Medicine: A Review. *Spatula DD - Peer Rev. J. Complement. Med. Drug Discov.* **2014**, *4*, 1–16.

(126) Walton Kimberly A.; Cole Amy L.; Yeh Michael; Subbanagounder Ganesamoorthy; Krutzik Stephan R.; Modlin Robert L.; Lucas Robert M.; Nakai Junko; Smart Eric J.; Vora Deven K.; Berliner Judith A. Specific Phospholipid Oxidation Products Inhibit Ligand Activation of Toll-Like Receptors 4 and 2. *Arterioscler. Thromb. Vasc. Biol.* **2003**, *23* (7), 1197–1203.

(127) Jurkiewicz, P.; Olżyńska, A.; Cwiklik, L.; Conte, E.; Jungwirth, P.; Megli, F. M.; Hof, M. Biophysics of Lipid Bilayers Containing Oxidatively Modified Phospholipids: Insights from Fluorescence and EPR Experiments and from MD Simulations. *Biochim. Biophys. Acta BBA - Biomembr.* **2012**, *1818* (10), 2388–2402.

(128) Sankhagowit, S.; Wu, S.-H.; Biswas, R.; Riche, C. T.; Povinelli, M. L.; Malmstadt, N. The Dynamics of Giant Unilamellar Vesicle Oxidation Probed by Morphological Transitions. *Biochim. Biophys. Acta BBA - Biomembr.* **2014**, *1838* (10), 2615–2624.

(129) Shukla, S.; Jin, R.; Robustelli, J.; Zimmerman, Z. E.; Baumgart, T. PIP2 Reshapes Membranes through Asymmetric Desorption. *Biophys. J.* **2019**, *117* (5), 962–974.

(130) Riske, K. A.; Sudbrack, T. P.; Archilha, N. L.; Uchoa, A. F.; Schroder, A. P.; Marques, C. M.; Baptista, M. S.; Itri, R. Giant Vesicles under Oxidative Stress Induced by a Membrane-Anchored Photosensitizer. *Biophys. J.* **2009**, *97* (5), 1362–1370.

(131) Mosca, M.; Ceglie, A.; Ambrosone, L. Effect of Membrane Composition on Lipid Oxidation in Liposomes. *Chem. Phys. Lipids* **2011**, *164* (2), 158–165.

(132) Fridovich, S. E.; Porter, N. A. Oxidation of Arachidonic Acid in Micelles by Superoxide and Hydrogen Peroxide. *J. Biol. Chem.* **1981**, *256* (1), 260–265.

(133) Gellert, F.; Ahrens, H.; Helm, C. A. Oxidation of Unsaturated Phospholipids: A Monolayer Study. *Langmuir* **2020**, *36* (41), 12213–12220.

(134) Makky, A.; Tanaka, M. Impact of Lipid Oxidization on Biophysical Properties of Model Cell Membranes. *J. Phys. Chem. B* **2015**, *119* (18), 5857–5863.

(135) Seifert, U. Configurations of Fluid Membranes and Vesicles. *Adv. Phys.* **1997**, *46* (1), 13–137.

(136) Kooijman, E. E.; Chupin, V.; Fuller, N. L.; Kozlov, M. M.; de Kruijff, B.; Burger, K. N. J.; Rand, P. R. Spontaneous Curvature of Phosphatidic Acid and Lysophosphatidic Acid †. *Biochemistry* **2005**, *44* (6), 2097–2102.

(137) Khandelia, H.; Mouritsen, O. G. Lipid Gymnastics: Evidence of Complete Acyl Chain Reversal in Oxidized Phospholipids from Molecular Simulations. *Biophys. J.* **2009**, *96* (7), 2734–2743.

(138) Wong-ekkabut, J.; Xu, Z.; Triampo, W.; Tang, I.-M.; Peter Tieleman, D.; Monticelli, L. Effect of Lipid Peroxidation on the Properties of Lipid Bilayers: A Molecular Dynamics Study. *Biophys. J.* **2007**, *93* (12), 4225–4236.

(139) Ayuyan, A. G.; Cohen, F. S. Lipid Peroxides Promote Large Rafts: Effects of Excitation of Probes in Fluorescence Microscopy and Electrochemical Reactions during Vesicle Formation. *Biophys. J.* **2006**, *91* (6), 2172–2183.

(140) Khandelia, H.; Mouritsen, O. G. Lipid Gymnastics: Evidence of Complete Acyl Chain Reversal in Oxidized Phospholipids from Molecular Simulations. *Biophys. J.* **2009**, *96* (7), 2734–2743.

(141) Shichiri, M.; Yoshida, Y.; Niki, E. Chapter 4 - Unregulated Lipid Peroxidation in Neurological Dysfunction. In *Omega-3 Fatty Acids in Brain and Neurological Health*; Watson, R. R., De Meester, F., Eds.; Academic Press: Boston, 2014; pp 31–55.

(142) Lü, J.-M.; Lin, P. H.; Yao, Q.; Chen, C. Chemical and Molecular Mechanisms of Antioxidants: Experimental Approaches and Model Systems. *J. Cell. Mol. Med.* **2010**, *14* (4), 840–860.

(143) Castro, I. A.; Rogero, M. M.; Junqueira, R. M.; Carrapeiro, M. M. Free Radical Scavenger and Antioxidant Capacity Correlation of α-Tocopherol and Trolox Measured by Three in Vitro Methodologies. *Int. J. Food Sci. Nutr.* **2006**, *57* (1–2), 75–82.

(144) Duval, C.; Poelman, M. C. Research Articles: Scavenger Effect of Vitamin E and Derivatives on Free Radicals Generated by Photoirradiated Pheomelanin. *J. Pharm. Sci.* **1995**, *84* (1), 107–110.

(145) Rossi, M.; Alamprese, C.; Ratti, S. Tocopherols and Tocotrienols as Free Radical-Scavengers in Refined Vegetable Oils and Their Stability during Deep-Fat Frying. *Food Chem.* **2007**, *102* (3), 812–817.

(146) Traber, M. G.; Stevens, J. F. Vitamins C and E: Beneficial Effects from a Mechanistic Perspective. *Free Radic. Biol. Med.* **2011**, *51* (5), 1000–1013.

(147) Dhingra, S. Oxidants and Antioxidants in Complementary and Alternative Medicine: A Review. *Spatula DD - Peer Rev. J. Complement. Med. Drug Discov.* **2014**, *4*, 1–16.

(148) Beyer, R. E. The Role of Ascorbate in Antioxidant Protection of Biomembranes: Interaction with Vitamin E and Coenzyme Q. *J. Bioenerg. Biomembr.* **1994**, *26* (4), 349–358.

(149) Åberg, F.; Appelkvist, E.-L.; Dallner, G.; Ernster, L. Distribution and Redox State of Ubiquinones in Rat and Human Tissues. *Arch. Biochem. Biophys.* **1992**, *295* (2), 230–234.

(150) Berg, K.; Selbo, P. K.; Weyergang, A.; Dietze, A.; Prasmickaite, L.; Bonsted, A.; Engesaeter, B. Ø.; Angell-Petersen, E.; Warloe, T.; Frandsen, N.; Høgset, A. Porphyrin-Related Photosensitizers for Cancer Imaging and Therapeutic Applications. *J. Microsc.* **2005**, *218* (Pt 2), 133–147.

(151) Correia, J. H.; Rodrigues, J. A.; Pimenta, S.; Dong, T.; Yang, Z. Photodynamic Therapy Review: Principles, Photosensitizers, Applications, and Future Directions. *Pharmaceutics* **2021**, *13* (9), 1332.

(152) Donnelly, R. F.; McCarron, P. A.; Tunney, M. M. Antifungal Photodynamic Therapy. *Microbiol. Res.* **2008**, *163* (1), 1–12.

(153) Bacellar, I. O. L.; Oliveira, M. C.; Dantas, L. S.; Costa, E. B.; Junqueira, H. C.; Martins, W. K.; Durantini, A. M.; Cosa, G.; Di Mascio, P.; Wainwright, M.; Miotto, R.; Cordeiro, R. M.; Miyamoto, S.; Baptista, M. S. Photosensitized Membrane Permeabilization Requires Contact-Dependent Reactions between Photosensitizer and Lipids. *J. Am. Chem. Soc.* **2018**, *140* (30), 9606–9615.

(154) Dixon, M. C. Quartz Crystal Microbalance with Dissipation Monitoring: Enabling Real-Time Characterization of Biological Materials and Their Interactions. *J. Biomol. Tech. JBT* **2008**, *19* (3), 151–158.

(155) Naklua, W.; Suedee, R.; Lieberzeit, P. A. Dopaminergic Receptor–Ligand Binding Assays Based on Molecularly Imprinted Polymers on Quartz Crystal Microbalance Sensors. *Biosens. Bioelectron.* **2016**, *81*, 117–124.

(156) Sauerbrey, G. Verwendung von Schwingquarzen zur Wägung dünner Schichten und zur Mikrowägung. *Z. Für Phys.* **1959**, *155* (2), 206–222.

(157) Rodahl, M.; Höök, F.; Krozer, A.; Brzezinski, P.; Kasemo, B. Quartz Crystal Microbalance Setup for Frequency and Q-factor Measurements in Gaseous and Liquid Environments. *Rev. Sci. Instrum.* **1995**, *66* (7), 3924–3930.

(158) Arnau, A. A Review of Interface Electronic Systems for AT-Cut Quartz Crystal Microbalance Applications in Liquids. *Sensors* **2008**, *8* (1), 370–411.

(159) Alassi, A.; Benammar, M.; Brett, D. Quartz Crystal Microbalance Electronic Interfacing Systems: A Review. *Sensors* **2017**, *17* (12), 2799.

(160) Cho, N.-J.; Frank, C. W.; Kasemo, B.; Höök, F. Quartz Crystal Microbalance with Dissipation Monitoring of Supported Lipid Bilayers on Various Substrates. *Nat. Protoc.* **2010**, *5* (6), 1096–1106.

(161) Sanderson, M. J.; Smith, I.; Parker, I.; Bootman, M. D. Fluorescence Microscopy. *Cold Spring Harb. Protoc.* **2014**, *2014* (10), pdb.top071795.

(162) Soumpasis, D. M. Theoretical Analysis of Fluorescence Photobleaching Recovery Experiments. *Biophys. J.* **1983**, *41* (1), 95–97.

(163) Prasad, V.; Semwogerere, D.; Weeks, E. R. Confocal Microscopy of Colloids. *J. Phys. Condens. Matter* **2007**, *19* (11), 113102.

(164) Axelrod, D. Cell-Substrate Contacts Illuminated by Total Internal Reflection Fluorescence. *J. Cell Biol.* **1981**, *89* (1), 141–145.

(165) Fish, K. N. Total Internal Reflection Fluorescence (TIRF) Microscopy. *Curr. Protoc. Cytom.* **2009**, *50* (1), 12.18.1-12.18.13.

(166) Trache, A.; Meininger, G. A. Total Internal Reflection Fluorescence (TIRF) Microscopy. *Curr. Protoc. Microbiol.* **2008**, *Chapter 2*, Unit 2A.2.1-2A.2.22.

(167) Ockenga, W. Total Internal Reflection Fluorescence (TIRF) Microscopy. **2012**.

(168) Rozovsky, S.; Forstner, M. B.; Sondermann, H.; Groves, J. T. Single Molecule Kinetics of ENTH Binding to Lipid Membranes. *J. Phys. Chem. B* **2012**, *116* (17), 5122–5131.

Chapter 2: Excitation of Fluorescent Lipid Probes Accelerates Supported Lipid Bilayer Formation via Photosensitized Lipid Oxidation

2.1 Abstract

Fluorescently-conjugated lipid probes are common molecules that are used to label and visualize cell membranes as well as model membranes such as supported lipid bilayers (SLBs), giant vesicles, and liposomes. Within this chapter, I show that the excitation of lipid probes conjugated with BODIPY-like fluorophores with broadband visible light results in significant acceleration of the liposome rupture and SLB formation pathway of unsaturated phospholipid liposomes on SiO_2 surfaces. The SLBs that are formed from these liposomes with the excited probes have smaller measured masses, which indicates a reduction in membrane thickness and/or a decreased membrane density. Conversely, the excitation of NBD- and Texas Red-conjugated fluorescent probes does not accelerate the SLB formation process. The inclusion of oxidized phospholipids in liposomes also shows accelerated SLB formation when these liposomes are not excited with visible light. The excitation-induced acceleration caused by BODIPY-like probes is eliminated when liposomes are made of saturated phospholipids, which are not susceptible to oxidation. The accelerated SLB formation process is greatly attenuated when a lipophilic antioxidant (α-tocopherol) is included in the liposomes. The results herein suggest that BODIPY-conjugated phospholipids act as photosensitizers, and their excitation causes oxidation of lipid membranes which greatly alters the properties of membrane formation. Lipid oxidation is verified by FT-IR spectroscopy, and area expansion is observed in Langmuir trough experiments.

2.2 Introduction

Living organisms use O_2 to perform many metabolic processes; however, in using O_2, reactive oxygen species (ROS) such as peroxides, superoxide, hydroxyl radicals, and singlet oxygen can be produced.[1] ROS are produced endogenously within cells and organelles such as the mitochondria,[2] endoplasmic reticulum,[3] and peroxisomes[4] during biochemical reactions. At first believed to be dangerous and deleterious molecules, it was later discovered that some ROS are also important signaling molecules for many cells.[5] The bilayer membranes that define the boundaries of cells and organelles are built from molecules that are susceptible to oxidation by ROS. Unsaturated lipids are particularly vulnerable to oxidation by ROS, and these oxidative stresses have been implicated in aging and a number of diseases.[6–8] Consequences of lipid oxidation include an increase in the area per lipid molecule, a decrease in membrane thickness, membrane phase separation, and membrane permeabilization.[9]

The impacts of lipid oxidation on the chemical and physical properties of membranes can be studied in model membrane systems like supported lipid bilayers (SLB).[10,11] A SLB can be formed on a solid substrate by the spontaneous rupture of phospholipid vesicles,[12,13] and many factors can influence the process of the SLB formation by vesicle rupture.[14–16] To create a fluorescent SLB, the precursor liposomes often contain one or more fluorescent lipid probes. The inclusion of these probes is not without some consequences, however. The presence of fluorescent lipid probes can increase phase transition temperatures of lipid membranes,[17] and probe excitation can initiate photochemical reactions that alter the chemical and physical properties of

membranes.[18,19] Interestingly, single-vesicle electrochemical impact studies showed that illumination of chromaffin cell vesicles containing rhodamine- or NBD-conjugated lipids significantly increased the frequency of vesicle rupture on carbon fiber electrodes[20] and excitation of soluble fluorophores can initiate photo-redox processes that cause vesicle division.[21]

Here, I show that vesicles composed of unsaturated phospholipids and lipid probes with BODIPY-like conjugated fluorophores rupture much more readily on SiO_2 surfaces after the probes have been excited. In contrast, SLB formation is not influenced by excitation when NBD- or Texas Red-conjugated probes are present. The light-induced modulation of SLB formation is sensitive to the position of BODIPY-like fluorophore conjugation, dependent upon unsaturated lipids, can be influenced by the antioxidant α-tocopherol, and is recapitulated by the inclusion of oxidized phospholipids without illumination. This evidence suggests that photosensitized lipid oxidation initiated by BODIPY-conjugated lipids is responsible for these effects.

2.3 Results and Discussion

2.3.1 Phospholipid Structures and Excitation Spectra of Fluorophore-Lipid Conjugates

The structures of the phospholipids and fluorescent lipid probes that were used in the following experiments are shown in Figure 2.1. Liposomes were composed of two different phosphatidylcholines—dioleoylphosphatidylcholine (DOPC) or diphytanoylphosphatidylcholine (DiPhyPC)—and were doped with 2 mol% of different fluorescently-conjugated lipid probes. Some probes had fluorophores conjugated to their

head groups (BODIPY-PE, NBD-PE, and Texas Red-DHPE), while other probes had fluorophores conjugated to their tail groups (TopFluor-PC (TF-PC) and NBD-PC). TF-PC and BODIPY-PE fluorophores are structurally similar, differing only in the number of pendent methyl groups.

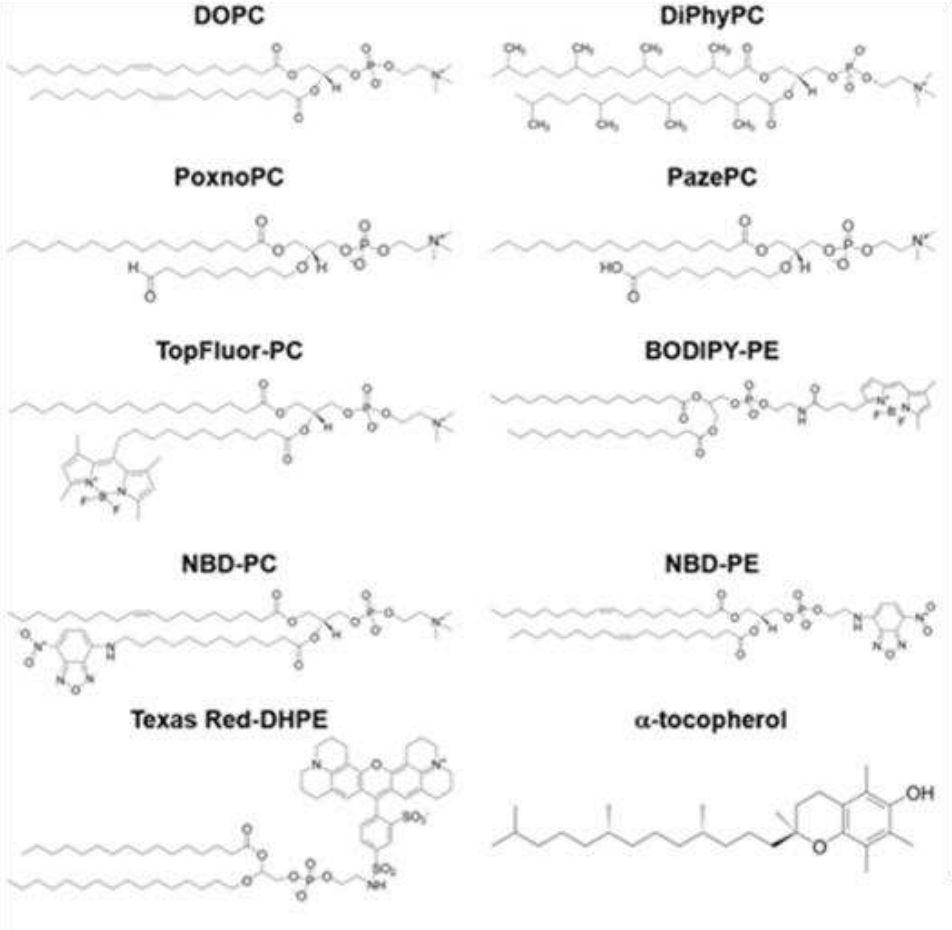

Figure 2.1. Structures of the phospholipids, fluorescently-conjugated lipids, and α-tocopherol used in this study.

The fluorophore excitation spectra of all of the fluorescently-conjugated lipid probes and the output spectrum of the LED light source are shown in Figure 2.2.

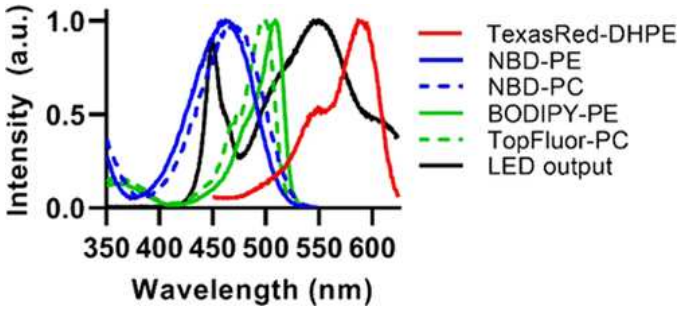

Figure 2.2. Excitation spectra and spectrum of LED light source. The excitation spectra of TF-PC, BODIPY-PE, NBD-PC, NBD-PE, and Texas Red-DHPE were collected from liposomes composed of DOPC and 2 mol% of each of the fluorescent lipid probes. Spectra were normalized to their maximum values.

2.3.2 The Inclusion of a Lipid-Conjugated Fluorophore does not Impact SLB Formation

I examined the formation of SLBs from DOPC precursor liposomes with and without TF-PC to show that the presence of 2 mol% TF-PC does not significantly alter the formation of a SLB. Figure 2.3 shows liposomes containing 2 mol% TF-PC form SLB membranes much the same as the liposomes that are composed solely of DOPC.

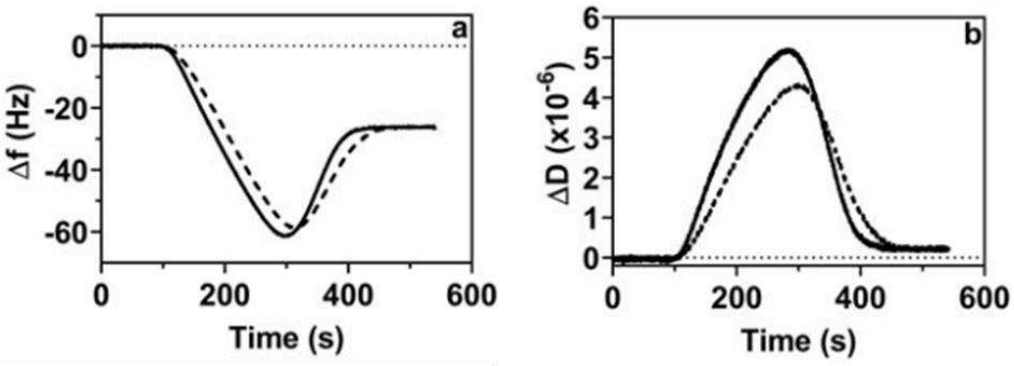

Figure 2.3. TF-PC does not significantly alter SLB formation. (a) QCM-D frequency shift (Δf) and (b) QCM-D dissipation shift (ΔD) curves from DOPC (solid line) and DOPC/2 mol% TF-PC (dashed line) liposomes.

The frequency (Δf) and dissipation (ΔD) responses are shown in Figure 2.3. For both liposome preparations, a characteristic two-step (adsorption and then rupture) profile was observed. The critical frequency (Δf_{min}) and dissipation (ΔD_{max}) were slightly more pronounced for the liposomes that did not contain 2% TF-PC. The average (±s.d.) Δf_{min} for DOPC and DOPC/2% TF-PC were -57.5 ± 5.8 Hz and 57.7 ± 2.8 Hz, respectively. The average (±s.d.) ΔD_{max} for DOPC and DOPC/2% TF-PC were (4.4 ± 0.7) x 10^{-6} and (4.40 ± 0.04) x 10^{-6}, respectively. The final Δf_{SLB} for DOPC and DOPC/2% TF-PC were -25.9 ± 0.3 Hz and -26.3 ± 0.3 Hz, respectively, which is expected for a uniform lipid bilayer formed on a SiO_2 substrate.[22] There was no significant difference in the final Δf or ΔD values. Thus, the presence of 2 mol% TF-PC in DOPC liposomes does not result in significantly different SLB characteristics, compared to TF-PC-free controls.

2.3.3 Accelerated SLB Formation

Liposomes composed of DOPC with 2 mol% of TF-PC, BODIPY-PE, NBD-PC, NBD-PE, or Texas Red-DHPE were formed via extrusion through a 50 nm pore-size polycarbonate membrane filter. The final lipid concentration was 1 mg mL^{-1}. These liposomes were diluted to 0.1 mg mL^{-1}, then illuminated with a broadband visible light-emitting diode (LED) to excite the fluorescent probes prior to study.

Quartz crystal microbalance with dissipation monitoring (QCM-D) is a common instrumental technique to study the adsorption and rupture pathway of liposomes on a

variety of surfaces (SiO_2, Au, TiO_2, Al_2O_3, etc.). QCM-D can simultaneously collect frequency (Δf) and dissipation (ΔD) data.[23,24] This is the technique that I used throughout a majority of this chapter. I examined the SLB formation process on a SiO_2 sensor.

The typical QCM-D signal response for 100% DOPC liposome adsorption and rupture to form a SLB is shown in Figure 2.4a. These liposomes show distinct minima and maxima frequency and dissipation signals, respectively. These liposomes were exposed to broadband visible light prior to QCM-D injection; the instrument response is shown in Figure 2.4b. Liposomes that were illuminated for 30 min with broadband visible light prior to injection into the QCM-D had no significant Δf or ΔD signal differences when compared to liposomes that underwent no illumination before injection into the QCM-D.

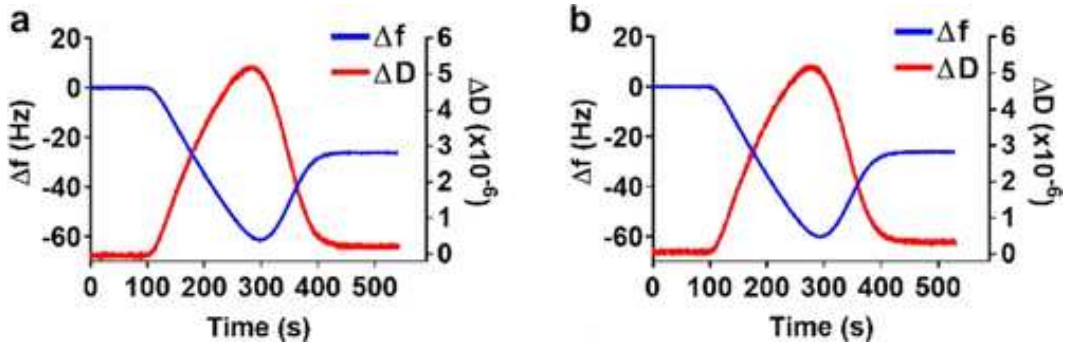

Figure 2.4. Illumination does not affect DOPC liposomes. (a, b) QCM-D frequency (Δf) and dissipation (ΔD) responses for SLB formation from DOPC liposomes without prior illumination (a) and after 30 min illumination (b).

When 2 mol% TF-PC was added to DOPC liposomes and illuminated prior to injection into the QCM-D, the instrument response changes from the tradition two-step process (adsorption of critical surface coverage of liposomes followed by liposome

rupture) to a one-step process (immediate liposome adsorption/rupture). This altered pathway is shown in Figure 2.5.

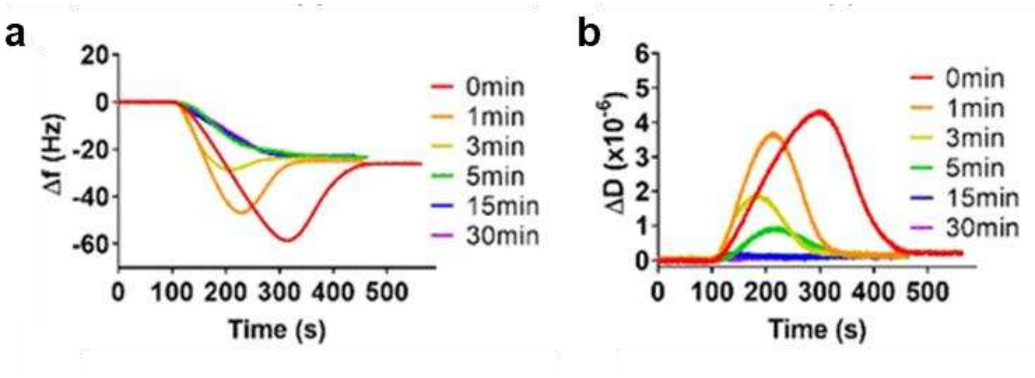

Figure 2.5. Influence of illumination of TF-PC-containing liposomes on SLB formation. Frequency (a) and dissipation (b) responses for SLB formation from DOPC liposomes containing 2 mol% TF-PC after 0-30 min illumination time.

Illuminated liposomes containing 2 mol% TF-PC reached critical liposome surface coverage and formed a SLB faster than unilluminated liposomes of the same composition. Without illumination, SLBs were formed in approximately 440 s, but after 30 min illumination, only 330 s was required to form a SLB. The SLB formation pathway changes from a two-step process to a one-step process after only 5 min of illumination. This one-step pathway indicates that liposomes rupture immediately upon contact with the SiO_2 surface. Similar behavior has been observed for the formation of SLBs from cationic liposomes[25] and from liposomes in hypertonic solutions.[26]

The excitation of liposomes containing 2 mol% BODIPY-PE also resulted in an acceleration of SLB formation. This QCM-D signal is shown in Figure 2.6.

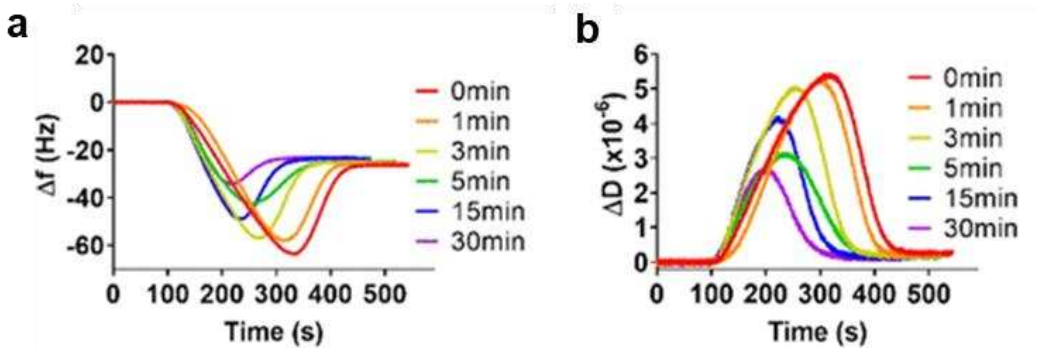

Figure 2.6. Influence of illumination of BODIPY-PE-containing liposomes on SLB formation. Frequency (a) and dissipation (b) responses for SLB formation from DOPC liposomes containing 2 mol% BODIPY-PE after 0-30 min illumination time.

When liposomes containing 2 mol% BODIPY-PE were illuminated for 30 min, there was an acceleration of the SLB formation time from 440 s to 365 s. Interestingly, the liposome rupture process never reaches the single-step profile that was observed with the TF-PC-containing liposomes. With TF-PC, the fluorophore moiety is embedded in the hydrophobic core of the membrane,[27,28] whereas with BODIPY-PE, the fluorophore is positioned on the phosphate headgroup, and therefore in the aqueous environment. Thus, the location of these fluorophores in relation to the membrane plays a role in how illumination alters the SLB formation process.

2.3.4 Concentration and Light Intensity Dependence

In addition to illumination time as a variable, I investigated the role of TF-PC concentration on SLB formation. As the concentration of TF-PC was reduced from 2 mol% to 0.2 and 0.02 mol%, the liposome rupture profile reverts to the classical two-step process even after 30 min illumination, as shown in Figure 2.7.

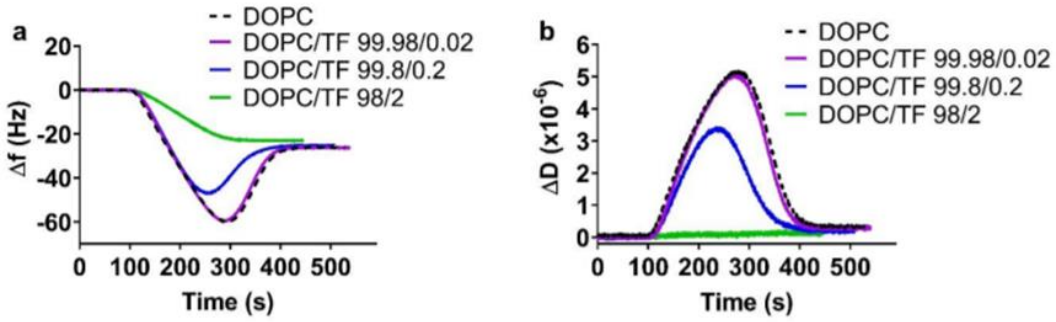

Figure 2.7. Effect of illumination and TF-PC concentration on SLB formation. All liposomes were illuminated for 30 min with broadband visible LED light prior to QCM-D injection. (a) Frequency shift (Δf) as a function of time for DOPC liposomes lacking TF-PC and for liposomes containing 2, 0.2, and 0.02 mol% TF-PC. (b) Dissipation shift (ΔD) as a function of time for DOPC liposomes lacking TF-PC and for liposomes containing 2 mol% (green line), 0.2 mol% (blue line), and 0.02 mol% (purple line) TF-PC.

Reducing the illumination intensity with neutral density (ND) filters caused a reversion to the classical two-step adsorption and rupture profile even after liposomes were illuminated with broadband visible light before injection into the QCM-D, as shown in Figure 2.8. In these studies, a ND 0.5 or ND 1.0 neutral density filter was placed in front of the LED light source during sample illumination. Samples were illuminated for either 5 min or 30 min, then injected into the QCM-D.

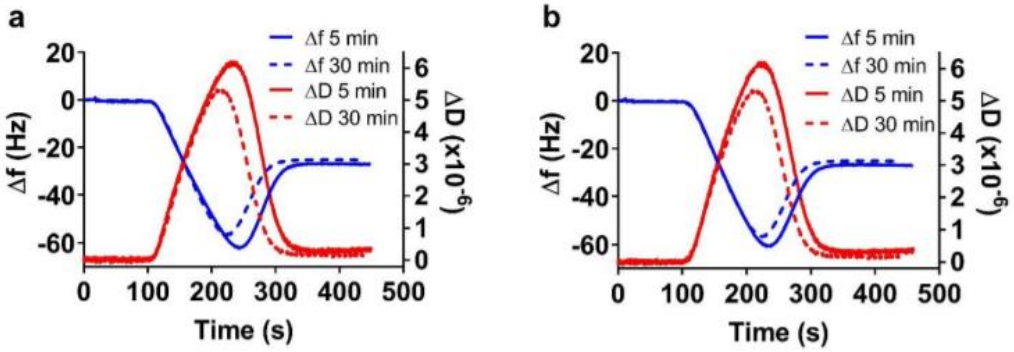

Figure 2.8. Effect of illumination intensity on SLB formation. Liposomes were composed of DOPC with 2 mol% TF-PC. Prior to QCM-D analysis, the liposomes were illuminated with broadband LED light that was passed through a ND 0.5 (a) or a ND 1.0 (b) neutral density filter. Samples were illuminated for 5 (solid curves) or 30 min (dashed curves).

Previously, without a filter in place, 5 min of illumination was enough time to shift a DOPC/2 mol% TF-PC liposome sample to the accelerated one-step SLB formation process (Figure 2.5). Regardless of ND 0.5 or ND 1.0, the rupture pathway remained classically two-step, implying a power intensity dependence to observe the accelerated rupture effects.

2.3.5 Excited Liposomes do not Spontaneously Rupture on Gold Surfaces

A number of optical sensors, such as surface plasmon resonance (SPR), or electrochemical sensors employ gold films. However, liposomes do not readily rupture on gold-coated surfaces.[23] Specialized surface coatings, such as SiO_2, are required for SLB formation via vesicle rupture, or polymeric layers (i.e. alkane-linked dexrans) are used for liposome immobilization on commercial SPR sensors.[29] Therefore, it was enticing to consider a method that might allow for the spontaneous rupture of liposomes on a gold-coated surface.

This prompted me to inject illuminated DOPC/TF-PC liposomes onto a gold-coated QCM-D sensor in the hopes that photo-oxidized liposomes would be more prone to rupturing on the surface. However, DOPC/TF-PC liposomes that have been illuminated for 30 min do not spontaneously rupture on gold surfaces (Figure 2.9b), similar to

unilluminated liposomes on gold surfaces (Figure 2.9a). This is in agreement with previous reports that studied the behavior of PC liposomes on gold QCM-D sensor surfaces.[23]

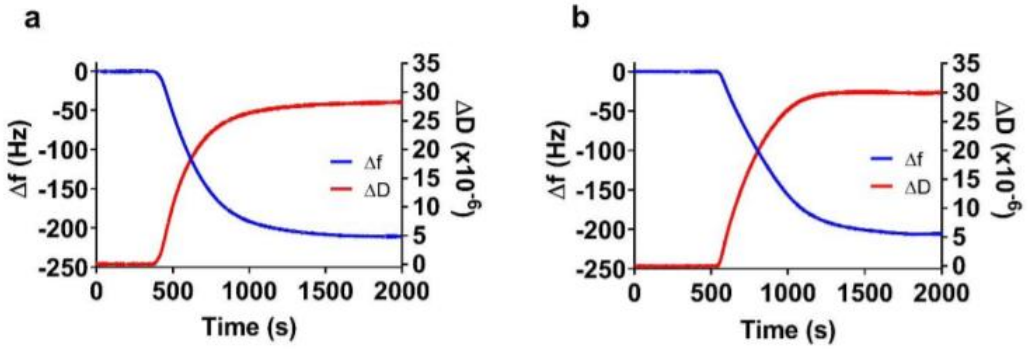

Figure 2.9. Illuminated DOPC/TF-PC liposomes do not spontaneously rupture on a gold surface. (a) QCM-D frequency (Δf) and dissipation (ΔD) responses for unilluminated DOPC/TF-PC liposomes adsorbing to a gold-coated sensor. (b) QCM-D frequency and dissipation responses for DOPC/TF-PC liposomes that had been illuminated for 30 min with broadband LED light prior to adsorption to a gold-coated sensor.

2.3.6 Larger Liposomes Also Show Accelerated SLB Formation

I also examined the influence of liposomes size on TF-PC-induced SLB formation acceleration. It has been shown that larger-diameter liposomes do not rupture as readily as smaller-diameter liposomes due to disrupted liposome-liposome contact (which is necessary for spontaneous liposome rupture and SLB formation) because of the steric hindrance that comes with larger liposome sizes.[30]

When the extrusion filter pore size was increased from 50 nm to 100 nm, the DOPC/TF-PF liposomes that were illuminated for 30 min ruptured on SiO_2 with a single-step accelerated rupture profile (Figure 2.10b).

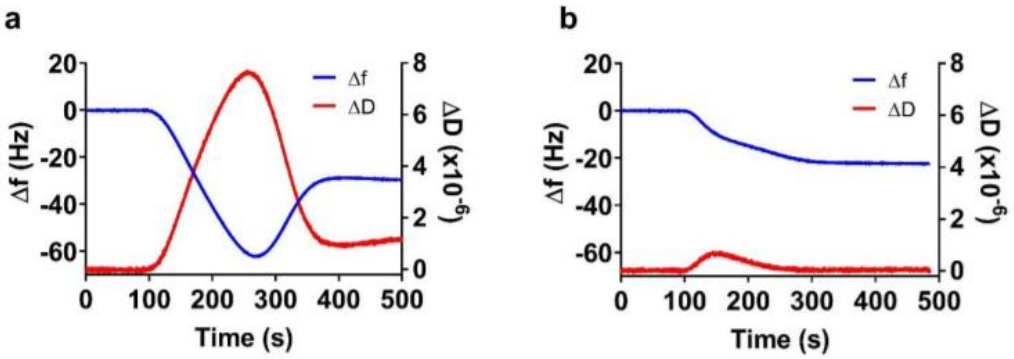

Figure 2.10. SLB formation from liposomes extruded through 100 nm pore size filters. QCM-D frequency (Δf) and dissipation (ΔD) responses for DOPC/TF-PC liposomes that did not receive illumination prior to injection (a) and liposomes that were illuminated for 30 min with broadband LED light prior to injection (b).

2.3.7 SLB Mass Decreases with Longer Illumination Times

When the final frequency shifts associated with complete SLB formation (Δf_{SLB}) are examined, an interesting trend emerges: for both DOPC/2 mol% TF-PC and DOPC/2 mol% BODIPY-PE compositions, as the illumination time increases, the Δf_{SLB} values become less negative (Figure 10a). Because a SLB can be considered a thin rigid film, its mass can be calculated using the Sauerbrey equation.[31]

$$\Delta m = -C_{QCM}\frac{\Delta f_n}{n} = \rho_{SLB} h_{SLB} \qquad \text{eq 2.1}$$

where Δm is the areal mass of the SLB (in units of ng cm^{-2}), C_{QCM} is the mass sensitivity constant (17.7 ng cm^{-2} Hz^{-1}), n is the overtone number, and Δf_n is the frequency shift of the nth overtone. Using eq 2.1, the SLB mass (Δm = mass$_{SLB}$) can be calculated as a function of illumination time (Figure 2.11b).

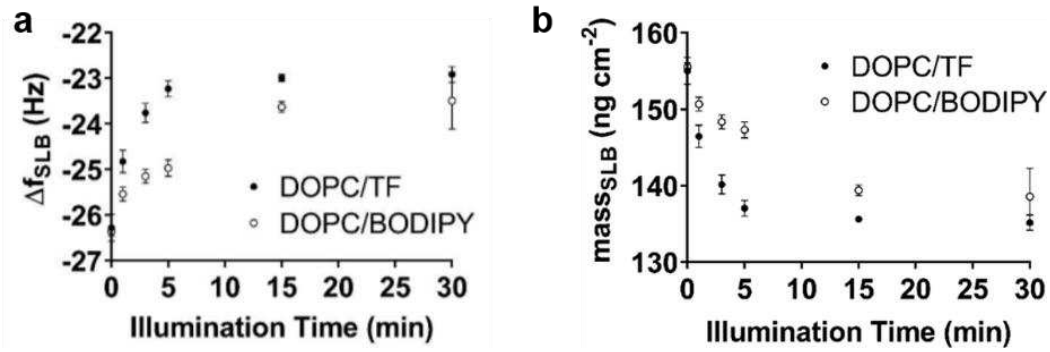

Figure 2.11. Liposome illumination reduces final frequency and SLB mass. (a) Final frequency (Δf_{SLB}) for DOPC SLBs containing TF-PC (TF) or BODIPY-PE as a function of illumination time. (b) SLB mass ($mass_{SLB}$) for DOPC SLBs containing TF-PC (TF) or BODIPY-PE as a function of illumination time.

Figure 2.11b shows that liposomes illuminated for longer durations lead to SLBs with smaller measured masses, and that TF-PC is more potent than BODIPY-PE in this regard. The areal mass is also equivalent to the product of the density of the SLB (ρ_{SLB}) and the SLB thickness (h_{SLB}).[31,32] Therefore, the frequency shift associated with a thin rigid film like a SLB is proportional to the areal mass of the film. This means that the smaller measured SLB masses after liposome illumination could arise from a decrease in film density due to an increase in the area per lipid molecule and/or a reduction in the SLB thickness.

2.3.8 SLBs Formed from Excited Liposomes are Relatively Free of Defects

Oxidized phospholipids are known to have a larger area per molecule (and thus reduced density), and oxidation can result in the thinning of the membrane.[33] Alternatively, a SLB with significant void spaces or defects would also have a smaller measured mass.

To probe whether this was the case, a solution of bovine serum albumin (BSA) was flowed into the QCM-D after SLBs were formed from illuminated liposomes.

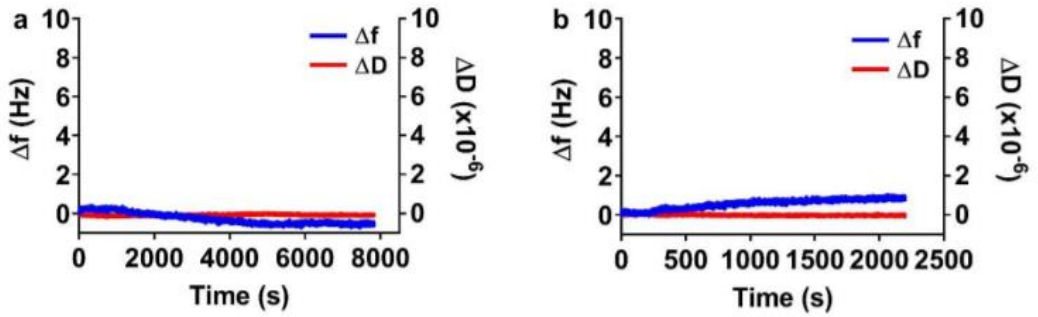

Figure 2.12. Examination of SLB continuity by exposure to bovine serum albumin (BSA). SLBs were formed from DOPC/2 mol% TF-PC liposomes that had not been illuminated (a) or from liposomes that had been illuminated for 30 min (b) prior to QCM-D injection. The SLBs were then exposed to BSA (105 nM) and frequency (Δf) and dissipation (ΔD) were monitored.

BSA strongly adsorbs on SiO_2 and if there were significant defects, large shifts in frequency would be expected due to mass accumulation. The lack of appreciable BSA adsorption (Figure 2.12b) beyond typical instrumental drift (< 1 Hz over the course of 10 min), indicates that these SLBs are largely free from defects that would expose the underlying SiO_2 surface. This rules out significant membrane defects as a cause for the decrease in the measured SLB mass (Figure 2.11b). This suggests that reductions in both the SLB density and membrane thinning are responsible for the decrease in SLB mass we observe when 2 mol% TF-PC or BODIPY-PE is present in illuminated liposomes.

2.3.9 Ambient Light has Negligible Effect on SLB Formation Process

To determine whether ambient light can have similar effects as the broadband visible LED light source on DOPC/2 mol% TF-PC liposomes, I exposed liposomes to ambient laboratory light for 1, 3, or 6 days, before injecting the sample into the QCM-D (Figure 2.13).

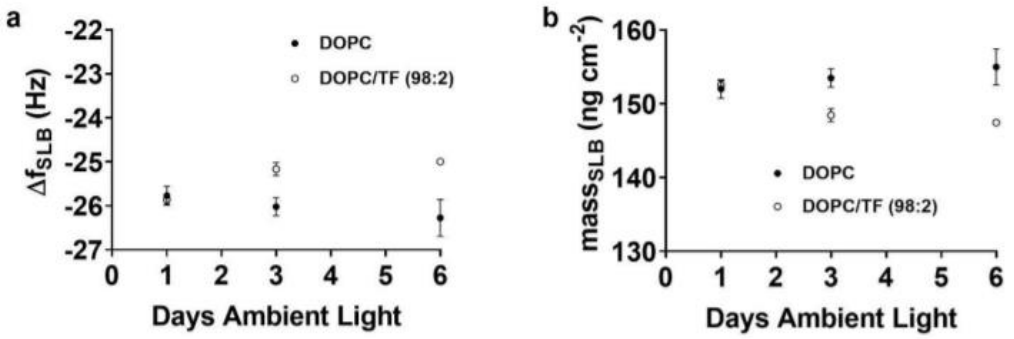

Figure 2.13. Effects of ambient light exposure on Δf_{SLB} (a) and $mass_{SLB}$ (b) for SLBs formed from liposomes composed of DOPC or DOPC/2% TF-PC.

Slightly reduced values of Δf_{SLB} and $mass_{SLB}$ were measured after 3 and 6 days of ambient light exposure (Figure 2.13). However, these reductions were not nearly as pronounced as the effects of $\leq$ 30 min illumination with the broadband LED (Figure 2.11).

2.3.10 Fluorescence Micrographs of SLBs Formed from Illuminated Liposomes

Fluorescence microscopy was used to examine SLBs formed from DOPC/2 mol% TF-PC liposomes with and without 30 min of illumination. However, after illumination of liposomes, the resulting SLBs were invisible by fluorescence microscopy due to complete photobleaching of the TF-PC probe (Figure 2.14b).

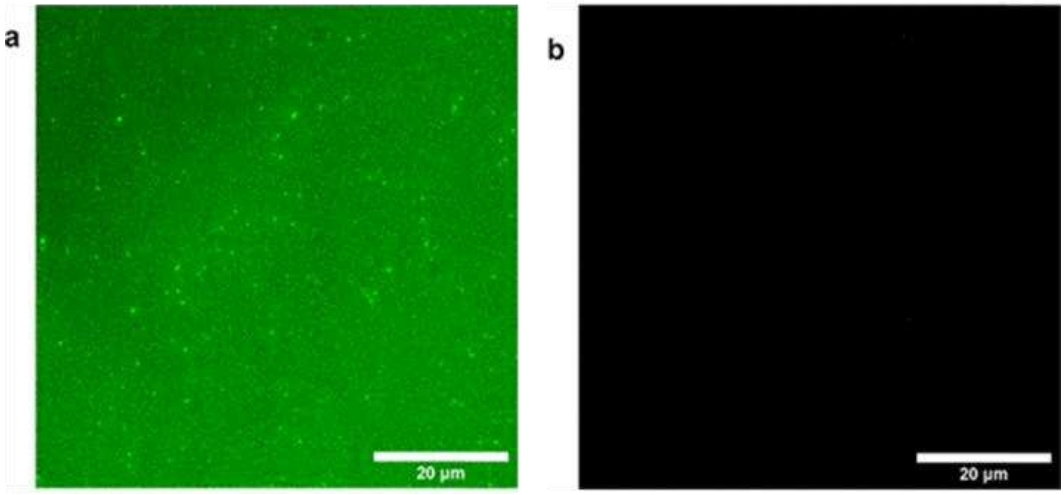

Figure 2.14. Fluorescence micrographs of SLBs. (a) A SLB formed from DOPC/2 mol% TF-PC liposomes that were not illuminated prior to deposition. (b) A completely photobleached SLB formed from DOPC/2 mol% TF-PC liposomes that were illuminated for 30 min prior to deposition on the glass substrate.

A few fluorescent membrane defects are observable in Figure 2.14a, which may be a result of SLB photo-oxidation that occurs during imaging. These defects will be discussed in much further detail in a later chapter of this dissertation.

2.3.11 Accelerated SLB Formation Process Depends on Fluorophore Identity

When liposomes were made of DOPC and 2 mol% of either NBD-PC, NBD-PE, or Texas Red-DHPE and illuminated for 30 min, there is no significant change to the liposome adsorption, rupture, and SLB formation process (Figure 2.15). Thus, the effects of fluorophore excitation on liposome rupture and SLB formation are specific to TF-PC and BODIPY-PE-lipid conjugates.

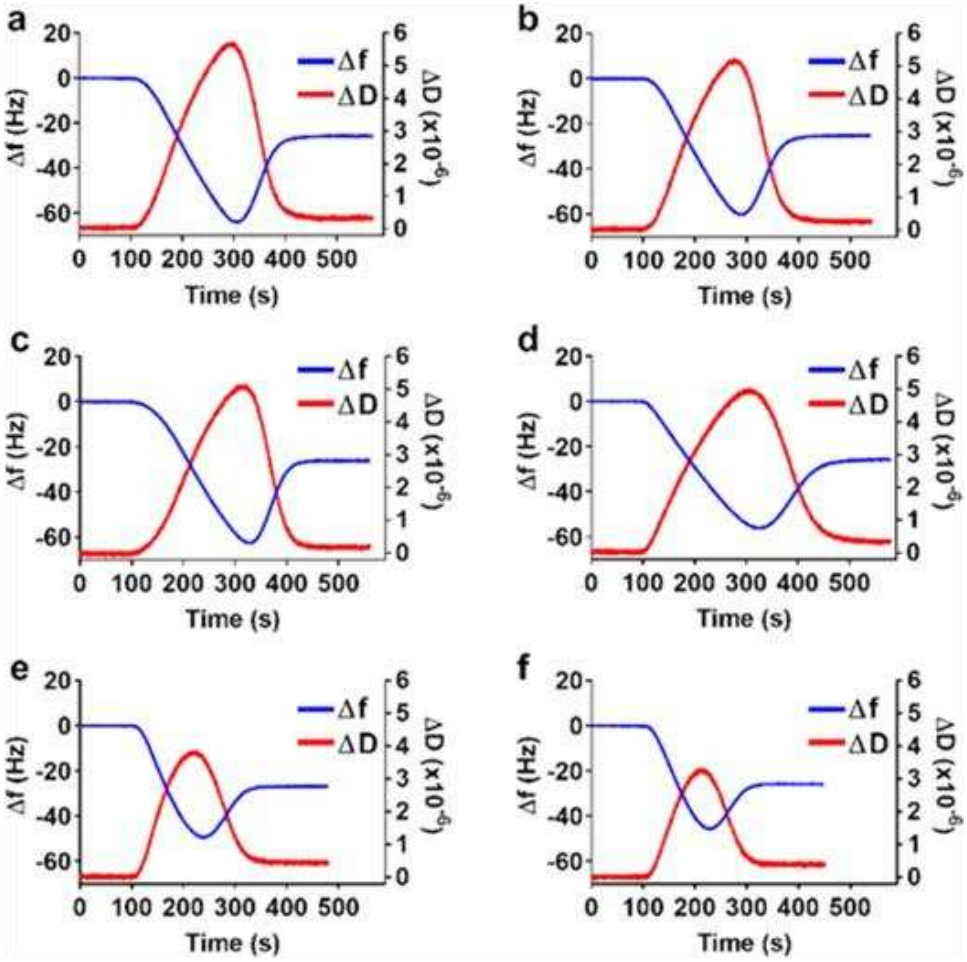

Figure 2.15. The influence of illumination on SLB formation from DOPC liposomes containing other fluorescently-conjugated lipid probes. (a, b) QCM-D response for DOPC liposomes containing 2 mol% NBD-PC without prior illumination (a) and after 30 min illumination (b). (c, d) QCM-D response for DOPC liposomes containing 2 mol% NBD-PE without prior illumination (c) and after 30 min illumination (d). (e, f) QCM-D response for DOPC liposomes containing 2 mol% Texas Red-DHPE without prior illumination (e) and after 30 min illumination (f).

For NBD-PC, the fluorophore is linked through the acyl chain of the lipid, similar to TF-PC. However, the tail-linked NBD moiety tends to reside near the aqueous interface,[34] whereas tail-linked TF-PC resides closer to the center of the membrane.[27]

Nevertheless, the presence of a tail group-conjugated fluorophore alone does not induce changes in the rupture pathway of illuminated liposomes. It is likely that the BODIPY-PE and TF-PC act as photosensitizers to trigger the oxidation of unsaturated DOPC fatty acid tails.[35]

2.3.12 Mimicking the Effects of Photo-Oxidation

The presence of oxidized phospholipids in liposomes can result in significant changes to the SLB formation process.[11] PoxnoPC and PazePC (Figure 2.1) are oxidized phospholipids that induce lipid flip-flop and cause increased tail group disorder, membrane bilayer thinning, and membrane pore formation.[33,36,37] Liposomes composed of DOPC and 20 mol% of PoxnoPC or PazePC were prepared and injected into the QCM-D to observe their rupture pathway on SiO_2 without any illumination (Figure 2.16).

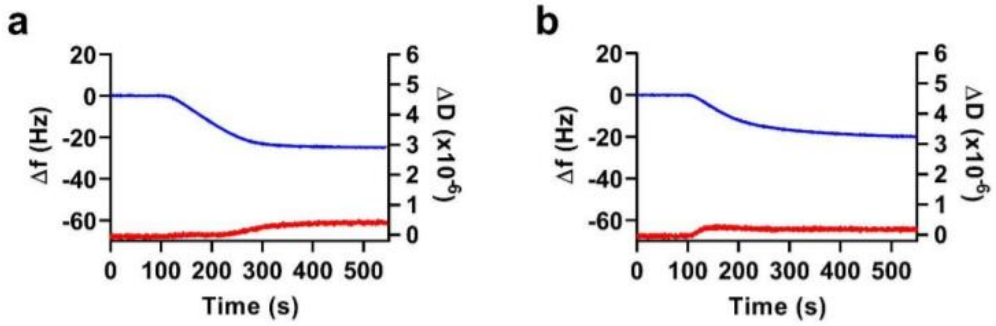

Figure 2.16. The influence of oxidized phospholipids on SLB formation. (a) Frequency and dissipation shifts for SLB formation from DOPC liposomes containing 20 mol% PoxnoPC. (b) Frequency and dissipation shifts for SLB formation from DOPC liposomes containing 20 mol% PazePC. These liposomes were not illuminated prior to QCM-D injection.

These liposomes rupture immediately upon contact with SiO_2. This agrees with previous results for POPC liposomes that contain PoxnoPC or PazePC.[11] The rupture process of liposomes containing these oxidized lipids is similar to the rupture process of liposomes containing 2 mol% TF-PC that have been illuminated prior to QCM-D injection, which suggests that photosensitized oxidation of lipid tails may be responsible for the accelerated SLB formation that I observed with TF-PC-containing liposomes.

Dimethylsulfoxide (DMSO) can partition into lipid bilayers, increasing the area per lipid molecule and thinning the membrane, which mimics the effects of lipid oxidation.[38] In work by another group, DMSO led to increased frequency of liposome rupture and cargo release events on carbon fiber electrodes.[20] However, the addition of 0.6 vol% DMSO into the buffer in which liposomes were dissolved did not induce changes to the SLB formation process (Figure 2.17).

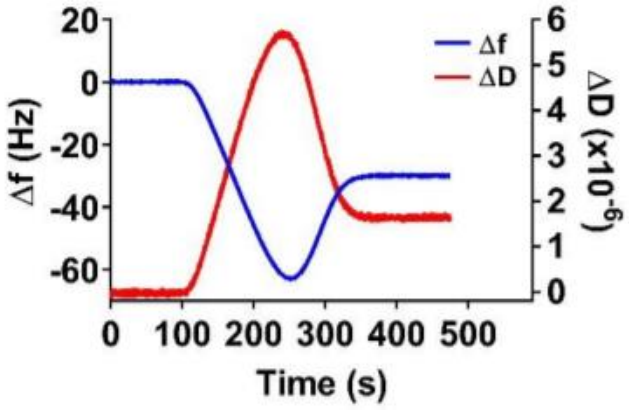

Figure 2.17. Influence of DMSO on liposome adsorption, rupture, and SLB formation. DOPC liposomes were suspended in PBS containing 0.6 vol % DMSO, then injected into the QCM-D where frequency (Δf) and dissipation (ΔD) shifts were monitored.

2.3.13 Attenuation of Accelerated SLB Formation Process

To determine if lipid unsaturation is required for the changes in the SLB formation process that are observed when TF-PC-containing liposomes are illuminated, liposomes composed of DiPhyPC and 2 mol% TF-PC were made. DiPhyPC is a saturated phospholipid (Figure 2.1) with a phase transition temperature below -120 °C and a bilayer thickness similar to DOPC.[39–41] Figure 2.18 shows the QCM-D response for SLB formation from DiPhyPC/2 mol% TF-PC liposomes in the absence and presence of illumination.

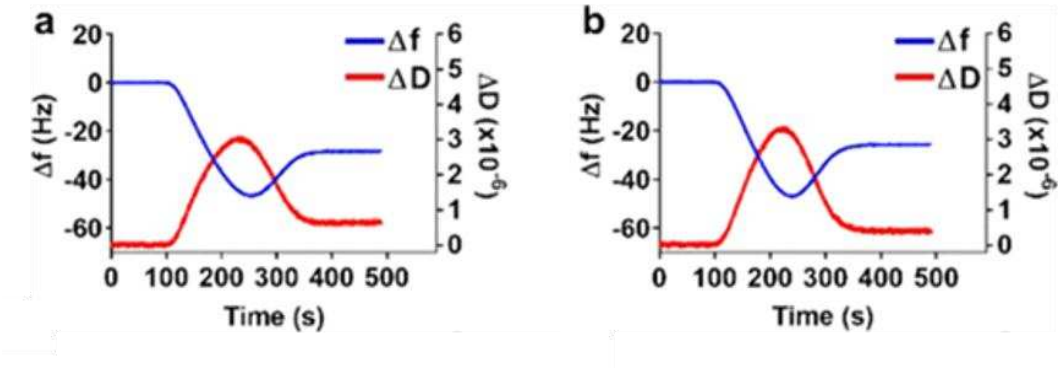

Figure 2.18. Influence of lipid saturation on SLB formation after liposome illumination. (a,b) QCM-D responses for SLB formation from DiPhyPC liposomes containing 2 mol% TF-PC without prior illumination (a) and after 30 min illumination (b).

There is no change in the SLB formation pathway after 30 min of illumination, suggesting that the presence of oxidizable bonds that are present in unsaturated lipids is required for the pronounced effect of illumination that was seen in DOPC/2 mol% TF-PC liposomes. Lipid oxidation occurs when ROS attacks sites of unsaturation within the fatty acid tails of the lipid molecule,[42,43] but there is no site of unsaturation within the DiPhyPC lipid tail, therefore those lipids cannot be readily oxidized via ROS attack.

I also tested whether a lipophilic antioxidant had any effect on the illumination-induced acceleration of SLB formation. The antioxidant α-tocopherol[44] (Figure 2.1) was included in DOPC liposomes in equimolar amounts to TF-PC (Figure 2.19). Unilluminated liposomes with this composition ruptured to form a SLB with the two-step profile. After 30 min of liposome illumination, the SLBs formed faster than those formed from unilluminated liposomes, but the frequency and dissipation signals still exhibited distinct minima and maxima.

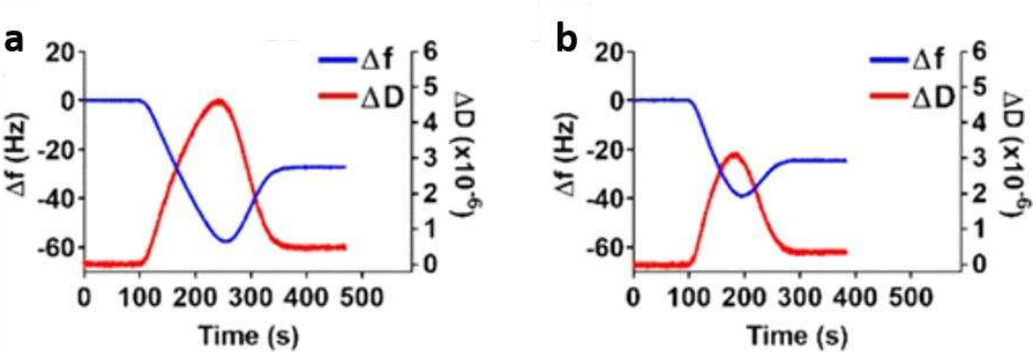

Figure 2.19. Influence of antioxidant on SLB formation after liposome illumination. (a,b) QCM-D responses for SLB formation from DOPC liposomes containing 2 mol% TF-PC and 2 mol% α-tocopherol without prior illumination (a) and after 30 min illumination (b).

Comparing Figure 2.19b with Figure 2.5 shows that α-tocopherol significantly reduces the influence of illumination on SLB formation from DOPC liposomes containing TF-PC. A membrane-embedded antioxidant does not completely eliminate illumination effects on liposome adsorption and rupture; however, it does significantly attenuate the effects of illumination, which further suggests TF-PC acts as a photosensitizer that initiates the oxidation of unsaturated lipids.

2.3.14 Evidence of Lipid Oxidation

To support my hypothesis that the alterations of the liposome rupture pathway is caused by lipid oxidation, I carried out Langmuir trough experiments (with the help of Monicka Kullappan and Professor Manoj Chaudhury of the Department of Chemical & Biomolecular Engineering at Lehigh University). In these Langmuir trough experiments, a liposome sample of DOPC/2 mol% TF-PC was exposed to a broadband visible LED before a monolayer was spread onto an aqueous PBS layer in the Langmuir trough.

Upon the compression of the monolayer, it is observed that there was a significant increase in the area-per-lipid molecule for the sample exposed to light compared with the sample that is not exposed to light, as shown in Figure 2.20. For example, at a surface pressure of 30 mN m^{-1}, the sample that was not exposed to illumination had an area-per-molecule of approximately 78 $Å^2$, whereas the sample that had been illuminated had an area-per-molecule of approximately 107 $Å^2$, an increase of 37%. The area-per-molecule values observed in the compression isotherm for nonilluminated DOPC/TF-PC compare well with other literature values.[45,46]

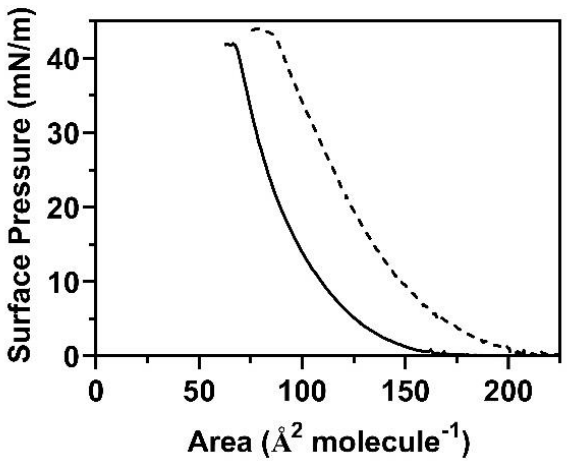

Figure 2.20. Surface pressure-area isotherms of monolayer of illuminated lipids. Plot of surface pressure versus area per molecule of DOPC/TF-PC in the absence (solid line) and presence (dashed line) of illumination. (Data collected by Monicka Kullappan of the Department of Chemical & Biomolecular Engineering at Lehigh University).

Additionally, I spectroscopically examined samples of DOPC/2 mol% TF-PC before and after light exposure. A number of lipid oxidation products have aldehyde or carboxyl functional groups, so I examined the IR absorbance in the C=O stretch region around 1730 cm^{-1}.[48] The absorbance at 1730 cm^{-1} of the sample that had been illuminated is approximately 3.6 times larger than that of its unilluminated counterpart (Figure 2.21).

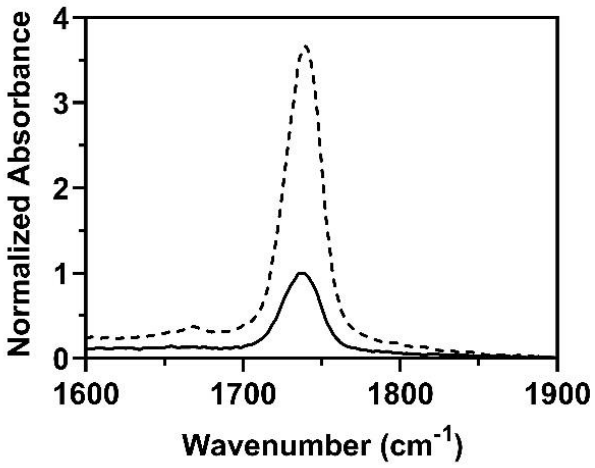

Figure 2.21. FT-IR spectra of illuminated lipids. IR absorbance of the carbonyl peak in a sample of DOPC/TF-PC before (solid line) and after (dashed line) illumination.

The fact that this peak is greatly enhanced in the illuminated sample lends weight to the argument that the sample has been photo-oxidized, resulting in products possessing aldehyde or carboxylic acid functional groups. Many oxidation products contain a carbonyl group, and though this group is also in the fatty acid of an unoxidized lipid, it appears in greater abundance after the lipid has been illuminated, and thus oxidized.

2.3.15 Dynamic Light Scattering and Zeta Potential of Liposomes

It is clear that illumination of DOPC liposomes containing 2 mol% TF-PC or BIDOPY-PE significantly accelerates SLB formation kinetics, and the data suggests that this is likely due to membrane oxidation. However, I sought to further characterize the consequences of illumination on liposome radius, surface area (assuming spherical geometry), and zeta potential. Dynamic light scattering (DLS) and a zeta potential analyzer

were used to examine liposomes before and after 30 min illumination with broadband visible light (Table 2.1).

	No illumination			30 min illumination			Comparison	
Liposome Composition	**Radius ± s.d. (nm)**	**Surface area ± s.d. ($\times 10^4$ nm^2)**	**Zeta Potential (mV)**	**Radius ± s.d. (nm)**	**Surface area ± s.d. ($\times 10^4$ nm^2)**	**Zeta Potential (mV)**	**% change in surface area ± error**	***P*-value[a]**
DOPC	57.8 ± 1.1	4.20 ± 0.16	-2.78 ± 4.63	58.3 ± 4.6	4.27 ± 0.67	-4.50 ± 5.65	+1.67 ± 16.4	0.869
DOPC/TopFluor-PC	61.1 ± 2.3	4.69 ± 0.35	-5.78 ± 2.01	56.3 ± 1.3	3.98 ± 0.18	-3.47 ± 5.53	-15.1 ± 8.5	0.035
DOPC/TopFluor-PC/α-tocopherol	62.7 ± 2.4	4.94 ± 0.38	-2.82 ± 4.43	58.4 ± 2.7	4.29 ± 0.40	-3.00 ± 4.69	-13.2 ± 11.1	0.111
DOPC/NBD-PC	58.5 ± 1.8	4.30 ± 0.26	-6.09 ± 5.77	54.4 ± 4.3	3.72 ± 0.59	-2.20 ± 5.42	-13.5 ± 15.0	0.194

Table 2.1. Liposome Radii, Surface Areas, and Zeta Potentials Before and After Illumination. [a]P-value for unpaired t-test comparing the surface area of unilluminated and illuminated vesicles.

Of the compositions that were tested, a significant decrease in liposome surface area was observed for DOPC/2 mol% TF-PC liposomes after 30 min illumination. Other compositions had changes in surface area that were not statistically significant. Although the inclusion of oxidized lipids in membranes has been shown to increase the area per lipid

molecule, the reduction in liposome surface area could be explained by some amount of liposome fission during the oxidation process, which has been observed in other liposome systems.[21] Alternatively, the presence of sodium ions, which are present in the buffer, can cause membrane condensation and a decrease in the area per lipid molecule in membranes that contain carboxylic acid-terminated oxidation products.[33] Additionally, the loss of oxidation scission products could result in a decrease in membrane surface area. Previous work has shown that the oxidation of PC liposomes with 2,2-azobis(2-amidinopropane) hydrochloride results in the formation of conjugated dienes and a significant reduction in liposome diameter.[49]

Zeta potentials for all liposomes were near zero and did not significantly change after 30 min illumination. Near-zero zeta potentials are to be expected from liposomes composed primarily of zwitterionic lipids (such as DOPC) under the conditions studied.[50]

2.3.16 Inclusion of Oxidation Products in Liposomes

Because oxidation products (short-chain aldehydes and carboxylic acids) reduce permeability in liposomes where oxidized phospholipids are also present,[51] I speculated that the addition of these oxidation products into liposomes might attenuate the acceleration of vesicle rupture when oxidized lipids such as PoxnoPC or PazePC are present.

I formed DOPC/PoxnoPC (80:20 mol%) liposomes in the presence of 25, 50, or 100 mM of hexanoic acid, then injected these liposomes into the QCM-D to monitor their rupture pathway (Figure 2.22). As seen earlier in Figure 2.16, the inclusion of 20 mol% oxidized lipid results in a one-step SLB formation pathway.

Liposomes formed in 25 mM and 50 mM hexanoic acid displayed the same one-step SLB formation pathway, indicating that the presence of hexanoic acid has little influence on altering the accelerated SLB rupture process. Interestingly, liposomes formed in 100 mM hexanoic acid showed no frequency or dissipation signal changes at all. This experiment was produced in triplicate, and each trial displayed this lack of signal change. This could be due to the high concentration of hexanoic acid in the buffer. Lipids could have a preference to remain soluble in hexanoic acid rather than form into liposomes.

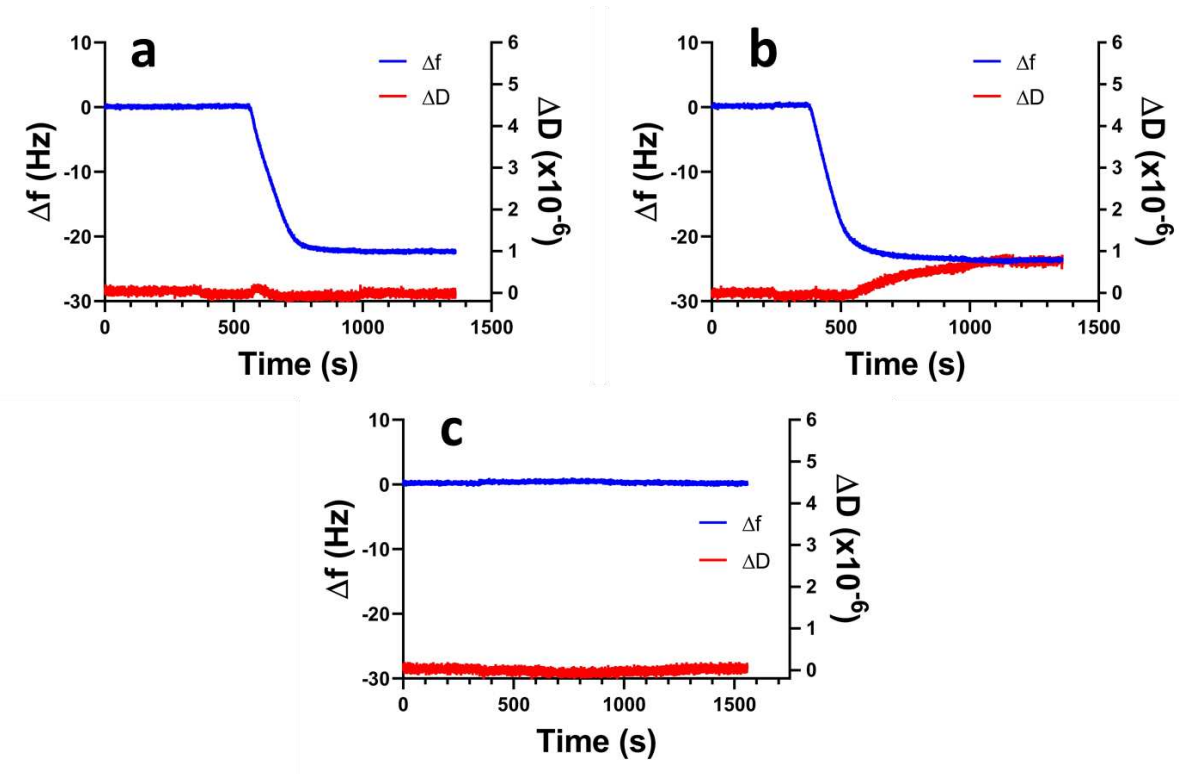

Figure 2.22. Effect of hexanoic acid on SLB formation. QCM-D signals of liposomes formed in the presence of 25mM (a), 50 mM (b), and 100 mM (c) hexanoic acid.

Further experimentation would need to be done to draw more accurate conclusions; however, from the preliminary data shown in Figure 2.22, it appears that the inclusion of a carboxylic acid oxidation product has no influence on the liposome rupture process. This behavior is also seen in the experiments of illuminated TC-PC-containing liposomes: those liposome samples would have their oxidation products in solution as well, yet those illuminated liposomes still displayed the accelerated one-step SLB formation pathway. This suggests that if short-chain oxidation products are indeed present, they have little to no influence on the liposome rupture process in the illuminated liposome systems studied.

2.4 Conclusions

In summary, SLB formation from DOPC liposomes that contain BODIPY-PE and TF-PC fluorescent lipid conjugates is significantly accelerated by fluorophore excitation using a broadband visible-light LED. The SLB formation pathway changes from a two-step process, wherein liposomes accumulate on a surface and then rupture to form a SLB, to a one-step process, wherein liposomes immediately rupture upon contact with a surface. This behavior can be eliminated by using liposomes composed of saturated phospholipids, which are more impervious to oxidation, and it can be attenuated by an antioxidant. Furthermore, single-step SLB formation is observed in the absence of illumination when oxidized lipids are present in liposomes. Together, the evidence suggests that photosensitized lipid oxidation changes the physiochemical properties of the liposomes and causes accelerated rupture and SLB formation.

The lipid oxidation products in our studies remain to be identified. The fact that inclusion of PC with oxidized fatty acid tails (PoxnoPC and PazePC) mimics the SLB

formation behavior of illuminated TF-PC-containing liposomes suggests that these molecules may be among the products of TF-PC- and BODIPY-PE-induced lipid oxidation. The oxidation of unsaturated lipids also results in cleavage of short-chain aldehydes[52] (e.g., hexanal), which can be further oxidized to a carboxylic acid (e.g., hexanoic acid). Malmstadt and coworkers showed that the presence of PoxnoPC in giant vesicles significantly increased the permeability of giant vesicles.[53] The inclusion of hexanal or hexanoic acid in combination with PoxnoPC decreased the membrane permeability compared to giant vesicles where PoxnoPC was the only oxidized species present.[51] However, in my system, the inclusion of hexanoic acid had no discernible effect on attenuating the accelerated SLB formation pathway.

The illumination protocol used in this study exposes samples to more optical energy than they would be exposed to during microscopy (for example, during fluorescence recovery after photobleaching (FRAP) of a SLB). Also, these studies do not establish an optical energy threshold for which excitation of lipid probes becomes a significant concern, though the reduction in excitation intensity (through use of neutral density filters) does cause liposomes to adsorb and rupture with a two-step profile (Figure 2.8). Nevertheless, it is shown that the excitation of BODIPY-based lipid probes likely causes significant changes to the properties of phospholipid liposomes with respect to their interaction with SiO_2.

Interestingly, BODIPY-based molecules are generally inefficient photosensitizers in the absence of heavy atoms or other substitutions due to their low intersystem crossing quantum yield.[35,54] However, it seems that the conjugation of BODIPY and TopFluor to PE and PC phospholipids, respectively, might facilitate intersystem crossing to a triplet

state, which in the presence of oxygen can lead to singlet oxygen formation. BODIPY- and TopFluor-conjugated lipid probes also display unique photoconversion properties, such as a lipid phase-dependent red-shift of its emission after periods of excitation with blue light, and changes in lipid phase partitioning after excitation.[19] However, these behaviors were attributed to changes in the structure of the lipid–fluorophore conjugate rather than the oxidation of background membrane lipids. Other groups have noted that photo-oxidation of lipids by NBD- and rhodamine-conjugated probes, which have no effects on the studies described here, can induce membrane phase separation.[18]

The data suggests that TF-PC is a more potent photosensitizer than BODIPY-PE. Of the two molecules, TF-PC resides within the membrane bilayer, whereas BODIPY-PE resides at the aqueous interface.[27] Although the exact ROS responsible for the observed effects is unknown, it is possible to consider the lifetime and diffusion coefficient of singlet oxygen to explain why BODIPY-PE, despite having the fluorophore farther from the point of lipid unsaturation, can also cause photosensitized oxidation. Singlet oxygen has decay times of roughly 3.5, 14, and 10 μs in pure water, pure lipid, and lipid/water suspensions, respectively.[55] The diffusion coefficients (*D*) for singlet oxygen in lipid membranes and water are 0.7 and 2.0 x 10^{-5} cm^2 s^{-1}, respectively.[56,57] The diffusion distance (*d*) for singlet oxygen can be calculated with the following equation:

$$d = (6Dt)^{1/2} \qquad \text{eq 2.2}$$

Using the singlet oxygen decay time (t = 14 μs) and the diffusion coefficient in a lipid membrane (D = 0.7 x 10^{-5} cm^2 s^{-1}), the diffusion distance for singlet oxygen is

approximately 240 nm. Given that a DOPC bilayer is roughly 4 nm thick,[58] singlet oxygen has to diffuse less than 2 nm from the BODIPY source to the point of unsaturation at the center of the membrane bilayer. Thus, the diffusion distance greatly exceeds the distance from the BODIPY group to the unsaturated acyl chain. BODIPY-PE is most likely a less-potent photosensitizer in this study because some ROS generated by BODIPY-PE can diffuse away from the membrane and decay prior to encountering another membrane, whereas ROS generated by TF-PC in the membrane core will encounter unsaturated lipids, regardless of the direction in which it diffuses.

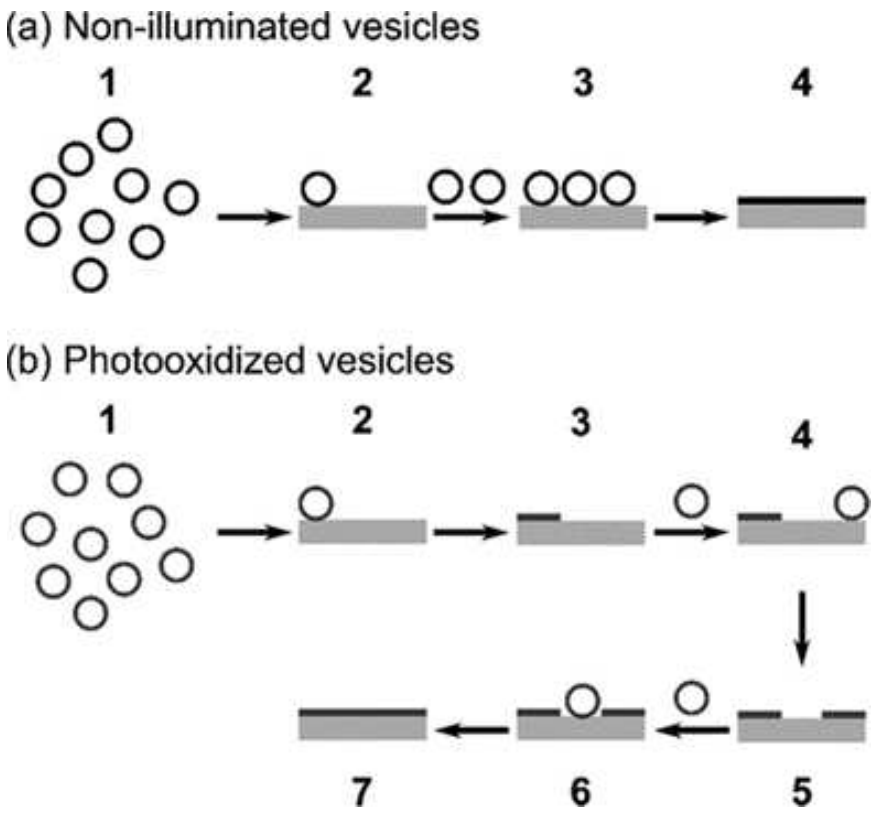

Figure 2.23. Schematic illustration of liposome rupture pathways. (a) Nonilluminated liposomes (a1) adsorb on the SiO_2 substrate (a2) until critical surface coverage is reached

(a3). Then, the rupture process commences resulting in the formation of a SLB (a4). (b) After illumination, photo-oxidized liposomes (b1) adsorb on the SiO_2 substrate (b2) and are able to rupture without the need for critical surface coverage (b3). This process continues (b4-b6) until a complete SLB is formed (b7).

The rupture of liposomes on a surface is driven largely by the stresses arising from liposome adhesion and deformation surpassing the cohesive intermolecular forces that maintain the closed-shell bilayer structure. Generally, for zwitterionic liposomes, such as DOPC, critical surface coverage of liposomes is required to initiate the rupture cascade. This process results in QCM-D signals that have a distinct minimum in the frequency signal and a distinct maximum in the dissipation signal. The liposome adsorption and then rupture process is shown above in Figure 2.23. Individual small liposomes can rupture upon contact with the substrate if liposome–substrate interactions give rise to significant adhesive forces. Such is the case for cationic liposomes on negatively-charged substrates, which display QCM-D responses similar to the illuminated and photo-oxidized liposomes that contain TF-PC.[24] An illustration of immediate liposome rupture upon adsorption is also shown in Figure 2.23. Alternatively, illumination of these liposomes could significantly reduce the cohesive energy of the membrane, making them much more likely to rupture. This is the more plausible scenario, as photosensitized lipid oxidation can permeabilize liposome bilayers, reduce their lysis tension, and induce membrane fusion.[59]

2.5 Materials and Methods

2.5.1 Preparation of Liposomes

DOPC, DiPhyPC, TF-PC, NBD-PC, NBD-PE, PazePC, and PoxnoPC were purchased from Avanti Polar Lipids. BODIPY-PE and Texas Red-DHPE were from Molecular Probes. Lipids dissolved in chloroform were mixed in glass vials with desired molar ratios to a final total lipid concentration of 1.0 mg mL^{-1}. To evaporate the chloroform, the lipid mixtures were placed under vacuum at room temperature for at least 4 h. The dry lipid films were rehydrated with phosphate buffered saline (PBS, pH 7.4) containing 10 mM phosphate, 137 mM NaCl, 2.7 mM KCl, and vortexed to suspend lipids. Aqueous lipid suspensions were sonicated using a bath sonicator (Branson 3510 Ultrasonic Cleaner) at room temperature for 10 min. The lipids were then passed through a 50 nm pore-size polycarbonate membrane filter 23 times inside a mini-extruder (Avanti). Concentrations of fluorescent lipid probes (TopFluor-PC, BODIPY-PE, NBD-PE, NBD-PC, and Texas Red-PE) in liposomes were 2 mol% unless stated otherwise.

Lipid films containing oxidized lipids (PazePC and PoxnoPC) were rehydrated with HEPES buffer (10 mM HEPES, 50 mM NaCl, pH 7.4). These liposomes were diluted to 0.10 mg mL^{-1} before QCM-D experiments in HEPES buffer (10 mM HEPES, 150 mM NaCl, pH 7.4). PazePC and PoxnoPC concentrations in liposomes were 20 mol%.

For studies including hexanoic acid, 25 mM, 50 mM, or 100 mM of hexanoic acid was included in HEPES buffer (10 mM HEPES, 150 mM NaCl, pH 7.4). Lipid films were rehydrated with this hexanoic acid-HEPES buffer, then extruded to 50 nm. Before injection into the QCM-D, liposome samples were diluted to 0.1 mg mL^{-1} in the hexanoic acid-HEPES buffer.

2.5.2 Collection of Spectra

Fluorescence excitation spectra were collected for all fluorescent lipid probes contained in DOPC liposomes using a Fluorolog TCSPC fluorometer (Horiba Scientific). The LED output spectrum was measured with an Ocean Optics FLAME Vis-NIR spectrometer.

2.5.3 Liposome Illumination

Liposomes were diluted to 0.10 mg mL^{-1} in PBS and placed inside a 15 mL conical tube prior to illumination. This tube was placed directly in front of a broadband visible LED light source (ACE, 15 W, model No. 3467875) and illuminated for designated durations. The output spectrum of the LED is shown in Figure 2.2. The illuminance of the LED was measured to be 3.75 x 10^5 lux using a visible light meter (DT-1308, NDT Supply, Inc.), placed 1 cm from the light source. The visible light meter was calibrated according to NIST standards prior to measurements. After illumination, the liposomes were immediately injected into the QCM-D.

For ambient illumination studies, liposome suspensions composed of DOPC or DOPC with 2 mol% TF-PC were placed in 15 mL conical tubes. Lipid concentrations were 0.10 mg mL^{-1} in PBS buffer. The tubes were placed inside a laboratory fume hood with the lights on continuously for 1, 3, or 6 days.

2.5.4 QCM-D Measurements

A QSense Explorer E1 QCM-D instrument (Biolin Scientific) was used for all QCM-D studies. Sensors for QCM-D studies were AT-cut SiO_2-coated quartz crystals (Biolin Scientific) with a fundamental frequency of 5 MHz. The internal temperature of

the QCM-D was held constant at 23.0 °C. Liposomes in PBS (with or without prior illumination) at a total lipid concentration of 0.10 mg mL^{-1} were injected into the QCM-D at a constant flow rate of 100 μL min^{-1}. Frequency and dissipation were monitored at the 1st, 3rd, 5th, 7th, 9th, and 11th overtones. The 3rd overtone is shown in all data here. To test the continuity of bilayers, a solution of 105 nM bovine serum albumin (BSA) in PBS was prepared and injected overtop normal and photo-oxidized DOPC/TF-PC SLBs. To determine the effects of DMSO exposure on the SLB formation, 0.10 mg mL^{-1} of DOPC liposomes were incubated with 0.60 vol % DMSO in PBS for 30 min and then injected into the QCM-D.

2.5.5 Lipid Monolayer Compression Isotherms

DOPC with 2 mol% TF-PC were dissolved in chloroform at a concentration of 1.0 mg/mL in clear glass test tubes. Some of the lipid solutions were exposed to broadband visible light with a LED source (ACE, 15 W, model no. 3467875) for 1 h, while others remained unilluminated. Chloroform lipid solutions were deposited atop a PBS subphase within a Langmuir trough (NIMA Technology Alternate layer Langmuir-Blodgett trough). Chloroform was allowed to evaporate for 1 min prior to monolayer compression. The monolayer was compressed at a rate of 15 cm^2 min^{-1} until collapse was observed.

2.5.6 FT-IR Spectroscopy

Two samples of DOPC and 2 mol% TF-PC lipids were dissolved in chloroform at a total lipid concentration of 5.0 mg mL^{-1} in individual clear glass test tubes. One sample was illuminated with a broadband visible LED light source (ACE, 15 W, model no.

3467875) for 1 h, while the other sample remained unilluminated. Samples were deposited on the Fourier transform infrared (FT-IR) crystal and the chloroform was allowed to evaporate. IR spectra (Thermo Scientific Nicolet iS10 FT-IR spectrometer with SMART iTR Nicolet iZ10 module) were collected for both samples.

2.5.7 Dynamic Light Scattering

Dynamic light scattering (DLS) measurements were collected using an ALV/CGS-3 Compact Goniometer System spectrometer. Liposome samples were diluted to 0.3 mg mL^{-1} in PBS buffer prior to DLS analysis.

2.5.8 Zeta Potential Analysis

Zeta potential measurements were collected using a ZetaPALS Zeta Potential Analyzer (Brookhaven Instruments Corporation). Liposome samples were diluted to 0.3 mg mL^{-1} in 10 mM NaCl prior to zeta potential analysis.

2.5.9 Fluorescence Microscopy

Liposomes composed of DOPC/2 mol% TF-PC were diluted to 0.1 mg mL^{-1} in PBS, then deposited on a glass coverslip. Prior to liposome deposition, the coverslips were cleaned in 2% (w/v) SDS solution, rinsed with MilliQ ultrapure H_2O (PureLab Classic UV, ELGA LabWater), dried under a stream of N_2, and then placed in a UV/Ozone ProCleaner Plus (BioForce Nanosciences) for 10 min. Liposomes were diluted to 0.1 mg mL^{-1}, then deposited onto the cleaned glass coverslips that were mounted in Attofluor imaging chambers (Thermo Fisher Scientific). The liposomes were incubated on the glass substrate

for 1 h, then rinsed with PBS buffer. In the case of illuminated liposomes, liposomes were placed in front of the LED light source for 30 min before being deposited on the glass coverslip. Fluorescence images were collected on an inverted microscope (Eclipse Ti, Nikon). Fluorescence was excited using an LED lamp source (Aura II, Lumencor) and captured with a 2048 x 2048-pixel sCMOS camera (Orca Flash 4.0 v2, Hamamatsu) controlled with the Nikon Elements software.

2.6 References

(1) Boveris, A. Mitochondrial Production of Superoxide Radical and Hydrogen Peroxide. In *Tissue Hypoxia and Ischemia*; Reivich, M., Coburn, R., Lahiri, S., Chance, B., Eds.; Advances in Experimental Medicine and Biology; Springer US: Boston, MA, 1977; pp 67–82.

(2) Boveris, A.; Oshino, N.; Chance, B. The Cellular Production of Hydrogen Peroxide. *Biochem. J.* **1972**, *128* (3), 617–630.

(3) Cao, S. S.; Kaufman, R. J. Endoplasmic Reticulum Stress and Oxidative Stress in Cell Fate Decision and Human Disease. *Antioxid. Redox Signal.* **2014**, *21* (3), 396–413.

(4) De Duve, C.; Baudhuin, P. Peroxisomes (Microbodies and Related Particles). *Physiol. Rev.* **1966**, *46* (2), 323–357.

(5) Corpas, F.; Gupta, D.; Palma, J. Production Sites of Reactive Oxygen Species (ROS) in Organelles from Plant Cells; 2015; pp 1–22.

(6) Aruoma, O. I. Free Radicals, Oxidative Stress, and Antioxidants in Human Health and Disease. *J. Am. Oil Chem. Soc.* **1998**, *75* (2), 199–212.

(7) Adibhatla, R. M.; Hatcher, J. F. Lipid Oxidation and Peroxidation in CNS Health and Disease: From Molecular Mechanisms to Therapeutic Opportunities. *Antioxid. Redox Signal.* **2010**, *12* (1), 125–169.

(8) Yang, W. S.; Stockwell, B. R. Ferroptosis: Death by Lipid Peroxidation. *Trends Cell Biol.* **2016**, *26* (3), 165–176.

(9) Jurkiewicz, P.; Olżyńska, A.; Cwiklik, L.; Conte, E.; Jungwirth, P.; Megli, F. M.; Hof, M. Biophysics of Lipid Bilayers Containing Oxidatively Modified Phospholipids: Insights from Fluorescence and EPR Experiments and from MD Simulations. *Biochim. Biophys. Acta BBA - Biomembr.* **2012**, *1818* (10), 2388–2402.

(10) Castellana, E. T.; Cremer, P. S. Solid Supported Lipid Bilayers: From Biophysical Studies to Sensor Design. *Surf. Sci. Rep.* **2006**, *61* (10), 429–444.

(11) Makky, A.; Tanaka, M. Impact of Lipid Oxidization on Biophysical Properties of Model Cell Membranes. *J. Phys. Chem. B* **2015**, *119* (18), 5857–5863.

(12) Brian, A. A.; McConnell, H. M. Allogeneic Stimulation of Cytotoxic T Cells by Supported Planar Membranes. *Proc. Natl. Acad. Sci.* **1984**, *81* (19), 6159–6163.

(13) Anderson, T. H.; Min, Y.; Weirich, K. L.; Zeng, H.; Fygenson, D.; Israelachvili, J. N. Formation of Supported Bilayers on Silica Substrates. *Langmuir* **2009**, *25* (12), 6997–7005.

(14) Reimhult, E.; Höök, F.; Kasemo, B. Intact Vesicle Adsorption and Supported Biomembrane Formation from Vesicles in Solution: Influence of Surface Chemistry, Vesicle Size, Temperature, and Osmotic Pressure. *Langmuir* **2003**, *19* (5), 1681–1691.

(15) Seantier, B.; Breffa, C.; Félix, O.; Decher, G. Dissipation-Enhanced Quartz Crystal Microbalance Studies on the Experimental Parameters Controlling the Formation of Supported Lipid Bilayers. *J. Phys. Chem. B* **2005**, *109* (46), 21755–21765.

(16) Rossetti, F. F.; Bally, M.; Michel, R.; Textor, M.; Reviakine, I. Interactions between Titanium Dioxide and Phosphatidyl Serine-Containing Liposomes: Formation and Patterning of Supported Phospholipid Bilayers on the Surface of a Medically Relevant Material. *Langmuir* **2005**, *21* (14), 6443–6450.

(17) Veatch, S. L.; Leung, S. S. W.; Hancock, R. E. W.; Thewalt, J. L. Fluorescent Probes Alter Miscibility Phase Boundaries in Ternary Vesicles. *J. Phys. Chem. B* **2007**, *111* (3), 502–504.

(18) Ayuyan, A. G.; Cohen, F. S. Lipid Peroxides Promote Large Rafts: Effects of Excitation of Probes in Fluorescence Microscopy and Electrochemical Reactions during Vesicle Formation. *Biophys. J.* **2006**, *91* (6), 2172–2183.

(19) Sezgin, E.; Chwastek, G.; Aydogan, G.; Levental, I.; Simons, K.; Schwille, P. Photoconversion of Bodipy-Labeled Lipid Analogues. *ChemBioChem* **2013**, *14* (6), 695–698.

(20) Najafinobar, N.; Lovrić, J.; Majdi, S.; Dunevall, J.; Cans, A.-S.; Ewing, A. Excited Fluorophores Enhance the Opening of Vesicles at Electrode Surfaces in Vesicle Electrochemical Cytometry. *Angew. Chem. Int. Ed.* **2016**, *55* (48), 15081–15085.

(21) Zhu, T. F.; Adamala, K.; Zhang, N.; Szostak, J. W. Photochemically Driven Redox Chemistry Induces Protocell Membrane Pearling and Division. *Proc. Natl. Acad. Sci.* **2012**, *109* (25), 9828–9832.

(22) Cho, N.-J.; Frank, C. W.; Kasemo, B.; Höök, F. Quartz Crystal Microbalance with Dissipation Monitoring of Supported Lipid Bilayers on Various Substrates. *Nat. Protoc.* **2010**, *5* (6), 1096–1106.

(23) Keller, C. A.; Kasemo, B. Surface Specific Kinetics of Lipid Vesicle Adsorption Measured with a Quartz Crystal Microbalance. *Biophys. J.* **1998**, *75* (3), 1397–1402.

(24) Cho, N.-J.; Frank, C. W.; Kasemo, B.; Höök, F. Quartz Crystal Microbalance with Dissipation Monitoring of Supported Lipid Bilayers on Various Substrates. *Nat. Protoc.* **2010**, *5* (6), 1096–1106.

(25) Richter, R.; Mukhopadhyay, A.; Brisson, A. Pathways of Lipid Vesicle Deposition on Solid Surfaces: A Combined QCM-D and AFM Study. *Biophys. J.* **2003**, *85* (5), 3035–3047.

(26) Jackman, J. A.; Choi, J.-H.; Zhdanov, V. P.; Cho, N.-J. Influence of Osmotic Pressure on Adhesion of Lipid Vesicles to Solid Supports. *Langmuir* **2013**, *29* (36), 11375–11384.

(27) Kay, J. G.; Koivusalo, M.; Ma, X.; Wohland, T.; Grinstein, S. Phosphatidylserine Dynamics in Cellular Membranes. *Mol. Biol. Cell* **2012**, *23* (11), 2198–2212.

(28) Shirey, C. M.; Ward, K. E.; Stahelin, R. V. Investigation of the Biophysical Properties of a Fluorescently Modified Ceramide-1-Phosphate. *Chem. Phys. Lipids* **2016**, *200*, 32–41.

(29) Baird, C. L.; Courtenay, E. S.; Myszka, D. G. Surface Plasmon Resonance Characterization of Drug/Liposome Interactions. *Anal. Biochem.* **2002**, *310* (1), 93–99.

(30) Jackman, J. A.; Kim, M. C.; Zhdanov, V. P.; Cho, N.-J. Relationship between Vesicle Size and Steric Hindrance Influences Vesicle Rupture on Solid Supports. *Phys. Chem. Chem. Phys.* **2016**, *18* (4), 3065–3072.

(31) Sauerbrey, G. Verwendung von Schwingquarzen zur Wägung dünner Schichten und zur Mikrowägung. *Z. Für Phys.* **1959**, *155* (2), 206–222.

(32) Reviakine, I.; Johannsmann, D.; Richter, R. P. Hearing What You Cannot See and Visualizing What You Hear: Interpreting Quartz Crystal Microbalance Data from Solvated Interfaces. *Anal. Chem.* **2011**, *83* (23), 8838–8848.

(33) Khandelia, H.; Mouritsen, O. G. Lipid Gymnastics: Evidence of Complete Acyl Chain Reversal in Oxidized Phospholipids from Molecular Simulations. *Biophys. J.* **2009**, *96* (7), 2734–2743.

(34) Chattopadhyay, A.; London, E. Parallax Method for Direct Measurement of Membrane Penetration Depth Utilizing Fluorescence Quenching by Spin-Labeled Phospholipids. *Biochemistry* **1987**, *26* (1), 39–45.

(35) Awuah, S. G.; You, Y. Boron Dipyrromethene (BODIPY)-Based Photosensitizers for Photodynamic Therapy. *RSC Adv.* **2012**, *2* (30), 11169–11183.

(36) Volinsky, R.; Cwiklik, L.; Jurkiewicz, P.; Hof, M.; Jungwirth, P.; Kinnunen, P. K. J. Oxidized Phosphatidylcholines Facilitate Phospholipid Flip-Flop in Liposomes. *Biophys. J.* **2011**, *101* (6), 1376–1384.

(37) Boonnoy, P.; Jarerattanachat, V.; Karttunen, M.; Wong-ekkabut, J. Bilayer Deformation, Pores, and Micellation Induced by Oxidized Lipids. *J. Phys. Chem. Lett.* **2015**, *6* (24), 4884–4888.

(38) Hughes, Z. E.; Mark, A. E.; Mancera, R. L. Molecular Dynamics Simulations of the Interactions of DMSO with DPPC and DOPC Phospholipid Membranes. *J. Phys. Chem. B* **2012**, *116* (39), 11911–11923.

(39) Redwood, W. R.; Pfeiffer, F. R.; Weisbach, J. A.; Thompson, T. E. Physical Properties of Bilayer Membranes Formed from a Synthetic Saturated Phospholipid in N-Decane. *Biochim. Biophys. Acta BBA - Biomembr.* **1971**, *233* (1), 1–6.

(40) Lindsey, H.; Petersen, N. O.; Chan, S. I. Physicochemical Characterization of 1,2-Diphytanoyl-Sn-Glycero-3-Phosphocholine in Model Membrane Systems. *Biochim. Biophys. Acta BBA - Biomembr.* **1979**, *555* (1), 147–167.

(41) Tristram-Nagle, S.; Kim, D. J.; Akhunzada, N.; Kučerka, N.; Mathai, J. C.; Katsaras, J.; Zeidel, M.; Nagle, J. F. Structure and Water Permeability of Fully Hydrated DiphytanoylPC. *Chem. Phys. Lipids* **2010**, *163* (6), 630–637.

(42) Hayyan, M.; Hashim, M. A.; AlNashef, I. M. Superoxide Ion: Generation and Chemical Implications. *Chem. Rev.* **2016**, *116* (5), 3029–3085.

(43) Yin, H.; Xu, L.; Porter, N. A. Free Radical Lipid Peroxidation: Mechanisms and Analysis. *Chem. Rev.* **2011**, *111* (10), 5944–5972.

(44) Wang, X.; Quinn, P. J. Vitamin E and Its Function in Membranes. *Prog. Lipid Res.* **1999**, *38* (4), 309–336.

(45) Lucero, A.; Rodríguez Niño, M. R.; Gunning, A. P.; Morris, V. J.; Wilde, P. J.; Rodríguez Patino, J. M. Effect of Hydrocarbon Chain and PH on Structural and Topographical Characteristics of Phospholipid Monolayers. *J. Phys. Chem. B* **2008**, *112* (25), 7651–7661.

(46) Guzmán, E.; Liggieri, L.; Santini, E.; Ferrari, M.; Ravera, F. DPPC–DOPC Langmuir Monolayers Modified by Hydrophilic Silica Nanoparticles: Phase Behaviour, Structure and Rheology. *Colloids Surf. Physicochem. Eng. Asp.* **2012**, *413*, 174–183.

(47) Zheng, Q.; Jockusch, S.; Zhou, Z.; Blanchard, S. C. The Contribution of Reactive Oxygen Species to the Photobleaching of Organic Fluorophores. *Photochem. Photobiol.* **2014**, *90* (2), 448–454.

(48) Pavia, D. L.; Lampman, G. M.; Kriz, G. S.; Vyvyan, J. R. *Introduction to Spectroscopy*, 5th Edition.; Cengage Learning: Stamford, CT, 2015.

(49) Mosca, M.; Ceglie, A.; Ambrosone, L. Effect of Membrane Composition on Lipid Oxidation in Liposomes. *Chem. Phys. Lipids* **2011**, *164* (2), 158–165.

(50) Melcrová, A.; Pokorna, S.; Pullanchery, S.; Kohagen, M.; Jurkiewicz, P.; Hof, M.; Jungwirth, P.; Cremer, P. S.; Cwiklik, L. The Complex Nature of Calcium Cation Interactions with Phospholipid Bilayers. *Sci. Rep.* **2016**, *6* (1), 38035.

(51) Runas, K. A.; Acharya, S. J.; Schmidt, J. J.; Malmstadt, N. Addition of Cleaved Tail Fragments during Lipid Oxidation Stabilizes Membrane Permeability Behavior. *Langmuir* **2016**, *32* (3), 779–786.

(52) Gardner, H. W.; Plattner, R. D. Linoleate Hydroperoxides Are Cleaved Heterolytically into Aldehydes by a Lewis Acid in Aprotic Solvent. *Lipids* **1984**, *19* (4), 294–299.

(53) Runas, K. A.; Malmstadt, N. Low Levels of Lipid Oxidation Radically Increase the Passive Permeability of Lipid Bilayers. *Soft Matter* **2014**, *11* (3), 499–505.

(54) Ulrich, G.; Ziessel, R.; Harriman, A. The Chemistry of Fluorescent Bodipy Dyes: Versatility Unsurpassed. *Angew. Chem. Int. Ed.* **2008**, *47* (7), 1184–1201.

(55) Baier, J.; Maier, M.; Engl, R.; Landthaler, M.; Bäumler, W. Time-Resolved Investigations of Singlet Oxygen Luminescence in Water, in Phosphatidylcholine, and in Aqueous Suspensions of Phosphatidylcholine or HT29 Cells. *J. Phys. Chem. B* **2005**, *109* (7), 3041–3046.

(56) Fischkoff, S.; Vanderkooi, J. M. Oxygen Diffusion in Biological and Artificial Membranes Determined by the Fluorochrome Pyrene. *J. Gen. Physiol.* **1975**, *65* (5), 663–676.

(57) St-Denis, C. E.; Fell, C. J. D. Diffusivity of Oxygen in Water. *Can. J. Chem. Eng.* **1971**, *49* (6), 885–885.

(58) Kučerka, N.; Nieh, M.-P.; Katsaras, J. Fluid Phase Lipid Areas and Bilayer Thicknesses of Commonly Used Phosphatidylcholines as a Function of Temperature. *Biochim. Biophys. Acta BBA - Biomembr.* **2011**, *1808* (11), 2761–2771.

(59) Heuvingh, J.; Bonneau, S. Asymmetric Oxidation of Giant Vesicles Triggers Curvature-Associated Shape Transition and Permeabilization. *Biophys. J.* **2009**, *97* (11), 2904–2912.

Chapter 3: Tubulation of Supported Lipid Bilayer Membranes Induced by Photosensitized Lipid Oxidation

3.1 Abstract

O_2 is a necessary molecule for many living organisms to undergo metabolic processes. A side effect of these metabolic processes is the production of reactive oxygen species (ROS). Though the cell contains machinery to help regulate the concentration of ROS, a buildup of ROS can be extremely harmful and begin to damage the lipids comprising the cell membrane. In this chapter, I show that photosensitized phospholipid oxidation, initiated by the lipid-conjugated fluorophore TopFluor-PC (TF-PC), causes defects, namely, membrane tubes and vesicle-like structures, in supported lipid bilayers (SLBs). Lipid oxidation is detrimental to the integrity of the lipid molecules; when oxidized, they undergo a conformational expansion, which causes membrane tubes to protrude from the SLB. Upon growing to a critical length, the membrane tubes arising from SLBs rapidly undergo a transition to vesicle-like structures. There is a correlation between the maximum tube length and the diameter of the resulting vesicle, suggesting the conservation of the surface area between these features. I use geometric modeling and the measured tube length and vesicle radius to calculate the tube radius; the calculated mean tube diameter of 243 nm is comparable to other groups' experimental findings. In the presence of fluid flow, membrane tubes can be extended to tens to hundreds of microns in length. I also show that the addition of divalent cations, such as Ca^{2+} and Mg^{2+}, inhibits oxidation-triggered membrane tubulation. SLBs composed of saturated lipids resist light-

induced tubulation, and the inclusion of the lipophilic antioxidant α-tocopherol attenuates the tubulation process and increases the light intensity threshold required for tubulation.

3.2 Introduction

Lipid bilayer membranes are abundant in nature, as they comprise the boundary of cells and organelles. These membranes are flexible, quasi-two-dimensional fluids, existing in a state which allows for lipid mixing and lateral diffusion within each leaflet of the bilayer.[1] With such flexibility comes the ability for a membrane to bend.[2] Membranes of cells and organelles frequency adopt highly-curved conformations throughout the course of cellular processes, such as cell division or exocytosis, among others.[3–5] Additionally, some proteins, such as dynamin, can induce membrane curvature and tubulation.[6–8]

These are not the only causes of membrane conformational changes, however; lipids—particularly unsaturated ones—are susceptible to oxidation via reactive oxygen species (ROS). This attack of ROS on lipid tails induces conformational changes on phospholipids and, in turn, on the conformation of lipid membranes.[9,10] Living organisms use O_2 to perform many metabolic processes, but in using O_2, ROS, such as peroxide, superoxide, hydroxyl radical, and singlet oxygen, can be produced.[11]

Lipid oxidation primarily occurs when ROS react with a site of unsaturation within the lipid tail, abstracting a hydrogen atom at the double bond.[12,13] There are a variety of mechanisms by which lipid oxidation can occur, and the mechanism can vary depending upon the number of sites of unsaturation in the lipid tail as well as on the exact ROS that is acting as the oxidizing agent. When ROS attack the unsaturated lipid tail, it often leads to fragmentation of the lipid molecule, creating oxidation products, such as lipid peroxides,

aldehydes, and carboxylic acids.[14–17] These oxidized lipids cause a number of structural changes to the lipid bilayer and can even alter the function of membrane proteins.[18] Some of the consequences of lipid oxidation are an increase in the area per lipid molecule that causes lateral membrane expansion, decrease in the lipid order, decreased membrane thickness, increased membrane permeability, increased lipid mobility, and increased lipid flip-flop.[19] Studies have also shown the induction of highly curved membrane structures, such as buds or tubes, upon lipid oxidation.[20]

Discussed in this section is lipid oxidation, initiated by the membrane-linked photosensitizer TopFluor-PC (TF-PC),[21] which causes the tubulation of SLBs. Photo-oxidation occurs when a photosensitizer is excited, creating reactive species that attack the surrounding lipids; photodynamic therapy exploits this process and has become an approved cancer treatment method in recent years.[22,23] Unlike GUVs, which are capable of inward or outward tubulation,[24] SLBs can only tubulate outward due to the presence of an underlying substrate. In this regard, SLBs are perhaps a better mimic for cellular membranes where the inward membrane tubulation may be inhibited by cytoskeletal elements.

The membrane tubes that are observed in this chapter grow away from the substrate until they abruptly retract to form round, liposome-like structures. The membrane tube lengths and the corresponding liposome sizes are correlated with one another, which suggests that there is a conservation of the membrane area during the tube-to-liposome transition. The conservation of the surface area allows me to calculate the membrane tube diameter, which is 243 nm on average. I also show that membrane tubes can be extended to tens of microns in length by hydrodynamic forces.

My work here focuses on the characterization of membrane tubes that erupt from SLBs upon photosensitized oxidation, as well as the factors that modulate tubulation, such as lipid unsaturation, antioxidants, and illumination intensity. My approach has the potential to enable studies where localized membrane oxidation and curvature are generated with a focused optical stimulus to investigate the interplay between lipid oxidation, membrane curvature, and biomolecular (e.g., lipid–protein) interactions.

3.3 Results and Discussion

3.3.1 TF-PC Causes Membrane Tubulation

The structures of the phospholipids and fluorescent lipid probes that were used in the following experiments are shown in Figure 3.1.

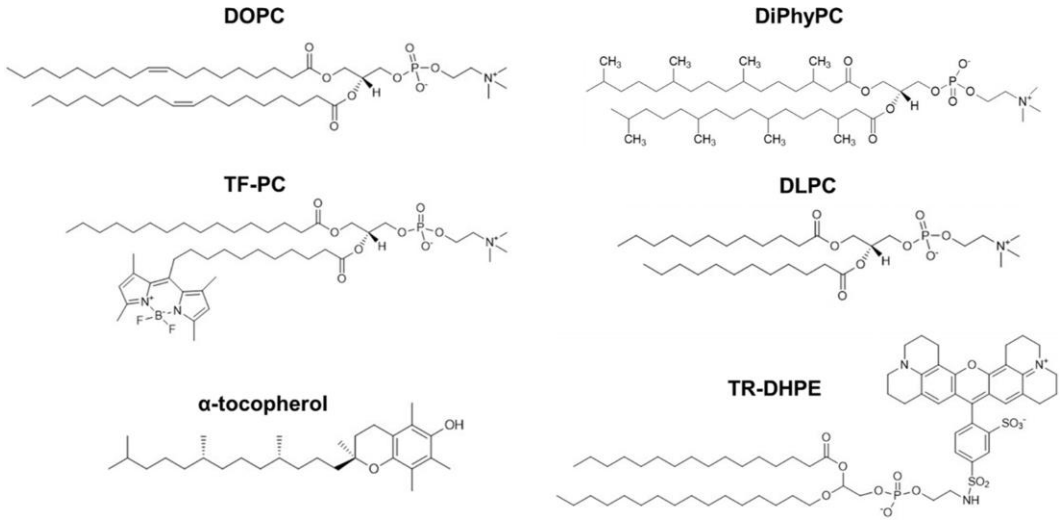

Figure 3.1. Structures of the phospholipids, fluorescently-conjugated lipids, and α-tocopherol used in this study.

Fluorescence microscopy was used to observe the light-triggered tubulation and vesiculation of a planar SLB composed of DOPC and 2 mol% TF-PC (Figure 3.2). After the formation of the SLB atop a glass coverslip in an imaging chamber, the samples were mounted on a microscope. The excitation of TF-PC was initiated using the microscope's LED light source. Upon illumination and observation of the sample, small defects began to form across the SLB. The defects began as small bright spots, then fluorescent tubes eventually formed across the bilayer. The tubes grew as time progressed and they fluctuated in space, indicating that tubes were attached only at one end. After the passage of time with continuous illumination, most tubes transitioned to round vesicle-like structures. Before transitioning into the spherical structures, some of the tubules appear to become self-entangled. Other groups have reported similar phenomena of tubule formation across a SLB followed by budding.[25,26]

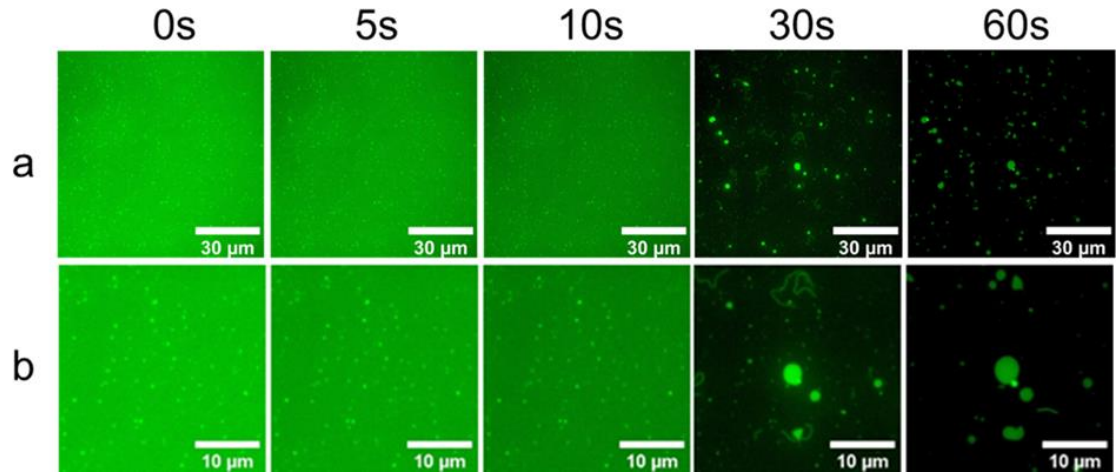

Figure 3.2. Fluorescence micrographs of DOPC/TF-PC SLBs. Large area (a) and zoomed-in (b) fluorescence micrographs of the processes of SLB tubulation and vesiculation of a membrane composed of DOPC and 2 mol% TF-PC.

During the tubulation and vesiculation processes, the background intensity decreases while the tubes and liposomes remain relatively bright. This is due to image intensity scaling factors, photobleaching, and the potential redistribution of TF-PC to the tubular and vesicular structures. Photobleaching is a result of photo-induced oxidation reactions,[27] and the structural changes of the lipids in the membrane associated with these reactions may also contribute a to the overall increase in the area-per-molecule, as was discussed in the last chapter of this dissertation, in the Langmuir trough section (Figure 2.20).

I also probed lower concentrations of TF-PC by forming SLBs containing 1 and 0.5 mol% TF-PC (Figure 3.3). Tubules grew across the surface in the SLB with 1 mol % TF-PC, though they were slightly less abundant than the tubes that formed across the 2 mol % TF-PC SLBs. However, no tubules or vesicular structures formed across the SLB containing only 0.5 mol % TF-PC, suggesting this tubulation process is dependent upon the concentration of the photosensitizing fluorophore in order for enough ROS to be generated to have a deformative effect across the SLB surface.

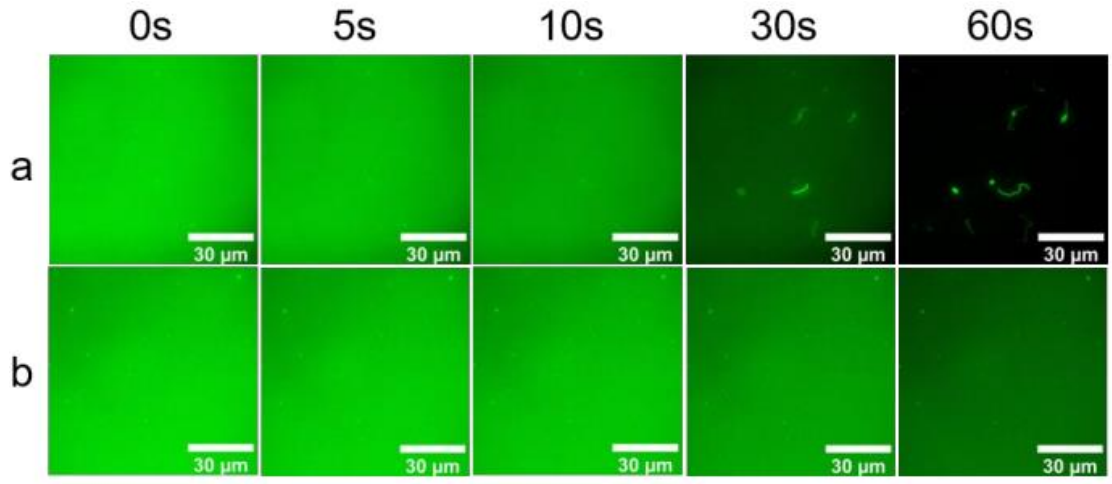

Figure 3.3. Tubulation is reduced by lower concentration of fluorophore. A SLB formed from (a) DOPC/1 mol% TF-PC and (b) DOPC/0.5 mol% TF-PC.

3.3.2 Attenuation of Membrane Tubulation

The tubulation of SLBs composed of DOPC and TF-PC could be due to lipid oxidation, where TF-PC is acting as a photosensitizer to generate ROS, which in turn oxidizes DOPC tail groups and causes an increase in the area per molecule. To investigate this further, I formed SLBs composed of DLPC and 2 mol% TF-PC. DLPC is a fully saturated straight-chain lipid lacking oxidizable carbon-carbon double bonds (Figure 3.1), allowing me to probe the relationship between tubulation and the propensity for the lipid to be oxidized. Figure 3.4a shows that no membrane tubulation is observed across a SLB of this composition.

To test a second saturated lipid, I formed a SLB with DiPhyPC and 2% TF-PC. DiPhyPC has fully saturated, branched tail groups (Figure 3.1) and a phase transition temperature below -120 °C.[28] It also has a bilayer thickness that is similar to DOPC.[29] Figure 3.4b shows that no membrane tubulation is observed when the SLB is composed of DiPhyPC and 2 mol% TF-PC. The studies with DLPC and DiPhyPC show that lipid unsaturation is required for SLB tubulation.

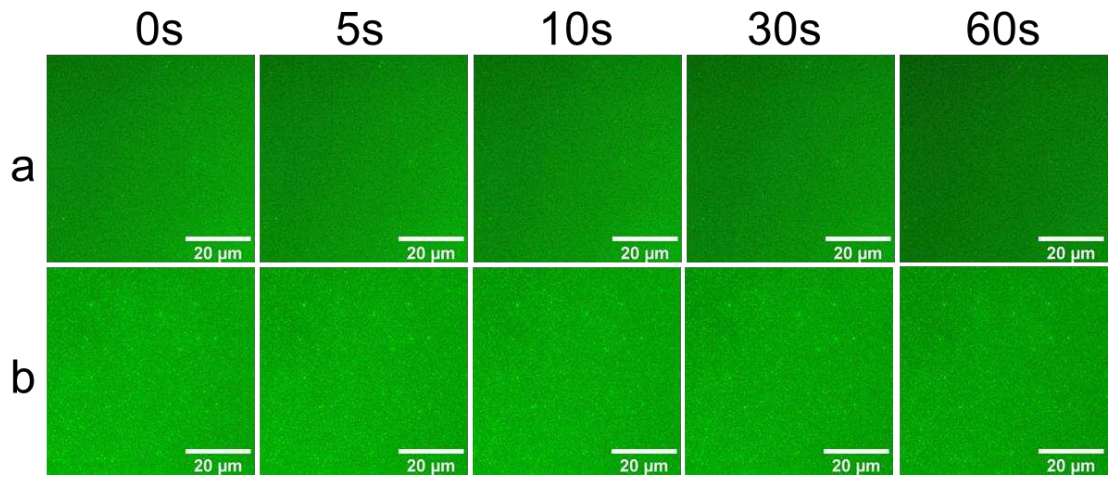

Figure 3.4. Tubulation is inhibited by saturated lipids. A SLB formed from (a) DLPC/2 mol% TF-PC and (b) DiPhyPC/2 mol%TF-PC.

Below, Figure 3.5 shows an analogous SLB that was composed of DOPC and 2% TR-DHPE. Over the course of 60 s, no tubular or vesicular structures were observed. In my previous chapter, I observed that illuminated liposomes composed of DOPC and 2 mol% TR-DHPE ruptured on SiO_2 surfaces similarly to the same liposomes that had not been illuminated (Figure 2.15e,f), suggesting that TR-DHPE is an ineffective photosensitizer for lipid oxidation, at least at the 2 mol% level.[21] Thus, the lack of light-triggered membrane tubulation in SLBs containing TR-DHPE agrees with my earlier conclusions that TR-DHPE is not an effective photosensitizer.

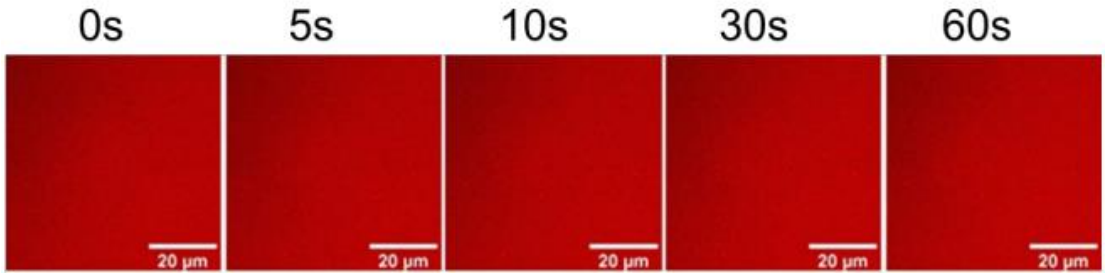

Figure 3.5. Tubulation is inhibited by a non-sensitizer fluorophore. A SLB formed from DOPC/2 mol% TR-DHPE.

Next, I examined the effect of an antioxidant, α-tocopherol, on membrane tubulation. When 2 mol% of α-tocopherol was incorporated into the SLB, the tubulation process is significantly attenuated (Figure 3.6). Not only is there a significant delay in the start of the tubulation process, the tubes that do form are generally not as long as those that form from DOPC/2 mol% TF-PC SLBs that lack an antioxidant. Also, there are fewer tube-to-vesicle transitions observed in SLBs that contain α-tocopherol.

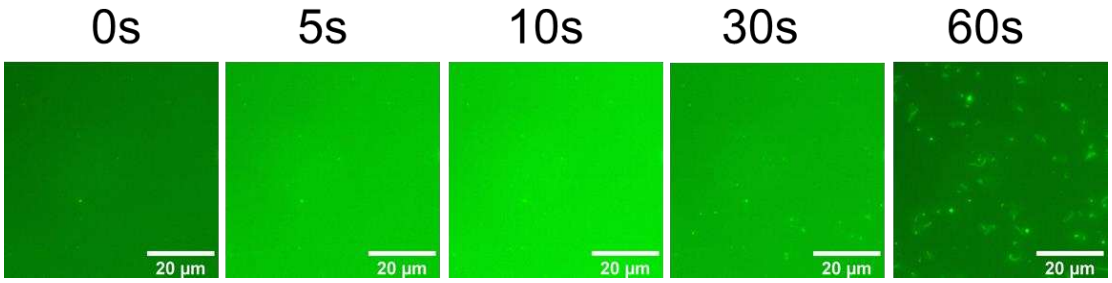

Figure 3.6. Tubulation is attenuated by an antioxidant. A SLB formed from DOPC/2 mol% TF-PC/2 mol% α-tocopherol.

The fact that no tubulation is observed when the SLB is composed of DLPC or DiPhyPC and it is attenuated in the presence of an antioxidant again points to lipid oxidation as the primary cause of membrane tubulation.

3.3.3 Correlation of Power Intensity and Lag Time of Membrane Tubules

I determined the relationship between excitation power and the lag time prior to the initiation of tube growth. The lag time is defined as the time between the initiation of illumination to the appearance of the first membrane tube. For both DOPC/2 mol% TF-PC SLBs with and without α-tocopherol, the lag time decreased as a function of excitation power (Figure 3.7). For all powers examined, DOPC/2 mol% TF-PC SLBs eventually tubulated. However, there was a threshold power of 51 mW to initiate the tubulation of the SLBs that contained 2 mol% α-tocopherol. These experiments were conducted for 90 s; at a power or 51 mW or lower, no tubes or liposome defects appeared across the SLB within this time frame. Furthermore, for immediate tubulation (lag time = 0 s), the threshold was 75 mW for DOPC/2 mol% TF-PC and 100 mW for DOPC/2 mol% TF-PC/2 mol% α-tocopherol.

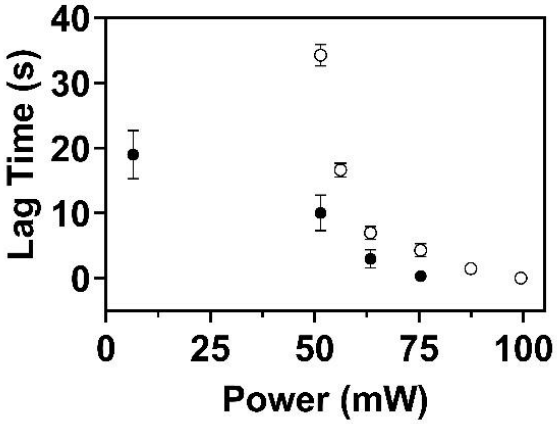

Figure 3.7. Light power dependence of SLB tubulation. The lag time of the first moment of tube formation across the DOPC/2 mol% TF-PC (solid circles) and DOPC/2 mol% TF-PC/2 mol% α-tocopherol (open circles) SLB as a function of microscope LED power. Error bars represent standard deviations.

Because the conditions that cause membrane tubulation cause an increase in the area-per-molecule and an increase in the IR absorbance of the C=O stretch, as discussed in the previous chapter of this dissertation (Figure 2.21), and the presence of saturated lipids eliminates membrane tubulation (Figure 3.4), my experiments point to lipid oxidation as the driving force for membrane tubulation. This is also supported by my observations that an antioxidant attenuates membrane tubulation (Figure 3.6). Lipid peroxidation occurs when ROS attacks the double bond in the acyl chain and forms a lipid radical, which can react and oxidize the surrounding lipids; this peroxidation process continues (known as "propagation") until all lipids have been oxidized.[30]

The role of an antioxidant is to react with the radical species,[31] and thereby being oxidized instead, which interrupts the propagation step of the lipid oxidation mechanism. Tocopherols, specifically, act as free-radical scavengers and H donors to the lipid radical, helping to minimize the oxidative damage to the membrane.[32–35] In my system, this means that α-tocopherol is being oxidized rather than the DOPC lipid tails.

At the concentration of α-tocopherol I worked with (2 mol%), there was still tubule formation, indicating that the antioxidant was not in excess and therefore lipid tails were still targeted by excess ROS. However, the longer lag time and necessity for a higher power of illumination to induce tubulation when α-tocopherol is present indicate that it takes longer for there to be pronounced oxidative damage of the lipid tails that leads to the

tubulation I observe. The fact that an antioxidant attenuated the effects I observe is further indication that lipid oxidation is the prime factor causing the membrane tubulation.

3.3.4 Tube-to-Liposome Transitions

As shown earlier in Figure 3.2, most of the membrane tubes that grow from DOPC/2 mol% TF-PC SLBs eventually transition into vesicular structures. I measured the length of individual tubes just prior to vesiculation, then measured the diameter of the resulting liposomes immediately after vesiculation. The distribution of tube lengths just prior to vesiculation is shown below in Figure 3.8a. The tubes ranged in length from approximately 2.0 to 23 μm, with a mean length of 6.7 ± 3.4 μm (mean ± s.d.). The resulting vesicular structures ranged in diameter from less than 1.0 μm to 3.0 μm, with a mean diameter of 1.3 ± 0.4 μm (mean ± s.d.) (Figure 3.8b).

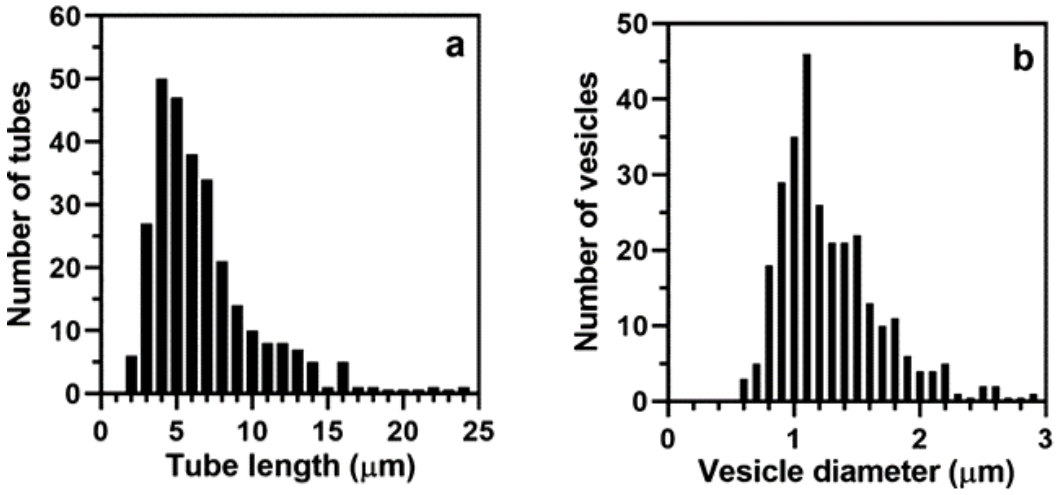

Figure 3.8. Membrane tube length and vesicle size distributions. (a) Distribution of tube lengths immediately prior to their vesiculation. (b) Distribution of vesicle diameters immediately after vesiculation.

For these experiments, images were recorded at a frame rate of 5 Hz. The vesiculation process occurred quickly, with many tube-to-liposome transitions occurring during the delay between frame acquisitions, that is, faster than 200 ms. A plot of liposome diameter versus tube length (Figure 3.9a) shows that longer tubes tend to transform into larger liposomes. The correlation between tube length and liposome diameter suggests that the surface area is conserved during the tube-to-liposome transition process. If there is a conservation of the surface area between tubes and vesicular structures, it is possible to use geometric representations of the tubes and liposomes to calculate the tube diameter.

To calculate the diameter of the tubes, I made several assumptions: first, that the surface areas of the tube just prior to transition and the corresponding liposome immediately after transition were conserved; second, that the tube and vesicular structures were unilamellar; and third, that the geometric shape of the tube is a cylinder with a hemispherical cap, while the shape of a vesicle is a sphere. Using these assumptions, and setting the surface area of the tube equal to the surface area of the corresponding vesicle, the following equation could be used to calculate the radius of an individual tube:

$$4\pi r_v^2 = 2\pi r_t L_t + 2\pi r_t^2 \qquad \text{(eq 3.1)}$$

where r_v is the measured radius of the liposome, L_t is the measured length of the tube, and r_t is the radius of the tube. Rearranging eq 3.1 gives a quadratic equation in which r_t can be solved for.

$$r_t^2 + L_t r_t - 2r_v^2 = 0 \qquad \text{(eq 3.2)}$$

Using this equation and the measured values of L_t and r_v, the radius of the membrane tubes can be calculated (which I plotted as diameters). The distribution of these calculated diameters is shown below in Figure 3.9b. The mean (± s.d.) was found to be 243 ± 67 nm, with a range of 105–745 nm.

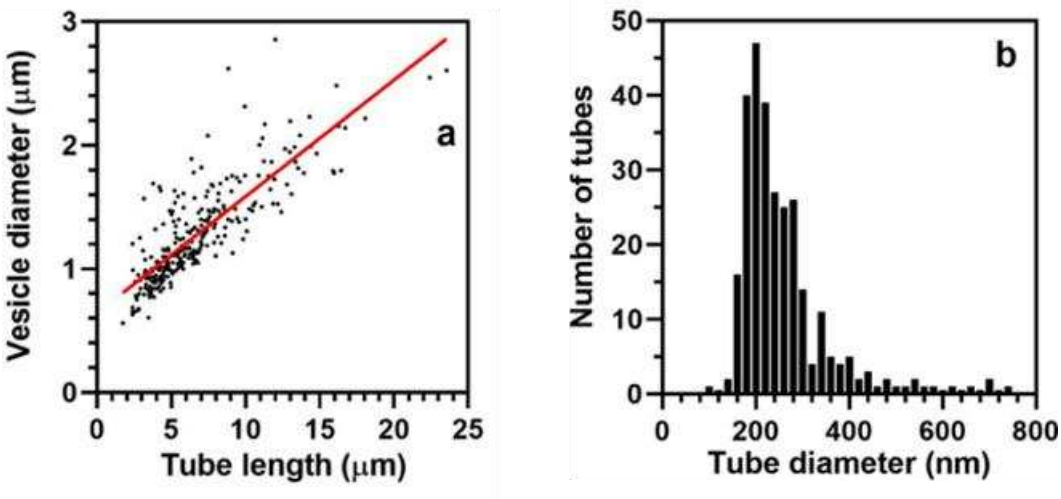

Figure 3.9. Tube-to-vesicle transitions. (a) Correlation between the maximum tube length (just prior to vesiculation) and the corresponding vesicle diameter (immediately after vesiculation). (b) Distribution of the tube diameter calculated from the conservation of the surface area between tubes and the corresponding liposomes using eq 3.2.

The mean tube diameter is in good agreement with membrane tubes measured in natural and synthetic systems. For example, in an early work on cell membrane mechanics, Hochmuth and co-workers determined that membrane tubes pulled from the red blood cells by hydrodynamic shear forces had diameters in the 100–200 nm range.[36] Tunneling nanotubes with diameters between 50 and 200 nm have been observed between a variety

of different cell types.[37,38] In synthetic lipid nanotube-vesicle networks, the connecting tubes were estimated to be 100–200 nm in diameter,[39–41] and tethers pulled from GUVs are also typically in this size range or slightly smaller.[42,43] Membrane tubes resulting from the lysis of spreading multilamellar liposomes have diameters estimated to be in the 100–200 nm range.[44] In experiments with SLBs, tubes of less than 250 nm in diameter could be induced by the adsorption of antimicrobial peptides.[45]

3.3.5 Tube and Liposome Growth Dynamics

The growth rate of membrane tubes and their corresponding liposomes was determined by measuring the change in length (tubes) or diameter (vesicles) as a function of time. Figure 3.10a shows that the membrane tubes extended at roughly a constant rate over the first 5 s of their existence, but then their extension rate slowed in a roughly linear fashion until they transitioned to vesicles. Similarly, after vesicles formed, they grew over time, then their growth rate declined with the passage of time (Figure 3.10b).

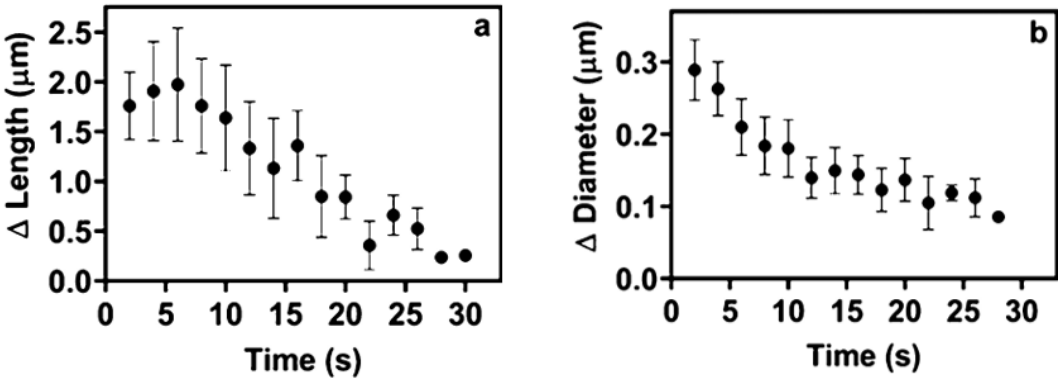

Figure 3.10. Rate of tube length and vesicle diameter growth. Progression of the changes in the (a) tube length and (b) vesicle diameter for a DOPC/2 mol% TF-PC SLB as a function of time. Error bars are the standard deviation.

The nonlinear decline in the vesicle diameter growth rate as a function of time suggests that the vesicle surface area growth rate may be constant as a function of time.

3.3.6 Tube Extension in Flow

In stagnant solutions, the membrane tubes I observed transitioned to vesicular structures when the tubes reached a mean length of 6.7 μm. They also fluctuated randomly in space. To determine if the tubes could be elongated in a prescribed direction by hydrodynamic forces, I carried out photo-oxidation experiments in the presence of flow using a microfluidic channel that was 400 μm wide and 50 μm high. A SLB composed of DOPC/2 mol% TF-PC was formed on the glass substrate, then flow was initiated with a volume flow rate of 1 μL min^{-1}, which corresponds to a linear flow velocity of 833 μm s^{-1}. Under these conditions, membrane tubes could be extended to lengths that greatly exceeded those observed in stagnant solutions, up to hundreds of μm in length (Figure 3.11).

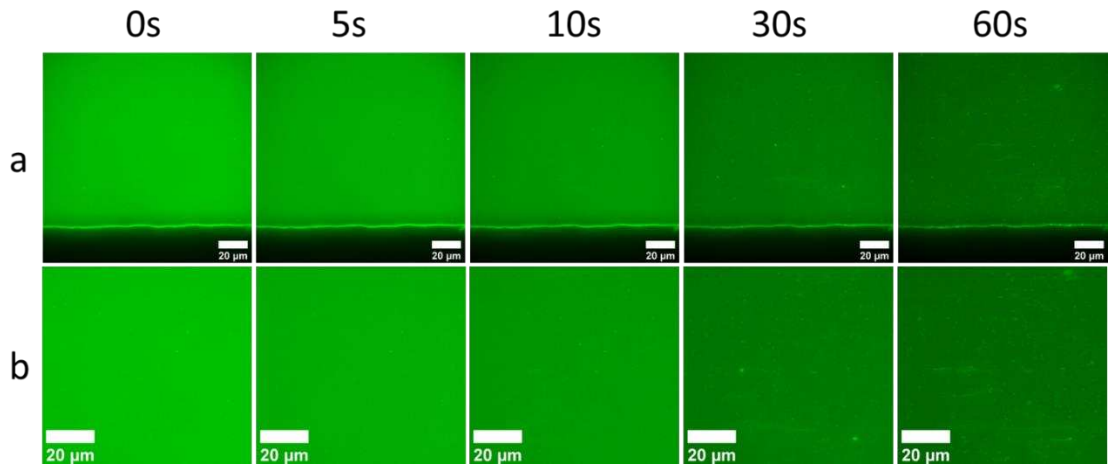

Figure 3.11. Membrane tubules extend under flow. Large area (a) and zoomed-in (b) fluorescence micrographs of the processes of SLB tubulation and vesiculation of a membrane composed of DOPC and 2 mol% TF-PC under flow.

Additionally, fewer tubes transitioned to liposomes in the presence of flow. Therefore, the drag force on the membrane tube due to the flowing liquid is more than enough to counterbalance the retraction force that drives tube vesiculation. Other groups have observed flow-driven membrane tube extension.[46–48] Notably, Pucadyil and co-workers used the flow to produce long tubes from surface-immobilized giant vesicles and used the tubes to investigate membrane scission by the protein dynamin.[49] While I did not undertake studies of lipid–protein interactions, my approach to generate extended membrane tubes could provide a unique platform to probe the interplay between the lipid oxidative state, membrane curvature, and curvature-dependent protein–lipid interactions.

3.3.7 The Effects of Divalent Cations on Membrane Tubulation

Ca^{2+} ions play an important role in biology as a signaling molecule as well as helping maintain the electrical homeostasis across cell membranes; therefore, the

concentration of Ca^{2+} is tightly controlled and regulated within cells.[50,51] Because of the importance of Ca^{2+} and other divalent cations like Mg^{2+} in cellular processes, I explored the effects of divalent cations on oxidation-triggered membrane tubulation. In these experiments, SLBs composed of DOPC/2 mol% TF-PC were formed in a HEPES buffer containing 10 mM of either Ca^{2+}, Mg^{2+}, or Sr^{2+}. Samples were washed with this buffer as well.

Illumination of SLBs in the presence of Ca^{2+} inhibited the tubulation process entirely, and instead caused vesicular blisters to form across the SLB (Figure 3.12a). Mg^{2+} did not have nearly as a pronounced effect as Ca^{2+}, but it still attenuated the tubulation process. Some tubes still formed across the SLB surface in the presence of Mg^{2+} (Figure 3.12b), but not nearly as many as in the absence of the divalent cations. In the presence of Mg^{2+}, vesicles that formed without tubular precursors were generally larger and were not nearly as uniform in size as those formed in the presence of Ca^{2+}. Finally, Sr^{2+} did not have a strong effect on membrane tubulation (Figure 3.12c). Tubes and vesicles formed across SLBs containing Sr^{2+}, nearly to the extent of a DOPC/2 mol% TF-PC SLB in the absence of divalent cations.

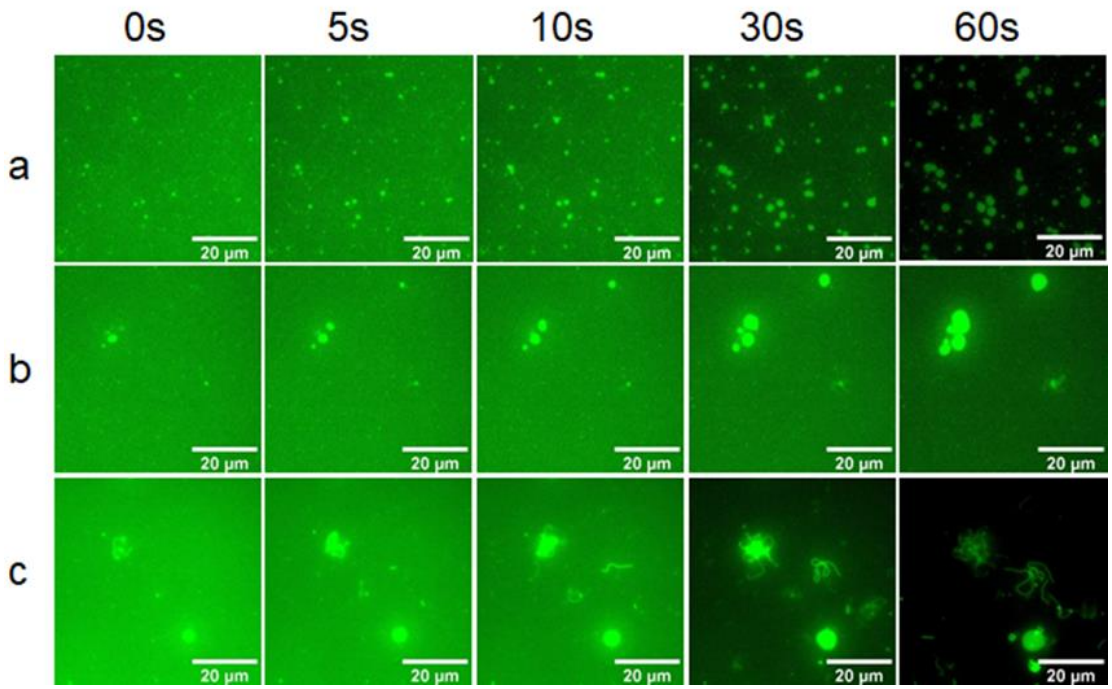

Figure 3.12. Fluorescence micrographs of the influence of divalent cations on the progression of SLB tubulation. A SLB formed from DOPC/2 mol% TF-PC liposomes in the presence of (a) Ca^{2+}, (b) Mg^{2+}, and (c) Sr^{2+}.

Divalent cations have been shown to interact strongly with the phosphate head group of lipids in a SLB.[52–54] Ca^{2+}, specifically, has been shown to increase membrane order[55,56] and cause localized increases in membrane tension.[57] Ca^{2+} also has a condensing effect on the membrane lipids.[58,59] Other studies have shown that localized exposure of Ca^{2+} on a GUV containing negatively-charged lipids generates localized membrane bending, which causes inward tubulation and vesiculation,[60,61] and can cause protrusion of double bilayer stacks.[57] Ca^{2+} can also promote tubulation of membranes during the rehydration process.[62]

We observe a rather different phenomenon; instead of promoting membrane tubulation, the presence of Ca^{2+} inhibits the tubulation process. Of course, due to the

presence of the solid substrate, SLBs cannot tubulate inward as is observed in GUVs. I hypothesize that the rigid binding of Ca^{2+} to the phosphate head groups stabilizes the membrane so that, upon lipid areal expansion due to photooxidation, the SLB blisters or vesiculates rather than tubulates. The formation of blisters or vesicles from a SLB generally does not occur because additional membrane area has to become detached from the substrate, which is energetically unfavorable due to attractive adhesion forces. However, if the energy penalty for bending a rigid membrane is greater than the adhesion energy, it is possible for enough of the membrane to detach from the substrate to form a low-curvature (compared to a tube) membrane vesicle or blister.

3.3.8 Mechanism of SLB Tubulation and Vesiculation

In general, planar SLBs are stable over long periods of time and do not spontaneously tubulate. From my results and the results of other groups, it is clear that a chemical or mechanical stimulus is required to drive the formation of tubes from the membrane. Other groups have shown that a variety of stimuli or chemical agents, including ions and peptides,[63–65] can induce SLB tubulation through their binding to the distal membrane leaflet. Reagents such as single-chain amphiphiles have been known to destabilize lipid membranes, inducing SLB tubulation and subsequent budding.[25,26,66] There have also been studies that show that lipopolysaccharide, an important component in the outer membrane of Gram-negative bacteria, causes significant morphological effects in the form of membrane tubules across a DOPC bilayer.[67] Additionally, light-triggered tubulation of giant vesicles through structural changes in membrane lipids of both leaflets has also been observed.[20,68]

Lipowsky put forth an explanation for why membrane tubes growing from SLBs are energetically favorable, while liposomes or blisters are not.[69] This tubulation mechanism relies upon the membrane acquiring a spontaneous curvature due to the adsorption of molecules or particles to the distal leaflet and is associated with spontaneous tension. In the case of my studies, the tubulation is likely due to a different effect, specifically membrane area expansion. Upon oxidation, each lipid molecule takes up more space (as discussed in the previous chapter, and shown in Figure 2.20) which in turn causes the membrane to expand.[70–72]

The drive to expand is opposed by the fixed area of the substrate which causes compression within the membrane. The result of this compression is the expulsion of membrane tubes away from the substrate to accommodate the additional membrane area. In a previous work, Staykova and co-workers formed SLBs on flexible PDMS substrates that could be expanded or compressed.[73] They observed supported bilayer tubulation when the relative area compression reached a threshold of 0.02–0.10. Furthermore, they also observed tube retraction into spherical structures that occurred by gradual or "snap-like" pathways. I only observed rapid tube-to-vesicle transitions that are analogous to the "snap-like" pathway.

The mechanism for tube-to-vesicle transitions in photo-oxidized membranes remains enigmatic at this time. It is possible that initial lipid oxidation and membrane area expansion drives tubulation, but the stability of the tubes decreases as the concentration of oxidized lipids in the membrane increases and oxidation products exit the membrane. Alternatively, the retraction of tubes into vesicular structures could be related to the membrane area decrease that is observed after an initial period of membrane expansion.[20]

The transition of membrane tubes into a network of vesicular structures has been previously observed,[74,75] though here I observe a singular vesicular structure arising from each tube. While the membrane surface area is conserved between the tube and the resulting vesicle, the internal volume of the vesicle exceeds that of the tube. This means that in order for a tube-to-vesicle transition to take place, mechanical work must be performed with the following energy:[69]

$$\Delta E = \Delta V(P_{t,ex} - P_{t,in}) \qquad \text{(eq 3.3)}$$

where ΔV is the volume difference between the vesicle and membrane tube, and is always positive. $P_{t,ex}$ is the osmotic pressure exterior to the tube, and $P_{t,in}$ is the osmotic pressure of the tube interior. When $P_{t,ex} > P_{t,in}$ the energy change is positive and the tube remains stable. Conversely, when $P_{t,in} > P_{t,ex}$, the energy change is negative and therefore favorable toward a tube-to-vesicle transition.

Note that eq 3.3 lacks a membrane bending energy term. This is because it assumes that the tube radius, $r_t = 1/2m$ and the liposome radius, $r_v = 1/m$, where m is the spontaneous curvature. Under these conditions, the mean curvature of both the tube and vesicle are equal to the spontaneous curvature of the membrane, which drives the bending energy to zero. The oxidation of the membrane results in the generation of products that can diffuse out of the membrane. The diffusion of these products from the distal membrane leaflet into the bulk liquid results in their rapid dilution. However, the accumulation of these products inside the tubule due to the oxidation of the proximal leaflet results in an increase in the osmotic pressure inside the tube. This results in a situation

where $P_{t,in} > P_{t,ex}$ and a tube-to-vesicle transition is energetically favorable. Osmotic gradients caused by asymmetric sugar concentrations have been previously shown to induce tube-to-vesicle transitions.[75]

3.4 Conclusions

In conclusion, I show that SLBs containing a membrane-embedded photosensitizer (TF-PC) will tubulate upon illumination. This tubulation is due to lipid oxidation initiated by ROS production by the photosensitizer. Evidence for tubulation being driven by oxidation is provided by the fact that DOPC illuminated in the presence of TF-PC has a larger area-per-molecule than nonilluminated controls (discussed in the previous chapter) and that a significant increase in the C=O stretch is observed after illumination (also discussed in the previous chapter). Furthermore, SLBs formed from saturated lipids do not tubulate, and the inclusion of a lipophilic antioxidant attenuates the tubulation process.

I calculated the membrane tube diameter through geometric representations of the tube and the resulting vesicular structure, and my results are in agreement with previous measurements of membrane tubes. The on-demand generation of membrane tubes via light exposure could provide a simple method for generating highly curved membrane structures for studies on the interplay between lipid oxidation, membrane curvature, and lipid–protein interactions. Furthermore, my in-depth characterization of the membrane tubes will allow the examination on how various factors, such as the degree of lipid unsaturation, the nature of the oxidizing agent, and the presence of antioxidants, alter the length and diameter of membrane tubes formed as a result of lipid oxidation.

3.5 Materials and Methods

3.5.1 Buffers

The following buffers were used:

Phosphate buffered saline (PBS) containing 10 mM phosphate, 137 mM NaCl, 2.7 mM KCl, pH 7.4.

HEPES: 10 mM 4-(2-hydroxyethyl)-1-piperazineethanesulfonic acid (HEPES), 150mM NaCl, pH 7.4.

HEPES with Ca^{2+}: 10 mM HEPES, 150 mM NaCl, 10 mM $CaCl_2$, pH 7.4.

HEPES with Mg^{2+}: 10 mM HEPES, 150 mM NaCl, 10 mM $MgCl_2$, pH 7.4.

HEPES with Sr^{2+}: 10 mM HEPES, 150 mM NaCl, 10 mM $SrCl_2$, pH 7.4.

3.5.2 Preparation of Liposomes

Dioleoylphosphatidylcholine (DOPC), diphytanoylphosphatidycholine (DiPhyPC), dilauroylphosphatidylcholine (DLPC), and TF-PC were purchased from Avanti Polar Lipids. Texas Red-dihexanoylphosphatidylethanolamine (TR-DHPE) and α-tocopherol were purchased from Fisher Scientific. Lipids were dissolved in chloroform and then were mixed in glass vials at the desired molar ratios to a final lipid concentration of 1.0 mg mL^{-1}. The fluorescent lipid and α-tocopherol concentrations were held constant at 2 mol % unless otherwise noted. Chloroform was evaporated by placing the lipid mixtures under vacuum at room temperature for at least 4 h. The resulting lipid films were rehydrated in PBS, then vortexed to resuspend the lipids. The rehydrated lipids were bath-sonicated (Branson 3510 Ultrasonic Cleaner) at room temperature for 10 min and then passed through

a 50 nm pore-size polycarbonate membrane filter 23 times within a mini-extruder (Avanti). The structures of all molecules used in this work are shown in Figure 3.1.

For experiments evaluating the effect of divalent cations on membrane tubulation, dried lipid films were instead rehydrated in HEPES buffer with either Ca^{2+}, Mg^{2+}, or Sr^{2+}.

3.5.3 Supported Bilayer Formation and Fluorescence Microscopy

Glass coverslips were cleaned in a 2% (w/v) sodium dodecyl sulfate (SDS) solution, rinsed with MilliQ ultrapure H_2O (PureLab Classic UV, ELGA LabWater), dried with N_2 gas, and finally placed in a UV/ozone chamber (ProCleaner Plus, BioForce Nanosciences) for 10 min. Liposomes were diluted to 0.1 mg mL^{-1}, then deposited onto the cleaned glass coverslips that were mounted in Attofluor imaging chambers (Thermo Fisher Scientific). Liposomes were incubated on the coverslips for approximately 1 h before being rinsed with buffer. Fluorescence images were collected on an inverted microscope (Eclipse Ti, Nikon). Fluorescence was excited using a light-emitting diode (LED) source (Aura II, Lumencor) and captured with a 2048 x 2048-pixel sCMOS camera (Orca Flash 4.0 v2, Hamamatsu) controlled with the Nikon Elements software. The excitation power at the sample stage was measured using a microscope slide photodiode power sensor (S170C, Thorlabs) coupled to a digital optical power meter (PM100D, Thorlabs). All image analysis and processing was performed with ImageJ software.

3.5.4 Fabrication of Microfluidic Channels

Glass coverslips were cleaned in a 2% (v/v) Hellmanex III solution, rinsed with ultrapure H_2O (MilliQ), and dried under a stream of N_2 gas. The surfaces of the coverslip

and a polydimethylsiloxane (PDMS) microfluidic channel (400 μm wide x 50 μm height) were activated by placing them in a plasma cleaner (Harrick Plasma, Ithaca, NY) at 270 mTorr for 1.5 min. The microfluidic channel was then bonded to the coverslip. A syringe pump (Harvard Apparatus Phd 2000 Programmable) was used to inject 0.1 mg mL^{-1} liposome samples in PBS through the microfluidic channel at a rate of 1 μL min^{-1}. Liposomes were incubated on the coverslip for approximately 10 min to form a SLB in the microfluidic channel. The channel was washed with PBS to remove unruptured liposomes before being imaged. The flow rate remained at 1 μL min^{-1} for the duration of experimentation.

3.6 References

(1) Nicolson, G. L. The Fluid—Mosaic Model of Membrane Structure: Still Relevant to Understanding the Structure, Function and Dynamics of Biological Membranes after More than 40years. *Biochim. Biophys. Acta BBA - Biomembr.* **2014**, *1838* (6), 1451–1466.

(2) McMahon, H. T.; Gallop, J. L. Membrane Curvature and Mechanisms of Dynamic Cell Membrane Remodelling. *Nature* **2005**, *438* (7068), 590–596.

(3) Heuser, J. Three-Dimensional Visualization of Coated Vesicle Formation in Fibroblasts. *J. Cell Biol.* **1980**, *84* (3), 560–583.

(4) Rothman, J. E.; Orci, L. Budding Vesicles in Living Cells. *Sci. Am.* **1996**, *274* (3), 70–75.

(5) Sciaky, N.; Presley, J.; Smith, C.; Zaal, K. J. M.; Cole, N.; Moreira, J. E.; Terasaki, M.; Siggia, E.; Lippincott-Schwartz, J. Golgi Tubule Traffic and the Effects of Brefeldin A Visualized in Living Cells. *J. Cell Biol.* **1997**, *139* (5), 1137–1155.

(6) Sweitzer, S. M.; Hinshaw, J. E. Dynamin Undergoes a GTP-Dependent Conformational Change Causing Vesiculation. *Cell* **1998**, *93* (6), 1021–1029.

(7) Takei, K.; Haucke, V.; Slepnev, V.; Farsad, K.; Salazar, M.; Chen, H.; De Camilli, P. Generation of Coated Intermediates of Clathrin-Mediated Endocytosis on Protein-Free Liposomes. *Cell* **1998**, *94* (1), 131–141.

(8) Stowell, M. H. B.; Marks, B.; Wigge, P.; McMahon, H. T. Nucleotide-Dependent Conformational Changes in Dynamin: Evidence for a Mechanochemical Molecular Spring. *Nat. Cell Biol.* **1999**, *1* (1), 27–32.

(9) Sevanian, A.; Hochstein, P. Mechanisms and Consequences of Lipid Peroxidation in Biological Systems. *Annu. Rev. Nutr.* **1985**, *5* (1), 365–390.

(10) van den Berg, J. J. M.; Op den Kamp, J. A. F.; Lubin, B. H.; Kuypers, F. A. Conformational Changes in Oxidized Phospholipids and Their Preferential Hydrolysis by Phospholipase A2: A Monolayer Study. *Biochemistry* **1993**, *32* (18), 4962–4967.

(11) Boveris, A. Mitochondrial Production of Superoxide Radical and Hydrogen Peroxide. In *Tissue Hypoxia and Ischemia*; Reivich, M., Coburn, R., Lahiri, S., Chance, B., Eds.; Advances in Experimental Medicine and Biology; Springer US: Boston, MA, 1977; pp 67–82.

(12) Hayyan, M.; Hashim, M. A.; AlNashef, I. M. Superoxide Ion: Generation and Chemical Implications. *Chem. Rev.* **2016**, *116* (5), 3029–3085.

(13) Yin, H.; Xu, L.; Porter, N. A. Free Radical Lipid Peroxidation: Mechanisms and Analysis. *Chem. Rev.* **2011**, *111* (10), 5944–5972.

(14) Wang, T.-Y.; Libardo, M. D. J.; Angeles-Boza, A. M.; Pellois, J.-P. Membrane Oxidation in Cell Delivery and Cell Killing Applications. *ACS Chem. Biol.* **2017**, *12* (5), 1170–1182.

(15) Reis, A.; Spickett, C. M. Chemistry of Phospholipid Oxidation. *Biochim. Biophys. Acta BBA - Biomembr.* **2012**, *1818* (10), 2374–2387.

(16) Spiteller, G. The Important Role of Lipid Peroxidation Processes in Aging and Age Dependent Diseases. *Mol. Biotechnol.* **2007**, *37* (1), 5–12.

(17) Vieira, S. A.; Zhang, G.; Decker, E. A. Biological Implications of Lipid Oxidation Products. *J. Am. Oil Chem. Soc.* **2017**, *94* (3), 339–351.

(18) Walton Kimberly A.; Cole Amy L.; Yeh Michael; Subbanagounder Ganesamoorthy; Krutzik Stephan R.; Modlin Robert L.; Lucas Robert M.; Nakai Junko; Smart Eric J.; Vora Deven K.; Berliner Judith A. Specific Phospholipid Oxidation Products Inhibit Ligand Activation of Toll-Like Receptors 4 and 2. *Arterioscler. Thromb. Vasc. Biol.* **2003**, *23* (7), 1197–1203.

(19) Jurkiewicz, P.; Olżyńska, A.; Cwiklik, L.; Conte, E.; Jungwirth, P.; Megli, F. M.; Hof, M. Biophysics of Lipid Bilayers Containing Oxidatively Modified Phospholipids: Insights from Fluorescence and EPR Experiments and from MD Simulations. *Biochim. Biophys. Acta BBA - Biomembr.* **2012**, *1818* (10), 2388–2402.

(20) Sankhagowit, S.; Wu, S.-H.; Biswas, R.; Riche, C. T.; Povinelli, M. L.; Malmstadt, N. The Dynamics of Giant Unilamellar Vesicle Oxidation Probed by Morphological Transitions. *Biochim. Biophys. Acta BBA - Biomembr.* **2014**, *1838* (10), 2615–2624.

(21) Baxter, A. M.; Wittenberg, N. J. Excitation of Fluorescent Lipid Probes Accelerates Supported Lipid Bilayer Formation via Photosensitized Lipid Oxidation. *Langmuir* **2019**, *35* (35), 11542–11549.

(22) Bacellar, I. O. L.; Baptista, M. S. Mechanisms of Photosensitized Lipid Oxidation and Membrane Permeabilization. *ACS Omega* **2019**, *4* (26), 21636–21646.

(23) Bacellar, I. O. L.; Tsubone, T. M.; Pavani, C.; Baptista, M. S. Photodynamic Efficiency: From Molecular Photochemistry to Cell Death. *Int. J. Mol. Sci.* **2015**, *16* (9), 20523–20559.

(24) Shukla, S.; Jin, R.; Robustelli, J.; Zimmerman, Z. E.; Baumgart, T. PIP2 Reshapes Membranes through Asymmetric Desorption. *Biophys. J.* **2019**, *117* (5), 962–974.

(25) Yoon, B. K.; Park, S.; Ma, G. J.; Kolahdouzan, K.; Zhdanov, V. P.; Jackman, J. A.; Cho, N.-J. Competing Interactions of Fatty Acids and Monoglycerides Trigger Synergistic Phospholipid Membrane Remodeling. *J. Phys. Chem. Lett.* **2020**, *11* (13), 4951–4957.

(26) Yoon, B. K.; Jackman, J. A.; Kim, M. C.; Cho, N.-J. Spectrum of Membrane Morphological Responses to Antibacterial Fatty Acids and Related Surfactants. *Langmuir* **2015**, *31* (37), 10223–10232.

(27) Zheng, Q.; Jockusch, S.; Zhou, Z.; Blanchard, S. C. The Contribution of Reactive Oxygen Species to the Photobleaching of Organic Fluorophores. *Photochem. Photobiol.* **2014**, *90* (2), 448–454.

(28) Lindsey, H.; Petersen, N. O.; Chan, S. I. Physicochemical Characterization of 1,2-Diphytanoyl-Sn-Glycero-3-Phosphocholine in Model Membrane Systems. *Biochim. Biophys. Acta BBA - Biomembr.* **1979**, *555* (1), 147–167.

(29) Tristram-Nagle, S.; Kim, D. J.; Akhunzada, N.; Kučerka, N.; Mathai, J. C.; Katsaras, J.; Zeidel, M.; Nagle, J. F. Structure and Water Permeability of Fully Hydrated DiphytanoylPC. *Chem. Phys. Lipids* **2010**, *163* (6), 630–637.

(30) Porter, N. A.; Caldwell, S. E.; Mills, K. A. Mechanisms of Free Radical Oxidation of Unsaturated Lipids. *Lipids* **1995**, *30* (4), 277–290.

(31) Shichiri, M.; Yoshida, Y.; Niki, E. Chapter 4 - Unregulated Lipid Peroxidation in Neurological Dysfunction. In *Omega-3 Fatty Acids in Brain and Neurological Health*; Watson, R. R., De Meester, F., Eds.; Academic Press: Boston, 2014; pp 31–55.

(32) Castro, I. A.; Rogero, M. M.; Junqueira, R. M.; Carrapeiro, M. M. Free Radical Scavenger and Antioxidant Capacity Correlation of α-Tocopherol and Trolox Measured by Three in Vitro Methodologies. *Int. J. Food Sci. Nutr.* **2006**, *57* (1–2), 75–82.

(33) Duval, C.; Poelman, M. C. Research Articles: Scavenger Effect of Vitamin E and Derivatives on Free Radicals Generated by Photoirradiated Pheomelanin. *J. Pharm. Sci.* **1995**, *84* (1), 107–110.

(34) Rossi, M.; Alamprese, C.; Ratti, S. Tocopherols and Tocotrienols as Free Radical-Scavengers in Refined Vegetable Oils and Their Stability during Deep-Fat Frying. *Food Chem.* **2007**, *102* (3), 812–817.

(35) Traber, M. G.; Stevens, J. F. Vitamins C and E: Beneficial Effects from a Mechanistic Perspective. *Free Radic. Biol. Med.* **2011**, *51* (5), 1000–1013.

(36) Hochmuth, R. M.; Mohandas, N.; Blackshear, P. L. Measurement of the Elastic Modulus for Red Cell Membrane Using a Fluid Mechanical Technique. *Biophys. J.* **1973**, *13* (8), 747–762.

(37) Önfelt, B.; Nedvetzki, S.; Benninger, R. K. P.; Purbhoo, M. A.; Sowinski, S.; Hume, A. N.; Seabra, M. C.; Neil, M. A. A.; French, P. M. W.; Davis, D. M. Structurally Distinct Membrane Nanotubes between Human Macrophages Support Long-Distance Vesicular Traffic or Surfing of Bacteria. *J. Immunol.* **2006**, *177* (12), 8476–8483.

(38) Rustom, A.; Saffrich, R.; Markovic, I.; Walther, P.; Gerdes, H.-H. Nanotubular Highways for Intercellular Organelle Transport. *Science* **2004**, *303* (5660), 1007–1010.

(39) Adams, K. L.; Engelbrektsson, J.; Voinova, M.; Zhang, B.; Eves, D. J.; Karlsson, R.; Heien, M. L.; Cans, A.-S.; Ewing, A. G. Steady-State Electrochemical Determination of Lipidic Nanotube Diameter Utilizing an Artificial Cell Model. *Anal. Chem.* **2010**, *82* (3), 1020–1026.

(40) Stepanyants, N.; Jeffries, G. D. M.; Orwar, O.; Jesorka, A. Radial Sizing of Lipid Nanotubes Using Membrane Displacement Analysis. *Nano Lett.* **2012**, *12* (3), 1372–1378.

(41) Karlsson, A.; Karlsson, R.; Karlsson, M.; Cans, A.-S.; Strömberg, A.; Ryttsén, F.; Orwar, O. Networks of Nanotubes and Containers. *Nature* **2001**, *409* (6817), 150–152.

(42) Bo, L.; Waugh, R. E. Determination of Bilayer Membrane Bending Stiffness by Tether Formation from Giant, Thin-Walled Vesicles. *Biophys. J.* **1989**, *55* (3), 509–517.

(43) Waugh, R. E.; Song, J.; Svetina, S.; Zeks, B. Local and Nonlocal Curvature Elasticity in Bilayer Membranes by Tether Formation from Lecithin Vesicles. *Biophys. J.* **1992**, *61* (4), 974–982.

(44) Köksal, E. S.; Liese, S.; Kantarci, I.; Olsson, R.; Carlson, A.; Gözen, I. Nanotube-Mediated Path to Protocell Formation. *ACS Nano* **2019**, *13* (6), 6867–6878.

(45) Domanov, Y. A.; Kinnunen, P. K. J. Antimicrobial Peptides Temporins B and L Induce Formation of Tubular Lipid Protrusions from Supported Phospholipid Bilayers. *Biophys. J.* **2006**, *91* (12), 4427–4439.

(46) Rossier, O.; Cuvelier, D.; Borghi, N.; Puech, P. H.; Derényi, I.; Buguin, A.; Nassoy, P.; Brochard-Wyart, F. Giant Vesicles under Flows: Extrusion and Retraction of Tubes. *Langmuir* **2003**, *19* (3), 575–584.

(47) Kantsler, V.; Segre, E.; Steinberg, V. Critical Dynamics of Vesicle Stretching Transition in Elongational Flow. *Phys. Rev. Lett.* **2008**, *101* (4), 048101.

(48) Zhao, H.; Shaqfeh, E. S. G. The Shape Stability of a Lipid Vesicle in a Uniaxial Extensional Flow. *J. Fluid Mech.* **2013**, *719*, 345–361.

(49) Dar, S.; Kamerkar, S. C.; Pucadyil, T. J. A High-Throughput Platform for Real-Time Analysis of Membrane Fission Reactions Reveals Dynamin Function. *Nat. Cell Biol.* **2015**, *17* (12), 1588–1596.

(50) *Interrelations between Essential Metal Ions and Human Diseases*; Sigel, A., Sigel, H., Sigel, R. K. O., Eds.; Metal Ions in Life Sciences; Springer Netherlands, 2013.

(51) Brini, M.; Calì, T.; Ottolini, D.; Carafoli, E. Intracellular Calcium Homeostasis and Signaling. *Met. Ions Life Sci.* **2013**, *12*, 119–168.

(52) McLaughlin, S.; Mulrine, N.; Gresalfi, T.; Vaio, G.; McLaughlin, A. Adsorption of Divalent Cations to Bilayer Membranes Containing Phosphatidylserine. *J. Gen. Physiol.* **1981**, *77* (4), 445–473.

(53) Alsop, R. J.; Schober, R. M.; Rheinstädter, M. C. Swelling of Phospholipid Membranes by Divalent Metal Ions Depends on the Location of the Ions in the Bilayers. *Soft Matter* **2016**, *12* (32), 6737–6748.

(54) Das, A.; Adhikari, C.; Chakraborty, A. Interaction of Different Divalent Metal Ions with Lipid Bilayer: Impact on the Encapsulation of Doxorubicin by Lipid Bilayer and Lipoplex Mediated Deintercalation. *J. Phys. Chem. B* **2017**, *121* (8), 1854–1865.

(55) Dluhy, R.; Cameron, D. G.; Mantsch, H. H.; Mendelsohn, R. Fourier Transform Infrared Spectroscopic Studies of the Effect of Calcium Ions on Phosphatidylserine. *Biochemistry* **1983**, *22* (26), 6318–6325.

(56) Binder, H.; Zschörnig, O. The Effect of Metal Cations on the Phase Behavior and Hydration Characteristics of Phospholipid Membranes. *Chem. Phys. Lipids* **2002**, *115* (1–2), 39–61.

(57) Lobovkina, T.; Gözen, I.; Erkan, Y.; Olofsson, J.; Weber, S. G.; Orwar, O. Protrusive Growth and Periodic Contractile Motion in Surface-Adhered Vesicles Induced by Ca2+-Gradients. *Soft Matter* **2010**, *6* (2), 268–272.

(58) Pedersen, U. R.; Leidy, C.; Westh, P.; Peters, G. H. The Effect of Calcium on the Properties of Charged Phospholipid Bilayers. *Biochim. Biophys. Acta BBA - Biomembr.* **2006**, *1758* (5), 573–582.

(59) Graber, Z.; Shi, Z.; Baumgart, T. Cations Induce Shape Remodeling of Negatively Charged Phospholipid Membranes. *Phys. Chem. Chem. Phys. PCCP* **2017**, *19* (23), 15285–15295.

(60) Ali Doosti, B.; Pezeshkian, W.; Bruhn, D. S.; Ipsen, J. H.; Khandelia, H.; Jeffries, G. D. M.; Lobovkina, T. Membrane Tubulation in Lipid Vesicles Triggered by the Local Application of Calcium Ions. *Langmuir* **2017**, *33* (41), 11010–11017.

(61) Ali Doosti, B.; Fjällborg, D.; Kustanovich, K.; Jesorka, A.; Cans, A.-S.; Lobovkina, T. Generation of Interconnected Vesicles in a Liposomal Cell Model. *Sci. Rep.* **2020**, *10* (1), 14040.

(62) Jones, S.; Huynh, A.; Gao, Y.; Yu, Y. Calcium Ion-Assisted Lipid Tubule Formation. *Mater. Chem. Front.* **2018**, *2* (3), 603–608.

(63) Inaba, T.; Kishimoto, T.; Murate, M.; Tajima, T.; Sakai, S.; Abe, M.; Makino, A.; Tomishige, N.; Ishitsuka, R.; Ikeda, Y.; Takeoka, S.; Kobayashi, T. Phospholipase Cβ1 Induces Membrane Tubulation and Is Involved in Caveolae Formation. *Proc. Natl. Acad. Sci.* **2016**, *113* (28), 7834–7839.

(64) Lamazière, A.; Burlina, F.; Wolf, C.; Chassaing, G.; Trugnan, G.; Ayala-Sanmartin, J. Non-Metabolic Membrane Tubulation and Permeability Induced by Bioactive Peptides. *PLoS ONE* **2007**, *2* (2).

(65) Arouri, A.; Kiessling, V.; Tamm, L.; Dathe, M.; Blume, A. Morphological Changes Induced by the Action of Antimicrobial Peptides on Supported Lipid Bilayers. *J. Phys. Chem. B* **2011**, *115* (1), 158–167.

(66) Thid, D.; Benkoski, J. J.; Svedhem, S.; Kasemo, B.; Gold, J. DHA-Induced Changes of Supported Lipid Membrane Morphology. *Langmuir* **2007**, *23* (11), 5878–5881.

(67) Adams, P. G.; Lamoureux, L.; Swingle, K. L.; Mukundan, H.; Montaño, G. A. Lipopolysaccharide-Induced Dynamic Lipid Membrane Reorganization: Tubules, Perforations, and Stacks. *Biophys. J.* **2014**, *106* (11), 2395–2407.

(68) Pernpeintner, C.; Frank, J. A.; Urban, P.; Roeske, C. R.; Pritzl, S. D.; Trauner, D.; Lohmüller, T. Light-Controlled Membrane Mechanics and Shape Transitions of Photoswitchable Lipid Vesicles. *Langmuir* **2017**, *33* (16), 4083–4089.

(69) Lipowsky, R. Spontaneous Tubulation of Membranes and Vesicles Reveals Membrane Tension Generated by Spontaneous Curvature. *Faraday Discuss.* **2013**, *161* (0), 305–331.

(70) Khandelia, H.; Mouritsen, O. G. Lipid Gymnastics: Evidence of Complete Acyl Chain Reversal in Oxidized Phospholipids from Molecular Simulations. *Biophys. J.* **2009**, *96* (7), 2734–2743.

(71) Wong-ekkabut, J.; Xu, Z.; Triampo, W.; Tang, I.-M.; Peter Tieleman, D.; Monticelli, L. Effect of Lipid Peroxidation on the Properties of Lipid Bilayers: A Molecular Dynamics Study. *Biophys. J.* **2007**, *93* (12), 4225–4236.

(72) Rudolphi-Skórska, E.; Filek, M.; Zembala, M. The Effects of the Structure and Composition of the Hydrophobic Parts of Phosphatidylcholine-Containing Systems on Phosphatidylcholine Oxidation by Ozone. *J. Membr. Biol.* **2017**, *250* (5), 493–505.

(73) Staykova, M.; Holmes, D. P.; Read, C.; Stone, H. A. Mechanics of Surface Area Regulation in Cells Examined with Confined Lipid Membranes. *Proc. Natl. Acad. Sci.* **2011**.

(74) Yu, Y.; Granick, S. Pearling of Lipid Vesicles Induced by Nanoparticles. *J. Am. Chem. Soc.* **2009**, *131* (40), 14158–14159.

(75) Sanborn, J.; Oglęcka, K.; S. Kraut, R.; N. Parikh, A. Transient Pearling and Vesiculation of Membrane Tubes under Osmotic Gradients. *Faraday Discuss.* **2013**, *161* (0), 167–176.

Chapter 4: Effects of Cholesterol on SLB Formation from Liposomes Containing Oxidized Lipids

4.1 Abstract

The presence of oxidized lipids within a lipid bilayer membrane causes a number of structural changes to the membrane. Cholesterol is a vital molecule found in high concentration in cell membranes and assists with bilayer support and permeabilization. Here, I explore the effects that cholesterol has with modulating the rupture pathway of supported lipid bilayers (SLBs) on a SiO_2 surface when oxidized lipids are also present in the liposomes. This chapter describes the work that has been done so far to probe the cholesterol-oxidized lipid interactions, and it describes the future work that must still be done with this project.

4.2 Introduction

The oxidation of unsaturated lipid tails via reactive oxygen species (ROS) induces chemical changes of the lipid molecule itself, which in turn creates a number of structural and morphological changes to the lipid bilayer membrane,[1,2] and can even alter the function of membrane proteins.[3] Membranes that have been oxidized have shown increased permeability and the formation of membrane pores,[4–7] which can be rather devastating to the lipid membrane, which aids in cellular structure, support, and organization. Studies have also shown that lipid peroxidation can promote the formation of membrane microdomains ("rafts").[8,9] Additionally, lipid oxidation has also been implicated in a

number of diseases and aging.[10–12] Thus, studying the effects of lipid oxidation is of vital importance.

Cholesterol is found in high percentages in eukaryotic cells, ranging from approximately 30–40 mol %,[13] and is necessary for cellular function.[14] Cholesterol has a fused-ring structure, rendering the bulk of the molecule very hydrophobic, while the polar hydroxyl headgroup orients itself towards the aqueous interface of a membrane. This orientation allows for tight packing, and as such, cholesterol can have a number of effects on the biophysical properties (mobility, melting point, etc.) of the membrane. Cholesterol is known to regulate membrane rigidity and permeability, and it can additionally play a role in membrane remodeling.[14–16]

A molecular dynamic simulation study from Van der Paal et al. showed that oxidized lipids lead to a decrease in lipid order in a membrane; however, when cholesterol is introduced into membranes that contain oxidized lipids, membrane order subsequently increases.[17] Their findings even suggested that cholesterol, when present in high enough quantities, can reduce or altogether eliminate membrane pore formation, thus protecting the membrane from further oxidative damage. In chapter two of this dissertation, I discussed at length how lipid oxidation, and by extension membrane permeability, is correlated with accelerated SLB formation. However, since cholesterol reverses permeability by causing tighter membrane packing, I hypothesize that the inclusion of cholesterol will influence SLB formation from liposomes that contain oxidized lipids. However, creating cholesterol-rich supported lipid bilayers (SLBs) is extremely challenging using the vesicle fusion method.[18] While Tabaei et al. have shown successful cholesterol-rich SLBs via the solvent-assisted lipid bilayer technique,[19,20] I herein describe

how the presence of oxidized phospholipids might enable the formation of cholesterol-rich SLBs via vesicle fusion.

4.3 Results and Discussion

The structures of the phospholipids and cholesterol that were used in the following experiments are shown in Figure 4.1. Liposomes were composed of 1-palmitoyl-2-linoleoyl-sn-glycero-3-phosphocholine (PLinPC), and were doped with 1-palmitoyl-2-azelaoyl-sn-glycero-3-phosphocholine (PazePC), and/or cholesterol at varying mol % as specified in each subsequent section.

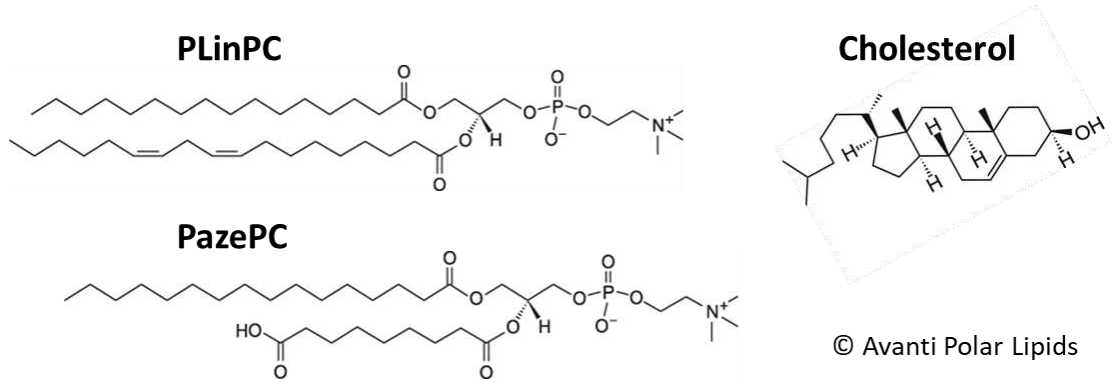

Figure 4.1. Structures of the phospholipids and cholesterol used in this study. © Avanti Polar Lipids.

4.3.1 Oxidized Phospholipids Alter Liposome Rupture Pathway

My research and the work of others has established that the presence of oxidized phospholipids changes the liposome rupture pathway from a two-step process (adsorption of critical surface coverage of liposomes followed by liposomes rupture) to a one-step process (immediate adsorption/rupture).[21,22] Below, in figure 4.2, I show the frequency (Δf)

and dissipation (ΔD) signals from QCM-D studies of 0.1 mg mL^{-1} liposomes composed of PLinPC with 0, 5, 7.5, and 10 mol% PazePC.

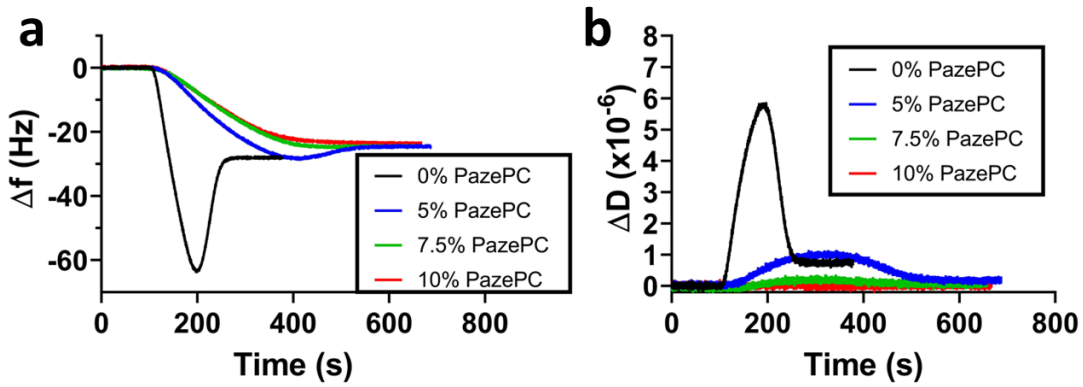

Figure 4.2. QCM-D response of SLB formation with increasing concentrations of oxidized lipids. (a) Frequency shift (Δf) and (b) dissipation shift (ΔD) curves liposomes composed of PLinPC (black line) and PLinPC with 5 mol% (green line), 7.5 mol% (blue line), and 10 mol% (red line) PazePC.

As little as 5 mol% PazePC is enough to revert the liposome rupture pathway to a one-step process. Interestingly, the presence of PazePC seems to slow the liposome rupture process, from approximately 285 s for 100% PLinPC liposomes, to 620 s, 548 s, and 558 s for liposomes containing 5, 7.5, and 10 mol% PazePC, respectively. This is at odds with my conclusions from chapter two of this dissertation, where I observed an acceleration of SLB formation when DOPC/TF-PC liposomes had been illuminated prior to QCM-D injection. The differences may arise in the fact that the base lipid is different: PLinPC here, versus DOPC in the studies discussed in chapter two. PLinPC is the natural precursor to PazePC, whereas DOPC is not. Additionally, it is worth mentioning that liposomes containing higher mole fractions (7.5 or 10 mol%) of PazePC rupture slightly faster than liposomes containing only 5 mol% PazePC.

4.3.2 Cholesterol Alters Rupture Pathway of Liposomes Containing Oxidized Lipids

It is known that forming SLBs with high mole fractions of cholesterol is extremely difficult,[18] yet the addition of oxidized lipids in liposomes causes liposomes to rupture more readily on SiO_2 surfaces. Therefore, I decided to attempt to incorporate high mole fractions (40, 50, and 60 mol%) cholesterol in liposomes containing 5, 7.5, and 10 mol% PazePC.

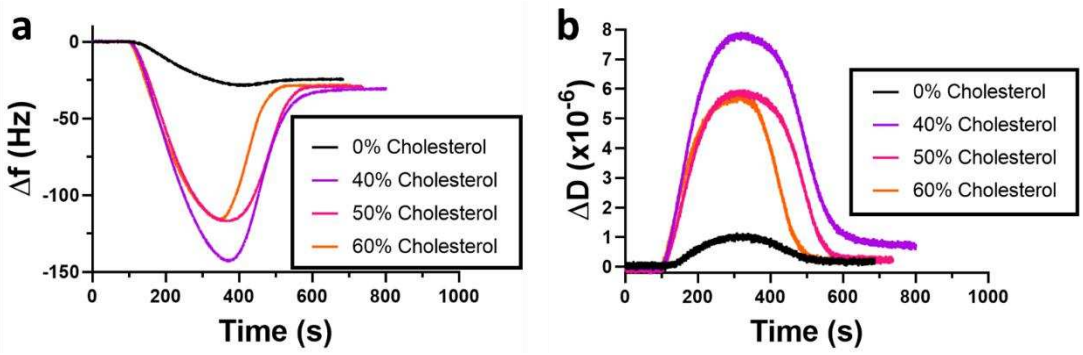

Figure 4.3. QCM-D response of SLB formation with 5 mol% PazePC and increasing concentrations of cholesterol. (a) Frequency shift (Δf) and (b) dissipation shift (ΔD) curves from liposomes composed of PLinPC and 5 mol% PazePC with 0 mol% (black line), 40 mol% (purple line), 50 mol% (pink line), and 60 mol% (orange line) cholesterol.

Above, Figure 4.3 shows the Δf and ΔD signals obtained from QCM-D experiments of PLinPC liposomes containing 5 mol% PazePC and either 40, 50, or 60 mol% cholesterol. Studies have shown that it is difficult to incorporate more than approximately 10 mol% cholesterol into liposomes and have them rupture spontaneously via the vesicle fusion method.[19,20,23] Yet when the aforementioned mole fractions of cholesterol are included in liposome precursors along with 5 mol% PazePC, I see the distinct two-step adsorption and

then rupture pathway of SLB formation. It is interesting to note that the addition of cholesterol has reverted the SLB formation pathway from a one-step process back to a two-step process. The time it takes to form a SLB does not change much despite the elevated concentrations of cholesterol. The time to form a SLB from liposomes containing 5 mol% cholesterol and no cholesterol is approximately 620 s, whereas it takes approximately 668, 610, and 567 s to form a SLB when 40, 50, and 60 mol% cholesterol (respectively) is included in the liposomes.

The final frequency shifts of these cholesterol-containing SLBs range from approximately -28 Hz to -31 Hz, which is slightly heavier than a typical intact SLB;[24] however, the slightly elevated frequency can be attributed to the mass of incorporated cholesterol within the formed SLB. Because the dissipation values are all less than 1 x 10^{-6}, I can confidently say that the more negative frequency shifts are not a result of adsorbed liposomes adhered to the surface. If this were the case, the dissipation shift would be much larger, since adsorbed liposomes are much less rigid than a SLB.

I next performed QCM-D experiments on liposomes composed of PLinPC with 7.5 mol% PazePC and 40, 50, and 60 mol% cholesterol (Figure 4.4). Once more, I saw a return of the liposomes rupture process to a two-step profile rather than the one-step profile when cholesterol is not incorporated into the liposomes.

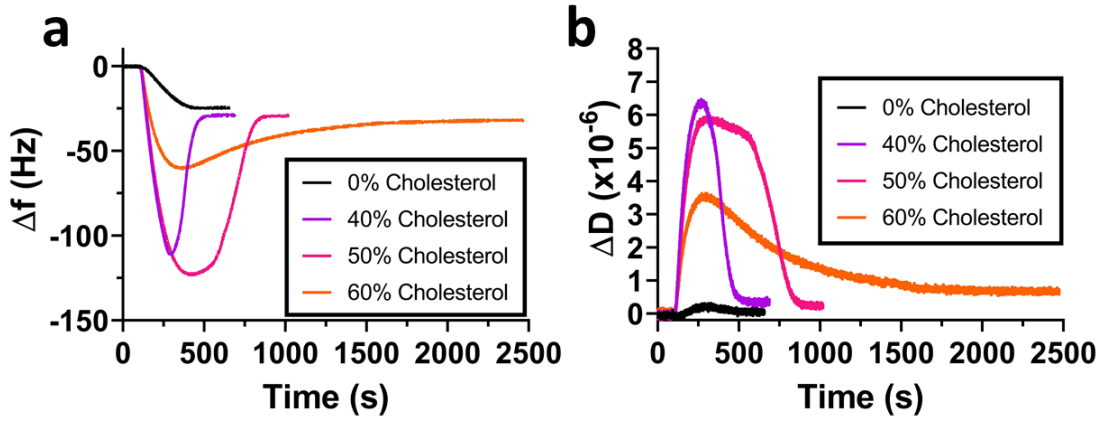

Figure 4.4. QCM-D response of SLB formation with 7.5 mol% PazePC and increasing concentrations of cholesterol. (a) Frequency shift (Δf) and (b) dissipation shift (ΔD) curves from liposomes composed of PLinPC and 7.5 mol% PazePC with 0 mol% (black line), 40 mol% (purple line), 50 mol% (pink line), and 60 mol% (orange line) cholesterol.

The rupture pathways for the liposomes containing 7.5 mol% PazePC and increasing mole fractions of cholesterol are slightly different from their 5 mol% PazePC counterparts. The time it takes to form a completed SLB is the biggest and most obvious difference. Without cholesterol, a liposome containing 7.5 mol% PazePC forms a completed SLB after approximately 548 s. Liposomes that contain 7.5 mol% PazePC and 40 mol% cholesterol form a SLB after approximately 588 s, though the differences between these two times are not statistically significant. However, when 50 mol% of cholesterol is included in these liposomes, the time it takes to form a SLB increases drastically to approximately 904 s, about 1.6 times longer than liposomes that only contain 7.5 mol% PazePC. Furthermore, when the cholesterol concentration is increased to 60 mol%, the time it takes to form a SLB increases dramatically to approximately 2105 s.

Again, the final frequency shifts for these liposome compositions falls within the expected range of an intact SLB, and their dissipations are all less than 1 x 10^{-6}, suggesting that the liposomes have indeed ruptured and are not simply adsorbed to the surface.

Finally, I performed QCM-D experiments on liposomes composed of PLinPC with 10 mol% PazePC and 40, 50, and 60 mol% cholesterol (Figure 4.5). Interestingly, the rupture pathway of these liposomes remained a one-step process, rather than reverting to a two-step process as was seen when 5 and 7.5 mol% PazePC was incorporated into liposomes.

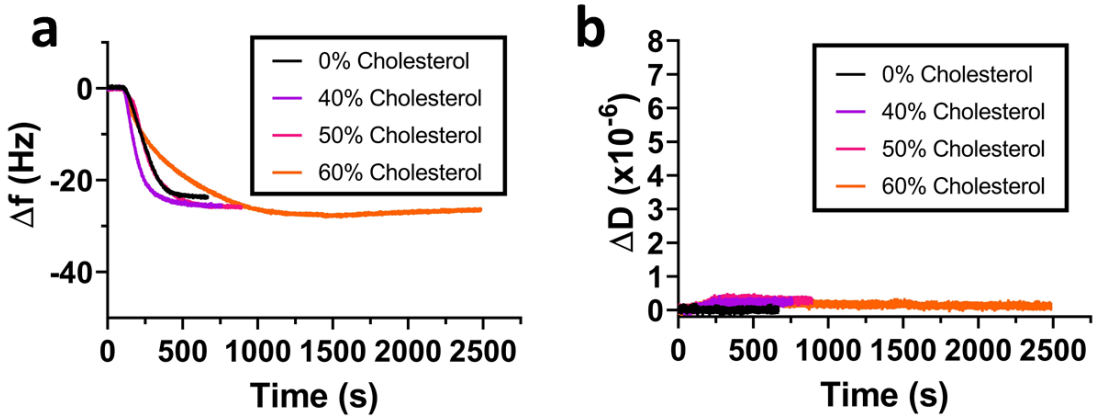

Figure 4.5. QCM-D response of SLB formation with 10 mol% PazePC and increasing concentrations of cholesterol. (a) Frequency shift (Δf) and (b) dissipation shift (ΔD) curves from liposomes composed of PLinPC and 10 mol% PazePC with 0 mol% (black line), 40 mol% (purple line), 50 mol% (pink line), and 60 mol% (orange line) cholesterol.

The time for SLB formation for liposomes containing 10 mol% PazePC and no cholesterol is approximately 558 s, while the SLB formation time for liposomes containing 10 mol% PazePC and 40, 50, and 60 mol% cholesterol is approximately 650, 940, and 2178s, respectively. Again, there is a huge increase in the time it takes for a SLB to form

when 60 mol% cholesterol is included in these liposomes, which is similar to the results from liposomes containing 7.5 mol% PazePC and 60 mol% cholesterol.

The increase in the time it takes to form a SLB with 60 mol% cholesterol could be due to several factors. Firstly, it is possible that not all of the cholesterol was incorporated into the liposomes. If cholesterol is free in solution or has formed micellar structures, then the total lipid concentration is much lower, thus the actual liposome concentration is far more dilute than expected; SLBs form much more slowly at reduced total lipid concentrations.[25,26]

The molecules β-cyclodextrin (BCD) and methyl-β-cyclodextrin (MBCD) have been shown to be effective at sequestering and removing cholesterol from lipid membranes, with MCBD showing slightly more efficacy than BCD at this endeavor.[27–29] Therefore, MBCD could be used to remove cholesterol from formed SLBs to test whether such high concentrations of cholesterol do indeed incorporate into a SLB. While the precise concentration of cholesterol cannot be determined by removal with MCBD, the relative ratios of removed cholesterol can be determined. For example, if a SLB was formed with 30 mol% and 60 mol% cholesterol, it would be expected that the frequency shift associated with cholesterol removal would be twice as much for the SLB supposedly containing 60 mol% cholesterol than the SLB containing 30 mol%.

Secondly, it is known that cholesterol rigidifies membranes.[14–16] The cholesterol may be stiffening the liposomes and rendering them less likely to rupture. There are competing forces of liposome-liposome cohesive forces and liposome-surface adhesive forces, which are necessary for spontaneous liposome rupture on certain solid supports such as SiO_2. Liposomes require a certain level of flexibility (deformation) in order to

rupture, but if cholesterol is rigidifying the membrane, the liposomes may take much longer to spontaneously rupture.

4.4 Conclusions and Future Directions

There is still much work to be done to make definitive conclusions about the effect that cholesterol has with modulating SLB formation from precursor liposomes containing oxidized lipids. I have continued experimenting with 10, 20, and 30 mol% cholesterol (data not shown), and have seen a reversion to the two-step rupture profile for both 5 and 7.5 mol% PazePC at all of these cholesterol concentrations. This further confirms that even minute amounts of cholesterol are enough to modulate liposome behavior. Additionally, further experiments can be run with a different oxidized lipid. PazePC is an oxidized lipid with a carboxyl moiety on its tail group. PoxnoPC is its counterpart—it has an identical structure, except it has an aldehyde moiety on its tail.

Fluorescence microscopy and fluorescence recovery after photobleaching (FRAP) experiments should also be performed on all of the various PLinPC/PazePC/cholesterol compositions. Firstly, this would further confirm that a SLB is formed. Secondly, FRAP would allow for the calculation of lipid diffusion coefficients. Because oxidized lipids tend to increase membrane permeability and increase the area per lipid molecule,[30] this would imply that the rate of lipid diffusion would increase. However, because cholesterol rigidifies membranes, it would be expected that the diffusion coefficient would then decrease with increasing concentrations of cholesterol.

4.5 Materials and Methods

4.5.1 Preparation of Liposomes

PLinPC, PazePC, PoxnoPC, and cholesterol were purchased from Avanti Polar Lipids. Lipids dissolved in chloroform were mixed in glass vials with desired molar ratios to a final total lipid concentration of 1.0 mg mL^{-1}. To evaporate the chloroform, the lipid mixtures were placed under vacuum at room temperature for at least 4 h. The dry lipid films were rehydrated with HEPES buffer (10 mM HEPES, 150 mM NaCl, pH 7.4), and vortexed to resuspend the lipids. Aqueous lipid suspensions were sonicated using a bath sonicator (Branson 3510 Ultrasonic Cleaner) at room temperature for 10 min. The lipids were then passed through a 50 nm pore-size polycarbonate membrane filter 23 times inside a mini-extruder (Avanti).

4.5.2 QCM-D Measurements

A QSense Explorer E1 QCM-D instrument (Biolin Scientific) was used for all QCM-D studies. Sensors for QCM-D studies were AT-cut SiO_2-coated quartz crystals (Biolin Scientific) with a fundamental frequency of 5 MHz. The internal temperature of the QCM-D was held constant at 23.0 °C. Liposomes in PBS (with or without prior illumination) at a total lipid concentration of 0.10 mg mL^{-1} were injected into the QCM-D at a constant flow rate of 100 μL min^{-1}. Frequency and dissipation were monitored at the 1st, 3rd, 5th, 7th, 9th, and 11th overtones. The 3rd overtone is shown in all data here.

4.6 References

(1) Sevanian, A.; Hochstein, P. Mechanisms and Consequences of Lipid Peroxidation in Biological Systems. *Annu. Rev. Nutr.* **1985**, *5* (1), 365–390.

(2) van den Berg, J. J. M.; Op den Kamp, J. A. F.; Lubin, B. H.; Kuypers, F. A. Conformational Changes in Oxidized Phospholipids and Their Preferential Hydrolysis by Phospholipase A2: A Monolayer Study. *Biochemistry* **1993**, *32* (18), 4962–4967.

(3) Walton Kimberly A.; Cole Amy L.; Yeh Michael; Subbanagounder Ganesamoorthy; Krutzik Stephan R.; Modlin Robert L.; Lucas Robert M.; Nakai Junko; Smart Eric J.; Vora Deven K.; Berliner Judith A. Specific Phospholipid Oxidation Products Inhibit Ligand Activation of Toll-Like Receptors 4 and 2. *Arterioscler. Thromb. Vasc. Biol.* **2003**, *23* (7), 1197–1203.

(4) Runas, K. A.; Malmstadt, N. Low Levels of Lipid Oxidation Radically Increase the Passive Permeability of Lipid Bilayers. *Soft Matter* **2014**, *11* (3), 499–505.

(5) Weber, G.; Charitat, T.; Baptista, M. S.; Uchoa, A. F.; Pavani, C.; Junqueira, H. C.; Guo, Y.; Baulin, V. A.; Itri, R.; Marques, C. M.; Schroder, A. P. Lipid Oxidation Induces Structural Changes in Biomimetic Membranes. *Soft Matter* **2014**, *10* (24), 4241–4247.

(6) Boonnoy, P.; Jarerattanachat, V.; Karttunen, M.; Wong-ekkabut, J. Bilayer Deformation, Pores, and Micellation Induced by Oxidized Lipids. *J. Phys. Chem. Lett.* **2015**, *6* (24), 4884–4888.

(7) Lis, M.; Wizert, A.; Przybylo, M.; Langner, M.; Swiatek, J.; Jungwirth, P.; Cwiklik, L. The Effect of Lipid Oxidation on the Water Permeability of Phospholipids Bilayers. *Phys. Chem. Chem. Phys.* **2011**, *13* (39), 17555–17563.

(8) Tsubone, T. M.; Junqueira, H. C.; Baptista, M. S.; Itri, R. Contrasting Roles of Oxidized Lipids in Modulating Membrane Microdomains. *Biochim. Biophys. Acta BBA - Biomembr.* **2019**, *1861* (3), 660–669.

(9) Tsubone, T. M.; Baptista, M. S.; Itri, R. Understanding Membrane Remodelling Initiated by Photosensitized Lipid Oxidation. *Biophys. Chem.* **2019**, *254*, 106263.

(10) Aruoma, O. I. Free Radicals, Oxidative Stress, and Antioxidants in Human Health and Disease. *J. Am. Oil Chem. Soc.* **1998**, *75* (2), 199–212.

(11) Adibhatla, R. M.; Hatcher, J. F. Lipid Oxidation and Peroxidation in CNS Health and Disease: From Molecular Mechanisms to Therapeutic Opportunities. *Antioxid. Redox Signal.* **2010**, *12* (1), 125–169.

(12) Yang, W. S.; Stockwell, B. R. Ferroptosis: Death by Lipid Peroxidation. *Trends Cell Biol.* **2016**, *26* (3), 165–176.

(13) Purves, W. K.; Orians, G. H.; Heller, H. C. *Life, the Science of Biology*; Sinauer Associates, 1992.

(14) Yeagle, P. L. Cholesterol and the Cell Membrane. *Biochim. Biophys. Acta BBA - Rev. Biomembr.* **1985**, *822* (3), 267–287.

(15) McMullen, T. P. W.; Lewis, R. N. A. H.; McElhaney, R. N. Cholesterol–Phospholipid Interactions, the Liquid-Ordered Phase and Lipid Rafts in Model and Biological Membranes. *Curr. Opin. Colloid Interface Sci.* **2004**, *8* (6), 459–468.

(16) Ohvo-Rekilä, H.; Ramstedt, B.; Leppimäki, P.; Peter Slotte, J. Cholesterol Interactions with Phospholipids in Membranes. *Prog. Lipid Res.* **2002**, *41* (1), 66–97.

(17) Paal, J. V. der; Neyts, E. C.; Verlackt, C. C. W.; Bogaerts, A. Effect of Lipid Peroxidation on Membrane Permeability of Cancer and Normal Cells Subjected to Oxidative Stress. *Chem. Sci.* **2015**, *7* (1), 489–498.

(18) Sundh, M.; Svedhem, S.; Sutherland, D. S. Influence of Phase Separating Lipids on Supported Lipid Bilayer Formation at SiO2 Surfaces. *Phys. Chem. Chem. Phys.* **2009**, *12* (2), 453–460.

(19) Tabaei, S. R.; Jackman, J. A.; Kim, S.-O.; Liedberg, B.; Knoll, W.; Parikh, A. N.; Cho, N.-J. Formation of Cholesterol-Rich Supported Membranes Using Solvent-Assisted Lipid Self-Assembly. *Langmuir* **2014**, *30* (44), 13345–13352.

(20) Tabaei, S. R.; Jackman, J. A.; Liedberg, B.; Parikh, A. N.; Cho, N.-J. Observation of Stripe Superstructure in the β-Two-Phase Coexistence Region of Cholesterol–Phospholipid Mixtures in Supported Membranes. *J. Am. Chem. Soc.* **2014**, *136* (49), 16962–16965.

(21) Makky, A.; Tanaka, M. Impact of Lipid Oxidization on Biophysical Properties of Model Cell Membranes. *J. Phys. Chem. B* **2015**, *119* (18), 5857–5863.

(22) Baxter, A. M.; Wittenberg, N. J. Excitation of Fluorescent Lipid Probes Accelerates Supported Lipid Bilayer Formation via Photosensitized Lipid Oxidation. *Langmuir* **2019**, *35* (35), 11542–11549.

(23) Sut, T. N.; Park, S.; Choe, Y.; Cho, N.-J. Characterizing the Supported Lipid Membrane Formation from Cholesterol-Rich Bicelles. *Langmuir* **2019**, *35* (47), 15063–15070.

(24) Cho, N.-J.; Frank, C. W.; Kasemo, B.; Höök, F. Quartz Crystal Microbalance with Dissipation Monitoring of Supported Lipid Bilayers on Various Substrates. *Nat. Protoc.* **2010**, *5* (6), 1096–1106.

(25) Reimhult, E.; Kasemo, B.; Höök, F. Rupture Pathway of Phosphatidylcholine Liposomes on Silicon Dioxide. *Int. J. Mol. Sci.* **2009**, *10* (4), 1683–1696.

(26) Zhdanov, V. P.; Keller, C. A.; Glasmästar, K.; Kasemo, B. Simulation of Adsorption Kinetics of Lipid Vesicles. *J. Chem. Phys.* **2000**, *112* (2), 900–909.

(27) Ohtani, Y.; Irie, T.; Uekama, K.; Fukunaga, K.; Pitha, J. Differential Effects of Alpha-, Beta- and Gamma-Cyclodextrins on Human Erythrocytes. *Eur. J. Biochem.* **1989**, *186* (1–2), 17–22.

(28) Kilsdonk, E. P.; Yancey, P. G.; Stoudt, G. W.; Bangerter, F. W.; Johnson, W. J.; Phillips, M. C.; Rothblat, G. H. Cellular Cholesterol Efflux Mediated by Cyclodextrins. *J. Biol. Chem.* **1995**, *270* (29), 17250–17256.

(29) Klein, U.; Gimpl, G.; Fahrenholz, F. Alteration of the Myometrial Plasma Membrane Cholesterol Content with Beta-Cyclodextrin Modulates the Binding Affinity of the Oxytocin Receptor. *Biochemistry* **1995**, *34* (42), 13784–13793.

(30) Jurkiewicz, P.; Olżyńska, A.; Cwiklik, L.; Conte, E.; Jungwirth, P.; Megli, F. M.; Hof, M. Biophysics of Lipid Bilayers Containing Oxidatively Modified Phospholipids: Insights from Fluorescence and EPR Experiments and from MD Simulations. *Biochim. Biophys. Acta BBA - Biomembr.* **2012**, *1818* (10), 2388–2402.

Chapter 5: Influence of Brain Gangliosides on the Formation and Properties of Supported Lipid Bilayers

Note: The work described in this chapter is thanks to a collaborative effort among several members of the Wittenberg lab. Luke Jordan, Megan Blauch, and Jennie Cawley all had a hand in this project.

5.1 Abstract

Gangliosides are glycolipids that are enriched on the outer surface of cell membranes. Gangliosides are receptors for a number of signaling molecules and toxins, and therefore are often incorporated into biosensors. Many of these biosensors incorporate gangliosides into supported lipid bilayers which are formed by the spontaneous rupture of liposomes on glass or SiO_2 substrates. In this work, we used quartz crystal microbalance with dissipation monitoring (QCM-D) to investigate how the presence of the four major brain gangliosides (GM1, GD1a, GD1b, and GT1b) influences the process of supported lipid bilayer (SLB) formation on SiO_2 surfaces. We show that the rate of SLB formation is dependent on both the charge and position of sialic acid moieties on ganglioside molecules. Additionally, Ca^{2+} can accelerate ganglioside-rich SLB formation, but the degree of acceleration differs for liposomes containing different gangliosides. Fluorescence recovery after photobleaching (FRAP) measurements show that the presence of all gangliosides reduces lipid diffusion coefficients in a concentration-dependent manner, and that Ca^{2+} slows lipid diffusion in membranes with and without gangliosides. Finally, we use ganglioside-rich supported bilayers to measure binding constants for a GD1a-binding

antibody that has similar properties to antibodies present in a variant of Guillain-Barré syndrome.

5.2 Introduction

The cellular plasma membrane is a complex environment composed of a wide variety of lipids, embedded with proteins, and decorated with carbohydrates. Lipid-carbohydrate conjugates (glycolipids) play essential roles in cellular recognition, adhesion, and infection. One family of glycolipids, gangliosides, are found in particularly high abundance in the vertebrate nervous system.[1] Gangliosides contain one or more sialic acid residues which are deprotonated at physiological pH. The predominant sialic acid found on human gangliosides is N-acetylneuraminic acid.[2] The most common gangliosides in the nervous system are GM1, GD1a, GD1b, and GT1b. Together, these four gangliosides account for roughly 94% of the gangliosides found in the human brain.[3] Gangliosides are enriched on the extracellular membrane leaflet, and in model membranes they are known to cluster with cholesterol[4,5] and cluster with themselves in the absence of cholesterol.[6]

In cells and tissues, gangliosides interact with a number of different molecules. For example, GD1a and GT1b on axons interact with Siglec-4, also called myelin-associated glycoprotein (MAG), in the periaxonal space between an axon and the first wrap of myelin.[7] Ganglioside-binding antibodies are also a hallmark of Guillain-Barré syndrome.[8] In addition to endogenous interactions, gangliosides can function as receptors for a number of toxins and viruses.[9] Perhaps the best-known example is cholera toxin, in which the cholera toxin B subunit (CTB) binds GM1 with high affinity.[10] Gangliosides are also

receptors for heat labile enterotoxin,[11] tetanus toxin,[12] and botulinum toxin.[12] Gangliosides also interact with pathogenic fibrils of β-amyloid[13] and α-synuclein.[14]

Because gangliosides bind important endogenous molecules, toxins, and viruses, a number of sensing strategies have been devised to quantitatively probe these interactions. Many approaches use model membrane systems, like giant unilamellar vesicles (GUVs), liposomes, or SLBs. The lipid composition of these model membranes can be precisely controlled, and the membranes can be incorporated into a number of sensor architectures with relative ease.[15–17] A variety of fluorescence assays have been used to investigate binding between glycolipids or gangliosides in model membranes and toxins or virus particles.[18–22] Ganglioside binding can also be detected with label-free methods like backscattering interferometry,[23] colloidal bead assembly,[24] surface plasmon resonance (SPR),[10,25,26] localized surface plasmon resonance,[27] isothermal titration calorimetry,[28] and quartz crystal microbalance with dissipation monitoring (QCM-D).[29,30]

Many strategies for characterizing ganglioside interactions rely upon the creation of ganglioside-rich SLBs. Formation of SLBs can be accomplished by the spontaneous rupture of lipsomes,[31] Langmuir-Blodgett methods,[32] or other techniques.[33,34] It is well established that a number of factors, including the substrate chemistry and the lipid composition of precursor liposomes, can influence SLB formation via vesicle rupture.[35] While the influence of GM1 on SLB formation by vesicle rupture has been examined,[30] there are few studies on the effects of the more highly-charged GD1a, GD1b, and GT1b on SLB formation. In this work, we examine the influence of the four major brain gangliosides on the formation of SLBs by vesicle rupture. We show that not only the ganglioside charge but also the position of sialic acid moieties has a significant influence on the transition from

adsorbed liposomes to a SLB. We also find that the presence of Ca^{2+} can significantly accelerate liposome rupture kinetics. FRAP studies show that increasing ganglioside concentrations reduces lipid diffusion coefficients significantly, and the presence of Ca^{2+} slows lipid diffusion in SLBs with and without gangliosides. Finally, we use membranes rich in GD1a to examine antibody binding kinetics with QCM-D.

5.3 Results and Discussion

5.3.1 Formation of SLBs Containing Brain Gangliosides

The four brain gangliosides examined in these studies are GM1, GD1a, GD1b, and GT1b. The structures, both in schematic illustrations as well as molecular models created with the glycolipid modeler in CHARMM-GUI[36] are shown below in Figure 5.1.

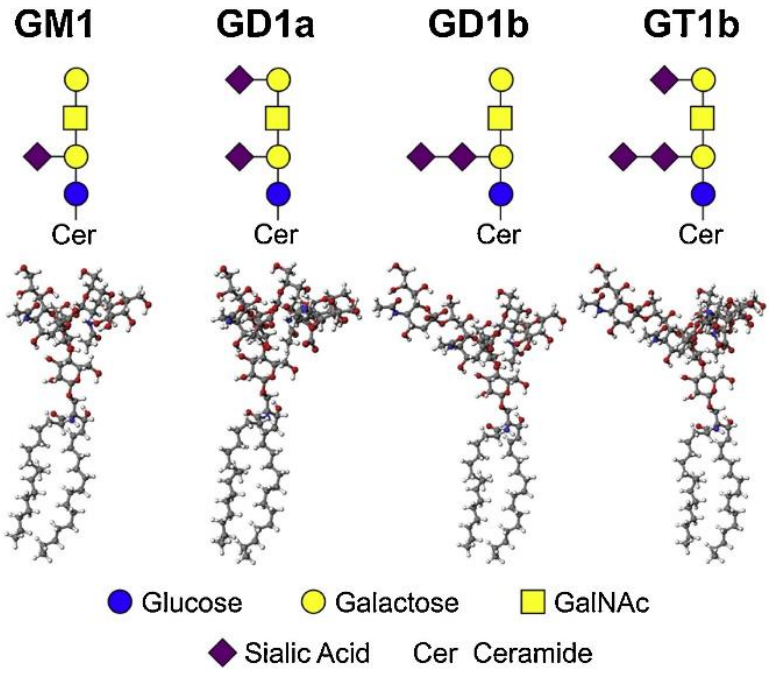

Figure 5.1. Structures of GM1, GD1a, GD1b, and GT1b gangliosides. (Top) Schematic illustrations of ganglioside structures. (Middle) Ball-and-stick models of ganglioside structures. (Bottom) Legend for the illustrated structures.

The four gangliosides have head groups with a common glycan backbone consisting of glucose, galactose, and N-acetylgalactosamine (GalNAc).[37] Where they differ, however, is in the number and linkages of sialic acid moieties. At physiological pH the sialic acid groups confer a net negative charge on gangliosides, with the charge equal to the number of sialic acids per molecule. Thus GM1, GD1a, GD1b, and GT1b have charges of -1, -2, -2, and -3, respectively. Simulations[38] and atomic force microscopy (AFM) measurements on lipid monolayers[39] and SLBs[6] have shown that the glycan head groups of gangliosides extend 0.7–2.0 nm above the head groups of the background phospholipids. This makes it likely that during the liposome adsorption process, the glycan head groups are the first entities on liposomes that encounter the substrate.

As precursors to the SLBs, we formed liposomes composed of dioleoylphosphatidylcholine (DOPC) and 1–5 mol % gangliosides by hydration in Tris buffer, bath sonication, and extrusion through 50-nm pore size filters. To monitor the formation of SLBs on SiO_2 surfaces, we employed QCM-D. Using QCM-D, it is possible to monitor the adsorption of liposomes to surfaces by observing negative shifts in the resonant frequency (Δf) of the QCM-D sensor, which correspond to mass added to the surface.[40] As the liposomes adsorb to the surface, the dissipation signal (ΔD) also increases due to the viscoelasticity of a layer of intact, unruptured liposomes.[41–43]

For the case of zwitterionic liposomes on a SiO_2 surface, a critical population of liposomes must be adsorbed to the surface before the liposome rupture cascade can begin.[44]

Once liposomes begin to rupture, the frequency shift reaches a minimum, then shifts back toward more positive values as aqueous solution from the interior of liposomes is liberated. The dissipation signal also exhibits a maximum as the viscoelastic adsorbed liposome layer begins the transition into a rigid SLB film.[41] The time required to reach the minimum in the frequency curve is t_{crit}, and the magnitude of frequency shifts at this time is Δf_{crit}. The value of ΔD_{crit} was taken from the maximum in the dissipation curve.

Once the liposome rupture process is complete and a SLB is formed, the Δf and ΔD signals reach stable plateaus, which are referred to as Δf_{SLB} and ΔD_{SLB}, respectively. The critical and SLB values are illustrated in the annotated QCM-D curves in Figure 5.2. Values of t_{crit}, Δf_{crit}, and ΔD_{crit} can depend on a number of factors, including liposome size, charge, infusion rate, and concentration, as well as buffer ionic strength, buffer pH, presence of divalent cations, and temperature.[35,42,45–54] The values of Δf_{crit}, ΔD_{crit}, Δf_{SLB}, and ΔD_{SLB} we measured for DOPC SLB formation agree with previous reports.[42,55]

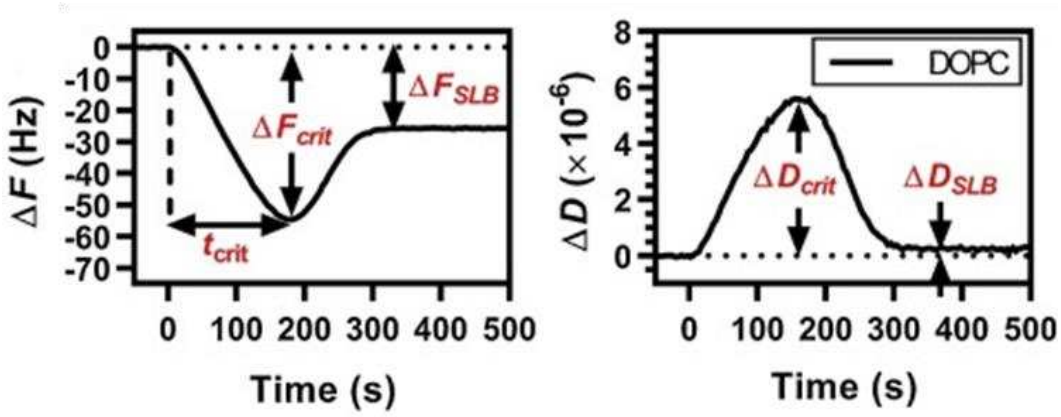

Figure 5.2. Representative frequency and dissipation curves for QCM-D monitoring of the formation of DOPC SLBs. Frequency (left) and dissipation (right) shifts for adsorption and rupture of DOPC liposomes. The annotations are defined in the text.

Next, we evaluated the influence of increasing mole fractions of GM1, GD1a, GD1b, and GT1b on the adsorption and rupture of DOPC liposomes in Tris buffer. Liposomes were prepared containing 1, 2, 3, 4, or 5% of the gangliosides and were injected into the QCM-D. Figure 5.3a,b show frequency and dissipation curves for liposomes containing either 1 or 5% of the gangliosides. Frequency and dissipation curves from liposomes containing 2, 3, and 4% ganglioside are shown in Figure 5.4. Figure 5.3a shows curves for the rupture of 1% ganglioside liposomes which are not statistically different than the pure DOPC control.

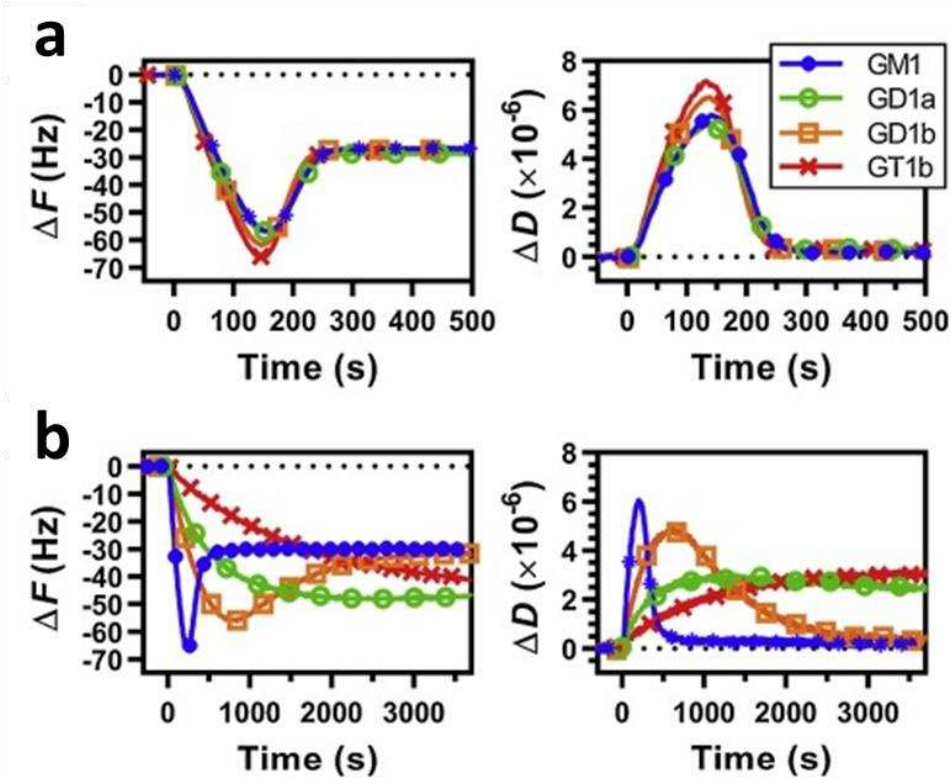

Figure 5.3. Representative frequency and dissipation curves for QCM-D monitoring of the formation of ganglioside-rich SLBs. (a) Frequency (left) and dissipation (right) shifts for adsorption and rupture of DOPC liposomes containing 1% GM1, GD1a, GD1b, or GT1b.

(b) Frequency (left) and dissipation (right) shifts for adsorption and rupture of DOPC liposomes containing 5% GM1, GD1a, GD1b, or GT1b.

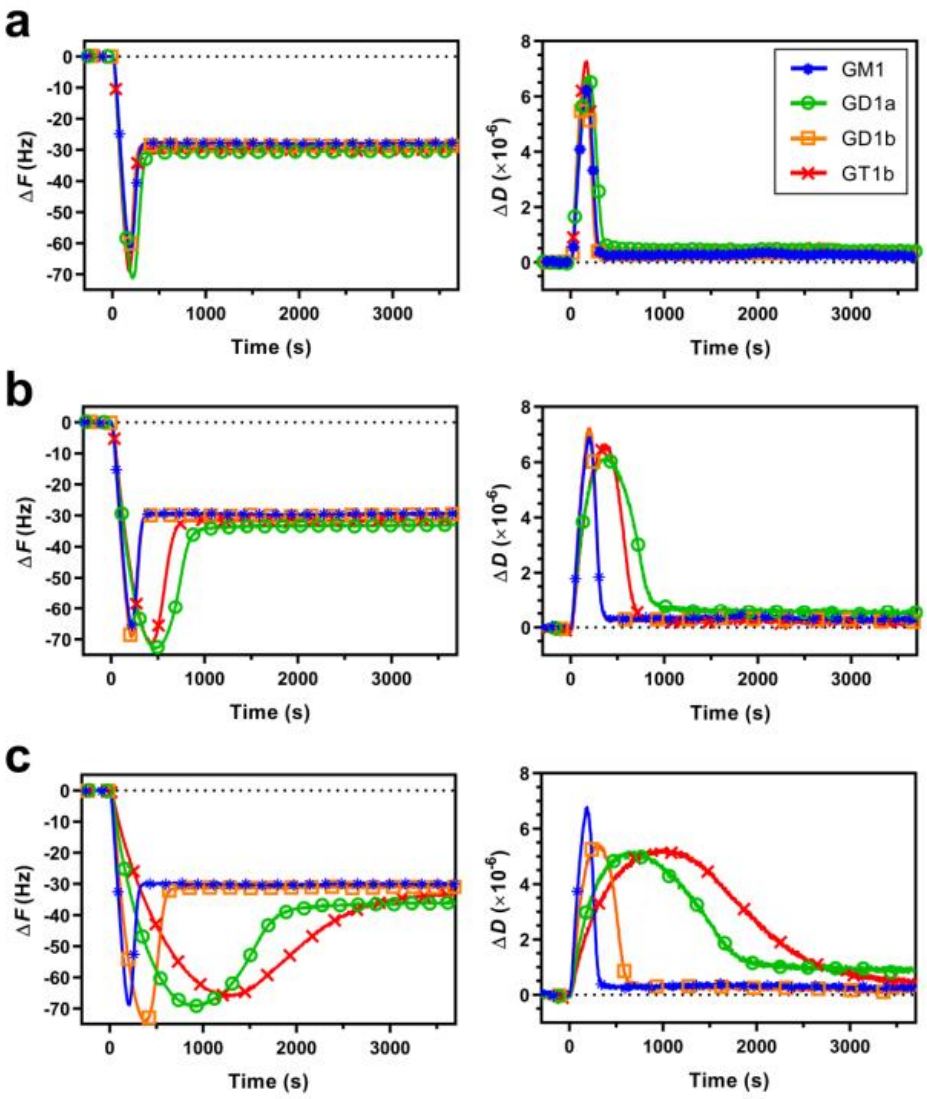

Figure 5.4. Formation of SLBs containing 2–4% gangliosides. Frequency (left) and dissipation (right) shifts for adsorption and rupture of DOPC liposomes with (b) 2%, (c) 3%, and (d) 4% gangliosides (GM1, GD1a, GD1b, and GT1b).

The effects of gangliosides on SLB formation become significant at higher mole fractions (Figure 5.4). Liposomes containing 5% GM1 or GD1b form SLBs via a two-step

adsorption-rupture pathway. The ΔF and ΔD signals indicate that liposomes containing 5% GD1a or GT1b do not rupture to form complete SLBs. While Figure 5.3b only shows the first hour (3600 s) of the QCM-D recordings, the samples with 5% GD1a and GT1b were exposed to the QCM-D sensor for up to 7.5 h, but we did not observe a frequency or dissipation plateau to indicate formation of a complete SLB (Figure 5.5).

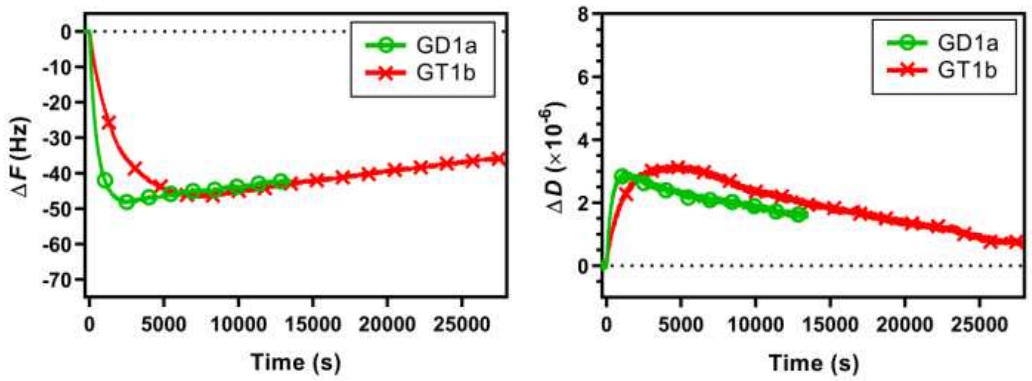

Figure 5.5. Time course of adsorption and rupture of liposomes with 5% GD1a and 5% GT1b in Tris buffer lacking Ca^{2+}. Panels show QCM-D frequency (left) and dissipation (right) shifts.

A summary of all figures of merit (Δf_{crit}, ΔD_{crit}, t_{crit}, and Δf_{SLB}) is shown below in Figure 5.6. In general, as the concentration of gangliosides in the liposomes increases, the values of Δf_{crit} increase. This indicates that as the ganglioside content increases, more liposomes need to adsorb to the surface before the rupture cascade begins. This could stem from weaker adhesion of liposomes to the SiO_2 substrate. Negative surface charges on both the SiO_2 and the ganglioside-containing liposomes results in electrostatic repulsion that counteracts attractive van der Waals interactions between the liposomes and the SiO_2.[50] Furthermore, increasing the concentration of gangliosides increases the amount of

hydrogen bonding between water and the liposomes surface, and thus increases the hydration repulsive force.[56]

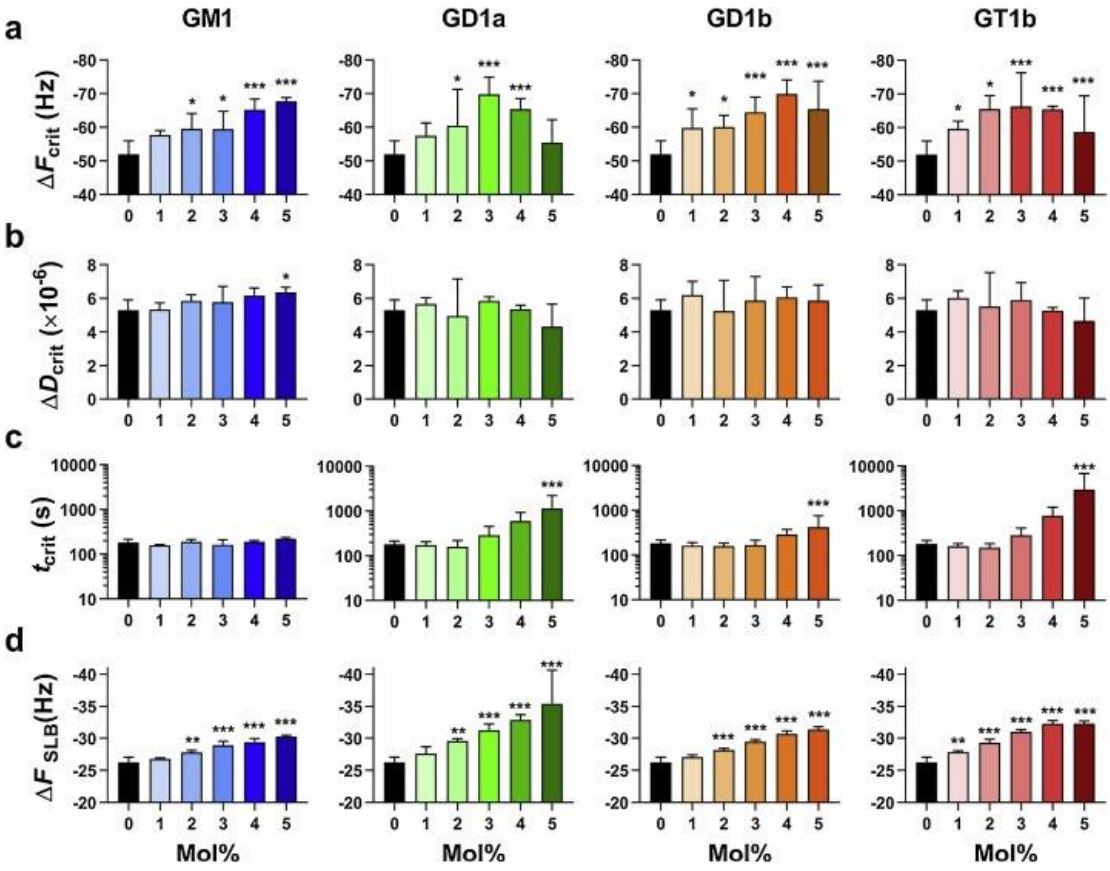

Figure 5.6. Influence of ganglioside type and concentration on liposomes adsorption and rupture. (a) Δf_{crit} values as a function of ganglioside type and concentration. (b) ΔD_{crit} values as a function of ganglioside type and concentration. (c) t_{crit} values as a function of ganglioside type and concentration. (d) Δf_{SLB} values as a function of ganglioside type and concentration. Data represented as mean ± s.d with an N = 3. *p < 0.05, **p < 0.01, ***p < 0.001 compared to liposomes composed solely of DOPC.

Because hydration repulsive forces and electrostatic repulsion oppose adhesion, liposomes with higher ganglioside content will have lower adhesion energies. For a constant membrane bending modulus, lowering the adhesion energy reduces liposome

deformation by decreasing the size of the membrane-substrate contact patch.[57] Thus, for the rupture cascade to begin, the liposomes need to pack more tightly, which induces stresses on the liposome membranes that can initiate their rupture.[58] The liposomes with 5% GD1a and GT1b exhibit a Δf_{crit} value that is less than the Δf_{crit} of liposomes with 4% GD1a and GT1b. Critical values were taken from the minimum point in the frequency curves. In the case of 5% GD1a and GT1b liposomes, a minimum is observed; however, the frequency never reaches a stable plateau (Figure 5.5). This suggests that 5% GD1a and GT1b liposomes transition from an intact adsorbed liposome state to a SLB very slowly.

While the critical frequencies increase as ganglioside concentration increases, the critical dissipation values (ΔD_{crit}) across all gangliosides at all concentrations, with the exception of 5% GM1, do not significantly differ from DOPC controls (Figure 5.6b). The t_{crit} is significantly different from DOPC controls for 5% GD1a, GD1b, and GT1b (Figure 5.6c). When comparing t_{crit} for GD1a, GD1b, and GT1b, a dependence on ganglioside charge and structure emerges. The t_{crit} values for 5% GD1a and GT1b are much larger than those of 5% GD1b. Among the gangliosides studied here, GT1b has the largest negative charge (-3) and the most negative zeta potential (Figure 5.7). It is likely that liposomes with GT1b take the longest to reach the critical point for liposome rupture due to increased electrostatic and hydration repulsive forces between the liposomes and the SiO_2 surface.

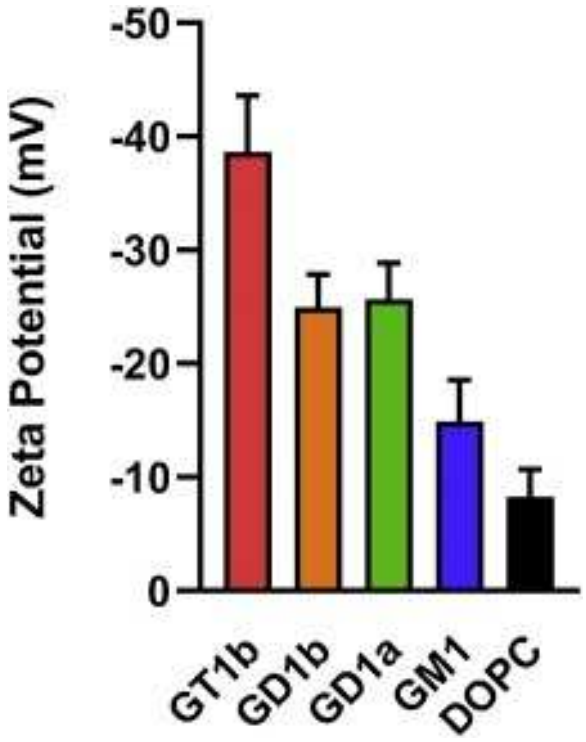

Figure 5.7. Zeta potential of liposomes composed solely of DOPC and DOPC liposomes containing 5% GM1, GD1a, GD1b, and GT1b.

Increased membrane-membrane repulsion between surface-adsorbed liposomes also contribute to the increase in t_{crit}. Increased repulsion between the liposomes and the surface reduces the degree of liposome deformation arising from adhesive interactions that stress liposomes, which ultimately drive liposome rupture. Analogous results were obtained by Richter et al. when examining the rupture of phosphatidylserine (PS)-rich liposomes on SiO_2. PS lipids have a -1 charge, and when the PS fraction was increased from zero to 33%, there was more than a 20-fold increase in the time required to form a SLB.[42]

Liposomes containing 5% GD1a have a t_{crit} that is nearly twice that of 5% GD1b liposomes. GD1a and GD1b both contain two sialic acid groups, and therefore both have a

charge of -2. Furthermore, liposomes with 5% GD1a and GD1b have similar zeta potentials (-25.7 ± 3.2 and -25.0 ± 2.9 mV, respectively) that lie as expected between those of liposomes containing 5% GT1b (-38.7 ± 5.0 mV) and 5% GM1 (-14.9 ± 3.7 mV) (Figure 5.7). However, the position of sialic acid linkages differ between GD1a and GD1b. GD1b has two sialic acids linked to the internal galactose, while GD1a has one sialic acid linked to the internal galactose and one linked to the terminal galactose (Figure 5.1). This structural difference may alter liposome-substrate and liposome-liposome interactions for liposomes containing these gangliosides. Though GD1b has two sialic acid groups, one of them is somewhat hidden and could cause steric screening. A compounding effect is the sialic acid on the terminal galactose of GD1a, which is more likely to have direct interactions with both the substrate and terminal sialic acids on GD1a molecules on neighboring liposomes. GT1b also has a sialic acid on its terminal galactose, which may further explain the hindering effect it has on liposomes rupture. To isolate the effects of sialic acid moieties on the terminal galactose of gangliosides, one would need to investigate the adsorption and rupture of liposomes containing GM1b or GD1c. However, these gangliosides are either expressed transiently during brain development or are present only in trace amounts in the developed mammalian brain,[59] and thus are quite difficult to isolate in appreciable quantities.

The final frequency shift corresponding to the formation of a SLB (Δf_{SLB}) increases as the concentration of gangliosides in the liposomes increases (Figure 5.6d). The measured Δf_{SLB} value is proportional to the product of the SLB density and its thickness,[40] and the increase Δf_{SLB} occurs due to increases in both density and thickness. The presence of gangliosides has a condensing effect on the SLB,[30,60,61] which increases the density of the

SLB. Additionally, the glycan head groups of the gangliosides increase the SLB thickness.[62] Furthermore, QCM-D measures the hydrated mass of the film. Therefore, an increase in the amount of intimately coupled water via hydrogen bonding interactions could give rise to larger frequency shifts when gangliosides are present in the SLB.

5.3.2 The Effect of Ca^{2+} on SLB formation

Divalent cations, such as Ca^{2+} and Mg^{2+}, have been shown to accelerate the rate of liposome rupture on SiO_2.[54,63] Ca^{2+} can also accelerate the rupture of negatively charged liposomes to form SLBs on SiO_2 and TiO_2 surfaces.[42,64] Ca^{2+} binds lipid phosphates and carbonyls, which induces a slight positive charge to the membrane. This strengthens adhesion between liposomes and negatively charged surfaces.

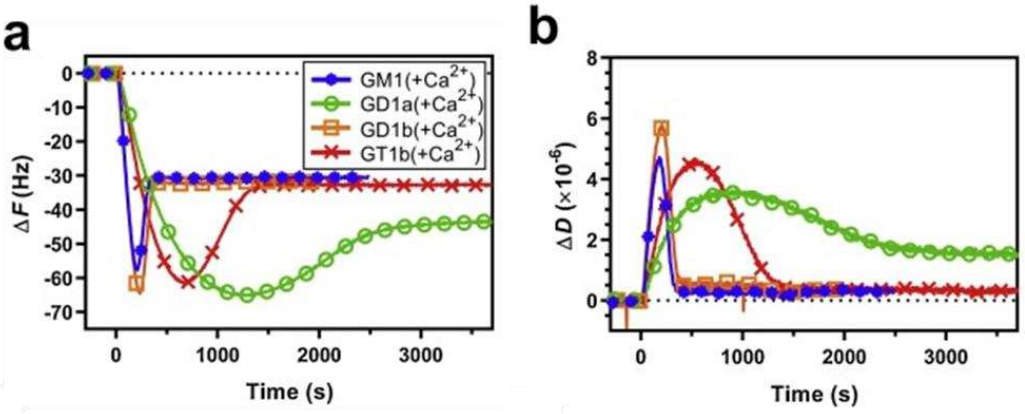

Figure 5.8. Effects of Ca^{2+} on the formation of ganglioside-rich SLBs. Representative QCM-D measurements of liposomes with 5% gangliosides: (a) Δf and (b) ΔD.

To demonstrate the effect of Ca^{2+} on the formation of ganglioside-rich SLBs, we prepared liposomes composed of DOPC and 1–5% of each of the brain gangliosides as

described earlier. Then, using QCM-D, we observed their adsorption and rupture in the presence of 2 mM Ca^{2+}. Frequency and dissipation responses for 5% ganglioside liposomes are shown in Figure 5.8a,b, respectively. Figure 5.9 compares the t_{crit} for all ganglioside concentrations in the absence and presence of Ca^{2+}.

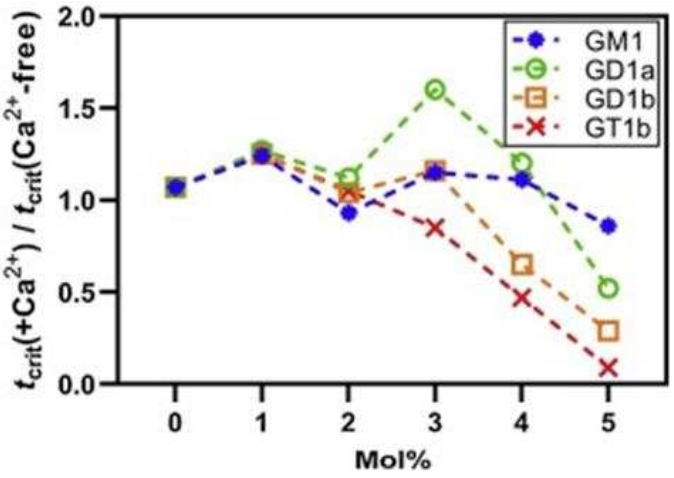

Figure 5.9. Ratio of $t_{crit}(+Ca^{2+})/t_{crit}(Ca^{2+}\text{-free})$ across all concentrations and different gangliosides.

For singly-charged GM1, Ca^{2+} makes little difference in t_{crit}. However, for GD1a, GD1b, and GT1b, the presence of Ca^{2+} has a pronounced acceleration effect. Liposomes with 5% GD1b and GT1b are the most susceptible to the presence of Ca^{2+}; their t_{crit} values decrease roughly 4- and 10-fold, respectively. Liposomes with GD1a also reach t_{crit} faster in the presence of Ca^{2+}, though the effect is more moderate (Figure 5.9). Even with Ca^{2+} present the Δf_{SLB} value for 5% GD1a does not indicate the presence of a complete SLB. Rather, the final configuration is a combination of intact liposomes and SLB patches, similar to when Ca^{2+} is absent. An alternative approach could be taken to form complete SLBs with high concentrations of GD1a. For example, solvent-assisted lipid bilayer

(SALB) formation[65] has been used to make SLBs on substrates where spontaneous rupture does not occur,[33] or with lipid compositions that are not susceptible to spontaneous rupture.[66]

5.3.3 The Influence of Gangliosides and Ca^{2+} on Lipid Diffusion

Lipid diffusion coefficients in SLBs were examined with fluorescence recovery after photobleaching (FRAP). In these experiments, SLBs containing DOPC, varying amounts of gangliosides, and 0.1% dihexanoylphosphatidylethanolamine-Texas Red (TR-DHPE) were formed on glass coverslips by vesicle rupture in Tris buffer with 2 mM Ca^{2+}. After photobleaching a small circular area (approx. 10 μm diameter) of the SLB, fluorescence recovery was recorded for 2 min. The SLBs were then washed with Tris buffer containing EDTA to chelate Ca^{2+}, and a second FRAP measurement was made after the subsequent washout of EDTA with Ca^{2+}-free Tris buffer. Fluorescence recovery before and after Ca^{2+} chelation was analyzed to calculate the lipid diffusion coefficient using the Hankel transform method described by Jönsson et al.[67] The FRAP results are summarized in Figure 5.10 and Table 5.1. FRAP micrograph images are shown in Figures 5.11-15.

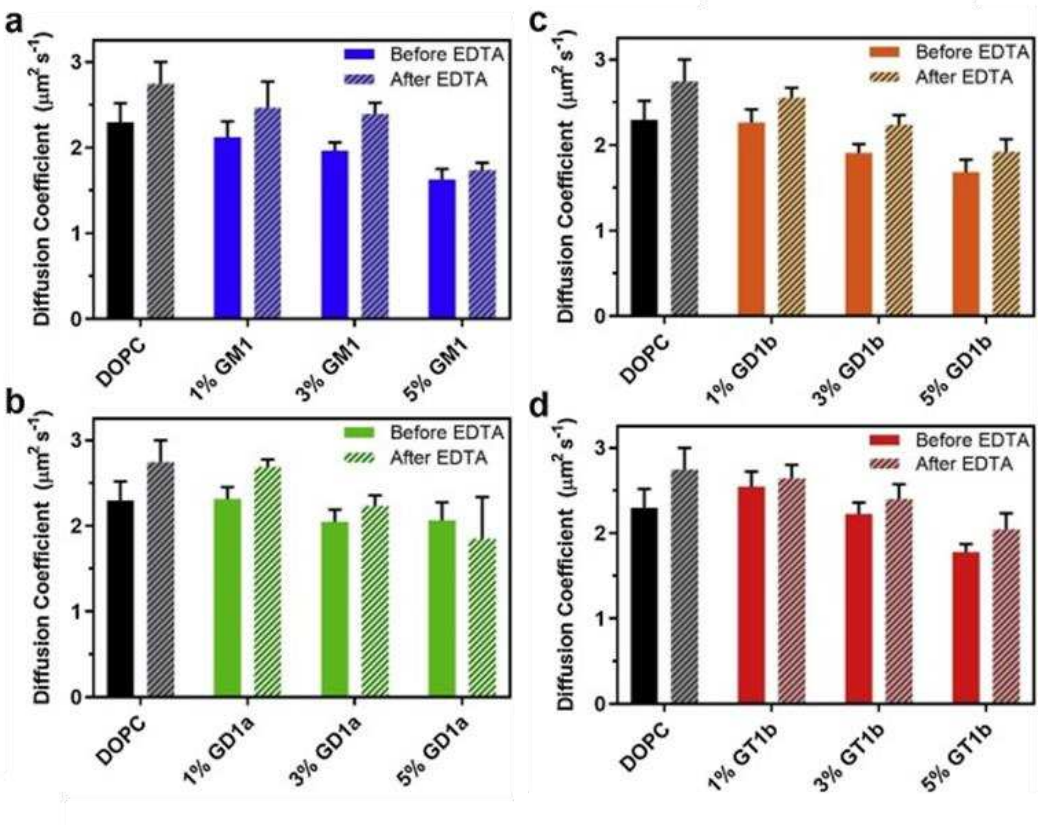

Figure 5.10. Influence of ganglioside concentration and Ca^{2+} on lipid diffusion coefficients in SLBs. Diffusion coefficients were measured with FRAP before (solid bars) and after (hatched bars) Ca^{2+} chelation with EDTA and subsequent washout. Data are represented as mean ± standard deviation.

We measured diffusion coefficients of 2.30 ± 0.22 μm^2 s^{-1} and 2.75 ± 0.26 μm^2 s^{-1} for a 100% DOPC SLB before and after chelation of Ca^{2+}, respectively. These values are within the range of values typically reported for fluid PC bilayers on solid supports.[67,68] Prior to addition of EDTA, the lipid diffusion coefficients in SLBs tend to decrease as the concentration of gangliosides increases. The same trend is observed after Ca^{2+} chelation with EDTA. Upon Ca^{2+} chelation with EDTA, the diffusion coefficients for a given SLB

composition generally increased. The increases of the diffusion coefficients are, for the most part, statistically significant (Table 5.1).

Sample	*D* before EDTA ($\mu m^2/s$) Mean ± S.D.	N before EDTA	*D* after EDTA ($\mu m^2/s$) Mean ± S.D.	N after EDTA	P value[a]	Significant?[b]
100% DOPC	2.30 ± 0.22	15	2.75 ± 0.26	15	<0.0001	Yes
1% GM1	2.12 ± 0.18	15	2.47 ± 0.30	15	0.0007	Yes
3% GM1	1.96 ± 0.10	14	2.40 ± 0.13	14	<0.0001	Yes
5% GM1	1.63 ± 0.12	15	1.74 ± 0.09	15	0.0005	Yes
1% GD1a	2.30 ± 0.14	14	2.69 ± 0.09	14	<0.0001	Yes
3% GD1a	2.05 ± 0.14	15	2.24 ± 0.12	15	0.0023	Yes
5% GD1a	2.05 ± 0.22	14	1.85 ± 0.48	14	0.0907	No
1% GD1b	2.26 ± 0.16	15	2.56 ± 0.11	15	<0.0001	Yes
3% GD1b	1.91 ± 0.10	14	2.22 ± 0.10	14	<0.0001	Yes
5% GD1b	1.67 ± 0.15	14	1.93 ± 0.14	14	<0.0001	Yes
1% GT1b	2.72 ± 0.18	14	2.64 ± 0.16	14	0.3084	No
3% GT1b	2.22 ± 0.13	15	2.40 ± 0.17	15	0.0074	Yes
5% GT1b	1.78 ± 0.09	15	2.05 ± 0.19	15	0.0002	Yes

Table 5.1. Lipid diffusion coefficients determined from FRAP measurements. [a]*P* value for paired t-tests comparing diffusion coefficients for SLBs before and after EDTA addition. [b]Samples were identified as significantly different if $P < 0.05$.

Thus, our FRAP results show that gangliosides reduce lipid diffusion coefficients in the presence and absence of Ca^{2+}. Furthermore, the presence of Ca^{2+} causes an overall reduction (slowing) of lipid diffusion coefficients. The 5% GD1a sample, which exhibited signs of intact liposomes and supported bilayer patches in the QCM-D experiments with Ca^{2+} (Figure 5.8a,b), showed complete SLB formation in the fluorescence microscopy experiments (Figure 5.13). This may reflect subtle differences in the preparation of the glass coverslips used for FRAP and the SiO_2 surfaces used for QCM-D.

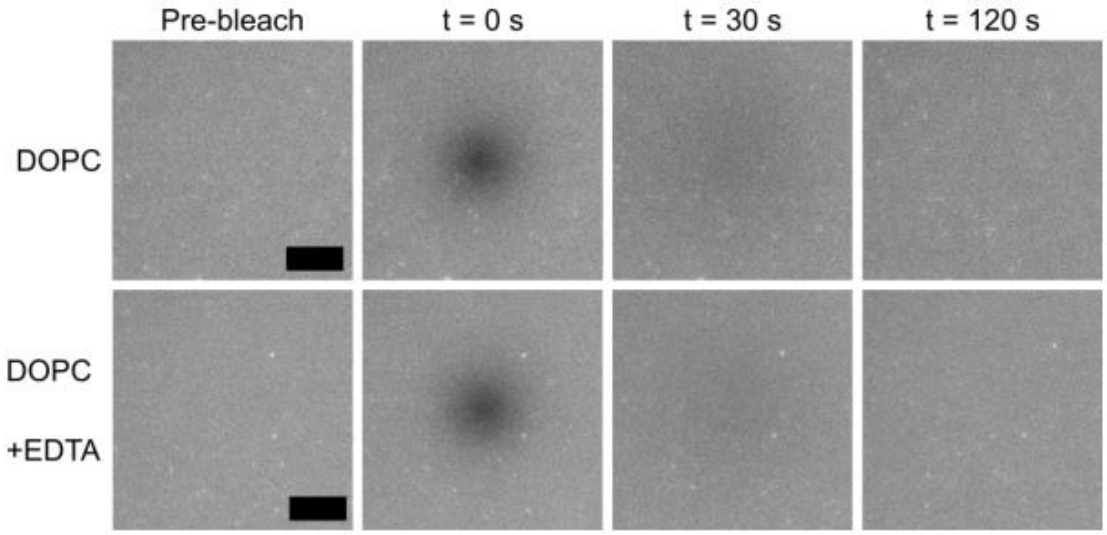

Figure 5.11. FRAP images of DOPC supported lipid bilayers before and after Ca^{2+} chelation with EDTA. Scale bar = 10 μm.

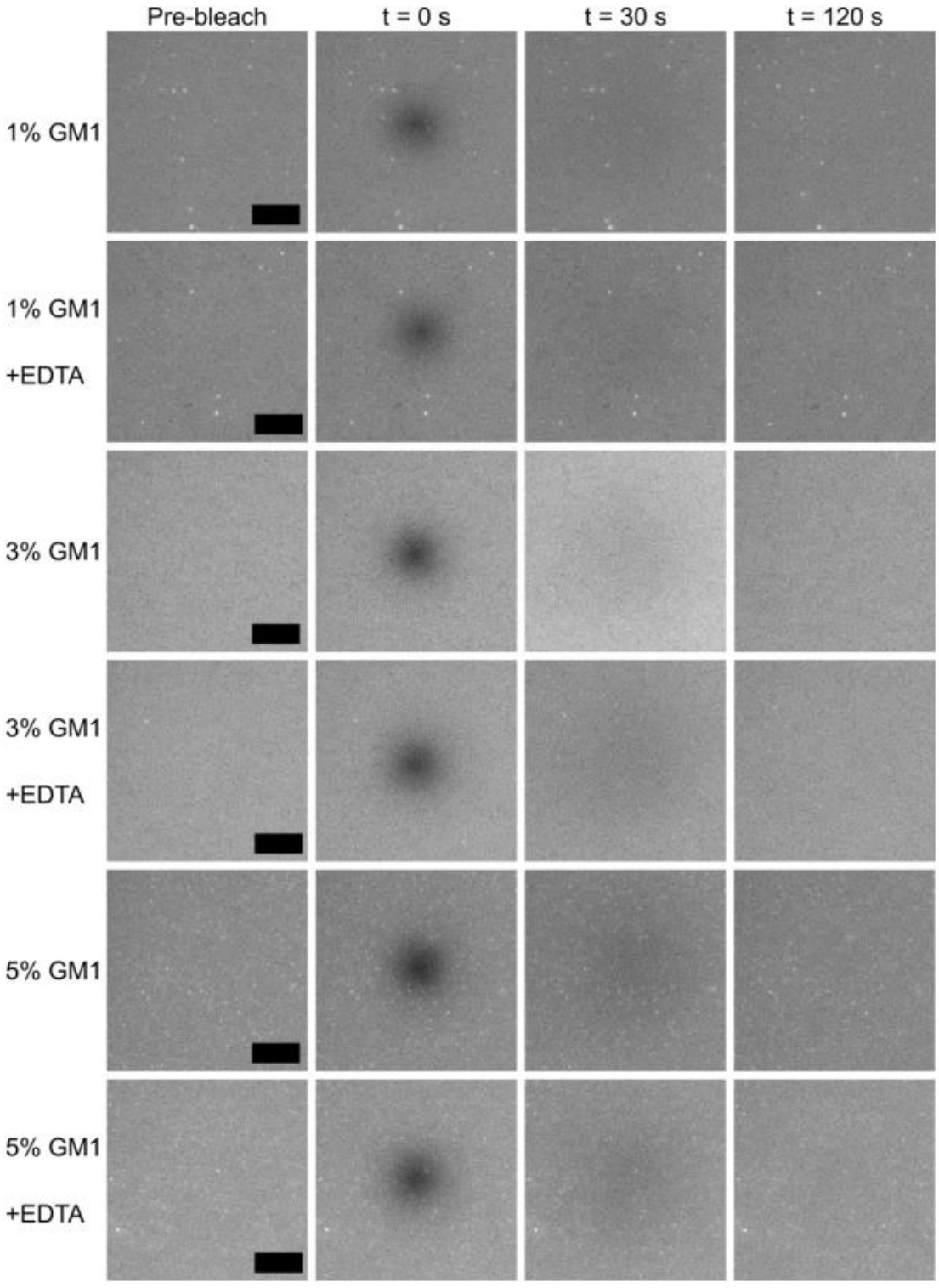

Figure 5.12. FRAP images of DOPC supported lipid bilayers containing 1, 3, or 5% GM1 before and after Ca^{2+} chelation with EDTA. Scale bar = 10 μm.

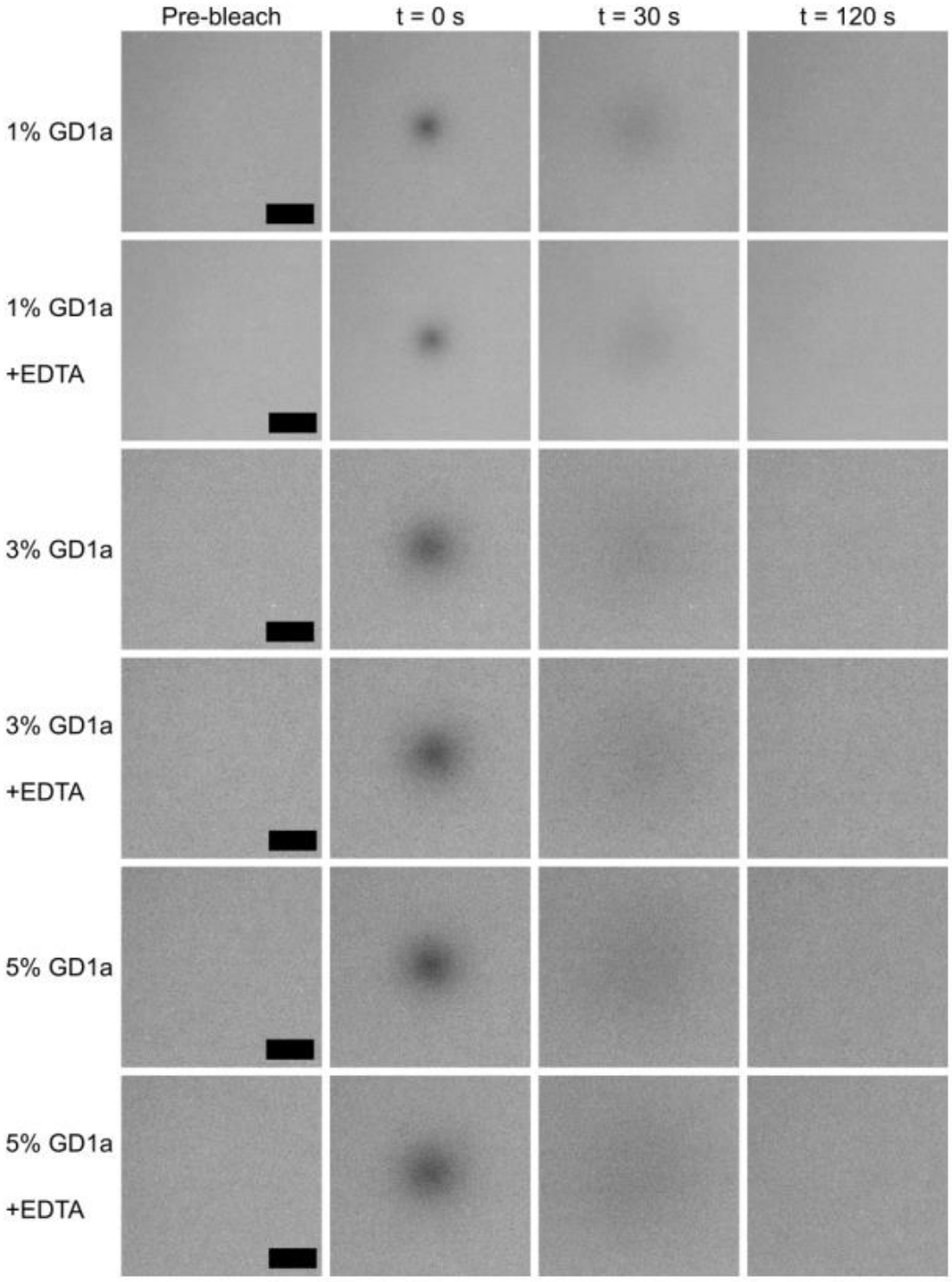

Figure 5.13. FRAP images of DOPC supported lipid bilayers containing 1, 3, or 5% GD1a before and after Ca^{2+} chelation with EDTA. Scale bar = 10 µm

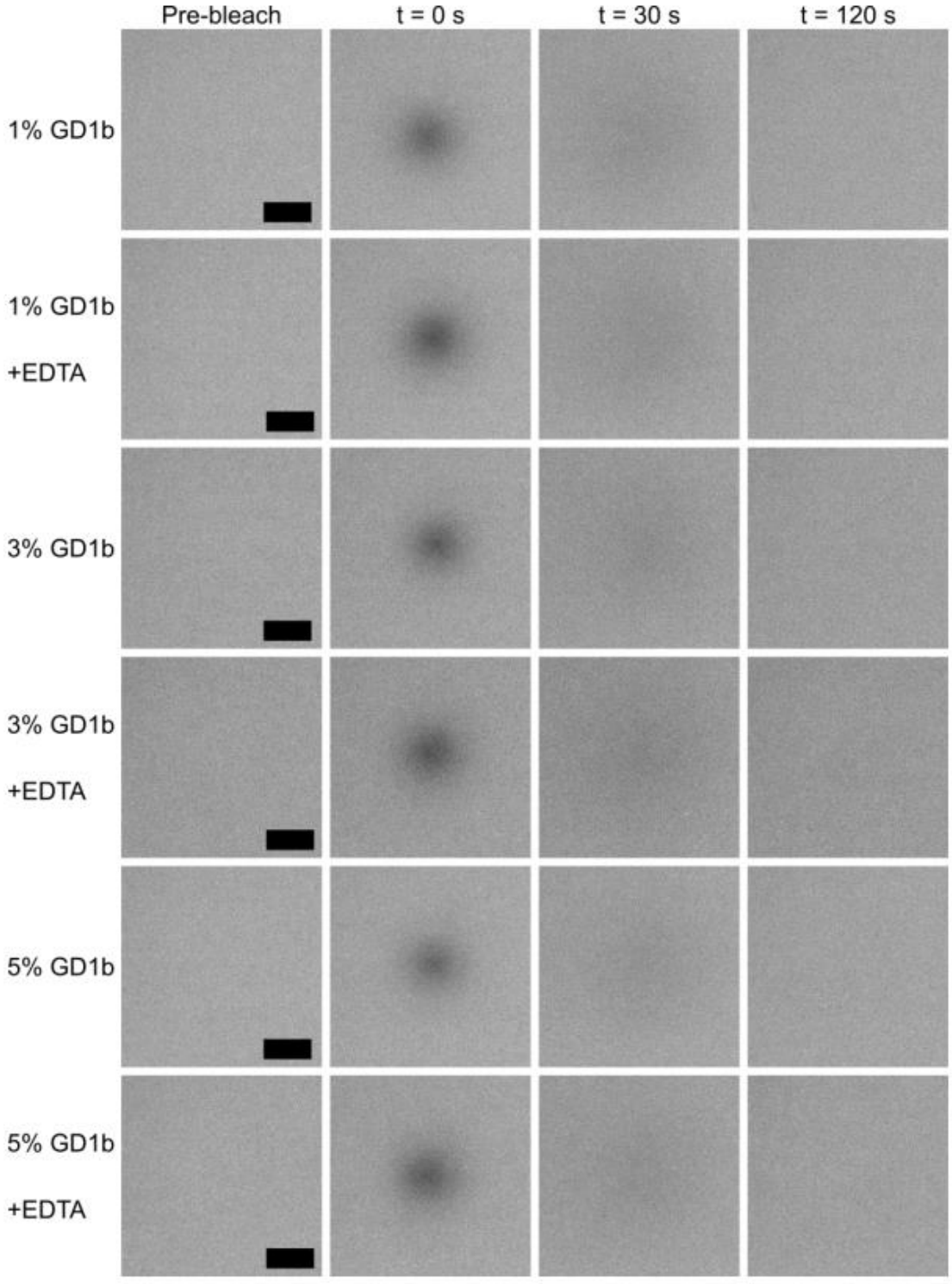

Figure 5.14. FRAP images of DOPC supported lipid bilayers containing 1, 3, or 5% GD1b before and after Ca^{2+} chelation with EDTA. Scale bar = 10 µm.

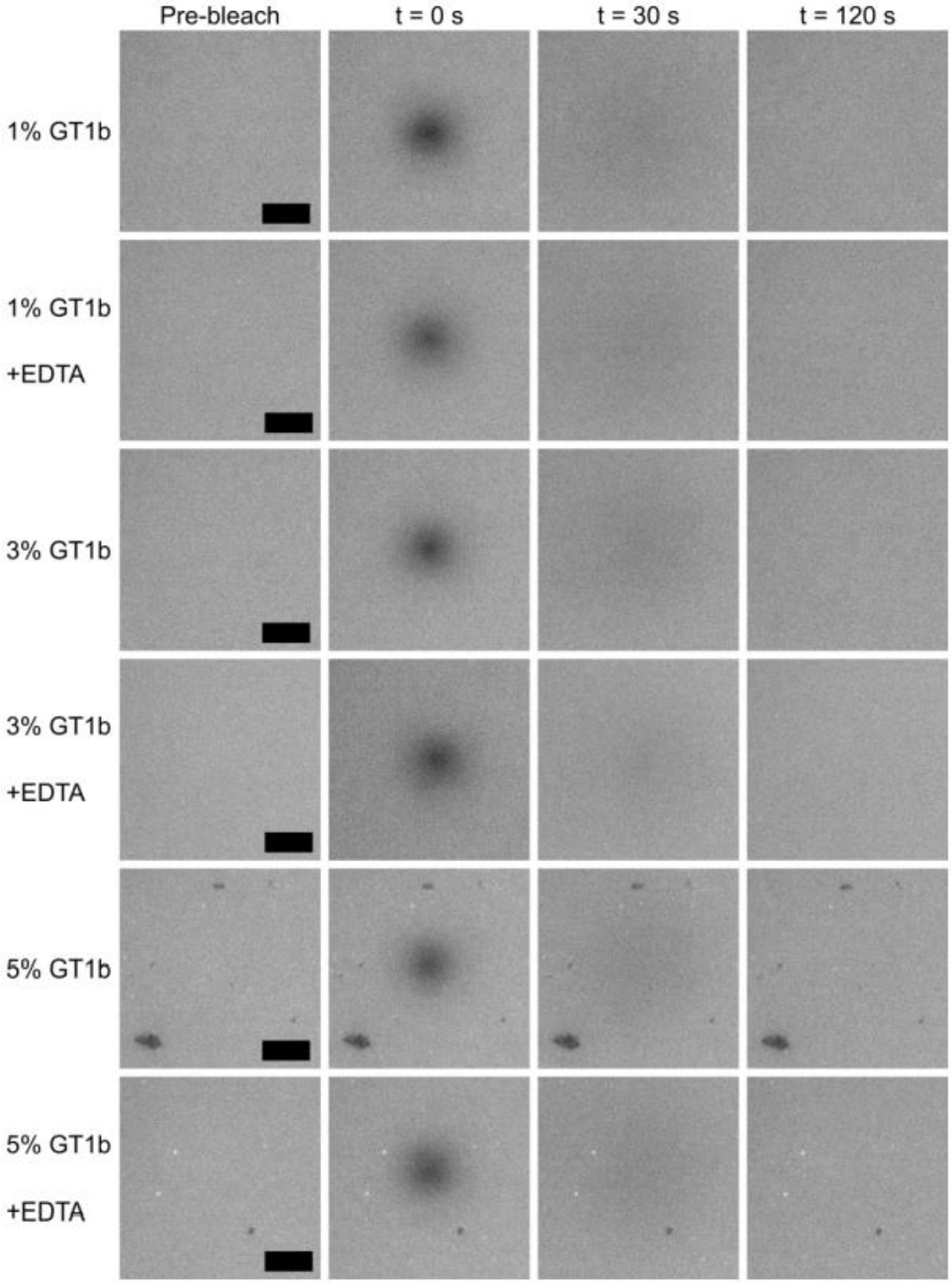

Figure 5.15. FRAP images of DOPC supported lipid bilayers containing 1, 3, or 5% GT1b before and after Ca^{2+} chelation with EDTA. Scale bar = 10 μm.

Other groups have also observed ganglioside-dependent reduction in lipid diffusion coefficients. For example, Weng et al. observed 9% and 16% reduction in diffusion coefficients for TR-DHPE in egg-PC SLBs containing 2% and 5% GM1, respectively.[30] Using POPC SLBs, Sagle et al. observed a 24% reduction in lipid diffusion coefficient when the GM1 concentration was raised from 0% to 8%.[69] We observed reductions in diffusion coefficients of 8% and 29% for SLBs containing 1% and 5% GM1, respectively. The reduction of diffusion coefficients could be due to formation of ganglioside clusters, which have been observed in SLBs in the absence of cholesterol. GM1 clusters in POPC SLBs were measured to be roughly 7 to 20 nm in diameter as the concentration of GM1 is increased from 0.1 to 10%.[6] Such clusters could act as obstacles to TR-DHPE diffusion, which would lower the observed diffusion coefficients.

Ganglioside clustering can be driven by a combination of hydrogen bonding interactions between glycan head groups[70] and ganglioside tail group interactions. Ganglioside tails are composed of ceramide that is made up of sphingosine and a fatty acid. The bovine ganglioside ceramide tails are primarily composed of a saturated (18:0) fatty acid chain and an unsaturated (18:1) sphingosine chain.[71] By itself, as little as 2% ceramide is able to induce a significant increase in lipid order in PC membranes.[72] Thus, it is likely that the reductions in diffusion coefficients we observed are due to ganglioside cluster formation driven by hydrogen bonding between glycan heads along with ceramide-ceramide interactions. Changes in lipid diffusion due to ganglioside-substrate interactions are expected to be minimal because up to 85% of gangliosides reside in the upper membrane leaflet.[62]

Ca^{2+} ions bind phospholipids and gangliosides in membrane bilayers.[73,74] Our results show that Ca^{2+} chelation increases lipid diffusion coefficients for membranes composed solely of DOPC as well as those containing gangliosides. Spectroscopic and molecular dynamics simulations have shown that Ca^{2+}-lipid interactions cause an increase in lipid packing density and tail group order,[75,76] which explains why lower diffusion coefficients are observed when Ca^{2+} is present. Stronger membrane-substrate interactions in the presence of Ca^{2+} can also contribute to reduction in lipid diffusion coefficients.

5.3.4 Measuring Antibody Binding Constants Using Ganglioside-Rich SLBs

We used QCM-D to investigate the binding between a monoclonal IgG anti-GD1a antibody and GD1a embedded in SLBs. Abnormally high levels of anti-GM1 and anti-GD1a antibodies are found in patients with the acute motor axon neuropathy (AMAN) variant of Guillain-Barré syndrome, which can result in the degeneration of motor neurons.[8] The anti-GD1a antibody used here (GD1a-1) binds motor neurons rather than sensory neurons, despite the two cell types having similar levels of GD1a.[77,78] Additionally, GD1a-1 displays similar tissue binding patterns as serum antibodies from AMAN patients.[79] To investigate how GD1a-1 interacts with GD1a in model membranes, we functionalized a SiO_2-coated QCM-D sensor with a SLB containing 1% GD1a.

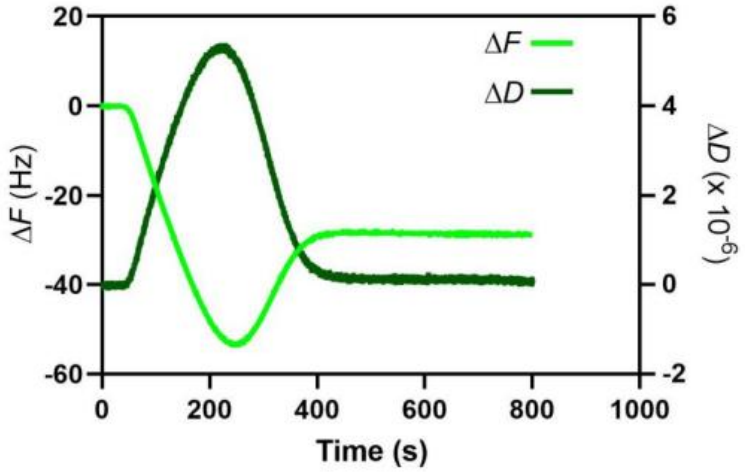

Figure 5.16. Formation of a SLB containing 1% GD1a in the presence of 2 mM Ca^{2+} monitored with QCM-D. The light green curve represents frequency shift (*ΔF*) and is plotted against the left y-axis. The dark green curve represents dissipation shift (*ΔD*) and is plotted against the right y-axis.

The SLB was formed by rupture of liposomes in Tris buffer containing 2 mM Ca^{2+} (Figure 5.16). Then as a negative control, 10 nM cholera toxin B-subunit (CTB) was injected over the SLB. The negligible frequency shift of the QCM-D indicates that CTB does not bind this lipid composition (Figure 5.17).

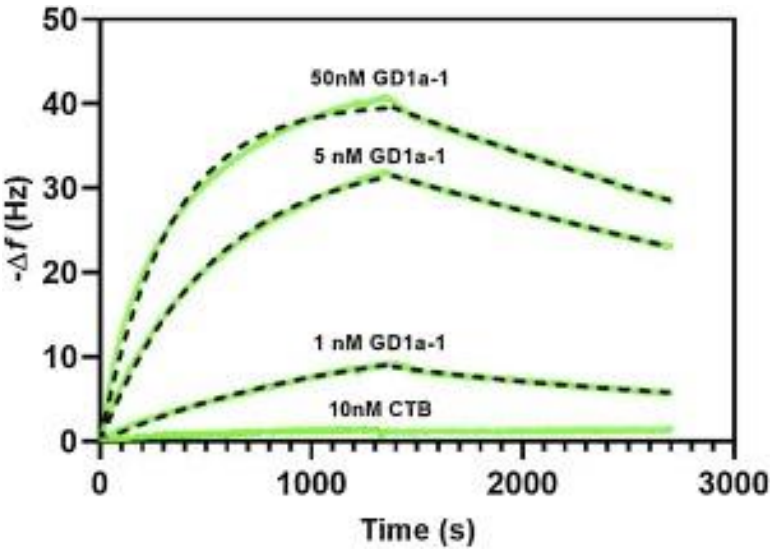

Figure 5.17. QCM-D frequency shift curves showing 1, 5, and 50 nM GD1a-1 antibody binding to SLBs with 1% GD1a. The experimental data is represented with solid green lines, and the fits are shown with dashed black lines. A curve showing 10 nM CTB does not bind to a 1% GD1a SLB is included as a negative control.

Additional SLBs containing 1% GD1a were exposed to 1, 5, or 50 nM GD1a-1 and binding was monitored with QCM-D. As expected, the maximum frequency shift increased with increasing GD1a-1 concentration (Figure 5.17). To determine the rate constants of association (k_a) and dissociation (k_d), the antibody binding curves were fit to exponential models for association and dissociation (dashed line in Figure 5.17). The ratio of the rate constants (k_d/k_a) gives the equilibrium dissociation constant K_D. For GD1a-1 binding to 1% GD1a in a SLB, we determined a K_D of 2.4 ± 1.3 nM (mean ± standard deviation). Monoclonal IgG antibodies typically display K_D values over a wide range, from low pM to nM. Thus, our measured K_D for the monoclonal GD1a-1 is within the expected range.

We conducted additional QCM-D binding assays and controls using GM1-rich SLBs. In these experiments, a SLB composed of DOPC and 5% GM1 was formed by vesicle rupture in the presence of 2 mM Ca^{2+} in Tris buffer. Next, we injected 10 nM GD1a-

1, which did not bind the GM1-rich SLB, indicating antibody specificity. Subsequent injections of escalating concentrations of CTB resulted in increasing shifts in the frequency signal (Figure 5.17). During the wash steps of our binding assay, the amount of CTB dissociation was negligible, which is expected due to the very high affinity CTB has for GM1.[10,25]

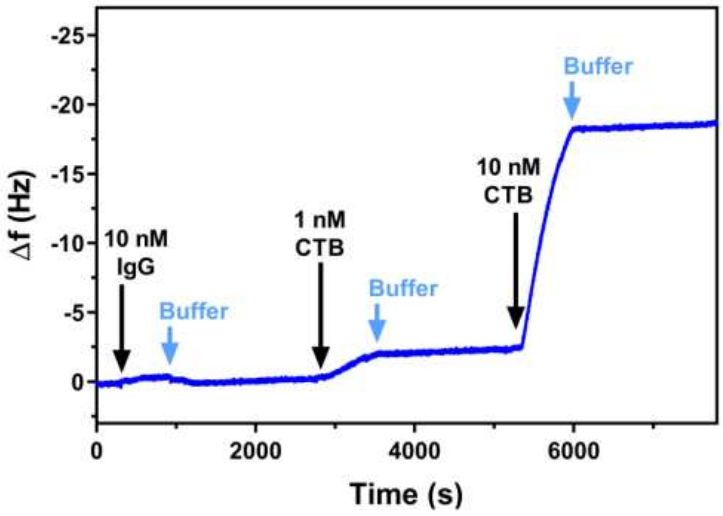

Figure 5.18. Cholera toxin B subunit (CTB) binding to SLB with 5% GM1. The GD1a-1 antibody was first injected over the SLB, and it did not appreciably bind to the SLB. Subsequent injections of 1 and 10 nM of CTB show significant binding and negligible dissociation, indicating a very high affinity interaction.

5.3.5 Curve Fitting for Antibody Binding Assays

Curves were fit to the QCM-D data of binding between anti-GD1a IgG to GD1a-rich SLBs in the following manner. First, an exponential curve was fit to the dissociation phase data, using the following equation:[80]

$$R_D(t) = R_o e^{-k_d t} \qquad \text{eq 5.1}$$

where $R_D(t)$ is the sensor response as a function of time (t), R_o is the magnitude of the sensor response when dissociation begins, and k_d is the dissociation rate constant.

Next, an exponential curve was fit to the association phase data using equation 5.2[80] by inserting the k_d value calculated in equation 5.1:

$$R_A(t) = \frac{Ck_aR_{max}[1 - e^{-(Ck_a+k_d)t}]}{Ck_a + k_d} \qquad \text{eq 5.2}$$

where $R_A(t)$ is the sensor response as a function of time (t), R_{max} is the maximum sensor response for a given antibody concentration, C is the bulk concentration of antibodies in solution, and k_a is the antibody association rate constant.

5.4 Summary and Conclusions

In summary, the presence of gangliosides in liposomes can significantly alter the process of SLB formation by spontaneous liposome rupture. The gangliosides GD1a and GT1b hinder the SLB formation process much more than GM1 and GD1b. This is likely due to the presence of sialic acids on the terminal galactose of the glycan head group. Electrostatic repulsion between the SiO_2 or glass substrates and the terminal sialic acid may account for the relatively slow liposome rupture kinetics. The inclusion of Ca^{2+} in buffers has been previously shown to accelerate liposome rupture, especially for lipid compositions containing anionic lipids. We observe similar effects, with Ca^{2+} resulting in up to a 10-fold reduction in the critical time for the liposome rupture cascade to begin when

gangliosides are present at the 5% level. Lipid diffusion coefficients tend to decrease as ganglioside concentrations in SLBs increase. This trend is observed in the presence of Ca^{2+} and after Ca^{2+} chelation. Chelation and removal of Ca^{2+} significantly increases lipid diffusion coefficients for most compositions studied. Finally, we used a QCM-D sensor functionalized with SLBs containing GD1a to measure the binding kinetics and affinity of GD1a-1, a monoclonal antibody with properties similar to those found in the AMAN variant of Guillain-Barré syndrome. This antibody binds GD1a with a K_D of 2.4 nM.

5.5 Materials and Methods

5.5.1 Reagents and Chemicals

Lipids were purchased and stored in chloroform or a chloroform/methanol mixture. All lipid stock vials were backfilled with Ar gas and stored in a -20 °C freezer. 1,2-dioleoyl-sn-glycero-3-phosphocholine (DOPC) and GM1 (ovine brain) were purchased from Avanti Polar Lipids. Gangliosides GD1a (bovine brain), GD1b (bovine brain), and GT1b (bovine brain) and bovine serum albumin (BSA) were purchased from Sigma-Aldrich. Texas Red DHPE and cholera toxin B subunit (CTB) were purchased from ThermoFisher Scientific. The GD1a-1 antibody was obtained from the Developmental Studies Hybridoma Bank at the University of Iowa (DSHB Hybridoma Product GD1a-1). All buffer chemicals and detergents were obtained from Sigma-Aldrich or Fisher and were used as received. All water used to make buffers was 18 MΩ-cm ultrapure H_2O (PureLab Classic UV, ELGA LabWater). Three different Tris buffers were used in this work: “Tris1” (10 mM Tris, 150 mM NaCl, pH 7.0), “Tris2” (10 mM Tris, 250 mM NaCl, pH 7.0), and

"Tris3" (10 mM Tris, 150 mM NaCl, 2.2 mM $CaCl_2$, pH 7.0), pH was adjusted dropwise with concentrated HCl.

5.5.2 Liposome Preparation

Liposomes were prepared by mixing lipids in chloroform or chloroform/methanol (2:1 v/v): DOPC only, DOPC/GM1 (1–5 mol%), DOPC/GD1a (1–5 mol%), DOPC/GD1b (1–5 mol%), or DOPC/GT1b (1–5 mol%). The solvent was then evaporated under vacuum for at least 4 h. Dried lipid films were rehydrated with Tris1 buffer to give a final lipid concentration of 1 mg mL^{-1}. Liposomes were made by high-speed vortexing the solution for 10 s, bath sonicating (Branson 3510 Ultrasonic Cleaner) at room temperature for 10 min, and finally extruding (Mini-Extruder, Avanti Polar Lipids) through a 50 nm diameter pore filter (polycarbonate track etch membranes, Avanti Polar Lipids) for a total of 23 passes. Prior to experiments, liposomes were diluted in either Tris1 buffer or Tris3 buffer to a lipid concentration of 0.1 mg mL^{-1}.

5.5.3 QCM-D Measurements

The QCM-D (Q-Sense E1 Explorer, Biolin Scientific) experiments were performed on AT-cut quartz crystals with a gold surface coated with SiO_2 (Biolin, Q-Sense chip QSX 303). Quartz crystals were prepared by cleaning with a stream of N_2 gas, 10 min UV ozone treatment (ProCleaner Plus, Bioforce Nanosciences), a 30 min soak in 2% (w/v) sodium dodecyl sulfate (SDS) solution, rinsing with ultrapure water, drying with N_2 gas, and 10 min UV ozone. After cleaning, the sensors were mounted in the flow cell and liquid was flowed over them within 5 min. The sensor was driven at 5 MHz and several overtones.

The third overtone was used for all analyses. The flow cell was held at 23.0 °C. The injection sequence for SLB formation was Tris1, liposomes in Tris1 or Tris3, Tris1, Tris2, Tris1. The goal of the short high ionic strength Tris2 injection was to induce the rupture of intact adsorbed liposomes with osmotic stress. In binding experiments with CTB or antibodies, the injection sequence was Tris1, liposomes in Tris3, Tris1, antibody in Tris1, Tris1. The flow rate was held at 100 µL min^{-1} throughout all steps. All QCM-D measurements of supported bilayer formation were repeated at least 3 times.

5.5.4 Zeta Potential Measurements

A ZetaPALS Zeta Potential Analyzer (Brookhaven Instruments Corp.) was used to measure zeta potential. Liposomes were diluted to 0.2 mg mL^{-1} in 10 mM NaCl. A total of 30 measurements were obtained for each sample. Temperature was held constant at 23 ± 1 °C. Data reported are as the mean ± standard deviation for each liposome composition.

5.5.5 FRAP Measurements

For FRAP experiments, 0.1 mol% of the lipid-conjugated fluorophore Texas Red-DHPE was included in all liposome mixtures. Liposomes were prepared with a 1 mg mL^{-1} lipid concentration in Tris1 buffer and diluted 10-fold in Tris3 right before adding to a glass coverslip. The glass coverslips were cleaned by soaking in 2% (v/v) Hellmanex III at 35°C for 40 min, followed by rinsing with ultrapure H_2O, and drying with a stream of N_2 gas. PDMS wells (6 mm diameter) were bonded to the coverslips by activating both surfaces with a plasma cleaner (Harrick Plasma, Ithaca, NY) using atmospheric gases at

approx. 270 mTorr on "high" for 1.5 min. Liposomes were added to the wells within 20 min, and then incubated for 1 h, followed by washing with Tris1 to rinse away loose liposomes. After the Tris1 wash, SLBs were examined with FRAP. Then the SLBs were washed with Tris1 containing 2 mM EDTA to chelate residual Ca^{2+}, and finally washed with Tris1 prior to additional FRAP analysis.

FRAP measurements were conducted with an inverted microscope (Eclipse Ti, Nikon) in epifluorescence mode with a 100x oil immersion objective (NA = 1.49). Fluorescence was excited using an LED lamp source (Aura II, Lumencor) and a Texas Red filter set (modified TRF49909, Chroma) and captured with an air-cooled 2048 x 2048-pixel sCMOS camera (Orca Flash 4.0 v2, Hamamatsu). Fluorophores were bleached in a circular spot by focusing a 405 nm laser (50 mW) on the sample for 3 s, and images collected with the Texas Red filter set every 1 s for 2 min. FRAP analysis was performed using the Hankel transform MATLAB code created by Jönsson et al.[67] FRAP images were made using the FIJI version of ImageJ.[81] The number of replicates for each of the FRAP experiments is listed in Table 5.1.

5.5.6 Statistical Analysis

Paired t-tests were used to compare diffusion coefficients before and after addition of EDTA. One-way ANOVAs (Dunnett test, grouped by ganglioside and compared to control DOPC-only liposomes) were used to compare QCM-D data. All statistical tests were done in Prism 8, GraphPad Software.

5.6 References

(1) Vajn, K.; Viljetić, B.; Degmečić, I. V.; Schnaar, R. L.; Heffer, M. Differential Distribution of Major Brain Gangliosides in the Adult Mouse Central Nervous System. *PLoS ONE* **2013**, *8* (9), e75720.

(2) Schnaar, R. L.; Gerardy-Schahn, R.; Hildebrandt, H. Sialic Acids in the Brain: Gangliosides and Polysialic Acid in Nervous System Development, Stability, Disease, and Regeneration. *Physiol. Rev.* **2014**, *94* (2), 461–518.

(3) Tettamanti, G.; Bonali, F.; Marchesini, S.; Zambotti, V. A New Procedure for the Extraction, Purification and Fractionation of Brain Gangliosides. *Biochim. Biophys. Acta BBA - Lipids Lipid Metab.* **1973**, *296* (1), 160–170.

(4) Sonnino, S.; Mauri, L.; Chigorno, V.; Prinetti, A. Gangliosides as Components of Lipid Membrane Domains. *Glycobiology* **2007**, *17* (1), 1R-13R.

(5) Lozano, M. M.; Liu, Z.; Sunnick, E.; Janshoff, A.; Kumar, K.; Boxer, S. G. Colocalization of the Ganglioside GM1 and Cholesterol Detected by Secondary Ion Mass Spectrometry. *J. Am. Chem. Soc.* **2013**, *135* (15), 5620–5630.

(6) Shi, J.; Yang, T.; Kataoka, S.; Zhang, Y.; Diaz, A. J.; Cremer, P. S. GM1 Clustering Inhibits Cholera Toxin Binding in Supported Phospholipid Membranes. *J. Am. Chem. Soc.* **2007**, *129* (18), 5954–5961.

(7) Yang, L. J.; Zeller, C. B.; Shaper, N. L.; Kiso, M.; Hasegawa, A.; Shapiro, R. E.; Schnaar, R. L. Gangliosides Are Neuronal Ligands for Myelin-Associated Glycoprotein. *Proc. Natl. Acad. Sci.* **1996**, *93* (2), 814–818.

(8) Hughes, R. A.; Cornblath, D. R. Guillain-Barré Syndrome. *The Lancet* **2005**, *366* (9497), 1653–1666.

(9) Ravindran, M. S.; Tanner, L. B.; Wenk, M. R. Sialic Acid Linkage in Glycosphingolipids Is a Molecular Correlate for Trafficking and Delivery of Extracellular Cargo. *Traffic* **2013**, *14* (11), 1182–1191.

(10) Kuziemko, G. M.; Stroh, M.; Stevens, R. C. Cholera Toxin Binding Affinity and Specificity for Gangliosides Determined by Surface Plasmon Resonance. *Biochemistry* **1996**, *35* (20), 6375–6384.

(11) Minke, W. E.; Roach, C.; Hol, W. G. J.; Verlinde, C. L. M. J. Structure-Based Exploration of the Ganglioside GM1 Binding Sites of Escherichia Coli Heat-Labile Enterotoxin and Cholera Toxin for the Discovery of Receptor Antagonists. *Biochemistry* **1999**, *38* (18), 5684–5692.

(12) Montecucco, C.; Schiavo, G. Structure and Function of Tetanus and Botulinum Neurotoxins. *Q. Rev. Biophys.* **1995**, *28* (4), 423–472.

(13) Yanagisawa, K.; Odaka, A.; Suzuki, N.; Ihara, Y. GM1 Ganglioside–Bound Amyloid β–Protein (Aβ): A Possible Form of Preamyloid in Alzheimer's Disease. *Nat. Med.* **1995**, *1* (10), 1062–1066.

(14) Gaspar, R.; Pallbo, J.; Weininger, U.; Linse, S.; Sparr, E. Ganglioside Lipids Accelerate α-Synuclein Amyloid Formation. *Biochim. Biophys. Acta BBA - Proteins Proteomics* **2018**, *1866* (10), 1062–1072.

(15) Castellana, E. T.; Cremer, P. S. Solid Supported Lipid Bilayers: From Biophysical Studies to Sensor Design. *Surf. Sci. Rep.* **2006**, *61* (10), 429–444.

(16) Richter, R. P.; Bérat, R.; Brisson, A. R. Formation of Solid-Supported Lipid Bilayers: An Integrated View. *Langmuir* **2006**, *22* (8), 3497–3505.

(17) Mazur, F.; Bally, M.; Städler, B.; Chandrawati, R. Liposomes and Lipid Bilayers in Biosensors. *Adv. Colloid Interface Sci.* **2017**, *249*, 88–99.

(18) Singh, A. K.; Harrison, S. H.; Schoeniger, J. S. Gangliosides as Receptors for Biological Toxins: Development of Sensitive Fluoroimmunoassays Using Ganglioside-Bearing Liposomes. *Anal. Chem.* **2000**, *72* (24), 6019–6024.

(19) Moran-Mirabal, J. M.; Edel, J. B.; Meyer, G. D.; Throckmorton, D.; Singh, A. K.; Craighead, H. G. Micrometer-Sized Supported Lipid Bilayer Arrays for Bacterial Toxin Binding Studies through Total Internal Reflection Fluorescence Microscopy. *Biophys. J.* **2005**, *89* (1), 296–305.

(20) Wittenberg, N. J.; Johnson, T. W.; Oh, S.-H. High-Density Arrays of Submicron Spherical Supported Lipid Bilayers. *Anal. Chem.* **2012**, *84* (19), 8207–8213.

(21) Kabbani, A. M.; Kelly, C. V. Nanoscale Membrane Budding Induced by CTxB and Detected via Polarized Localization Microscopy. *Biophys. J.* **2017**, *113* (8), 1795–1806.

(22) Parveen, N.; Rimkute, I.; Block, S.; Rydell, G. E.; Midtvedt, D.; Larson, G.; Hytönen, V. P.; Zhdanov, V. P.; Lundgren, A.; Höök, F. Membrane Deformation Induces Clustering of Norovirus Bound to Glycosphingolipids in a Supported Cell-Membrane Mimic. *J. Phys. Chem. Lett.* **2018**, *9* (9), 2278–2284.

(23) Baksh, M. M.; Kussrow, A. K.; Mileni, M.; Finn, M. G.; Bornhop, D. J. Label-Free Quantification of Membrane-Ligand Interactions Using Backscattering Interferometry. *Nat. Biotechnol.* **2011**, *29* (4), 357–360.

(24) Baksh, M. M.; Jaros, M.; Groves, J. T. Detection of Molecular Interactions at Membrane Surfaces through Colloid Phase Transitions. *Nature* **2004**, *427* (6970), 139–141.

(25) Lee, S. H.; Lindquist, N. C.; Wittenberg, N. J.; Jordan, L. R.; Oh, S.-H. Real-Time Full-Spectral Imaging and Affinity Measurements from 50 Microfluidic Channels Using Nanohole Surface Plasmon Resonance. *Lab. Chip* **2012**, *12* (20), 3882–3890.

(26) Xu, X.; Denic, A.; Jordan, L. R.; Wittenberg, N. J.; Warrington, A. E.; Wootla, B.; Papke, L. M.; Zoecklein, L. J.; Yoo, D.; Shaver, J.; Oh, S.-H.; Pease, L. R.; Rodriguez, M. A Natural Human IgM That Binds to Gangliosides Is Therapeutic in Murine Models of Amyotrophic Lateral Sclerosis. *Dis. Model. Mech.* **2015**, *8* (8), 831–842.

(27) Wu, H.-J.; Henzie, J.; Lin, W.-C.; Rhodes, C.; Li, Z.; Sartorel, E.; Thorner, J.; Yang, P.; Groves, J. T. Membrane-Protein Binding Measured with Solution-Phase Plasmonic Nanocube Sensors. *Nat. Methods* **2012**, *9* (12), 1189–1191.

(28) Turnbull, W. B.; Precious, B. L.; Homans, S. W. Dissecting the Cholera Toxin−Ganglioside GM1 Interaction by Isothermal Titration Calorimetry. *J. Am. Chem. Soc.* **2004**, *126* (4), 1047–1054.

(29) Janshoff, A.; Steinem, C.; Sieber, M.; el Bayâ, A.; Schmidt, M. A.; Galla, H.-J. Quartz Crystal Microbalance Investigation of the Interaction of Bacterial Toxins with Ganglioside Containing Solid Supported Membranes. *Eur. Biophys. J.* **1997**, *26* (3), 261–270.

(30) Weng, K. C.; Kanter, J. L.; Robinson, W. H.; Frank, C. W. Fluid Supported Lipid Bilayers Containing Monosialoganglioside GM1: A QCM-D and FRAP Study. *Colloids Surf. B Biointerfaces* **2006**, *50* (1), 76–84.

(31) Brian, A. A.; McConnell, H. M. Allogeneic Stimulation of Cytotoxic T Cells by Supported Planar Membranes. *Proc. Natl. Acad. Sci.* **1984**, *81* (19), 6159–6163.

(32) Tamm, L. K.; McConnell, H. M. Supported Phospholipid Bilayers. *Biophys. J.* **1985**, *47* (1), 105–113.

(33) Tabaei, S. R.; Choi, J.-H.; Haw Zan, G.; Zhdanov, V. P.; Cho, N.-J. Solvent-Assisted Lipid Bilayer Formation on Silicon Dioxide and Gold. *Langmuir* **2014**, *30* (34), 10363–10373.

(34) Mager, M. D.; Melosh, N. A. Lipid Bilayer Deposition and Patterning via Air Bubble Collapse. *Langmuir* **2007**, *23* (18), 9369–9377.

(35) Seantier, B.; Breffa, C.; Félix, O.; Decher, G. Dissipation-Enhanced Quartz Crystal Microbalance Studies on the Experimental Parameters Controlling the Formation of Supported Lipid Bilayers. *J. Phys. Chem. B* **2005**, *109* (46), 21755–21765.

(36) Jo, S.; Kim, T.; Iyer, V. G.; Im, W. CHARMM-GUI: A Web-Based Graphical User Interface for CHARMM. *J. Comput. Chem.* **2008**, *29* (11), 1859–1865.

(37) Groux-Degroote, S.; Guérardel, Y.; Delannoy, P. Gangliosides: Structures, Biosynthesis, Analysis, and Roles in Cancer. *ChemBioChem* **2017**, *18* (13), 1146–1154.

(38) Patel, R. Y.; Balaji, P. V. Characterization of Symmetric and Asymmetric Lipid Bilayers Composed of Varying Concentrations of Ganglioside GM1 and DPPC. *J. Phys. Chem. B* **2008**, *112* (11), 3346–3356.

(39) Yuan, C.; Johnston, L. J. Distribution of Ganglioside GM1 in L-α-Dipalmitoylphosphatidylcholine/Cholesterol Monolayers: A Model for Lipid Rafts1. *Biophys. J.* **2000**, *79* (5), 2768–2781.

(40) Reviakine, I.; Johannsmann, D.; Richter, R. P. Hearing What You Cannot See and Visualizing What You Hear: Interpreting Quartz Crystal Microbalance Data from Solvated Interfaces. *Anal. Chem.* **2011**, *83* (23), 8838–8848.

(41) Keller, C. A.; Kasemo, B. Surface Specific Kinetics of Lipid Vesicle Adsorption Measured with a Quartz Crystal Microbalance. *Biophys. J.* **1998**, *75* (3), 1397–1402.

(42) Richter, R.; Mukhopadhyay, A.; Brisson, A. Pathways of Lipid Vesicle Deposition on Solid Surfaces: A Combined QCM-D and AFM Study. *Biophys. J.* **2003**, *85* (5), 3035–3047.

(43) Richter, R. P.; Brisson, A. R. Following the Formation of Supported Lipid Bilayers on Mica: A Study Combining AFM, QCM-D, and Ellipsometry. *Biophys. J.* **2005**, *88* (5), 3422–3433.

(44) Keller, C. A.; Glasmästar, K.; Zhdanov, V. P.; Kasemo, B. Formation of Supported Membranes from Vesicles. *Phys. Rev. Lett.* **2000**, *84* (23), 5443–5446.

(45) Cremer, P. S.; Boxer, S. G. Formation and Spreading of Lipid Bilayers on Planar Glass Supports. *J. Phys. Chem. B* **1999**, *103* (13), 2554–2559.

(46) Reimhult, E.; Höök, F.; Kasemo, B. Temperature Dependence of Formation of a Supported Phospholipid Bilayer from Vesicles on SiO2. *Phys. Rev. E* **2002**, *66* (5), 051905.

(47) Reimhult, E.; Höök, F.; Kasemo, B. Vesicle Adsorption on SiO2 and TiO2: Dependence on Vesicle Size. *J. Chem. Phys.* **2002**, *117* (16), 7401–7404.

(48) Reimhult, E.; Höök, F.; Kasemo, B. Intact Vesicle Adsorption and Supported Biomembrane Formation from Vesicles in Solution: Influence of Surface Chemistry, Vesicle Size, Temperature, and Osmotic Pressure. *Langmuir* **2003**, *19* (5), 1681–1691.

(49) Bailey, C. M.; Tripathi, A.; Shukla, A. Effects of Flow and Bulk Vesicle Concentration on Supported Lipid Bilayer Formation. *Langmuir* **2017**, *33* (43), 11986–11997.

(50) Anderson, T. H.; Min, Y.; Weirich, K. L.; Zeng, H.; Fygenson, D.; Israelachvili, J. N. Formation of Supported Bilayers on Silica Substrates. *Langmuir* **2009**, *25* (12), 6997–7005.

(51) Hain, N.; Gallego, M.; Reviakine, I. Unraveling Supported Lipid Bilayer Formation Kinetics: Osmotic Effects. *Langmuir* **2013**, *29* (7), 2282–2288.

(52) Jackman, J. A.; Choi, J.-H.; Zhdanov, V. P.; Cho, N.-J. Influence of Osmotic Pressure on Adhesion of Lipid Vesicles to Solid Supports. *Langmuir* **2013**, *29* (36), 11375–11384.

(53) Cho, N.-J.; Jackman, J. A.; Liu, M.; Frank, C. W. PH-Driven Assembly of Various Supported Lipid Platforms: A Comparative Study on Silicon Oxide and Titanium Oxide. *Langmuir* **2011**, *27* (7), 3739–3748.

(54) Dacic, M.; Jackman, J. A.; Yorulmaz, S.; Zhdanov, V. P.; Kasemo, B.; Cho, N.-J. Influence of Divalent Cations on Deformation and Rupture of Adsorbed Lipid Vesicles. *Langmuir* **2016**, *32* (25), 6486–6495.

(55) Cho, N.-J.; Frank, C. W.; Kasemo, B.; Höök, F. Quartz Crystal Microbalance with Dissipation Monitoring of Supported Lipid Bilayers on Various Substrates. *Nat. Protoc.* **2010**, *5* (6), 1096–1106.

(56) McIntosh, T. J.; Simon, S. A. Hydration Force and Bilayer Deformation: A Reevaluation. *Biochemistry* **1986**, *25* (14), 4058–4066.

(57) Seifert, U.; Lipowsky, R. Adhesion of Vesicles. *Phys. Rev. A* **1990**, *42* (8), 4768–4771.

(58) Zhdanov, V. P.; Kasemo, B. Comments on Rupture of Adsorbed Vesicles. *Langmuir* **2001**, *17* (12), 3518–3521.

(59) Hirabayashi, Y.; Hyogo, A.; Nakao, T.; Tsuchiya, K.; Suzuki, Y.; Matsumoto, M.; Kon, K.; Ando, S. Isolation and Characterization of Extremely Minor Gangliosides, GM1b and GD1 Alpha, in Adult Bovine Brains as Developmentally Regulated Antigens. *J. Biol. Chem.* **1990**, *265* (14), 8144–8151.

(60) Frey, S. L.; Chi, E. Y.; Arratia, C.; Majewski, J.; Kjaer, K.; Lee, K. Y. C. Condensing and Fluidizing Effects of Ganglioside GM1 on Phospholipid Films. *Biophys. J.* **2008**, *94* (8), 3047–3064.

(61) Frey, S. L.; Lee, K. Y. C. Number of Sialic Acid Residues in Ganglioside Headgroup Affects Interactions with Neighboring Lipids. *Biophys. J.* **2013**, *105* (6), 1421–1431.

(62) Carton, I.; Lucy Malinina; Richter, R. P. Dynamic Modulation of the Glycosphingolipid Content in Supported Lipid Bilayers by Glycolipid Transfer Protein. *Biophys. J.* **2010**, *99* (9), 2947–2956.

(63) Seantier, B.; Kasemo, B. Influence of Mono- And Divalent Ions on the Formation of Supported Phospholipid Bilayers via Vesicle Adsorption. *Langmuir* **2009**, *25* (10), 5767–5772.

(64) Rossetti, F. F.; Bally, M.; Michel, R.; Textor, M.; Reviakine, I. Interactions between Titanium Dioxide and Phosphatidyl Serine-Containing Liposomes: Formation and Patterning of Supported Phospholipid Bilayers on the Surface of a Medically Relevant Material. *Langmuir* **2005**, *21* (14), 6443–6450.

(65) Tabaei, S. R.; Guo, F.; Rutaganira, F. U.; Vafaei, S.; Choong, I.; Shokat, K. M.; Glenn, J. S.; Cho, N.-J. Multistep Compositional Remodeling of Supported Lipid Membranes by Interfacially Active Phosphatidylinositol Kinases. *Anal. Chem.* **2016**, *88* (10), 5042–5045.

(66) Tabaei, S. R.; Jackman, J. A.; Kim, S.-O.; Liedberg, B.; Knoll, W.; Parikh, A. N.; Cho, N.-J. Formation of Cholesterol-Rich Supported Membranes Using Solvent-Assisted Lipid Self-Assembly. *Langmuir* **2014**, *30* (44), 13345–13352.

(67) Jönsson, P.; Jonsson, M. P.; Tegenfeldt, J. O.; Höök, F. A Method Improving the Accuracy of Fluorescence Recovery after Photobleaching Analysis. *Biophys. J.* **2008**, *95* (11), 5334–5348.

(68) Tamm, L. K. Lateral Diffusion and Fluorescence Microscope Studies on a Monoclonal Antibody Specifically Bound to Supported Phospholipid Bilayers. *Biochemistry* **1988**, *27* (5), 1450–1457.

(69) Sagle, L. B.; Ruvuna, L. K.; Bingham, J. M.; Liu, C.; Cremer, P. S.; Van Duyne, R. P. Single Plasmonic Nanoparticle Tracking Studies of Solid Supported Bilayers with Ganglioside Lipids. *J. Am. Chem. Soc.* **2012**, *134* (38), 15832–15839.

(70) Sharom, F. J.; Grant, C. W. M. A Model for Ganglioside Behaviour in Cell Membranes. *Biochim. Biophys. Acta BBA - Biomembr.* **1978**, *507* (2), 280–293.

(71) Svennerholm, L. The Gangliosides. *J. Lipid Res.* **1964**, *5* (2), 145–155.

(72) Silva, L.; De Almeida, R. F. M.; Fedorov, A.; Matos, A. P. A.; Prieto, M. Ceramide-Platform Formation and -Induced Biophysical Changes in a Fluid Phospholipid Membrane. *Mol. Membr. Biol.* **2006**, *23* (2), 137–148.

(73) Melcrová, A.; Pokorna, S.; Pullanchery, S.; Kohagen, M.; Jurkiewicz, P.; Hof, M.; Jungwirth, P.; Cremer, P. S.; Cwiklik, L. The Complex Nature of Calcium Cation Interactions with Phospholipid Bilayers. *Sci. Rep.* **2016**, *6* (1), 38035.

(74) McDaniel, R.; McLaughlin, S. The Interaction of Calcium with Gangliosides in Bilayer Membranes. *Biochim. Biophys. Acta BBA - Biomembr.* **1985**, *819* (2), 153–160.

(75) Böckmann, R. A.; Grubmüller, H. Multistep Binding of Divalent Cations to Phospholipid Bilayers: A Molecular Dynamics Study. *Angew. Chem. Int. Ed.* **2004**, *43* (8), 1021–1024.

(76) Binder, H.; Zschörnig, O. The Effect of Metal Cations on the Phase Behavior and Hydration Characteristics of Phospholipid Membranes. *Chem. Phys. Lipids* **2002**, *115* (1), 39–61.

(77) Svennerholm, L.; Boström, K.; Fredman, P.; Jungbjer, B.; Lekman, A.; Månsson, J.-E.; Rynmark, B.-M. Gangliosides and Allied Glycosphingolipids in Human Peripheral Nerve and Spinal Cord. *Biochim. Biophys. Acta BBA - Lipids Lipid Metab.* **1994**, *1214* (2), 115–123.

(78) Gong, Y.; Tagawa, Y.; Lunn, M. P. T.; Laroy, W.; Heffer-Lauc, M.; Li, C. Y.; Griffin, J. W.; Schnaar, R. L.; Sheikh, K. A. Localization of Major Gangliosides in the PNS: Implications for Immune Neuropathies. *Brain* **2002**, *125* (11), 2491–2506.

(79) Lopez, P. H. H.; Zhang, G.; Bianchet, M. A.; Schnaar, R. L.; Sheikh, K. A. Structural Requirements of Anti-GD1a Antibodies Determine Their Target Specificity. *Brain* **2008**, *131* (7), 1926–1939.

(80) O'Shannessy, D. J.; Brighamburke, M.; Soneson, K. K.; Hensley, P.; Brooks, I. Determination of Rate and Equilibrium Binding Constants for Macromolecular Interactions Using Surface Plasmon Resonance: Use of Nonlinear Least Squares Analysis Methods. *Anal. Biochem.* **1993**, *212* (2), 457–468.

(81) Schindelin, J.; Arganda-Carreras, I.; Frise, E.; Kaynig, V.; Longair, M.; Pietzsch, T.; Preibisch, S.; Rueden, C.; Saalfeld, S.; Schmid, B.; Tinevez, J.-Y.; White, D. J.; Hartenstein, V.; Eliceiri, K.; Tomancak, P.; Cardona, A. Fiji: An Open-Source Platform for Biological-Image Analysis. *Nat. Methods* **2012**, *9* (7), 676–682.

Chapter 6: Future Directions

6.1 Introduction

Apoptosis (cell death) leads to the generation of reactive oxygen species, which can result in oxidative stress to membranes. While a majority of this dissertation has discussed the negative consequences of lipid oxidation, cells also use the presence of oxidized lipids as signaling molecules and markers for injury or illness. Atherosclerosis, kidney disease, pathogenic infections, and other inflammatory or non-inflammatory tissue injuries can generate oxidized phospholipids in membranes.[1]

As previously discussed in earlier chapters, the oxidation of fatty acid tails leads to structural changes of the lipid. Oxidized tails are more polar in nature, and thus flip upwards/outwards to be closer to the aqueous interface rather than be buried in the hydrophobic core of a membrane. This results in short "whiskers" that protrude from the membrane.[2] It is thought that the presence of these whiskers trigger an immune response to oxidative stress.[3]

It is the responsibility of the innate immune system to detect the presence of oxidized lipids within cells or tissues, and to mediate an appropriate response.[4] CD36 is a protein found on the surface of many immune cells (i.e. macrophages, dendritic cells, and monocytes); the key function of CD36 is to recognize oxidized lipids.[5] The binding of CD36 to oxidized lipids (oxPC) triggers an immune response, prompting lipid uptake or phagocytosis via macrophages, along with an inflammatory response.[6] However, not much is currently known about the precise mechanism of modulation of CD36, nor about the recognition of oxPC by CD36. Therapies that target and block CD36 activity have been suggested for the treatment of kidney disease,[7] atherosclerosis,[8] diabetes,[9] and cancer

metastasis.[10] Determining the binding kinetics and affinity of CD36 to oxPC is critical in furthering understanding of those potential CD36-targeted therapies. This chapter outlines potential directions of future research in the Wittenberg lab that builds upon the foundations I have laid throughout my graduate career.

6.2 Binding Studies of CD36 to Oxidized Lipids

QCM-D is a viable option with which to monitor protein binding kinetics. SLBs rich in oxPC can be formed on SiO_2 sensors in a QCM-D instrument. Once a bilayer has been formed, CD36 can be flowed overtop the oxidized bilayer. If binding occurs, there will be a negative shift in the frequency signal, and a positive shift in the dissipation signal. By controlling the concentration of both the oxPC within the SLB and the CD36 protein, and by controlling the flowrate and flow times, association and dissociation constants can be calculated using the same approach as described in chapter five.

Similarly, SLBs containing oxPC can be formed on glass coverslips, and analyzed with fluorescence microscopy. FRAP analyses can be performed to monitor changes to lipid diffusion coefficients as a result of changing the concentration of oxPC containing within the SLB. Also, TIRFM can be a useful technique with which to also calculate binding kinetics of CD36 to SLBs containing oxPC (Figure 6.1).

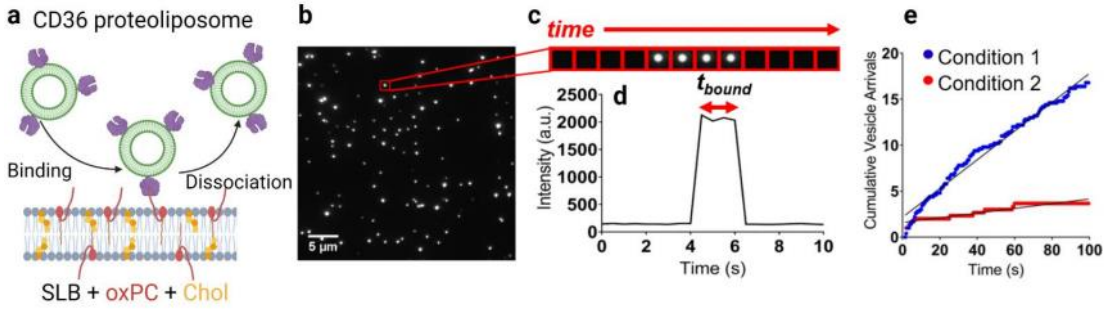

Figure 6.1. Approach to measure CD36-oxPC interaction kinetics and affinity. (a) Illustration of a supported lipid bilayer (SLB) possessing "whiskers" (red) and cholesterol (orange). Fluorescent CD36 proteoliposomes bind to the membrane giving a fluorescent spot in the TIRF image. Dissociation of the proteoliposome causes the fluorescent spot to vanish. (b) TIRF image and kymograph (c) of a fluorescent liposome transiently associating to SLB-bound receptors. (d) Bound state lifetime (t_{bound}) for an individual receptor-mediated liposome binding process, which is related to the dissociation rate constant for the interaction. (e) Cumulative liposome arrivals plot showing receptor-mediated liposome binding under two different conditions. The plot for Condition 1 has a greater slope, thus the association rate constant for Condition 1 is greater than for Condition 2. (Credit to Nathan Wittenberg for the creation of this figure.)

Fluorescent proteoliposomes incorporating CD36 can be made and incubated atop a bilayer rich in oxPC. Because TIRFM gives a surface-level view of samples,[11] binding of CD36 proteoliposomes would appear as bright spots, and when they dissociate, that bright spot would disappear. The length of time that the proteoliposome remains bound can be used to calculate binding kinetics. This technique can be used to probe the differences in binding kinetics when variables such as oxPC concentration, CD36 protein concentration, or cholesterol concentration are adjusted.

6.2.1 The Influence of Cholesterol on CD36 Binding

Cholesterol is abundant in cell membranes, though studies have shown that cholesterol can alter lipid packing and lipid conformation in membranes, which can

sometimes impede protein binding. The hydroxyl group on the head of cholesterol can alter hydrogen-bonding of nearby lipids in a membrane—essentially, cholesterol can sometimes "mask" receptors from proteins.[12] Chapter four of this dissertation discussed that the presence of oxidized lipids aids in the incorporation of higher cholesterol concentrations. Therefore, it would be interesting to perform the QCM-D and TIRFM experiments as described in the section above with increasing concentrations of cholesterol to observe the influence cholesterol has on CD36 binding kinetics.

6.3 Spatiotemporal Response of Immune Cells to Oxidized Lipid Gradients

As discussed in the introduction of this section, immune cells (such as macrophages) can recognize the presence of oxidized lipids, which triggers an immune response. To determine the spatiotemporal response of macrophages to the presence of oxidized lipids, gradients of oxidized lipid concentration can be generated in SLB membranes.

One option of creating such a gradient is through the use of a microfluidic device (Figure 6.2a). A microfluidic mixer contains multiple channels that eventually feed into one larger channel. Liposomes with different concentrations of oxPC can be flowed through the smaller channels. These liposomes then rupture, which will result in a gradient of oxidized lipids in a SLB. Macrophages can then be injected into the microfluidic device to determine their preference for adhesion to membranes with varying concentrations of oxidized lipids (Figure 6.2b). Additionally, gradients of cholesterol and oxPC concentration can be used to monitor the influence of cholesterol on macrophage migration.

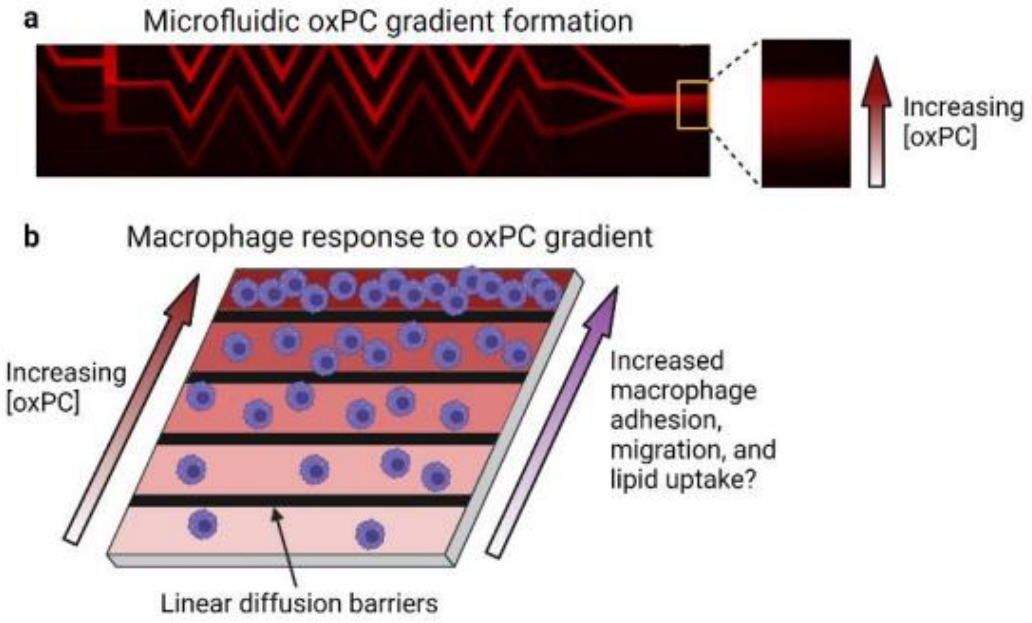

Figure 6.2. Spatiotemporal macrophage response to linear oxPC gradients. (a) A microfluidic mixer generates a concentration gradient of oxPC liposomes. (b) These liposomes rupture on a substrate possessing linear diffusion barriers, resulting in a concentration gradient of oxPC in SLBs. Macrophages will be cultured on the substrate and assayed for adhesion density, migration, and lipid uptake. (Credit to Nathan Wittenberg for the creation of this figure.)

A second option for investigating macrophage migration atop bilayers containing oxidized lipids is to locally photo-oxidize an area of a SLB. Initially, macrophages will be cultured atop SLBs that lack oxidized phospholipids in a presumably random array. As discussed extensively in chapter three of this dissertation, focused optical stimuli can be used to oxidize a lipid bilayer that contains of lipid-conjugated photosensitizer. The presence of diffusion barriers will keep the generated oxidized lipids from diffusing throughout the entire surface area of the solid support. The migratory behavior of macrophages across this locally-photo-oxidized surface can thus be monitored. Again,

cholesterol will be incorporated to investigate whether cholesterol influences the migration of macrophages across an oxidized lipid bilayer.

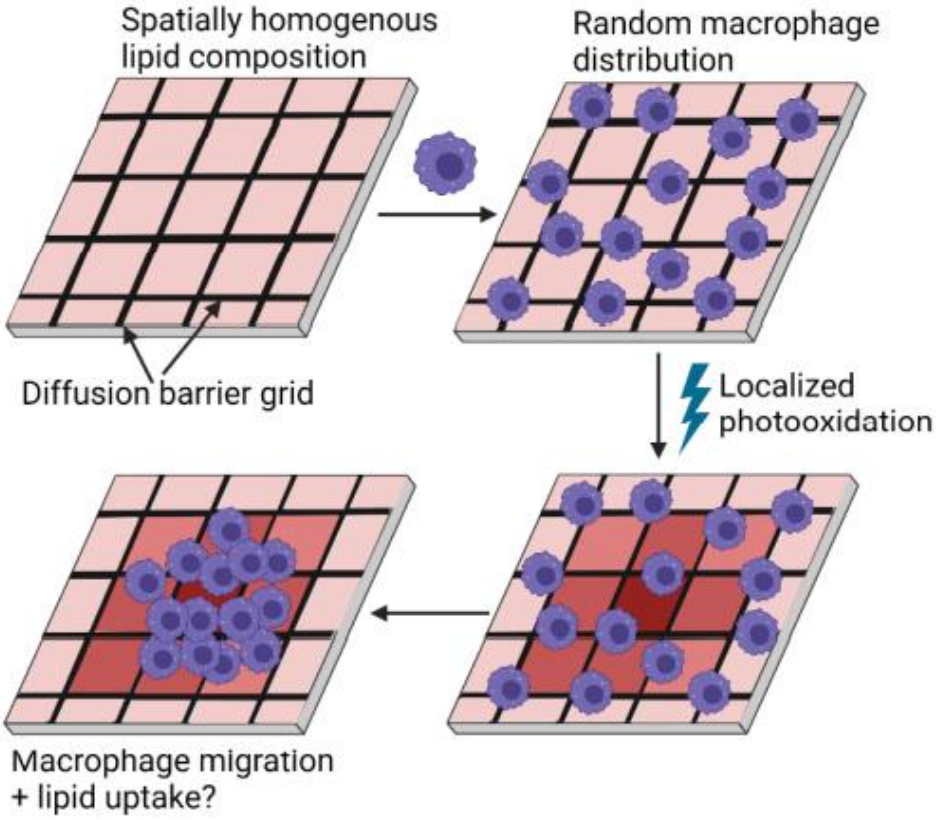

Figure 6.3. Spatiotemporal macrophage response to photochemically-generated oxPC gradients. A homogeneous SLB is initially present overtop a diffusion barrier grid. Macrophages are cultured on the SLB, then a focused optical stimulus initiates the localized generation of oxPC. This may trigger macrophage migration to the area enriched in oxPC and the uptake of membrane lipids. (Credit to Nathan Wittenberg for the creation of this figure.)

6.4 Cholesterol Modulation of Lipid-Lipid and Lipid-Protein Interactions

The addition of cholesterol in membranes has been shown to create raft domains as well as induce phase separation in non-oxidized membranes.[13–16] The Wittenberg lab has

done work with giant unilamellar vesicles (GUVs) and labeling liquid ordered (L_O) and liquid disordered (L_D) domains. As such, future work with the project I described in chapter four could include monitoring phase separation of GUVs when varying mole fractions of oxidized lipids and cholesterol are present.

The Wittenberg lab has also previously done studies that characterize lipid-protein interactions between myelin-associated glycoprotein (MAG) and gangliosides, which is an important model of the interface between axons and myelin in the nervous system.[17] Work can still be done to probe the effects that cholesterol has on these MAG-ganglioside interactions. Additionally, because oxidized lipids are often markers for an immune response due to injury or illness,[1] oxidized lipids can be incorporated into the axonal model to further understand MAG-ganglioside interactions when neurons have been damaged.

6.5 Conclusions

The foundations that I have laid throughout this dissertation serve as the groundwork for many important future studies. My system of photosensitized lipid oxidation via a lipid-conjugated fluorophore can be used to probe the interactions and kinetics of vital immune cells with oxidized phospholipids. These interactions are not currently well-known. Thus, the work suggested in this chapter is a starting point for many future studies and investigations that can be performed with the bioanalytical tools and techniques utilized by the Wittenberg Lab.

References 6.6

(1) Zhong, S.; Li, L.; Shen, X.; Li, Q.; Xu, W.; Wang, X.; Tao, Y.; Yin, H. An Update on Lipid Oxidation and Inflammation in Cardiovascular Diseases. *Free Radical Biology and Medicine* **2019**, *144*, 266–278.

(2) Greenberg, M. E.; Li, X.-M.; Gugiu, B. G.; Gu, X.; Qin, J.; Salomon, R. G.; Hazen, S. L. The Lipid Whisker Model of the Structure of Oxidized Cell Membranes. *Journal of Biological Chemistry* **2008**, *283* (4), 2385–2396.

(3) Hazen, S. L. Oxidized Phospholipids as Endogenous Pattern Recognition Ligands in Innate Immunity. *Journal of Biological Chemistry* **2008**, *283* (23), 15527–15531.

(4) Zhivaki, D.; Kagan, J. C. Innate Immune Detection of Lipid Oxidation as a Threat Assessment Strategy. *Nat Rev Immunol* **2021**, 1–9.

(5) Podrez, E. A.; Poliakov, E.; Shen, Z.; Zhang, R.; Deng, Y.; Sun, M.; Finton, P. J.; Shan, L.; Gugiu, B.; Fox, P. L.; Hoff, H. F.; Salomon, R. G.; Hazen, S. L. Identification of a Novel Family of Oxidized Phospholipids That Serve as Ligands for the Macrophage Scavenger Receptor CD36. *Journal of Biological Chemistry* **2002**, *277* (41), 38503–38516.

(6) Stewart, C. R.; Stuart, L. M.; Wilkinson, K.; van Gils, J. M.; Deng, J.; Halle, A.; Rayner, K. J.; Boyer, L.; Zhong, R.; Frazier, W. A.; Lacy-Hulbert, A.; Khoury, J. E.; Golenbock, D. T.; Moore, K. J. CD36 Ligands Promote Sterile Inflammation through Assembly of a Toll-like Receptor 4 and 6 Heterodimer. *Nat Immunol* **2010**, *11* (2), 155–161.

(7) Yang, X.; Okamura, D. M.; Lu, X.; Chen, Y.; Moorhead, J.; Varghese, Z.; Ruan, X. Z. CD36 in Chronic Kidney Disease: Novel Insights and Therapeutic Opportunities. *Nat Rev Nephrol* **2017**, *13* (12), 769–781.

(8) Park, Y. M. CD36, a Scavenger Receptor Implicated in Atherosclerosis. *Exp Mol Med* **2014**, *46* (6), e99–e99.

(9) Griffin, E.; Re, A.; Hamel, N.; Fu, C.; Bush, H.; McCaffrey, T.; Asch, A. S. A Link between Diabetes and Atherosclerosis: Glucose Regulates Expression of CD36 at the Level of Translation. *Nat Med* **2001**, *7* (7), 840–846.

(10) Wang, H.; Franco, F.; Tsui, Y.-C.; Xie, X.; Trefny, M. P.; Zappasodi, R.; Mohmood, S. R.; Fernández-García, J.; Tsai, C.-H.; Schulze, I.; Picard, F.; Meylan, E.; Silverstein, R.; Goldberg, I.; Fendt, S.-M.; Wolchok, J. D.; Merghoub, T.; Jandus, C.; Zippelius, A.; Ho, P.-C. CD36-Mediated Metabolic Adaptation Supports Regulatory T Cell Survival and Function in Tumors. *Nat Immunol* **2020**, *21* (3), 298–308.

(11) Axelrod, D. Cell-Substrate Contacts Illuminated by Total Internal Reflection Fluorescence. *Journal of Cell Biology* **1981**, *89* (1), 141–145.

(12) Lingwood, D.; Binnington, B.; Róg, T.; Vattulainen, I.; Grzybek, M.; Coskun, Ü.; Lingwood, C. A.; Simons, K. Cholesterol Modulates Glycolipid Conformation and Receptor Activity. *Nat Chem Biol* **2011**, *7* (5), 260–262.

(13) de Almeida, R. F. M.; Borst, J.; Fedorov, A.; Prieto, M.; Visser, A. J. W. G. Complexity of Lipid Domains and Rafts in Giant Unilamellar Vesicles Revealed by Combining Imaging and Microscopic and Macroscopic Time-Resolved Fluorescence. *Biophys J* **2007**, *93* (2), 539–553.

(14) Mills, T. T.; Toombes, G. E. S.; Tristram-Nagle, S.; Smilgies, D.-M.; Feigenson, G. W.; Nagle, J. F. Order Parameters and Areas in Fluid-Phase Oriented Lipid Membranes Using Wide Angle X-Ray Scattering. *Biophysical Journal* **2008**, *95* (2), 669–681.

(15) Alwarawrah, M.; Dai, J.; Huang, J. A Molecular View of the Cholesterol Condensing Effect in DOPC Lipid Bilayers. *J. Phys. Chem. B* **2010**, *114* (22), 7516–7523.

(16) Leeb, F.; Maibaum, L. Spatially Resolving the Condensing Effect of Cholesterol in Lipid Bilayers. *Biophys J* **2018**, *115* (11), 2179–2188.

(17) Cawley, J. L.; Jordan, L. R.; Wittenberg, N. J. Detection and Characterization of Vesicular Gangliosides Binding to Myelin-Associated Glycoprotein on Supported Lipid Bilayers. *Anal. Chem.* **2021**, *93* (2), 1185–1192.

Ashley M. Baxter
Department of Chemistry

Lehigh University
Seeley G. Mudd Building
6 E. Packer Ave
Bethlehem, PA 18015

EDUCATION

2018-2022 Ph.D. Chemistry, Lehigh University

2016-2018 M.S. Chemistry, Lehigh University

2012-2016 B.S. Biochemistry and Molecular Biology, DeSales University

PROFESSIONAL EXPERIENCE

2017-2022 Graduate Researcher

Performed variety of analytical techniques to further graduate research project. Catalogued chemical inventory. Placed purchasing orders for materials and equipment. Supervised, trained, and mentored undergraduate researchers.

2020-2021 General Chemistry Laboratory Teaching Assistant

Supervised students as they performed experiments. Assisted students with writing lab reports. Graded lab reports and provided feedback to students. Enforced laboratory safety. Enforced rules and regulations of the teaching laboratory. Assisted with proctoring and grading in-class exams.

2017-2020 General Chemistry Laboratory Instructor

Supervised students and teaching assistants as they performed experiments. Assisted students with writing lab reports. Introduced students to a laboratory setting and laboratory equipment. Enforced the rules and regulations of the teaching laboratory. Educated students about proper laboratory safety and waste disposal protocols. Assisted with proctoring and grading in-class exams.

2016-2017 General Chemistry Laboratory Teaching Assistant

RESEARCH EXPERIENCE

2017-2022 Graduate Research Assistant, Department of Chemistry, Lehigh University

Bioanalytical Techniques to Investigate the Consequences of Photosensitized Lipid Oxidation on Lipid Bilayer Formation and Structure
(advisor: Nathan J. Wittenberg)

2014-2016 Undergraduate Research Assistant, Department of Chemistry, DeSales University

Investigation of the Glycosidic Bond Energy of Disaccharides through Bomb Calorimetry
(advisor: Sara E.N. Hayik)

TEACHING EXPERIENCE

2020-2021 Teaching Assistant, General Chemistry Laboratory, Lehigh University

2017-2020 Instructor, General Chemistry Laboratory, Lehigh University

2016-2017 Teaching Assistant, General Chemistry Laboratory, Lehigh University

PUBLICATIONS

3. **A.M. Baxter**, L.R. Jordan, M. Kullappan, N.J. Wittenberg. Tubulation of supported lipid bilayer membranes induced by photosensitized lipid oxidation. *Langmuir*. **2021**. 37, 19, 5753-5762

2. **A.M. Baxter**, N.J. Wittenberg. Excitation of fluorescent lipid probes accelerates supported lipid bilayer formation via photosensitized lipid oxidation. *Langmuir*. **2019**. 35, 35, 11542-11549.

1. L.R. Jordan, M.E. Blauch, **A.M. Baxter**, J.E. Cawley, N.J. Wittenberg. Influence of brain gangliosides on the formation and properties of supported lipid bilayers. *Colloids and Surfaces B: Biointerfaces*. **2019**, 183, 110442.

PRESENTATIONS

7. Biophysical Society, Poster Presentation February 2022
Structural Defects of a Supported Lipid Bilayer Induced by Photosensitized Lipid Oxidation

6. Biophysical Society, Poster Presentation February 2020
The Effects of Photosensitized Lipid Oxidation on Supported Lipid Bilayer Formation and Membrane Deformation

5. Pittcon Conference and Expo, Oral Presentation March 2019
Photosensitized Lipid Peroxidation Accelerates Vesicle Rupture on SiO_2 Surfaces: A QCM-D Study

4. Lehigh University Thesis Proposal, Oral Presentation June 2018
The Effects of Lipid Oxidation on Bilayer Formation, Integrity, and Structure

3. ACS Mid-Atlantic Regional Meeting, Poster Presentation June 2018
Photosensitized Lipid Peroxidation Accelerates Vesicle Rupture on SiO_2 Surfaces: A QCM-D Study

2. Lehigh University Departmental Seminar, Oral Presentation April 2018
A Sampling of the Use of Cryo-EM to Provide Structural Insights into Biomolecular Systems

1. ACS National Meeting & Exposition, Poster Presentation March 2016
Investigation of the Glycosidic Bond Energy of Disaccharides through Bomb Calorimetry

SKILLS

Instrumentation/Equipment:

- Quartz Crystal Microbalance with Dissipation Monitoring (QCM-D)
- Fluorescence Microscopy
- UV-Vis Spectroscopy
- Infrared Spectroscopy
- Fluorescence Spectroscopy
- NMR Spectroscopy
- Dynamic Light Scattering (DLS)
- Zeta Potential

Computer Programs:

- Microsoft Office (MS Word, MS Excel, MS PowerPoint)
- GraphPad, Prism
- LoggerPro, Vernier
- ImageJ, NIH
- MATLAB, Mathworks